Activity-dependent Remodeling of *Drosophila* Olfactory Sensory Neurons During an Early-life Critical Period

By

Randall Michael Golovin

Dissertation

Submitted to the Faculty of the

Graduate School of Vanderbilt University

in partial fulfillment of the requirements

for the degree of

DOCTOR OF PHILOSOPHY

in

Neuroscience

February 28th, 2021

Nashville, Tennessee

Approved:

Kendal Broadie, Ph.D.

Bruce Carter, Ph.D.

David Miller III, Ph.D.

R. Jason Pitts, Ph.D.

To my lovely wife, Danielle, for her unwavering support

and

To our baby, whose critical periods are about to open

ACKNOWLEDGEMENTS

First off, I want to thank my family for instilling in me my love for science and joy of exploration. Dad, thank you for always making science seem like the coolest job. Mom, thank you for teaching me to stay calm and logical even in the most stressful of situations. Seth, thank you for expanding my imagination and teaching me how to dream big. Kevin, thank you for being a role model and pushing me to be my best. Hannah, thank you for keeping me sane and happy, as you know, life is no walk in the park. You all have always been a constant in my life and I am the better for it.

Next, I want to thank all the people in the Broadie lab who have helped me and improved my life. I thank my advisor, Kendal Broadie, who gave me the freedom to follow my passion. To the whole Broadie laboratory, thank you for your constant support and passion. I thank Emma Rushton for sharing her love of science and always having time to explain a complex genetic cross. I thank Cheryl Gatto for always being willing to have the difficult conversations and her unyielding belief and support of me. I thank Caleb Doll for blazing the critical period trail with me. I thank Patty Jumbo for showing me how to balance career and life with grace. I thank Jim Sears for his enthusiasm for innovation and always designing a new gismo or gadget for experiments. I thank Neil Dani for treating me like one of the crew even though we never overlapped in lab. I thank Mary Lynn Dear for being the best mentor and never saying no when I needed help. I thank Tyler Kennedy for demonstrating that you can be a great scientist while being true to yourself. I thank Shannon Leahy for not letting me go a whole day in lab without talking to someone. I thank Chunzhu Song for letting me vent my frustrations. I thank Dominic Vita for never being too busy to talk about cool science. I thank Darius Booth and Qing Xia Chen for keeping the lab running smoothly. I thank Josh Mitchell for spreading his infectious love for science and music. I thank Ryan Moore for keeping me company on the long nights in

lab and teaching me that rock climbing is both a physical and mental challenge. I thank Jarrod Shilts for sharing his wisdom well beyond his years. Finally, I thank Jacob Vest for help on my projects with his brilliant mind and more brilliant jokes. Through teaching you, I learned so much.

I want to also thank the other faculty and students who improved my graduate school journey. I want to thank my Neuroscience cohort JP, Katherine, Melissa and Robin. You are some of the most intelligent people I know, but your emotional, not intellectual, support got me through graduate school. I want to thank my unofficial cohort member Corey. Our car rides to and from the card shop are amongst my fondest memories. You have taught me so much about life, honor and friendship. To Quentin Gaudry, thank you for teaching me electrophysiology and sharing your wisdom. Science is great because of people like you. I would like to thank my thesis committee chair, David Miller and my other committee members Bruce Carter and Jason Pitts for their support of my scientific and my personal growth. I thank Anita Disney for adopting me into her lab and providing me with opportunities to expand my scientific horizons. I thank the administrators in the Neuroscience office including Roz Johnson and Beth Sims who took care of all the little things so I could focus on my science.

Finally, I would like to thank my wife, Danielle, for always believing in me and supporting me. If for nothing else, my Ph.D. was worth it because I met you. Thank you everyone one who has helped me along the way. I made it.

FUNDING

This work was supported by:

National Institutes of Health Grant MH084989 to K.B.

Table of Contents

Page

LIST OF TABLES

LIST OF FIGURES

ABBREVIATIONS

5-HT	serotonin
A	anterior
ACh	acetylcholine
AL	antennal lobe
APF	after puparium formation
ASD	autism spectrum disorder
A.U.	arbitrary units
BDNF	brain-derived neurotrophic factor
BRP	bruchpilot
BSA	bovine serum albumin
$CaCl_2$	calcium chloride
CAM	cell adhesion molecule
CAMKII	calcium-calmodulin dependent kinase II
cAMP	cyclic adenosine monophosphate
CREB-B	cAMP-responsive element binding protein B
CSPG	chondroitin sulfate proteoglycan
D	dorsal
Dally	division abnormally delayed
DAB	diaminobenzidine
DAN	dopaminergic neuron
Dfmr1	*Drosophila fragile x mental retardation 1*
DHSB	Developmental Studies Hybridoma Bank
DIW	deionized water
Dlp	Dally-like protein

DM5	dorsal medial 5
DN	dominant-negative
DNA	deoxyribonucleic acid
DoOR 2.0	database of Olfactory Responses 2.0
dpe	days post eclosion
E	excitation
E/I	excitation to inhibition ratio
EB	ethyl butyrate
EtOH	ethanol
Fmr1	*fragile x mental retardation 1*
FMRP	Fragile X Mental Retardation Protein
FXS	Fragile X Syndrome
Fz2	frizzled-2 receptor
GA	geranyl acetate
GABA	gamma-Aminobutyric acid
GAD	glutamic acid decarboxylase
GAT	GABA transporter
GCaMP	circularly permutated GFP, Calmodulin, M13 peptide
GFP	green fluorescent protein
GLT1	glutamate type 1 transporter
GluLNs	glutamatergic local interneurons
GOF	gain of function
GTA	glutaraldehyde
HEPES	4-(2-hydroxyethyl)-1-piperazineethanesulfonic acid
I	inhibition
ID	intellectual disability

IR	ionotropic receptor
Kir2.1	inward rectifying potassium channel 2.1
KO	knockout
KC	Kenyon cells
KCl	potassium chloride
LH	lateral horn
LHN	lateral horn neuron
LN	local interneuron
LOF	loss of function
LTH	long-term habituation
Lynx1	Ly6/Neurotoxin1
MAP1B	microtubule-associated protein 1B
MB	mushroom body
MBON	mushroom body output neuron
$MgCl_2$	magnesium chloride
miniSOG	mini singlet oxygen generator
mM	millimolar
MMP	matrix metalloproteinase
MP	maxillary palp
NaCl	sodium chloride
NE	norepinephrine
NIH	National Institutes of Health
NMDA	N-Methyl-D-aspartic acid
NMJ	neuromuscular junction
Nogo-66	neurite outgrowth inhibitor 66
N.S.	non-significant

O/N	overnight
OR	olfactory receptor
Orco	olfactory co-receptor
ORK	open rectifier potassium (K+) channel
OSN	olfactory sensory neuron
OsO_4	osmium tetroxide
Otx2	Orthodenticle Homeobox 2
P	posterior
PBS	phosphate buffered saline
PBS-T	phosphate buffered saline with triton X-100
PCR	polymerase chain reaction
Peb-Gal4	*Pebbled*-Gal4
PFA	paraformaldehyde
PKA	protein kinase A
PN	projection neuron
PNN	perineuronal net
PO	propylene oxide
PS	phosphatidylserine
PSD-95	postsynaptic density protein 95
PV	parvalbumin
qPCR	quantitative polymerase chain reaction
RDL	resistant to Dieldrin
RFP	red fluorescent protein
RNA	ribonucleic acid
RNAi	ribonucleic acid interference
RoI	region of interest

SC	sodium cacodylate
SEM	standard error of the mean
SER	standard error of the regression
Sgg	Shaggy
STaR	synaptic tagging with recombination
SV	synaptic vesicle
TBS-T	tris buffered saline with tween-20
TDE	2,2-thiodiethanol
TEM	transmission electron microscopy
TeTxLc	tetanus toxin light-chain
tPA	tissue plasminogen
Trpv1	transient receptor potential cation channel subfamily V member 1
UA	uranyl acetate
V	ventral
V1	primary visual cortex
VM7	ventral medial 7
Wg	wingless

Chapter I

Introduction

Critical Periods of Development

Critical periods are epochs of nervous system development with heightened adaptability to environmental stimulation. Studies from Konrad Lorenz on newly-hatched geese provide the classic example of a critical period. He found that geese would follow the first moving object encountered and treat it as their mother (Lorenz, 1935). Later experiments demonstrated this imprinting peaked between 12-17 hours after hatching and ended by ~32 hours (Hess, 1958). Imprinting epitomizes the key concept of the critical period, with an all-or-nothing behavioral change occurring between defined opening and closing times. Building on the idea of critical periods from ethology, Eric Lenneberg applied these principals to language development. He argued that language is built upon largely innate scaffolds, with the words of the caregiver refining sound discernment and reproduction during language maturation (Lenneberg, 1967). As anyone who has tried to learn a second language in their teenage years or beyond can attest, it is much more difficult than 'child's play'. However, unlike the imprinting behavior characterized by Lorenz, the ability to learn language does not disappear completely, but is only dampened after the early critical period. This distinction has led some to distinguish the all-or-nothing "critical periods" from such "sensitive periods" that never fully close (Knudsen, 2004). For the purposes of this discussion, the term "critical period" is used to refer to both "critical" and "sensitive" periods, as the words are often used interchangeably and, in many cases, no experimental evidence exists to distinguish them (Knudsen, 2004). Regardless of semantics, the critical period framework in parallel developmental psychology to developmental biology paved the way for seminal work by neuroscientists linking these two previously disparate fields.

The ground-breaking experiments of Hubel and Wiesel in the cat visual system married behavioral observations of developing animals with the structure and function of brain circuitry. Early work highlighted the pronounced effects of monocular visual deprivation on the developing cat visual system (Wiesel and Hubel, 1963a, 1963b), demonstrating the dramatic preference for the open eye over the closed eye. Later studies systematically defined a critical period from eye opening to the fourth month (Hubel and Wiesel, 1970). This “ocular dominance plasticity” paved the way for critical period research, which now extends from many sensory systems to a variety of higher brain centers. For instance, the auditory system refines tuning to sound frequencies by exposure to broadband sounds in a frequency-tuning critical period (Sanes and Constantine-Paton, 1983), wherein exposure to a single frequency sharpens and shifts the tuning of auditory cortex to that particular sound (Zhang et al., 2001a). Similarly, the rodent whisker barrel system displays robust plasticity during a critical period soon after birth, with barrels in the somatosensory cortex shifting to a spared whisker when all others are removed (Fox, 1992). Improved tools and greater understand of the brain have led to the discovery of critical periods for complicated cognitive behaviors. For instance, mice show a critical period for social reward learning in a nucleus accumbens reward circuit that opens at weaning and closes at maturity (Nardou et al., 2019). Likewise, male social isolation during a critical period between weaning and sexual maturity in mice decreases later sociability by reducing feedback projections in the prefrontal cortex (Bicks et al., 2020; Yamamuro et al., 2020). Overall, critical period studies show a commonality implying similar circuit mechanisms operate across disparate brain regions.

The cellular and molecular mechanisms that underlie critical period plasticity across the developing brain highlight a transition between intrinsic neuronal activity and sensory input experience (Hooks and Chen, 2007; Espinosa and Stryker, 2012). Critical periods open with the onset of experience and close when the circuitry matures and stabilizes to resist further change (Hensch, 2005). Studies of critical periods have focused mainly on brain circuits activated primarily by one particular sensory modality, making it easy to control the onset of sensory

experience and manipulate the sensory environment. This work has defined four critical period phases – pre-experience, onset of experience, refinement and stabilization – which highlight the dynamic changes occurring (Fig. 1; Hensch, 2005). It is important to note that although these phases are used as a general reference framework, the extent to which different circuits are influenced by sensory experience varies greatly between varying species and brain regions within species (Dehorter and Del Pino, 2020; Reh et al., 2020). In addition, transitions between these phases are somewhat fluid, and any given developmental snapshot could represent a hybrid state. In the pre-experience phase, brain circuits are proposed to be in largely “hard-wired”, mainly determined by morphogen signaling, cell-adhesion molecules and intrinsic activity (Fig. 1; Rakic, 1988; O’Leary, 1989; Cadwell et al., 2019). These factors converge to regulate both the positional and cellular identity of neurons that delineate the “protomap” of the pre-experience prenatal brain (Antón-Bolaños et al., 2019; Cadwell et al., 2019). At this phase, the neural circuit organization of the brain roughly approximates the mature state, but will undergo both continued development and activity-dependent modification with the onset of sensory experience.

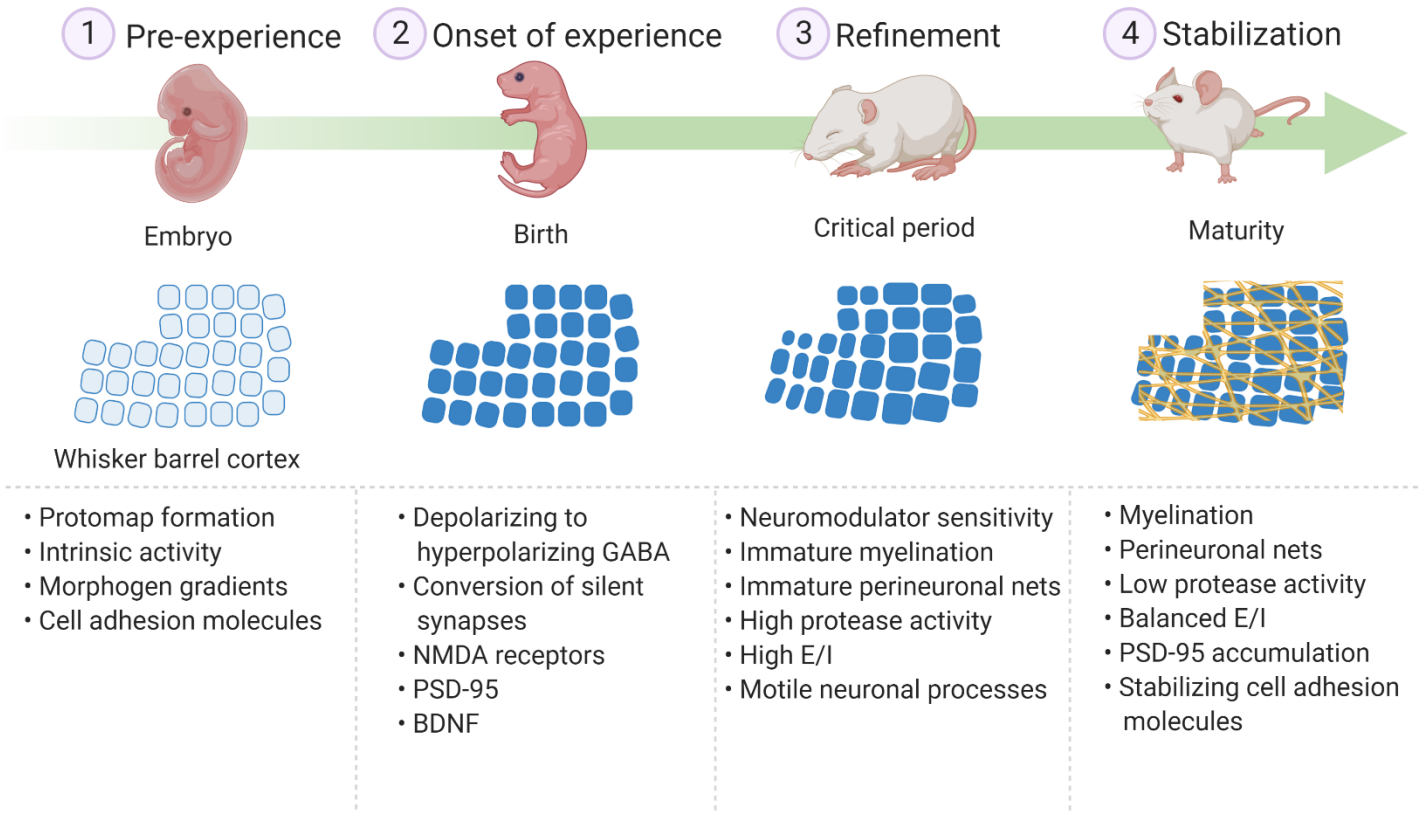

Figure 1. Phases of Critical Periods
1) Pre-experience. Prior to experience, the brain is assembled into a rough "protomap" that approximates the adult structures. These maps are formed by a combination of the intrinsic activity of input neurons, cell adhesion molecules and morphogen gradients. **2) Onset of Experience.** The onset of experience triggers events in the brain that lead to the opening of the critical period. During this stage, sensory input drives the early depolarizing actions of GABA which activate NMDA receptors to convert silent synapses by recruiting AMPA receptors and post-synaptic density protein 95 (PSD-95). This initial activity also leads to the release of brain-derived neurotrophic factor (BDNF) that allows for GABAergic neuron maturation. **3) Refinement**. The heightened plasticity defining critical periods occurs during the refinement stage. The profound change during this critical period phase relies on neuromodulator sensitivity, high levels of protease activity and greater relative windows of excitation compared to inhibition (high E/I) within developing circuits. The brain during the critical period also has immature myelination and perineuronal nets leading to more motile neuronal processes. **4) Stabilization.** The closer of the critical period is brought about by the accumulation of myelin, perineuronal nets, PSD-95 and cell adhesion molecules. This is possible due to a reduction in the amount of protease activity and leads to the maturation of inhibitory GABAergic neurons which balance the E/I. Created with BioRender.com.

The dramatic increase in sensory experience at birth marks the start of the earliest critical periods, and a switch to sensory-driven input activity (Fig. 1; Hooks and Chen, 2007; Reh et al., 2020). Although it is generally accepted that critical periods first begin with this initial onset of sensory experience, there have been few studies that capture the molecular features of this first burst of sensory input activity. However, one striking example of the transition at the onset of sensory experience comes from studies on the *Xenopus* tadpole optic tectum (Rheede et al., 2015). With the onset of vision, the excitatory glutamatergic neurons do not fire action potential spikes in response to early visual stimulation. Rather, the neurons receiving the initial visual input respond with weak excitatory responses characterized by many silent synapses (Rheede et al., 2015). Relatively short duration visual experience (e.g. 15 minutes) is able to convert 30-40% of these non-spiking neurons to visually-spiking neurons (Rheede et al., 2015). This rapid conversion involves three steps; 1) visual stimulation drives activation of both glutamatergic and GABAergic neurons, 2) the combination of glutamate binding and depolarizing GABA conductance during this developmental time point activates NMDA receptors, and 3) opening of NMDA receptors drives activity-dependent plasticity leading to the insertion of AMPA receptors and unsilencing of the glutamatergic synapses (Rheede et al., 2015). This work taking advantage of the *Xenopus* model system highlights the transition to sensory-driven network activity, and epitomizes the second phase of critical periods. Although other systems are not as amenable for the observation of the initial onset of sensory-driven activity, regulators that control the opening of critical periods have been inferred from delays in the emergence of critical period plasticity.

Studies of the mammalian sensory cortex indicate that the conversion of silent synapses and maturation of GABAergic interneurons generally play important roles in critical period onset (Hensch et al., 1998; Huang et al., 2015; Oh et al., 2016). As above in *Xenopus* optic tectum, activation of silent synapses appears to be one underlying mechanism to convert brain circuits to a primarily sensory-driven state. The conversion of a silent synapse to an active synapse results

from AMPA receptor recruitment via the PDZ scaffold postsynaptic density protein 95 (PSD-95) anchoring receptors in the appropriate membrane subdomains (Béïque et al., 2006; Kerchner and Nicoll, 2008). In PSD-95 knockout (KO) mice, silent synapses cannot recruit AMPA receptors, and brain circuits are left in a perpetually immature state (Huang et al., 2015). In addition to the central role of silent synapse activation in critical period plasticity, the maturation of GABAergic interneurons controls critical period timing (Hensch et al., 1998; Fagiolini and Hensch, 2000; Deidda et al., 2015; Kobayashi et al., 2015). During earlier development, high levels of intracellular chloride lead to membrane depolarization in response to opening of GABA-gated chloride channels (Ben-Ari et al., 1989). Local GABA administration can drive the formation of both inhibitory synapses and excitatory dendritic spines in the developing mouse cortex through this initial GABA depolarizing action (Oh et al., 2016). Transiently disrupting these depolarizing GABA currents has been shown to extend the critical period for ocular dominance plasticity within the rat primary visual cortex (V1; Deidda et al., 2015). These depolarizing GABA currents trigger the release of neurotrophic factors, which further push circuit maturation forward.

One driver of the extended duration of the critical period by disrupting early depolarizing GABA is the lower expression of the secreted brain-derived neurotrophic factor (BDNF), and the consequent slowed development of GABAergic inhibitory tone within the rodent V1 visual cortex (Huang et al., 1999). Similarly, ablation of subplate neurons providing the initial excitatory input to the cortex stops maturation from depolarizing to hyperpolarizing GABAergic currents, and thereby disrupts critical period plasticity (Kanold and Shatz, 2006). The normal maturation of GABAergic inhibition leads to the proper formation of the visual ocular dominance columns, and the critical period can only proceed once this network structure has been properly established (Fagiolini and Hensch, 2000). Indeed, the incorporation of proper inhibitory GABAergic neurons appears to be a common feature of critical periods (Takesian et al., 2018; Yaeger et al., 2019; Reh et al., 2020). Together this work highlights a general set of mechanisms that may lead to the onset of critical periods. The early pre-critical period protomap responds to initial sensory activity,

which drives the activation of immature GABAergic and glutamatergic neurons. This maturation in turn triggers conversion of silent synapses to functional AMPA receptor-containing synapses, and also drives the switch of GABA currents from excitatory to inhibitory signaling (Tyzio et al., 2014; Rheede et al., 2015; Oh et al., 2016). By pairing activation of glutamatergic silent synapses to GABAergic neuron incorporation, developing brain circuits are able to ensure matching excitation (E) and inhibition (I), and develop proper E/I balance (Akerman and Cline, 2006). Once the transition to sensory-driven input is completed in this second critical period phase, the stage is set for more profound changes during the third phase of refinement.

The critical period refinement phase represents a shift from a genetically-driven state to a sensory-driven state (Fig. 1). This phase is characterized by a low threshold for synaptic plasticity, which is enabled by neuromodulator signaling that facilitates plasticity and the lack of stabilizing molecules that gradually build up to mark the fourth critical period phase (Hensch, 2005; Hensch and Quinlan, 2018; Reh et al., 2020). Early depletion studies showed the importance of norepinephrine (NE) and acetylcholine (ACh) for visual ocular dominance plasticity in kittens (Bear and Singer, 1986). NE appears less specific to the critical period, as it facilitates adult plasticity in the auditory cortex and is a key mediator of attention and arousal (Martins and Froemke, 2015). However, NE still plays an important role during the critical period (Shepard et al., 2015). Conversely, ACh appears to have a more specific role during the critical period. In both visual and auditory systems, GABAergic interneurons have a specific sensitivity to cholinergic stimulation during the critical period, which facilitates plasticity by creating windows of disinhibition (Takesian et al., 2018; Yaeger et al., 2019). Moreover, serotonin (5-HT) appears to play a similar role, as early serotonin depletion blocks ocular dominance plasticity in the V1 (Gu and Singer, 1995), and administration of a serotonin selective reuptake inhibitor in adult mice reopens critical period-like plasticity (Vetencourt et al., 2008). In addition to these classic neuromodulators, oxytocin has more recently emerged as an important facilitator of critical period cross-modal plasticity in sensory cortices and social reward learning (Zheng et al., 2014; Nardou et al., 2019).

Together, neuromodulators lead to robust plasticity during the critical period, and the progressive decrease in neuromodulator signaling with structural and functional stabilization progressively leads to the closing of critical periods.

The fourth phase of the critical period is circuit stabilization (Fig. 1; Hensch, 2005; Bavelier et al., 2010; Espinosa and Stryker, 2012). This late window is highlighted by increasing inhibition, decreased sensitivity to neuromodulators, and a profound stabilization of circuit connectivity (Hensch and Quinlan, 2018). While critical periods open with the onset of functional GABAergic inhibition, the progressive increase in the inhibitory tone over the critical period eventually culminates in its closure (Fagiolini and Hensch, 2000; Reh et al., 2020). The maturation of inhibitory interneurons serves to balance excitation, providing stability in adult brain circuits. One reason for this excitation-inhibition balance is the reduced sensitivity to above neuromodulators (Morishita et al., 2010; Nardou et al., 2019). For instance, in the visual system, parvalbumin-expressing (PV) and somatostatin-expressing GABAergic interneurons both show lowered responses to ACh stimulation as the critical period expires (Morishita et al., 2010; Takesian et al., 2018; Yaeger et al., 2019). PV interneurons respond less to ACh after the close of the critical period due to expression of Ly6/Neurotoxin1 (Lynx1), a nicotinic ACh receptor-binding protein that reduces the activity of the receptor channels (Morishita et al., 2010). Indeed, Lynx1 expression helps to close the critical periods in both the visual and auditory systems, and the removal of Lynx1 leads to critical period-like plasticity in the adult brain (Morishita et al., 2010; Takesian et al., 2018). Similarly, loss of oxytocin sensitivity in the nucleus accumbens leads to the end of the social reward critical period, which can be later reinstated by boosting oxytocin levels (Nardou et al., 2019). This functional stabilization is paralleled by a progressive solidifying of the structure of the neurons and the surrounding extracellular matrix.

A final piece of the critical period closure mechanism is the structural stabilization of the circuit architecture (Hensch and Quinlan, 2018). For instance, PV interneurons are stabilized by the progressive emergence of extracellular proteoglycan perineuronal nets (PNNs), which provide

structural support and also sequester key signaling molecules, such as the transcription factor Orthodenticle Homeobox 2 (Otx2) that facilitates plasticity (Sugiyama et al., 2008). Disrupting extracellular PNN integrity with exogenous enzymes (chondroitinase; Liu et al., 2013) or secreted matrix metalloproteinases (e.g. matrix metalloproteinase 9 (MMP9); Murase et al., 2017) can reinstate critical period plasticity in the adult brain. Glial astrocytes secrete MMP9 to regulate PNN formation and thus control critical period closure (Ribot et al., 2020). Similarly, the protease tissue plasminogen (tPA) activator is upregulated during critical periods to facilitate dendritic spine synaptic pruning, whereas decreased tPA activity is causally associated with critical period closure (Mataga et al., 2004). During this transition, postsynaptic spines are also stabilized by the accumulation of the PSD-95 scaffold, cell adhesion molecule (CAM) cadherins and intercellular linker catenins (Bian et al., 2015; Huang et al., 2015). In addition to this postsynaptic stabilization, myelination of the presynaptic axons leads to the release of signaling molecules that bind to the neurite outgrowth inhibitor 66 (Nogo-66) receptor, and thus help to bring about the closure of the critical period for ocular dominance plasticity (McGee et al., 2005). Overall, these phases of critical periods serve as important markers of the progressive transition of brain circuits from genetically-wired to environmentally-refined, allowing brain neural circuits and animal behaviors to dynamically adapt to an ever-changing, unpredictable world.

The Drosophila Antennal Lobe as a Critical Period Model System

In this Ph.D. thesis work, I took advantage of *Drosophila melanogaster*, and the highly characterized and well-mapped brain olfactory antennal lobe (AL; Fig. 2,3 Vosshall et a., 2000; Couto et a., 2005; Wilson, 2013), to explore the genetic and molecular underpinnings of critical periods. *Drosophila* have numerous advantages that make it a powerful system for the genetic study of developmental neuroscience and sensory modality processing. The very short generation time (10 days) and large number of offspring (100s per female) facilitate developmental studies with tight time windows. The *Drosophila* model system also boasts a sophisticated genetic

toolbox, including extensive collections of genetic mutant and transgenic RNA interference (RNAi) lines; the UAS/Gal4 (Brand and Perrimon, 1993), Q-system (Potter et al., 2010) and LexA/LexAop (Szüts and Bienz, 2000) binary transgenic driver expression systems; excitatory and inhibitory optogenetic lines to manipulate neuronal excitability during development (Kazama, 2015); neurotoxin expression lines (e.g. tetanus toxin light-chain; TeTxLC) for targeted blockage of synaptic function (Sweeney and Broadie et al., 1995); transgenic reporter lines (e.g. membrane marker mCD8::GFP) to reveal neuronal architecture and trace neuronal circuits (Lee and Luo, 1999); and transgenic indicator lines (e.g. circularly permutated GFP, Calmodulin, M13 peptide; GCaMPs) to assess neuronal and synaptic function (Nakai et al., 2001). Compared to mammals, *Drosophila* have reduced complexity of both gene families and neural circuity maps to accelerate the connection of genes to critical period changes in the brain. Finally, the size and accessibility of the *Drosophila* brain allows for whole brain imaging and transgenic manipulation of individually-identified neurons within exquisitely-defined brain circuits. These benefits together provide a strong foundation to study critical period mechanisms.

The *Drosophila* olfactory circuitry comprises three levels of processing across five nodes in the periphery and brain. Olfactory processing begins in antenna and maxillary palps (MPs) where olfactory sensory neurons (OSNs) transduce odorant binding into electrical activity (Fig. 2,3; Coute et al., 2005; Van Naters and Carlson, 2007; Wilson, 2013). OSN dendrites extend into thin hair-like protrusions in both antenna and MPs (Brochtrup and Hummel, 2011). Odorants dissolve in a sensillar lymph to bind odorant receptor (OR) and ionotropic receptor (IR) channels. Both ORs and IRs are heteromeric ligand-gated cation channels formed of one class of odorant-binding subunit and an essential co-receptor subunit (Larsson et al., 2004; Benton et al., 2009; Butterwick et al., 2018). ORs have only a single obligate co-receptor (Orco), but IRs have a few different co-receptors (Larsson et al., 2004; Benton et al., 2009). In general, OSNs express just a single olfactory receptor class along with the required co-receptor; however, some exceptions do exist (Coute et al., 2005; Grabe and Sachse, 2018). Each sensilla houses 2-3 OSNs, each

expressing a different class of receptor. Just below the superficial OSN dendrites are the OSN cell bodies, which upon sufficient depolarization propagate actional potentials along the antennal or labial tract for antennal OSN axons and MP OSN axon, respectively (Wilson, 2013). Glial cells wrap OSN cell bodies as well as their axons, but do not extend into the dendrites. Although the antenna and MP seem to serve similar functions, the antenna contains more OSNs and seems particularly important for the detection of long-range odors, while the MP contains fewer OSNs and may serve a more prominent role in short-range odor detection and the olfactory enhancement of gustatory behaviors (Shiraiwa, 2008; Dweck et al., 2016).

Following initial sensory detection of odorants in both the antenna and MPs, olfactory information is shuttled along OSN axons to the antennal lobe (AL) in the central brain (Fig. 2,3; Couto et al., 2005). The AL serves as the first synaptic node information processing center of the brain by representing the odor identity and concentration in the activity of synaptic compartments called glomeruli (Wilson, 2013; Grabe and Sachse, 2018). The AL synaptic glomeruli represent separate functional channels of olfactory processing. OSNs which express the same olfactory receptor send convergent input onto the same target glomerulus, and do not overlap with other classes of OSNs (Vosshall et al., 2000 Coute et al., 2005; Grabe et al., 2016). Postsynaptic to the OSNs are olfactory projection neurons (PNs), which receive input from multiple OSNs of the same class. In addition to these principal neurons, local interneurons (LNs) regulate the activity of AL synapses through the release of excitatory, inhibitory and modulatory neurotransmitters as well as through gap junction mediated electrical synapses (Olsen and Wilson, 2008; Yaksi and Wilson, 2010; Wilson, 2013; Grabe and Sachse, 2018). Glial cells are also an important feature of the AL. PN and LN cell bodies reside surrounding the AL and cortex glial cells wrap the cell bodies of these neurons (Kremer et al., 2017). Ensheathing glia wrap the OSN axons of the labial and antennal tracts as well as demarcate individual glomeruli by covering OSNs as they enter the glomerular region (Kremer et al., 2017). Astrocyte-like glia send projections into glomeruli and interact more directly with AL synapses (Kremer et al., 2017). The AL extracts olfactory

information from the convergent input of OSNs onto PNs and sends these second order olfactory neurons to the final stage of information processing within the mushroom body (MB) and lateral horn (LH).

The MB mediates olfactory learning and the LH is required for innate olfactory behavior (Fig. 2; Belle and Heisenberg, 1994; Grabe and Sachse, 2018). PNs occur is three classes; excitatory PNs projecting to MB and LH, excitatory PNs projecting to just LH, and inhibitory PNs to just LH (Liang et al., 2013; Grabe and Sachse, 2018). PNs innervate the MB calyx with inputs on a small number Kenyon cells (KCs) and KCs receive input from about 10 PNs (Masse et al., 2009; Groschner and Miesenböck, 2019), although MB connectivity differs between animals (Masse et al., 2009; Hige et al., 2015) Thus, odor representation occurs in only a small number of KCs, allowing the MB to uniquely encode different odors (Wang et al., 2004). KCs have weak presynaptic inputs to MB output neurons (MBONs) under naïve conditions, but odors associated with a reward or punishment potentiate KC-MBON synapses via dopaminergic neurons (DANs) to drive associative memories (Hige et al., 2015). LH connectivity is much more stereotyped (Jeanne et al., 2018; Dolan et al., 2019), with a single PN or small subsets of PNs connecting to lateral horn neurons (LHNs; Fişek and Wilson, 2014). PNs responding to similar odor classes or eliciting similar behaviors tend to connect to the same LHNs (Jeanne et al., 2018). Olfactory processing has only begun to be explored, but >80 cell types have been genetically identified, suggesting complex LH odorant information regulation upstream of output motor behaviors (Dolan et al., 2019). Despite the MB/LH separation for olfactory processing, MB and LH outputs seem to converge on downstream neurons to drive motor behaviors (Dolan et al., 2019). Together, this extensive exploration of the *Drosophila* olfactory system, and especially the AL, makes it an excellent system to study experience-dependent remodeling.

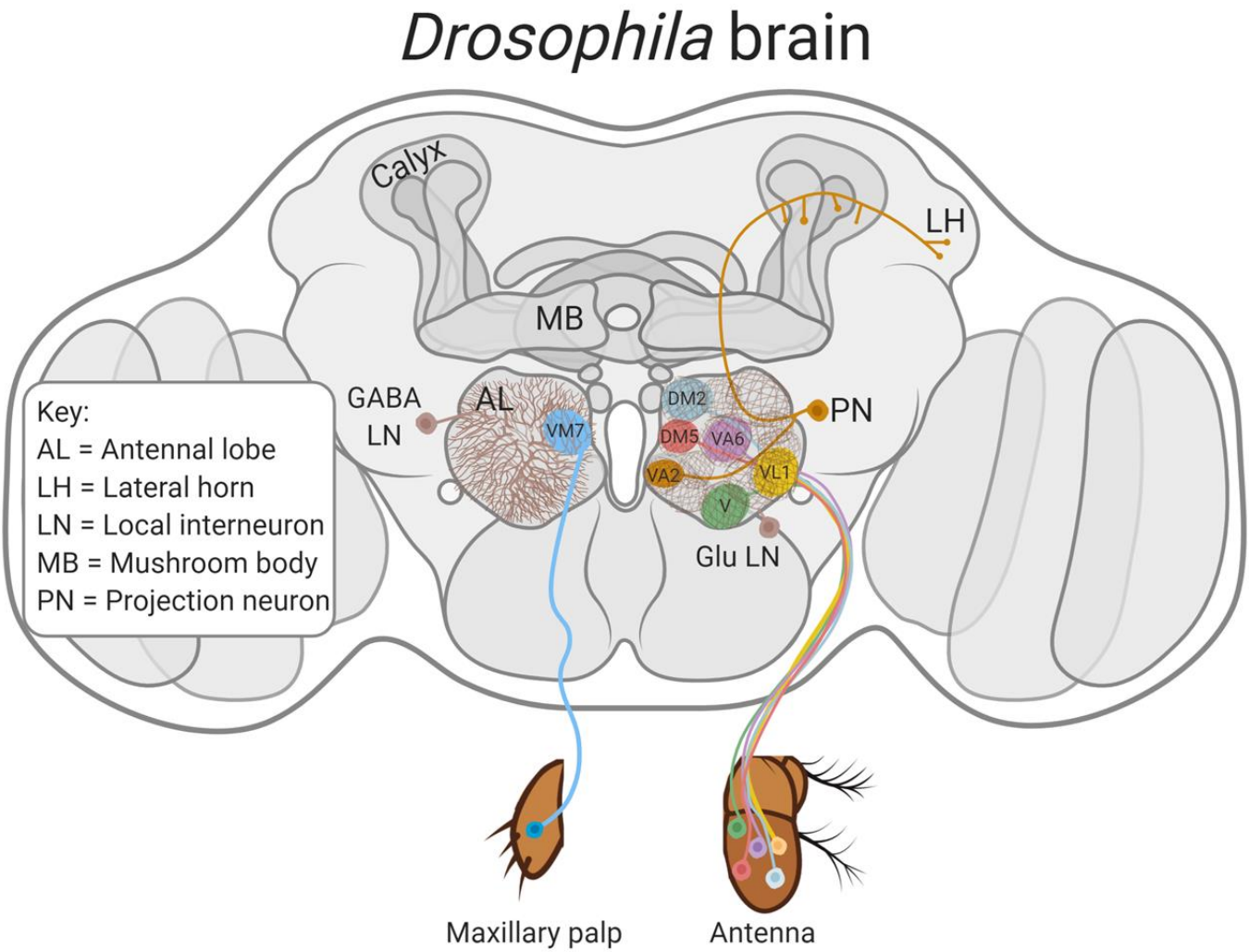

Figure 2. *Drosophila* Brain Antennal Lobe Circuitry
Cartoon representation of the *Drosophila* brain highlighting different neuron classes with in the antennal lobe (AL). Olfactory sensory neurons (OSNs) housed in the antenna or maxillary palp send axonal projections to target glomeruli in the AL. OSNs which express the same receptor class send projections to the same glomerulus. The Or42a-expressing OSNs from the maxillary palp send axons to the ventral medial 7 (VM7) glomerulus. Several classes of antennal OSNs are shown Or22a (dorsal medial 2, DM2), Or85a (DM5), Or82a (ventral anterior 6, VA6), IR75d (ventral lateral 1, VL1), GR21a (V). In addition to OSNs, the AL has GABAergic local interneurons (GABA LNs), glutamatergic LNs (Glu LNs) and olfactory projection neurons (PNs; VA2 PN shown). GABA LNs send broad glomerulus penetrating projections across the AL. Glu LNs have processes spanning the AL similar to GABA LNs, but these processes wrap around rather than penetrate into glomeruli. PNs are unipolar neurons which send a single projection which bifurcates; leading to one branch making the dendrites in the AL and a second branch sending an axonal projection which forms presynaptic boutons in the mushroom body (MB) calyx and lateral horn (LH). Created with BioRender.com.

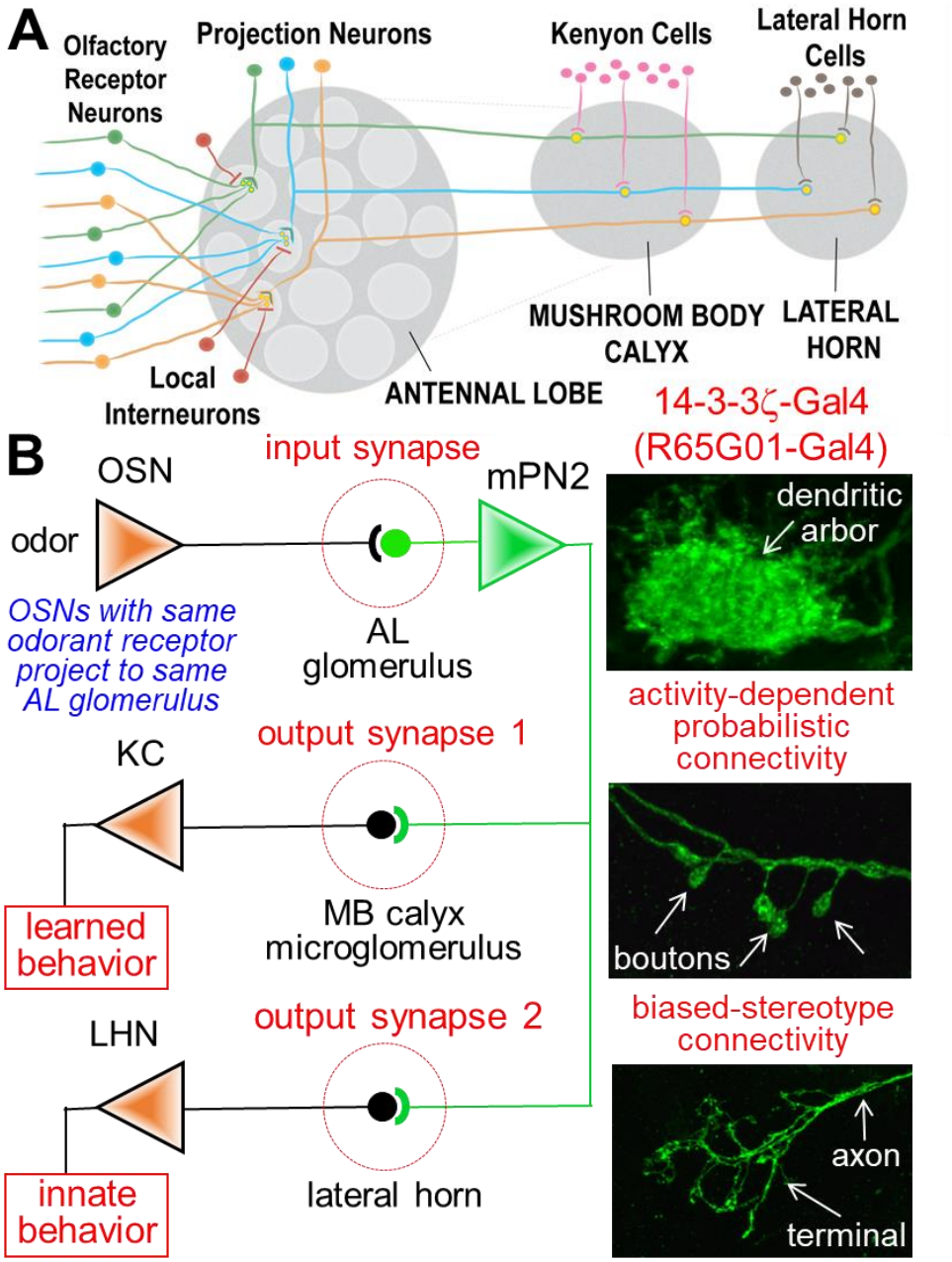

Figure 3. *Drosophila* Olfactory Circuitry

A) Schematic of the *Drosophila* olfactory system showing the antennal lobe (AL), mushroom body (MB) and lateral horn (LH). Olfactory sensory neurons (OSNs) transduce odorants from the environment and send axons into glomeruli of the AL. Within a glomerulus OSNs synapse with local interneurons (LNs) and postsynaptic projection neurons (PNs). These second order olfactory PNs send axons to both the MB calyx synapsing with Kenyon cells (KC) and the LH synapsing with LH neurons (LHNs). **B)** Connectivity of the PN labeled by the 14-3-3ζ-Gal4 (mPN2; R65G01-Gal4) within the AL, MB and LH. Within the AL OSNs which express the same receptor (Ir75d) project to the same target glomerulus (VL1). These PNs then send axons to the MB calyx and synapse with KC important for learned behaviors and the LH and synapse with LHNs important for innate behaviors.

The AL is an excellent model to study the genetic, molecular and circuit mechanisms that control critical periods because of its extensively studied development, well-characterized functional map and available genetic toolkit (Couto et al., 2005; Grabe et al., 2016). As in the above section, I will explore the development, function, plasticity and associated behaviors of the AL in the context of the critical period phases of 1) pre-experience, 2) onset of experience, 3) refinement and 4) stabilization. Prior to the onset of olfactory experience, the development of the adult brain AL is composed of five steps; 1) degeneration of the larval AL, 2) dendrite targeting of the PNs, 3) axon targeting of the ORNs, 4) process targeting of the LNs, and 5) formation of functional synapses (Jefferis et al., 2004; Hong and Luo, 2014). The end result of these processes is a stereotyped glomerular map, where OSNs expressing the same receptor send convergent input to target AL synaptic glomeruli (Vosshall et al., 2000; Coute et al., 2005; Grabe et al., 2016). At the onset of pupation, the larval AL is degenerated (Jefferis et al., 2004). Crucially, the degeneration of larval OSNs secreted morphogens, like semaphorins, which direct the general positioning of PN dendrites (Sweeney et al., 2011). The fine-scale segregation of PN dendrites into their proper positioning is determined by downstream transcription factor expression and an ensemble of cell-surface proteins (Komiyama and Luo, 2006; Hong and Luo, 2014). In addition to PN dendrite targeting, N-cadherin and DsCAM signaling promote dendritic arborize of the entire glomeruluar space to allow room for later targeting of LNs and OSNs (Zhu and Luo, 2004; Zhu et al., 2006). It is perhaps not surprising that OSN axons take longer to innervate the AL than PN dendrites, as the processes have a much farther distance to travel (Jefferis et al., 2004).

As with PN dendrite targeting, the proper positioning of OSN axons follows a stepwise process with coarse morphogen gradients giving way to progressively more restricted signals, and eventually specific OSN-PN matching (Hong and Luo, 2014). Early arriving OSN axons from the antenna are initially split into ventromedial and dorsolateral projecting bundles by the same semaphorin gradient that directs PN dendrite targeting (Joo et al., 2013). Later arriving OSNs from the antenna and MP are sorted through interactions with the early arriving pioneer axons

(Sweeney et al., 2007). Once the OSN axons have arrived at the AL periphery, both DsCAM and N-cadherin are needed for neuropil infiltration (Hummel et al., 2003; Hummel and Zipursky, 2004). Following OSN axon infiltration into the AL, specific trans-synaptic adhesion molecules help match OSNs and PNs, with the best studied example being the tenurins, ten-m and ten-a (Hong et al., 2012). Although LNs might be under some of the same control mechanisms to PN dendrites (Zhu et al., 2006), the complexity of LN processes and the variability in their structure suggests that these neurons are prime candidates for structural and functional plasticity during later development (Chou et al., 2010). While much of the AL synaptic connectivity occurs prior to adult eclosion, the emergence from the pupal case, the volume of the AL synaptic glomeruli continues to change during the first week of life (Devaud et al., 2003a) In addition, OSN activity is required for the maintenance of synaptic connections (Chiang et al., 2009). Overall, the development of the AL creates a precise OSN-PN glomerular map, but the relative immaturity of AL synapses at birth along with the dynamic nature of LN connectivity paves the way for olfactory experience to modify the AL circuitry.

The eclosion of the adult marks the release of the antennae and MPs from the confines of the pupal case and the sudden burst of environmental olfactory stimulation. Correspondingly, the onset of olfactory experience at eclosion is the transition point that demarcates the onset of the olfactory critical period in the brain AL (Devaud et al., 2003a; Sachse et al., 2007; Chiang et al., 2009; Doll and Broadie, 2015, 2016; Chodankar et al., 2020). Although the molecular changes that occur at the onset of olfactory experience remain largely unknown, two studies provide compelling evidence that the onset of sensory activity provides the important cues for AL remodeling and refinement. In the first study, it was shown that OSNs that have been genetically silenced for the first week of life by *orco* mutation, Kir2.1 expression or TeTxLc expression progressively degenerate after this period (Chiang et al., 2009). Importantly, the delayed OSN degeneration can be prevented by allowing activity for only the few days following eclosion by the temporally controlled re-expression of Orco protein in *orco* mutant animals using a temperature-

sensitive Gal4 repressor, Gal80^{TS}. This indicates that early olfactory activity is absolutely required for the activity-dependent maintenance of the olfactory circuitry (Chiang et al., 2009). In the second study, it was shown that genetically silencing OSNs during the first two days of life by again combining *orco* mutants and Gal80^{TS} controlled Orco expression could extend the AL olfactory critical period by the corresponding amount of time (Chodankar et al., 2020). Thus, the onset of olfactory experience at the opening of the critical period permits experience-dependent changes in the AL circuit for only a short time after eclosion. As olfactory information begins to percolate through the AL circuit, the AL neurons undergo a period of enhanced refinement with the definte closing point characteristic of a critical period.

During the third critical period refinement phase, AL synaptic remodeling is associated with changes in odor valance, OSN/PN glomerulus innervation volume and functional changes in PNs and LNs (Devaud et al., 2003a; Sachse et al., 2007; Das et al., 2011; Doll and Broadie, 2015, 2016). The original observation was that prolonged odorant exposure led to a long-lasting habituation in behavioral avoidance to repulsive odors with a coincident decrease in AL glomeruli volume (Devaud et al., 2001; Devaud et al., 2003a). These early studies suggested a critical period between 2-5 days post eclosion (dpe), but subsequent work shows most change occurs in the first day of life (Devaud et al., 2003a; Doll and Broadie, 2015, 2016). It is not clear what controls the direction of the change in AL glomerulus volume. While the early studies show decreased volumes in response to benzaldehyde and isoamyl acetate (Devaud et al., 2001), subsequent studies using CO_2, ethyl butyrate (EB) and geranyl acetate (GA) have all shown increased volumes (Sachse et al., 2007; Das et al., 2011; Kidd et al., 2015). Direct optogenetic activation of VL1 PNs decreases their volume (Fig. 3; Doll and Broadie, 2015). This finding supports the conclusion of recent work demonstrating that innervation volumes are regulated, at least partially, by glomerulus-specific mechanisms during the critical period (Chodankar et al., 2020). A consistent result amongst the studies where it was tested is that the change in AL glomerulus volume occurs in both OSN axons and PN dendrites (Sachse et al., 2007; Chodankar

et al., 2020). The results of behavioral analyses show that animals exposed to repulsive odorants exhibit habituation and those exposed to attractive odorants exhibit sensitization (Devaud et al., 2001; Sachse et al., 2007; Das et al., 2011). However, since only one attractant has been tested to date, more behavioral experiments are needed to confirm this framework.

Odorant experience is the main driver of AL critical period refinement (Fig. 4; Sachse et al., 2007; Das et al., 2011; Doll et al., 2017), with direct neuron activation via heat (Trpv1; Das et al., 2011) or light (channelrhodopsin; Doll and Broadie, 2015) effectively substituting for odorant. OSN-PN synaptic activity is necessary for critical period change, but LNs also play a major role. For instance, inhibitory LN output is required for long-term habituation (LTH) behavior following EB or CO_2 exposure, and LTH is elicited by direct LN activation (Das et al., 2011). Differential LN activation is likely an important determinant for critical period remodeling, as not all odor-responsive glomeruli are affected by experience (Sudhakaran et al., 2014), and LNs are key for critical period structural and functional changes (Sachse et al., 2007; Das et al., 2011). LNs release both GABA and glutamate onto OSNs and PNs. The coincidence of glutamate and depolarization in OSNs and PNs activates NMDA receptors and potentiates or depresses LN connectivity (Das et al., 2011). This proposed mechanism holds for most studies to explain how increased glomerulus innervation is associated with decreased PN responses and vice versa (Sachse et al., 2007; Das et al., 2011; Doll and Broadie, 2015), but this model does not explain all reported studies (Kidd et al., 2015). The molecular mechanisms downstream of activity have not been well explored, but there is a requirement for cAMP signaling, calcium-calmodulin dependent kinase II (CaMKII) and RNA-binding proteins Ataxin-2 and FMRP (see more on FMRP below; Devaud et al., 2003a; Sachse et al., 2007; Sudhakaran et al., 2014; Chodankar et al., 2020). Similar to the opening of the AL critical period, the mechanisms associated with the fourth and final phase to close the critical period by the end of the first week of life, remain a mystery.

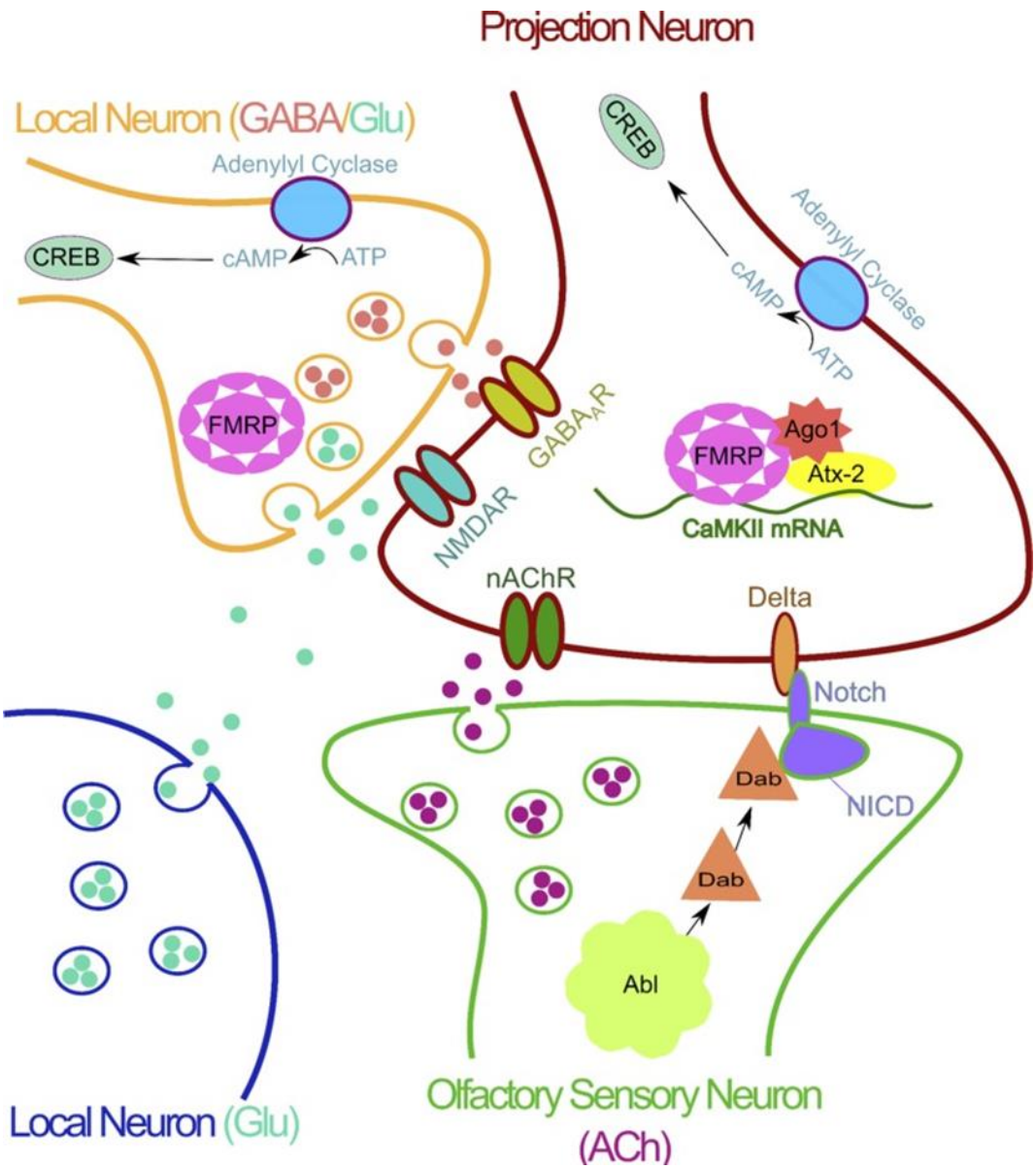

Figure 4. The Antennal Lobe Circuitry Underlying Long-term Habituation (LTH)
Olfactory sensory neuron (OSN): the OSN provides the odor signal to the antennal lobe via synaptic release of acetylcholine (ACh). LTH volume changes are mediated by noncanonical Notch signaling with the Abl target Disabled (Dab) acting on the Notch receptor. Volume changes are controlled by a retrograde Delta signal activating a canonical Notch signaling pathway. Projection neuron (PN): the PN is the output of the antennal lobe. Changes in PN function require 3 different receptor classes: nicotinic acetylcholine receptors (nAChRs), N-methyl-D-aspartate receptors (NMDARs), and ionotropic -aminobutyric acid receptors (GABAARs). Functional presentation of LTH requires Delta expression on the PN. RNA-binding proteins fragile X mental retardation protein (FMRP) and ataxin-2 (Atx-2) interact with the RNA-induced silencing complex (RISC) protein Argonaut1 (Ago1) to mediate translation of activity-dependent transcripts. One target transcript bound by both FMRP and Atx-2 encodes calcium/calmodulin-dependent kinase II (CaMKII). Local interneurons (LNs): local interneurons modify PN output via the release of GABA, glutamate (Glu), and other neuromodulators. A variety of LNs are important for LTH presentation. The release of both GABA and Glu from LNs is required for LTH. Two sites of Glu release are 1) synaptic corelease with GABA and 2) volume release from distinct glutamatergic neurons. FMRP and cAMP-response element binding protein (CREB) are both required in LNs for LTH. Originally from Golovin, R. M. & Broadie, K. J Neurophysiol 116, 2730–2738 (2016).

The Role of FMRP in the Drosophila Olfactory System Critical Period

Fragile X Syndrome (FXS) is a monogenetic disorder caused by the loss of Fragile X Mental Retardation Protein (FMRP), occurring in ~1/4,000-7,000 males and ~1/6,000-11,000 females world-wide (Fragile X Syndrome: Prevalence, 2021). FXS patient symptoms include intellectual disability, autistic behaviors, developmental speech delay, hypersensitivity to sensory input (touch, sound and light), hyperactivity and childhood seizures (Fragile X Syndrome – Symptoms and Signs*,* 2021). The most common cause for FXS is a CGG trinucleotide repeat expansion upstream of the causative *fragile X mental retardation 1* (*FMR1*) gene, which leads to hypermethylation and epigenetic silencing of FMRP transcription (Verkerk et al. 1991). From this initial characterization of FMRP loss as causative in FXS, much effort identified the major FMRP role as an mRNA-binding translational regulator that functions primarily to suppress neuronal and synaptic protein synthesis (Brown et al., 2001; Darnell et al., 2001; Zalfa et al., 2003). FMRP selectively binds only to an estimated 4% of brain transcripts (Ashley et al. 1993). FMRP operates in the activity-dependent regulation of synaptic protein synthesis and plays an important role in experience-dependent critical periods (Yun et al., 2006; Dölen, et al., 2007; Bureau et al., 2008; Harlow et al., 2010; Gonçalves et al., 2013; Kim et al., 2013; He et al., 2014 Sudaharkan et al., 2014; Tyzio et al., 2014; Doll and Broadie, 2015, 2016; Doll et al., 2017). Indispensable in these discoveries have been animal FXS disease models from *Aplysia* and *Drosophila* to zebrafish and mice (The Dutch-Belgian Fragile X Consortium, 1994; Zhang et al., 2001b; Broeder et al., 2009; Till et al., 2010). Here, I will continue my focus on the *Drosophila* olfactory circuit, and examine how FMRP regulates remodeling during the olfactory critical period.

Drosophila FMR1 null mutants (*dfmr1)* exhibit conserved phenotypes including elevated neuronal excitability, hyperactivity, increased E/I ratio, repetitive behaviors, impaired learning/ memory and disrupted sensory-experience critical periods (Zhang et al., 2001b; Tessier and Broadie, 2008; Kanellopoulos et al., 2012; Gatto et al., 2014; Doll et al., 2017 Franco et al., 2017; Russo and DiAntonio, 2019). The *Drosophila* olfactory system has defects in structure, function

and activity-dependent refinement (Bolduc et al., 2008; Tessier and Broadie, 2008, 2009, 2011; Kanellopoulos et al., 2012; Gatto et al., 2014; Sudhakaran et al., 2014; Doll and Broadie, 2015, 2016; Dong et al., 2016; Doll et al., 2017; Franco et al., 2017; Vita and Broadie, 2017; Russo and DiAntonio, 2019; Sears et al., 2019; Sears and Broadie, 2020). Olfactory MB-dependent learning/memory processes show aberrant mGluR signaling, cAMP transduction and protein synthesis (Bolduc et al., 2008; Kanellopoulos et al., 2012). In the olfactory critical period, MB neurons exhibit aberrant activity-dependent structural and functional changes (Tessier and Broadie, 2008, 2009, 2011; Gatto et al., 2014; Doll and Broadie, 2015, 2016; Doll et al., 2017; Sears et al., 2019). PN axon inputs to the MB are overgrown during the critical period and fail to respond to odorant exposure or activity manipulations (Doll et al., 2017; Vita and Broadie, 2017). Moreover, PNs show elevated calcium transients during the critical period insensitive to critical period odorant experience or optogenetic activation (Sudharkan et al., 2014; Doll and Broadie, 2016). Downstream KC axons normally pruned by the onset of olfactory experience (Tessier and Broadie, 2008), fail to manifest activity-dependent pruning and maintain enlarged calcium transients in the absence of FMRP (Tessier and Broadie, 2011). A GABAergic MBON of *dfmr1* mutant flies has overgrown dendritic processes and fails to show arbor expansion after optogenetic stimulation as is seen in control animals (Doll and Broadie, 2015). The lack of activity-dependent modifications to both excitatory and inhibitory MB neurons contributes to E/I imbalance indicative of FXS.

FMRP regulates the excitability of neurons and their response to inhibition by controlling the protein levels of ion channels and neurotransmitter synthesis enzymes and by directly interacting with several classes of potassium channels (Meredith et al., 2007; Brown et al., 2010; Gross et al., 2011; Paluszkiewicz et al., 2011; Deng et al., 2013; Ferron et al., 2014; Gatto et al., 2014; Martin et al., 2014; Zhang et al., 2014; Contractor et al., 2015; Myrick et al., 2015; Franco et al., 2017). The changes in neuronal excitability have been linked to the levels of a variety of potassium channels within FXS model systems (Gross et al., 2011; Zhang et al., 2014). FMRP

also controls calcium channel levels, which leads to altered thresholds for synaptic plasticity (Meredith et al., 2007). In addition, a more recently discovered translation-independent FMRP role involves protein-protein interactions between FMRP and both potassium and calcium channels leading to changes in channel kinetics and stability (Brown et al., 2010; Deng et al., 2013; Ferron et al., 2014; Myrick et al., 2015). On top of hyperexcitation, FXS model neurons often display decreased inhibition (Paluszkiewicz et al., 2011; Gatto et al., 2014; Martin et al., 2014; Franco et al., 2017). The mouse FXS model has reduced levels of $GABA_A$ receptors while both the mouse and *Drosophila* FXS models display reduced levels of the GABA synthesis enzyme glutamic acid decarboxylase (GAD; Paluszkiewicz et al., 2011; Gatto et al., 2014). FXS mice also show reduced inhibitory tone in the hippocampus and amygdala (Curia et al., 2009; Olmos-Serrano et al., 2010), and *dfmr1* flies show lower responses to inhibitory LNs in the AL despite increased activity within this LN population (Franco et al., 2017). In addition, pharmacologically correcting GABAergic disfunction in FXS flies corrects structural abnormalities (Chang et al., 2008) while genetically restoring GABAergic neuron function ameliorates perceptual learning in FXS mice (Goel et al., 2018). This overall increase in E/I in FXS (Contractor et al., 2019), may contribute to the overgrown and immature state of the *Drosophila* MB during the critical period.

Cyclic adenosine monophosphate (cAMP)-signaling is a second major player linking FXS to the *Drosophila* olfactory critical period. FXS patients and model animals produce less cAMP (Berry-Kravis et al., 1995; Kelley et al., 2007) and olfactory learning in the MB and critical period LTH in the AL require Ca^{2+}/Calmodulin-dependent adenylyl cyclase (Rutabaga; Levin et al., 1992) and cAMP-dependent phosphodiesterase II (Dunce; Byers et al., 1981) important in cAMP processing (Dudai et al., 1976; Zars et al., 2000; Devaud et sl., 2001; Das et al., 2011). Downstream of cAMP, protein kinase A (PKA) acts to control actin cytoskeleton stability (Lin et al., 2005; Cingolani and Goda, 2008; Zhu et al., 2015). *Dfmr1* mutant *Drosophila* have decreased cAMP (Kelley et al., 2007), leading to lower PKA activity and a corresponding increase in

filamentous actin (Sears et al., 2019). The reduced PKA activity also stems from less of the PKA-binding protein, Rugose, in FXS model flies (Sears et al., 2019). The increase in filamentous actin could help explain the expanded neuronal arbors of PNs and MBONs. In *dfmr1* flies (Doll and Broadie, 2015). In the AL, *dunce* and *rutabaga* mutants fail to show LTH or the corresponding changes in glomerulus volume following critical period odorant exposure (Devaud et al., 2001; Das et al., 2011). These genes function alongside FMRP within PNs and LNs to control LTH behavior (Sudhakaran et al., 2014), possibly indicating an interaction between FMRP and PKA signaling similar to the MB circuit. The altered cAMP within the inhibitory LNs of the AL is especially important since exogenously activating this population using Trpv1 drives LTH in the absence of critical period odorant exposure (Das et al., 2011). Altogether, reduced cAMP signaling in the *Drosophila* FXS model serves as an important bridge from disrupted function to altered morphology.

Studies of FXS have primarily focused on neurons. However, a growing body of work has shown that FMRP acts in both neurons and glia and neuron-glia interactions contribute to FXS phenotypes (Wang et al., 2014; Gholizadeh et al., 2015; Higashimori et al., 2016; O'Connor et al., 2017; Jawaid et al., 2018; Doll et al., 2020). Glial cells play an important part in the development and function of the nervous system (Banner et al., 2002; Stevens et al., 2007; Wu et al., 2009; Stacey et al., 2010; Schafer et al., 2012; Chung et al., 2013; Khakh and Sofroniew, 2015; Blanco-Suarez et al., 2018; Vainchtein et al., 2018; Wilton et al., 2019; Takano et al., 2020). During development, astrocytes secrete cytokines and signaling molecules to drive microglial phagocytosis of synapses (Blanco-Suarez et al., 2018; Vainchtein et al., 2018) as well as actively participating in phagocytosis in the developing visual system of mice (Chung et al., 2013). At the mouse neuromuscular junction (NMJ), glia mediate synaptic competition. While at the *Drosophila* NMJ glia engulf destabilized presynaptic boutons (Fuentes-Medel et al., 2009; Darabid et al., 2013). Furthermore, Jedi-1 and its *Drosophila* homolog, Draper, control the clearance of neurons after programmed cell death (Wu et al., 2009; Vita et al., 2021). Astrocytes express cell adhesion

molecules and secrete extracellular proteases to control inhibitory synapse formation and maturation (Ackerman et al., 2020; Ribot et al., 2020; Takano et al., 2020) and drive the closure of critical periods (Ackerman et al., 2020; Ribot et al., 2020). Since FMRP regulates glial phagocytosis of MB axons during metamorphosis and AL OSN clearance following axotomy (O'Connor et al., 2017), these cells are well situated to mediate critical period remodeling of *Drosophila* olfactory circuits. Glial cells also regulate the function of neurons through neurotransmitter clearance and the secretion of gliotransmitters (Stacey et al., 2010; Araque et al., 2014; Muthukumar et al., 2014; Higashimori et al., 2016; Zhiguo et al., 2016). The expression levels of the GABA transporters (GAT) and the glutamate type 1 transporter (GLT1) in astrocytes control the synaptic clearance rate of GABA and glutamate, respectively (Muthukumar et al., 2014; Higashimori et al., 2016;). FMRP has a specific role in astrocytes to promote GLT1 expression (Higashimori et al., 2016). Reduced GLT1 expression in the FXS mouse model contributes directly to the hyperexcitability phenotype of these animals (Higashimori et al., 2016). The levels of GAT in the *Drosophila* AL are determined by the response of astrocytes to GABA from LNs (Muthukumar et al., 2014) which may be altered in *dfmr1* mutants since AL neurons response more weakly to GABAergic LN stimulation (Franco et al., 2017). The ability of glia to directly influence neurons through gliotransmitters has been controversial in mammals (Fiacco and McCarthy, 2018), but clearly demonstrated *in vivo* using *Drosophila* larvae (Zhiguo et al., 2016). Although there is no clear link to gliotransmission defects in FXS, the increased calcium activity seen in *fmr1* mutant neurons (Contractor et al., 2015) could extend to hyperexcitable glial networks. Altogether, glial cells help to shape the function of the nervous system and contribute to FXS in direct and meaningful ways that are just beginning to be elucidated.

Neurons and glia together shape the extracellular matrix surrounding synapses (synaptomatrix) which are both integral in critical period closure and disrupted in FXS. In mammals, the end of critical periods is associated with an expansion of plasticity-inhibiting synaptomatrix PNNs, as discussed previously (Pizzorusso et al., 2002, 2006). These PNNs are

made up of chondroitin sulfate proteoglycans (CSPGs) and store important extracellular signaling molecules such as Otx2 (Sugiyama et al., 2008). MMP9 secretion from astrocytes prevents PNN accumulation during the ocular dominance critical period and reduced MMP9 levels close the critical period (Ribot et al., 2020). FXS model mice have elevated levels of MMP9 and reduced levels of PNNs on inhibitory GABAergic neurons (Sidhu et al., 2014; Wen et al., 2017). This suggests that FMRP acts directly in astrocytes or indirectly on neuron-glia signaling to increase levels of secreted MM9. At the NMJ of *dfmr1* mutant flies, MMP9 homolog, MMP1, is secreted at higher levels than wildtype animals under basal conditions, but fails to increase in response to neuronal activity (Dear et al., 2017). This activity-dependent enhancement of MMP1 depends on the heparan sulfate proteoglycan, division abnormally delayed (Dally)-like protein (Dlp), and reducing Dlp in the *dmfr1* mutant background restores MMP1 regulation (Dear et al., 2017). The role of extracellular proteoglycans in the *Drosophila* olfactory critical period has not been explored. However, many of the morphogens important for patterning the AL utilize proteoglycans to establish gradients (Wu et al., 2017) and HSPGs such as Dally and Dlp are expressed in the adult AL (Nagarkar-Jaiswal et al., 2015). Future work is needed to determine if the increased secretion of MMPs and HSPGs in FXS is causatively linked to alterations in critical period closure and the role of the synaptomatrix in closing the olfactory critical period of the AL.

These converging disruptions to critical period mechanisms accompanying the loss of FMRP impacts the structure, function and activity-dependent refinement of the AL during the olfactory critical period. Although *dfmr1* null mutants show normal performance on the olfactory T-maze assay (Bolduc et al., 2008), the more sensitive odor arena demonstrates impairments in odor perception (Franco et al., 2017). Furthermore, this study shows that the impaired olfactory performance results from decreased AL lateral inhibition from LNs onto other LNs and PNs, leading ultimately to much broader AL activation in response to odor stimulation (Franco et al., 2017). The reduced inhibition in the FXS disease model has important implications for critical period refinement of the AL circuitry since LN responses are required for activity-dependent

remodeling (Das et al., 2011). Indeed, FMRP removal from PNs or LNs can block LTH and FMRP loss from VL1 PNs eliminates their critical period response to optogenetic activation (Sudharkan et al., 2014; Doll and Broadie, 2015, 2016). To generate LTH, FMRP acts alongside RNA-binding Ataxin-2 to control CaMKII activation locally in PN processes (Sudharkan et al., 2014). Another way that FMRP may regulate the AL critical period is through reducing GABAergic signaling, as *dfmr1* mutants have diminished expression of the GABA synthesis enzyme GAD (Gatto et al., 2014). Overall, FMRP plays an important role during the *Drosophila* olfactory critical period to control neural development and facilitate experience-dependent plasticity of neural circuits. Although much work has been done to show a role for FMRP in the critical period refinement phase of several olfactory neurons, further research is needed to test FMRP in other neural cell types and to explore the involvement of FMRP in other critical period phases.

Chapter II

Activity-Dependent Remodeling of *Drosophila* Olfactory Sensory Neuron Brain Innervation During an Early-Life Critical Period[1]

Introduction

Abstract

Critical periods are windows of development when the environment has a pronounced effect on brain circuitry. Models of neurodevelopmental disorders including autism spectrum disorders, intellectual disabilities and schizophrenia are linked to disruption of critical period remodeling. Critical periods open with the onset of sensory experience, however it remains unclear exactly how sensory input modifies brain circuits. Here, we examine olfactory sensory neuron (OSN) innervation of the *Drosophila* antennal lobe (AL) of both sexes as a genetic model of this question. We find that olfactory sensory experience during an early-use critical period drives loss of OSN innervation of AL glomeruli and subsequent axon retraction in a dose-dependent mechanism. This remodeling does not result from olfactory receptor loss or OSN degeneration, but rather from rapid synapse elimination and axon pruning in the target olfactory glomerulus. Removal of the odorant stimulus only during the critical period leads to OSN re-innervation, demonstrating remodeling is transiently reversible. We find this synaptic refinement requires the OSN-specific olfactory receptor and downstream activity. Conversely, blocking OSN synaptic output elevates glomeruli remodeling.

[1] This work has been adapted from a published paper under the same name. See additional information below.

This chapter is adapted from *Activity-Dependent Remodeling of Drosophila Olfactory Sensory Neuron Brain Innervation During an Early-Life Critical Period* published in The Journal of Neuroscience and has been reproduced with the permission of the publisher and my co-authors, Jacob Vest, Dominic Vita and Kendal Broadie. Golovin, R. M., Vest, J., Vita, D. J. & Broadie, K. Activity-Dependent Remodeling of Drosophila Olfactory Sensory Neuron Brain Innervation During an Early-Life Critical Period. J Neurosci 39, 2223–18 (2019). The authors declare no competing financial interests. Abbreviated Title: Activity-Dependent Remodeling of *Drosophila* OSNs

We find that GABAergic neurotransmission has no detectable role, but that glutamatergic signaling via NMDA receptors is required for OSN synaptic refinement.Altogether, these results demonstrate that OSN inputs into the brain manifest robust, experience-dependent remodeling during an early-life critical period, which requires olfactory reception, OSN activity and NMDA receptor signaling. This work reveals a pathway linking initial olfactory sensory experience to glutamatergic neurotransmission in the activity-dependent remodeling of brain neural circuitry in an early-use critical period.

Significance statement

Neurodevelopmental disorders manifest symptoms at specific developmental milestones that suggest an intersection between early sensory experience and brain neural circuit remodeling. One classic example is Fragile X syndrome (FXS) caused by loss of an RNA-binding translation regulator of activity-dependent synaptic refinement. As a model, *Drosophila* olfactory circuitry is well characterized, genetically tractable and rapidly developing, and thus ideally suited to probe underlying mechanisms. Here, we find olfactory sensory neurons are dramatically remodeled by heightened sensory experience during an early-life critical period. We demonstrate removing the olfactory stimulus during the critical period can reverse the connectivity changes. We find this remodeling requires neural activity and NMDA receptor mediated glutamatergic transmission. This improved understanding may help us design treatments for neurodevelopmental disorders.

Background

Critical periods are discrete developmental time windows when the brain is especially susceptible to modification by sensory stimuli. Since the classical visual cortex work by Hubel and Wiesel (Hubel and Wiesel, 1970), enormous progress has been made in understanding critical period refinement (Vay et al., 1980; Hensch, 2005; Morishita et al., 2010) and how it goes awry in neurological diseases (Dölen et al., 2007; Contractor et al., 2015; Doll and Broadie, 2015, 2016;

Golovin and Broadie, 2016; Doll et al., 2017; Vita and Broadie, 2017). Typically, critical periods open with the onset of sensory experience and close after a defined period of refinement, during which neural circuitry is modified to better respond to the sensory environment (Hensch, 2005). Although initial studies painted a stark black-and-white picture regarding opening and closing of critical periods, it is now known that numerous factors can reopen critical period-like states in mature animals (McGee et al., 2005; Vetencourt et al., 2008; Morishita et al., 2010; Hensch and Bilimoria, 2012; Baroncelli et al., 2016). Critical period work has focused primarily on vertebrate systems, but there are excellent examples of critical periods in invertebrate models (Fielde et al., 1904; Remy and Hobert, 2005; Doll and Broadie, 2015; Jin et al., 2016). The short generation time and powerful genetic tools available in these systems make them attractive candidates for furthering our understanding of critical periods.

The *Drosophila* antennal lobe (AL) circuitry is particularly well mapped (Vosshall et al., 2000; Wang et al., 2003; Grabe et al., 2016). In the AL, the axon termini from olfactory sensory neurons (OSNs) synapse onto projection neurons (PNs) and local interneurons (LNs) within discrete synaptic glomeruli (Couto et al., 2005; Fishilevich and Vosshall, 2005; Wilson, 2013). OSNs that express the same olfactory receptor innervate the same target AL glomerulus to form synaptic connections with the same PNs. Each glomerulus can be individually identified based both on anatomical position and by the expression of the defining specific olfactory receptor (Jefferis et al., 2001, 2002, 2004). The AL circuit is grossly hard-wired with no large-scale changes to the glomerular map even after complete loss of olfaction (Larsson et al., 2004). Although the overall glomerular map is stable, a growing body of work has shown that individual glomeruli can alter their morphology and functionality in response to the odorant environment (Devaud et al., 2001, 2003b, 2003a; Sachse et al., 2007; Acebes et al., 2012; Das et al., 2011; Doll and Broadie, 2015, 2016). Environmental odorants usually bind to multiple sensory odorant receptors with different affinities, which lead to a characteristic AL activity map dependent on different odorant

concentrations (Hallem and Carlson, 2006). Thus, olfactory sensory experience can be mapped onto central brain olfactory circuitry.

Seminal early papers demonstrated AL critical period refinement in response to olfactory experience (Devaud et al., 2001, 2003b, 2003a). Later studies showed selective remodeling of the CO_2-sensitive glomerulus (Sachse et al., 2007), and LN modulatory roles shaping the critical period (Acebes et al., 2011, 2012). Molecular pathways involved include NMDA-dependent glutamatergic signaling, cAMP signal transduction (*dunce, rutabaga, creb)* and translational regulation (FMRP, Ataxin2) (Devaud et al., 2001, 2003b; Das et al., 2011; Sudhakaran et al., 2014; Doll and Broadie, 2015, 2016). Previous studies have reported that odor activation of glomeruli during the early-life critical period can increase glomerular volume (Sachse et al., 2007; Das et al., 2011; Kidd et al., 2015). We tested this result taking advantage of genetic tools to probe OSN-specific structural and synaptic changes with the commonly used odorant ethyl butyrate (EB) on the strongly activated VM7 glomerulus (DoOR V2.0, Münch and Galizia, 2016); but, unexpectedly, discovered strongly reduced glomerular volume with critical period exposure. This finding shows that odorants can drive opposing remodeling changes in discrete glomeruli. Synaptic remodeling is reversible, activity-dependent and requires NMDA receptor signaling. Overall, this study expands our knowledge of mechanisms of critical period circuit remodeling, and provides a platform to investigate neuron-specific requirements.

Materials and Methods

Drosophila genetics

All animals were raised at 25°C on standard cornmeal/agar/molasses *Drosophila* food in a 12h light/dark cycling incubator until odorant exposure (see below). The following lines were used in genetic crosses: *Or42a*-Gal4 (RRID:BDSC_9969; Fishilevich and Vosshall, 2005) | UAS-mCD8::GFP (RRID:BDSC_5137; Doll and Broadie, 2015) | UAS-mCD8::RFP

(RRID:BDSC_32219) | Brp-FRT-GFP (Chen et al., 2014) | UAS-FLP1; *Or42a*-Gal4 (RRID:BDSC_4539/RRID:BDSC_9969) | *Or42a*^{F04305}; *Or42a*-mCD8::GFP (RRID:BDSC_18758; Thibault et al., 2004; Stephan et al., 2012) | UAS-mCD8::GFP;*Or42a*-Gal4 | UAS-TeTxLC (Wang et al., 2012) | UAS-Kir2.1-eGFP (RRID:BDSC_6596; Baines et al., 2001) | UAS-*GABAb R3* RNAi (RRID:BDSC_26729; Flockhart et al., 2006) | UAS-*NMDAR1* RNAi (RRID:BDSC_41666; Flockhart et al., 2006) | *wg*$^{l-17}$ (Baker, 1987) | UAS-dFz2-DN (Zhang and Carthew, 1998) | and UAS-Sgg-DN (RRID:BDSC_5360; Bourouis, 2002). All genotypes were confirmed with visible markers or PCR. *w*^{1118} (RRID:BDSC_3605) was used as a genetic background control. Transgenic controls used included *w*^{1118}*;* UAS-mCD8::GFP/+;Or42a-Gal4/+| and *w*^{1118}*;* Or42a-mCD8::GFP/Or42a-mCD8::GFP. Animals of both sexes were used in all studies, except where specifically noted in figure legends. All crosses were transferred to fresh food every 2-3 days, with rearing densities matched between genotypes.

Odorant exposure

Staged animals were sorted as dark pupae into separate vials based on sex, genotype and odor exposure (except for Figure 5C,D where animals were aged 7 days prior to exposure). A fine wire stainless steel mesh (Small Parts, Inc.) was secured with tape over the top of the vial to contain the flies, but still allow airflow. Vials were placed in an airtight 3700 mL Glasslock container with either 1 mL 15% or 25% ethyl butyrate (EB, Sigma-Aldrich; %V/V EB in mineral oil) or the vehicle only (mineral oil alone) in a 1.5 mL microcentrifuge tube attached to the side of the chamber. Exposure chambers were placed in temperature-controlled incubators (23°C) on 12h light/dark cycles. 18-21h after placing vials into the chambers, eclosed flies were rapidly transferred to clean vials with fresh food and placed in clean exposure chambers with freshly made odorants, as above. Except for experiments shown in Figure 7, animals were kept in the odor exposure chambers in incubators for 48h and then processed for immunohistochemistry. For Figure 7 experiments, animals were kept in the EB exposure chambers for 24h (1 Day), 48h

(2 Day) or 96h (4 Day); whereas 3 Day reversals were kept on EB for 24h then transferred to oil for 72h, and 2 Day reversals were kept on EB for 48h then transferred to oil for 48h. Testing indicates that exposing animals to odorant from the dark pupae stage causes a more consistent phenotype, indicating that odorant exposure immediately after eclosion is critically important.

Immunohistochemistry imaging

Staged animals were anesthetized on ice for 1-2 mins. Brains were then dissected using fine, sharpened forceps (Dumont #5) in physiological saline ([in mM]; 128 NaCl, 2 KCl, 4 $MgCl_2$, 1.8 $CaCl_2$, 64.6 Sucrose, 5 HEPES, pH 7.2; all reagents from Sigma-Aldrich). After dissection, brains were fixed for 30 mins at room temperature in 4% paraformaldehyde (EMS)/4% Sucrose in phosphate buffered saline (PBS), pH 7.4 (Life Technologies). Fixed brains were washed 3X with PBS and then blocked for 1h in 1% bovine serum albumin (BSA; Sigma Aldrich) in PBS-T (0.2% Triton X-100 in PBS; Fisher Chemical). Brains were incubated with primary antibodies diluted in 0.2% BSA in PBS-T at 4°C overnight (~14-18h). The primary antibodies used were: rabbit anti-GFP (Abcam 290; 1:3000 or 1:6000 empirically determined for each aliquot), mouse anti-BRP (Developmental Studies Hybridoma Bank (DSHB), nc82; 1:50) and rat anti-RFP (Chromotek 5F8; 1:500). The next day brains were washed 3X for 20 mins with PBS-T, and then incubated overnight (14-18h) with secondary antibodies conjugated to fluorescent tags. The secondary antibodies used were: AlexaFluor 488 goat anti-rabbit, AlexaFluor 546 goat anti-mouse, AlexaFluor 546 goat anti-rat and AlexaFluor 633 goat anti-mouse (all used at 1:250). Following secondary incubation, the brains were washed in PBS-T 3X for 20 mins followed by PBS 1X for 20 mins. Brains were then rinsed with dH_2O and mounted onto clean glass slides (*Probe On* Microscope Slides, Fisherbrand) with Fluoromount (EMS 17984-25) with a glass coverslip (No. 1.5H, Zeiss). Double-sided adhesive tape (Scotch) was used to raise coverslips above the brains, and clear nail polish (Sally Hansen) was used to seal a coverslip to the slide. For maxillary palps (Figure 6), whole proboscises were dissected and processed exactly like the

brains, except fixed for 45 mins with longer primary/secondary antibody incubations (38-42h). In Figure 8, brains were put through a concentration series of 2,2-thiodiethanol (TDE; Sigma-Aldrich) 10%, 25%, 50% and 97% TDE in PBS for 10 mins each, followed by 2X washes with 97% TDE in PBS and then mounting in 97% TDE in PBS as above. Fluorescent images were collected on a Zeiss 510 META laser-scanning confocal microscope with either a 40X or 63X oil-immersion lens. Images taken with the 40X objective were collected at 1024x1024 resolution with a Z-slice of 1 µm thickness. Images taken with the 63X objective were collected at 2048x2048 resolution with a Z-slice thickness of 0.8 µm. The microscope and imaging settings were kept constant within every experiment.

Glomerular measurements

For glomerular volume measurements, a region of interest was defined for the maximal borders of the VM7 glomerulus and the FIJI plugin 3D Objects Counter was used to quantify volume (Schindelin et al., 2012; RRID:SCR_002285). The threshold was chosen to minimize noise. When the signal from the glomerulus was sparse, multiple object volumes were summed to obtain a single data point. Data collected from different days of experiments were normalized to the appropriate control to account for variation between replicates. To count VM7 Bruchpilot (BRP) punctae, the “find maxima” tool in NIH ImageJ (Schneider et al., 2012) was used to identify local maxima above a chosen noise tolerance. The “find maxima stacks” macro in ImageJ allowed quantification for an entire image by using the find maxima function for each slice. BRP intensity measurements were derived from the “histogram function” in ImageJ, which provides pixels at brightness (range: 0-255). To generate intensity values, we used the weighted sum of all pixels, with the number of pixels at each level of brightness multiplied by the brightness value, and the products summed together to generate the overall intensity. Brightness values below 20 were dropped to account for image background.

Soma measurements

For maxillary palp measurements, blinded Z-stack images were analyzed using ImageJ (NIH) and the Or42a OSN cell bodies manually counted throughout the entire maxillary palp. For the fluorescence intensity measurements, the region of interest was defined on a blinded maximum intensity projection of the Or42a OSN cell bodies and proximal labial nerve within the maxillary palp. The ImageJ measurement tool was then used to quantify the mean fluorescence intensity of this region of interest.

Western blots

Western blots were performed as reported (Vita and Broadie, 2017), with slight modifications. Staged animals were exposed to oil or EB as described above. After exposure, animals were anesthetized on ice and maxillary palps were removed in dissecting saline with EDTA-free protease inhibitor (Roche - 04693132001). Palps were placed in 24 µl RIPA buffer (150 mM sodium chloride, 1% Triton X-100, 0.5% sodium deoxycholate, 0.1% sodium dodecyl sulfate, 50 mM Tris), immediately snap frozen on dry ice and stored at -80^{o}C for <1 week. Palps in RIPA buffer were then defrosted on ice followed by sonication (Branson Sonifier, setting:90% duty, output 2) for 20 secs, vortexed (Standard Mini Vortexer, VMR Scientific Products, speed 4) for 5 secs, and then centrifuged at 12000 RPM for 10 mins. 12 µl of lysate was then transferred to new prechilled tubes, 4 µl of NuPage LDS buffer (Invitrogen, NP007) and 0.8 µl of 2-mercaptoethanol (Sigma, M7154) were added, and the lysate vortexed as above. Samples were placed at RT to incubate for 20 mins and then boiled for 10 mins followed by centrifugation (14000 RPM, 10 mins). Samples were then loaded into precast NuPage 4-12% Bis-Tris gels (Invitrogen, NP0336) with NuPage Mes SDS running buffer (Life Technologies, NP002). Buffer in the middle chamber was supplemented with NuPage antioxidant (Invitrogen, NP0005) to ensure 2-mercaptoethanol movement into gel. Samples were run at 150 V until loading dye exited the gel. Transfers were performed overnight at 4^{o}C with constant 30 mA current. Proteins were transferred

to nitrocellulose membranes (PROTRAN, NBA085C001EA) in 4ºC NuPage transfer buffer (Life Technologies, NP0006-1) supplemented with 20% methanol (Honeywell, AH230-4). Membranes were rinsed with deionized water (DIW) for 5 mins, then air-dried for 1h. Total protein was analyzed via REVERT total protein stain (LI-COR, 926-11011) according to manufacturer's instructions. Membranes were then blocked with 2% powdered milk (Kroger: Instant nonfat dry milk) in TBS-T (0.1% Tween-20, 150 mM sodium chloride, 5mM potassium chloride, 25 mM Tris, pH 7.6) for 1h at RT with rotation. Primary antibody in 2% milk in TBS-T was incubated overnight at 4ºC with rotation. Membranes were then washed 5 X 6 mins with TBS-T at RT with rotation. Secondary antibody in 2% milk in TBS-T was incubated for 1h at RT with rotation, then washed as above. Membranes were imaged using a LI-COR Odyssey imager, with intensity measurements taken by Image Studio Lite (LI-COR Biosciences). Bands were normalized to REVRT total protein stain. Primary antibody used was rabbit anti-GFP (Abcam 290, 1:2,500). Secondary antibody was goat anti-rabbit 680 (AlexaFluor 680, 1:10,000). Due to differences in transgenic insert composition (1xGFP vs. 4xGFP) Or42a>mcd8::GFP runs at a smaller molecular weight than Or42a-mcd8::GFP (Couto et al., 2005; Hara et al., 2017).

Quantitative real-time PCR

As above, staged animals were exposed to EB or vehicle for 48h after eclosion, and then proboscises with maxillary palps were dissected free with fine forceps (Dumont) and transferred immediately to 10µL water with 1u/µL RNase inhibitor on ice (Applied Biosystems). In order to enhance signal, animals expressing 2 copies Or42a-Gal4 driving 2 copies of mCD8::GFP were used, with samples from 5 males and 5 females combined from each odorant condition, repeated in 3 independent replicates. RNA was extracted using the RNeasy Micro Kit (Qiangen) following manufacturer's instructions. cDNA synthesis from total RNA and quantitative real-time PCR (qPCR) was performed using the Power SYBR™ Green RNA-to-C_T™ 1-*Step* Kit (Applied Biosystems) following the manufacturer's instructions, except RNase inhibitor was added to the

PCR reaction at 1u/µL. For each reaction 1ng of total RNA was used with the following primers: 5'-AAGAAAAACC GAAGTGCGCC-3' and 5'-AGTCAGCGGA GACCTTTTGG-3' for *Gal4* (DNA-binding domain), 5'-TTTTGCGATT TGTTGACTGC CT-3' and 5'-TTAGGGTAAA GCCCAGCACC-3' for *Or42a*, 5'-TCACCCAAAT TCTGAGTCCC G-3' and 5'-CATCATGGCG GCAAATCCTG-3' for *Or71a*, 5'-TACAGGCCCA AGATCGTGAA-3' and 5'-TCTCCTTGCG CTTCTTGGA-3' for *rp49* (LaLonde et al., 2006), 5'-CGTTCATGCC ACCACCGCTA-3' and 5'-CCACGTCCAT CACGCCACAA-3' for *GAPDH2* (Ling and Salvaterra, 2011). Primers were tested and verified to produce a single peak using melting curve analysis. qPCR retractions were run on a Bio-Rad CFX-96 Real-Time System, with PCR reactions run in duplicate and expression values from each run averaged. Data was analyzed using the ΔΔ Ct method (Livak and Schmittgen 2001). Each expression level was normalized to housekeeping genes *GAPDH2* and *rp49*, with values then normalized to the mean vehicle control.

MiniSOG photoconversion

Photoconversion for electron microscopy was performed as described, with some minor revisions (Strickfaden et al., 2015; Ng et al., 2016). Note that it is imperative that all solutions are made fresh at pH 7.4 for photoconversion. Staged animals expressing membrane-tethered miniSOG (UAS-*myr-miniSOG*) driven by Or42a-Gal4 were exposed to oil vehicle or 25% EB, and then the brains were dissected as described above. All following steps were performed at RT, in a dark chamber, with end over end rotation. Immediately following dissection, brains were fixed for 30 mins with 4% paraformaldehyde (PFA, EMS 15714) in 0.1 M sodium cacodylate (SC, EMS 11652) buffer followed by 2X 20 mins washes with 0.1 M SC. Brains were then incubated for 30 mins in a solution of 5 mM aminotriazole (Sigma A8056) and 50 mM glycine (Sigma G8898) in 0.1 M SC buffer to reduce endogenous peroxidase activity (Strickfaden et al., 2015; Ng et al., 2016), followed by 2X 20 mins washes with 0.1M SC. Brains were individually placed in 1 mg/ml hyper-oxygenated diaminobenzidine (DAB, ESM 13802) dissolved in 0.1 M SC buffer. DAB was

hyper-oxygenated by bubbling medical grade O_2 through solution for 2h on ice prior to use. Brains were then exposed to strong blue light (480 nm) mercury lamp (powered by a LEP Ltd. ArcLamp Power Supply HBO100 DC IGN) until the DAB precipitate reaction was visible, typically 60-75 mins at RT. After light exposure, brains were placed in 0.1 M SC buffer on ice until all samples were completed.

Electron microscopy

The brain preparation for ultrastructure studies was performed as previously described (Doll et al., 2017; Vita and Broadie, 2017). All incubations were performed at RT with rotation unless otherwise stated. Briefly, following photoconversion, brains were post-fixed in fresh 2.5% glutaraldehyde (GTA, EMS 16120) in 0.1 M SC buffer overnight at 4^{o}C. Brains were then washed 3X 20 mins with 0.1 M SC buffer, with a final wash overnight at 4^{o}C. Brains were then incubated in 1% osmium tetroxide (OsO_4, EMS 19172) in 0.1 M SC buffer for 1h, followed by 3X 20 mins washes in 0.1 M SC buffer. Brains were then stained with 2% aqueous uranyl acetate (UA, EMS 22400-2) covered for 2h, followed by 3X 20 mins washes with DIW. Brains were then dehydrated in an ethanol series (EtOH, EMS 15055): 30, 50, 70, 90, 95, 2X 100% for 10 mins each. EtOH was then replaced with transitional solvent propylene oxide (PO, EMS 20401): 50/50 EtOH/PO, 2X 100% PO each for 10 mins. Resin (20 g EMBED 812 [EMS 14900], 9 g DDSA [EMS 19000], 12 g NMA [EMS 13710], 1.2 g BDMA [EMS 11400]) was then infiltrated into the samples: 75/25 PO/resin for 30 mins, 50/50 PO/resin for 1h, and 50/50 PO/resin overnight with vials open to allow PO to evaporate. Fresh resin was then applied to brains for 2, 4 and 24h. Flat block molds were half filled and heated at 60^{o}C, until resin was tacky but not yet firm (~4h). A small cavity was made in the resin to orient the brains anteriorly towards the block face (for sectioning in an anterior to posterior plane). Blocks were filled with resin and placed at 60^{o}C for 48h. Thick sections (500 nm) were cut using a Leica EM UC7 ultramicrotome until brain tissue was reached. After cutting 30 µm of thick sections (VM7 depth based on confocal measurements), thin sections (65 nm) were

cut for 20 µm. Sections were collected on formvar coated, slotted grids (EMS FCF2010-CU) at 20 sections/grid (~1.3 µm of tissue/grid). Brains were imaged using a FEI T-12 transmission electron microscope operating at 100kV. Imaging began at ~40 µm and ended at ~46.5µm (5 grids) to ensure no artifacts due to depth of measurement. One section per grid was imaged to limit double imaging of synaptic regions. Area measurements of labeled OSNs were made (one antennal lobe/brain) using ImageJ (Schneider et al., 2012). Synaptic active zone T-bars were quantified in two ways; 1) total within the entire section (6500X magnification), and 2) density per miniSOG-labeled Or42a OSN area.

Statistical analyses

All statistical analyses were performed with Prism software (GraphPad, San Diego, CA), except for the linear regressions done in R (R Project for Statistical Computing, RRID:SCR_001905; Version x64 3.2.1; Vienna, Austria). Statistics were done using n = number of preparations, unless otherwise stated. All groups that met the criteria for parametric statistics were analyzed with unpaired two-tailed t tests; otherwise, the Mann-Whitney test was used for comparisons. For data comparing $\geq$2 genotypes, a two-way ANOVA was used with odorant exposure and genotype as independent variables, followed up Sidak's multiple comparisons tests to compare the odorant vehicle and EB exposed conditions within a genotype. To compare between two genotypes, the interaction term from the two-way ANOVA was used. For data with more than two genotypes, a linear regression was performed in R with interaction terms between each experimental genotype and EB exposure assessed for significance with unpaired two-tailed t tests adjusted by Sidak's correction for multiple comparisons. These pairwise comparisons show how different genotypes impact the effect of EB exposure and are indicated in figures by dashed significance bars. For data comparing a genotype with $\geq$2 odor exposure paradigms (Figure 7), a Kruskal-Wallis one-way ANOVA with Dunn's multiple comparisons tests were used for pairwise comparisons between odor treatments. For analyses of synaptic t-bars per terminal area (Figure 9), a ROUT outlier test

was done with Q set to 1%. In all figures, significance levels are shown as $p>0.05$ (not significant; N.S.), $p<0.05$ (*), $p<0.01$ (**) and $p<0.001$ (***).

Results

Critical period odorant experience selectively reduces OSN glomerular innervation

Previous work from our lab and others has shown that specific antennal lobe (AL) glomeruli exhibit changes in response to odorant exposure in an early-use period immediately following eclosion (Devaud et al., 2001, 2003b, 2003a; Sachse et al., 2007; Das et al., 2011; Acebes et al., 2012; Sudhakaran et al., 2014; Doll and Broadie, 2015, 2016). Older work has shown this early sensory experience can result in expansion of olfactory sensory neuron (OSN) innervation of the activated glomeruli (Sachse et al., 2007; Das et al., 2011). We started this study by testing this result for Or42a OSNs innervating the VM7 glomerulus, which are strongly activated by the ethyl butyrate (EB) odorant (Münch and Galizia, 2016). To examine the VM7 innervation, we labeled the OSNs with an Or42a-Gal4 driving UAS-mCD8::GFP to mark neural membranes (Fig. 5). Or42a OSN innervation of the VM7 glomerulus was compared between an odorant vehicle control (mineral oil) and EB dissolved in mineral oil at low (15% EB; Fig. 5A) and high (25% EB; Fig. 5B) concentrations. Odorant exposure was compared between an early time period (0-2 days post-eclosion (dpe); Fig. 5A,B) within the well-defined early-use critical period (Devaud et al., 2003a; Sachse et al. 2007; Tessier and Broadie, 2008, 2011; Doll and Broadie, 2015, 2016; Doll et al., 2017; Vita and Broadie, 2017; Sears and Broadie, 2018) and a late time period of adult maturity following the critical period (7-9 days dpe; Figs. 1C,D). Sample images at both low and high magnification, as well as quantified glomerular volume data for all eight conditions are shown in Figure 5.

During the critical period, EB odorant exposure causes dramatic reduction in Or42a OSN innervation of VM7 glomeruli (Fig. 5A,B). With 15% EB, VM7 innervation is strongly reduced

compared to vehicle control (oil alone), with weak and sparse Or42a OSN labeling in the VM7 synaptic domain (Fig. 5A, left two panels). Despite a strong reduction in innervation, glomerulus integrity is not compromised, with similar glomerular boundaries and maintained scaffolding. Quantification of the innervation volume shows EB-exposed animals are significantly reduced (normalized vehicle control (oil) 1.0 $\pm$ 0.066 (n=9 brains) vs. 15% EB 0.429 ± 0.116 (n=10); t(17)=4.148, p=0.0007, two-tailed unpaired t test; Fig. 5A, right). The EB exposure effect is concentration dependent, with 25% EB causing an even greater loss of VM7 innervation, often resulting in an absence of detectable Or42a OSNs (Fig. 5B, left). The loss of VM7 innervation is accompanied by loss from the labial tract, which projects from the maxillary palps to AL. Quantification of glomerular volume reveals that EB-exposed animals show a greater and more significant loss of VM7 innervation compared to matched controls (Oil 1.0 ± 0.037 (n=23) vs. 25% EB 0.195 ± 0.054 (n=26); t(47)=11.95, p=7.53 x 10^{-16}, two-tailed unpaired t test; Fig. 5B, right). Or42a OSN remodeling after 25% EB can appear qualitatively similar to the 15% EB condition, but there is a greater extent of axon process retraction including many instances of complete loss of detectable Or42a OSN signal (Fig. 5B). These results show that EB odorant during the early-use critical period (0-2 dpe) exposure causes a dose-dependent reduction of Or42a OSN innervation of the VM7 glomerulus.

At maturity, EB odorant exposure causes little or no change in Or42a OSN innervation of VM7 glomeruli (Fig. 5C,D). With 15% EB for 2 days starting at 7 dpe, there is no significant difference in VM7 innervation compared to controls (Fig. 5C). The size and structure of Or42a OSN axon tracts entering the VM7 glomerulus (Fig. 5C, left), and the VM7 innervation by Or42a terminals (Fig. 5C, middle), both appear unchanged between EB exposure and vehicle controls. Quantification of innervation volume shows EB-exposed animals are not significantly different from controls (Oil 1.0 ± 0.055 (n=20) vs. 15% EB 0.841 ± 0.066 (n=18); t(36)=1.862, p=0.071, two-tailed unpaired t test; Fig. 5C, right). With the higher 25% EB exposure (7-9 dpe), there is weak Or42a OSN remodeling (Fig. 5D). Robust VM7 glomerulus innervation persists, although

there is evidence of some axon retraction and glomerular reduction (Fig. 5D, left and middle). Quantification shows a significant loss of the VM7 glomerular volume (Oil 1.0 ± 0.051 (n=21) vs. 25% EB 0.669 ± 0.059 (n=21); t(40)=4.262, p=0.0001, two-tailed unpaired t test; Fig. 5D, right). However, this change is small compared to critical period remodeling (~80% reduction in critical period vs. ~30% at maturity). This result is consistent with mammalian critical periods, in which heightened sensory stimulation can induce adult plasticity after critical period closure (Hensch and Bilimoria, 2012; Baroncelli et al., 2016). These results show that EB odorant exposure drives remodeling loss of Or42a OSN innervation in the VM7 glomeruli, which is concentration dependent and especially sensitive during the critical period (0-2 dpe).

Critical period odorant exposure does not alter OSN survival or odorant receptor expression

The dramatic loss of Or42a OSN innervation of the VM7 glomerulus after critical period EB exposure could be the result of the OSN cell death or reduced expression of the cell marker. However, studies of AL glomerular innervation after odorant exposure or neuronal silencing have reported no alterations of OSN cell bodies or peripheral odor responses, regardless of the direction of the glomerular volume change (Devaud et al., 2001; Sachse et al., 2007; Chiang et al., 2009). Moreover, despite the widespread use of genetically-encoded odorant receptor fluorescent reporters to measure AL glomerulus innervation volumes, no work to our knowledge has shown altered transgenic expression after odorant exposure (Sachse et al., 2007; Das et al., 2011; Acebes et al., 2012). Nevertheless, to test for any altered OSN survival after EB exposure during the critical period, Or42a OSN cell bodies located in the peripheral olfactory maxillary palp were quantified. As above, animals with Or42a-Gal4 driving UAS-mCD8::GFP were exposed to 25% EB or vehicle control for the first 2 days after eclosion. Critical period odor exposure does not alter Or42a OSN cell bodies (Fig. 6A). Quantification shows no significant difference in soma number (Oil 15.25 ± 0.335 cells/palp (n=16) vs. EB 14.15 ± 0.629 (n=13); t(27)=1.62, p=0.117; Fig. 6B). Likewise, critical period odor exposure does not alter Or42a-Gal4 driven GFP expression

in OSN cell bodies (Fig. 6A). Quantification shows no significant difference in fluorescence intensity of soma and basal processes (Oil 115.2 ± 5.261 (n=16) vs. EB 105.1 ± 7.37 (n = 13); t(27)=1.143, p=0.263; two-tailed unpaired t-tests; Fig. 6B).

To confirm and extend the above findings, we next used Western blot analyses to test maxillary palps for differences in Or42a-Gal4 driven UAS-mCD8::GFP expression between the same paired EB odorant exposed and oil vehicle control conditions. In agreement with the above immunocytochemistry imaging, Western blot analyses also do not show GFP expression changes after critical period EB exposure assayed in 3 independent replicates (Fig. 6C, top). Quantification of the fluorescence intensity normalized to total protein reveals no significant difference between the two conditions (Oil 1533±192.3 (n=3 replicates, >30 palps/replicate) vs. EB 1900±606.9 (n=3); U=3, p=0.7; two-tailed Mann-Whitney test; Fig. 6D, top). We also separately assayed mCD8::GFP expression under the direct control of the Or42a promoter (Or42a-mCD8::GFP), which provides a direct, Gal4-indendent read-out of Or42a expression (Stephan et al., 2012). Western blot analyses were done to test GFP expression changes after critical period EB exposure in 3 independent replicates. Maxillary palps from these animals also show no change in GFP expression following critical period EB exposure (Fig. 6C, bottom). Quantification of fluorescence intensity normalized to total protein again reveals no significant difference between the two conditions (Oil 4735±1008 (n=3 replicates, >20 palps/replicate vs. EB 6561±1722 (n=3); U=4, p>0.999; two-tailed Mann-Whitney test; Fig. 6D, bottom). Thus, both imaging and Western blot analyses indicate no change in Or42a driven expression in response to heightened EB odorant exposure during the critical period.

Finally, we used quantitative real-time PCR (qPCR) to directly test transcript levels following critical period EB exposure. After either oil vehicle or 25% EB exposure (0-2 days), proboscises with maxillary palps were dissected to extract RNA. We assessed the expression of 3 transcripts; 1) Gal4, 2) the Or42a receptor, and 3) an Or71a receptor control, all normalized to the housekeeping genes *GAPDH2* and *rp49.* Compared to *GAPDH2,* quantification of RNA

expression levels between EB-exposed animals and oil vehicle controls done using the ΔΔ Ct method show no significant differences (*Gal4*: Oil 1.061±0.262 fold expression (n=3 replicates, 10 proboscises for all replicates) vs. EB 0.551±0.221 (n=2), t(3)=1.354, p=0.2687; *Or42a*: Oil 1.12±0.32 (n=3) vs. EB 1.45±0.348 (n=3), t(4)=0.699, p=0.523 ; *Or71a*: Oil 1.348±0.574 (n=3) vs. EB 1.302±0.14 (n=3), t(4)=0.077, p=0.942; two-tailed unpaired t test; Fig. 6E). Compared to *rp49,* a second housekeeping gene, there are likewise no significant differences in RNA levels (*Gal4*: Oil 1.071±0.293 fold expression (n=3 replicates, 10 proboscises for all replicates) vs. EB 0.362±0.036 (n=2), t(3)=1.871, p=0.158; *Or42a*: Oil 1.163±0.371 (n=3) vs. EB 1.147±0.512 (n=3), t(4)=0.025, p=0.981; *Or71a*: Oil 1.415±0.623 (n=3) vs. EB 1.037±0.396 (n=3), t(4)=0.511, p=636; two-tailed Mann Whitney test). These results demonstrate the dramatic loss of Or42a OSN innervation of the VM7 glomeruli following heightened critical period odorant experience is independent of changes in OSN cell bodies, Or42a reporter expression or Or42a receptor level, and therefore due to local retraction of axon terminal innervation in the antennal lobe.

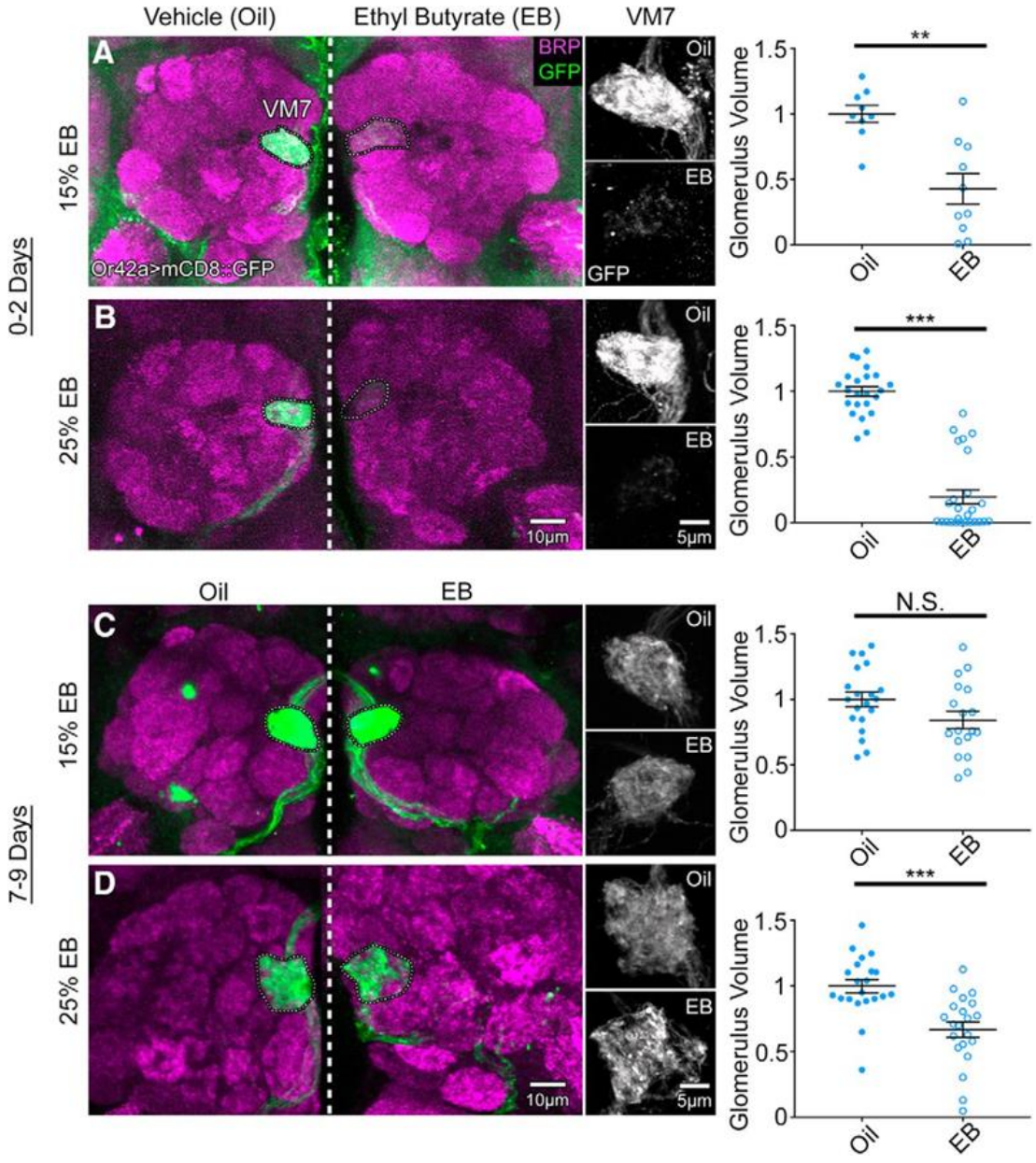

Figure 5: Critical period sensitive remodeling of olfactory glomeruli innervation
Representative confocal images of the Or42a-Gal4 driven UAS-mCD8::GFP membrane marker (green) in olfactory sensory neurons (OSNs) innervating antennal lobe (AL) glomerulus VM7 double-labeled with the anti-Bruchpilot (BRP; magenta) synaptic marker. Animals exposed to mineral oil vehicle (left) or ethyl butyrate (EB) odorant in oil during the early-use critical period (0-2 days post-eclosion) at **A)** 15% or **B)** 25% (%V/V; right). Middle: High magnification gray scale images of the Or42a-GFP channel only for the oil vehicle (top) and EB (bottom) at both odorant concentrations. Right: Quantification of the Or42a OSN innervation volume of the VM7 glomerulus for 15% (top) and 25% (bottom) odorant concentrations. The same experiment at maturity (7-9 days post-eclosion) comparing oil vehicle (left) to EB in oil at **C)** 15% or **D)** 25%. Middle: High magnification gray scale images of GFP channel only. Right: Quantification of Or42a OSN innervation volume of the VM7 glomerulus at both odorant concentrations. Scatter plots show all data points and the mean ± SEM. Significance from two-tailed unpaired t-test is indicated as not significant (N.S.; $p>0.05$), or significant at $p<0.01$ (**) and $p<0.001$ (***).

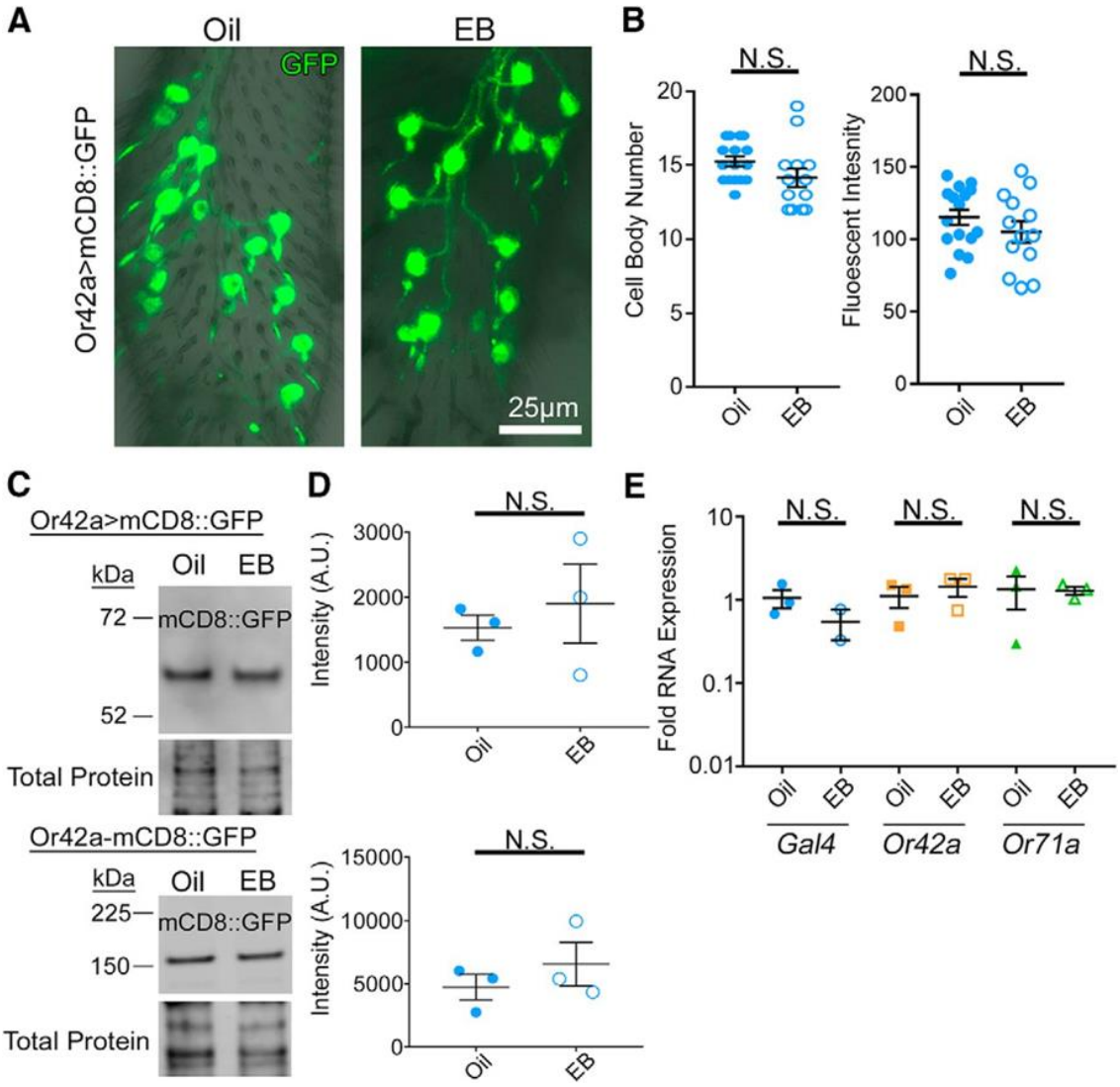

Figure 6: Odorant experience does not alter OSN survival or odorant receptor expression
A, Representative confocal images of Or42a-Gal4 driven UAS-mCD8::GFP membrane marker (green) in the olfactory sensory neuron (OSN) cell bodies, dendrites and labial tract within the maxillary palp. Staged animals exposed to either the mineral oil vehicle (Oil, left) or odorant ethyl butyrate in oil (EB, 25% V/V, right) during the critical period (0-2 days post-eclosion; dpe). **B**, Quantification of the number of Or42a OSN cell bodies (left) and total fluorescent intensity within each maxillary palp (right) comparing oil and EB conditions. **C**, Representative Western blots of maxillary palp homogenates from oil or EB-exposed animals (0-2 dpe) from both Or42a-Gal4 driven mCD8::GFP (Or42a>mCD8::GFP, top) and mCD8::GFP driven directly by a Or42a promoter (Or42a-mCD8::GFP, bottom). Both blots show the GFP channel (upper panel) and total protein (REVERT, lower panel). Molecular weights are shown to the left. The difference in mCD8::GFP size is due to the number of GFP molecules in reporter (1 GFP at top vs. 4 GFPs at bottom). **D**, Quantification of GFP Western blots for both Or42a-Gal4 driven mCD8::GFP (top) and Or42a promoter (bottom) normalized to the total protein. A sample size of 3 independent biological replicates is compared for all 4 conditions. **E**, Quantification of RNA level from the proboscis with attached maxillary palps from animals exposed to oil or EB from 0-2 dpe for the *Gal4* driver (left), *Or42a* receptor (middle) and *Or71a* (EB-insensitive control olfactory receptor, right) normalized to the *GAPDH2* housekeeping gene. Scatter plots show all data points and the mean ± SEM. Significance from two-tailed unpaired t-tests (B,E) or Mann-Whitney tests (D) is indicated as not significant (N.S.; p>0.05).

Retracted OSN glomerular innervation during critical period odorant exposure is reversible

Given the striking OSN axonal retraction caused by heightened odorant experience during the critical period (Fig. 5), we next wished to test whether removal of the odorant stimulus during this time window would enable re-innervation of the VM7 glomerulus by Or42a OSNs. Previous studies investigating the specialized CO_2-sensitive OSN showed odorant-dependent glomerular growth is reversible after CO_2 removal for at least 2 days during the critical period, but not at all reversible afterwards (Sachse et al. 2007). Similar critical period restricted reversibility characterizes the mammalian ocular dominance activity-dependent critical period (Blakemore et al., 1978). We therefore hypothesized that the removal of the EB odorant after inducing critical period remodeling would enable Or42a OSNs to re-innervate VM7 glomeruli, thus reversing the effect during the critical period. Using OSNs labeled with Or42a-Gal4 driving UAS-mCD8::GFP, we tested the reversibility of OSN axonal retraction by shifting animals after 1 or 2 days of EB odorant exposure immediately after eclosion, to oil through 4 days post-eclosion (Fig. 7A). We tested effects of EB exposure for 1, 2 and 4 days, demonstrating a similar strong axon retraction for all three critical period treatments (Fig. 7A,B). In parallel, we tested animals exposed to EB for one day (0-1 dpe) and then returned to the oil vehicle for the three remaining days (3-day reversal; Fig. 7A), as well as animals exposed to EB for two days (0-2 dpe) replaced with the oil vehicle for the two remaining days (2-day reversal; Fig. 7A). All animals were dissected at the same time at the end of day 4 (Fig. 7A), and the Or42a OSN innervation of the VM7 glomerulus imaged (Fig. 7B,C).

EB exposure for 1, 2 or 4 days during the critical period causes a similar reduction in the VM7 innervation compared to the oil controls (Fig. 7B,D; Kruskal-Wallis one-way ANOVA $KW(7)=84.94$, $p=1.348 \times 10^{-15}$). Note that the dimmer Or42a>GFP signal at day 1 post-eclosion reflects the earlier time point in reporter expression, but the extent of axonal retraction is similar for all three treatments. Quantification shows all EB exposures significantly reduce glomerular volume compared to oil controls (1 Day: Oil 1.184 ± 0.047 (n=26) vs. EB 0.571 ± 0.073 (n=23),

mean rank difference=80.82, $p=2.21x10^{-6}$; 2 Day: Oil 1.303 ± 0.053 (n=22) vs. EB 0.646 ± 0.093 (n=26), mean rank difference=82.33, $p=1.79x10^{-6}$; 4 Day: Oil 1.0 ± 0.040 (n=23) vs. EB 0.505 ± 0.070 (n=24), mean rank difference=58.32, p=0.0017, Dunn's multiple comparisons tests; Fig. 7D). We find that both the 2- and 3-day reversal returns innervation to levels indistinguishable from controls (Fig. 7C). Quantification shows that animals returned to the oil vehicle for 2 or 3 days during the critical period re-develop OSN innervation volumes that are not statistically different from day 4 controls never exposed to the EB odorant (3 Day reversal 1.164 ± 0.044 (n=25), mean rank difference=-10.3, p>0.9999; 2 Day reversal 1.01 ± 0.087 (n=24), mean rank difference=-27.82, p=0.424, Dunn's multiple comparisons tests; Fig. 7D). Note that, in addition to the reversal of the majority of animals after 2 days of EB exposure, 3 animals fail to reverse the axonal retraction (Fig. 7D), suggesting the approaching end of the early-use critical period. We conclude the Or42a OSN innervation remodeling within the VM7 glomerulus is reversible after removal from EB odor during the critical period.

Critical period odorant exposure drives OSN synapse elimination in AL glomeruli

The glomerular OSN volume measure represents a good proxy for synaptic innervation (Mosca and Luo, 2014), but does not directly measure OSN synaptic contacts. We therefore tested whether the Or42a OSN volume reduction in response to EB odorant exposure during the early-use critical period also affects synaptic organization within the VM7 glomerulus, by assaying the commonly used active zone marker Bruchpilot (BRP; Wagh et al., 2006). Based on the reduction in glomerular volume we hypothesized synapse number would be reduced. We employed the Synaptic Tagging with Recombination (STaR) labeling method (Chen et al., 2014) to investigate the Or42a OSN-specific changes in BRP expression and spatial distribution in synapses following critical period odorant exposure. The STaR method uses the transgenic FLP/FRT system to express tagged BRP::GFP under its endogenous promoter only in the neurons where FLP is expressed. Here, we employ the UAS/Gal4 system to specifically express

FLP using Or42a-Gal4 targeted to the OSNs innervating only the VM7 glomerulus. The resulting brains show green, punctate BRP::GFP synaptic labeling restricted to the mDC8::RFP co-labeled VM7 glomerulus (Fig. 8). The transgenic BRP::GFP label shows close overlap with anti-BRP staining for endogenous VM7 synapses. Or42a OSN synapses are compared between the odorant vehicle control (mineral oil) and 25% EB dissolved in the oil during the early-use critical period (0-2 dpe). Sample images and quantified data for VM7 glomerular volume, BRP punctae number and BRP expression levels are shown in Figure 8.

Vehicle control animals exhibit prominent BRP::GFP synaptic labeling of Or42a OSN presynaptic active zones in the VM7 glomerulus (Fig. 8A, top). In contrast, animals exposed to 25% EB during the critical period (0-2 dpe) show a striking decrease in both the number and intensity of BRP::GFP labeled synaptic punctae (Fig. 8A, bottom). As previously shown, Or42a OSN innervation of VM7 in EB-exposed animals is significantly reduced compared to controls (Oil 1.0 ± 0.0368 (n=16) vs. EB 0.332 ± 0.0898 (n=12); $t(26)=7.566$, $p=4.953 \times 10^{-8}$, two-tailed unpaired t test; Fig. 8B). Consistently, EB exposure also causes a highly significant reduction of local BRP signal maxima as a measure for BRP synaptic punctae (see Methods) compared to matched controls (Oil 1.0 ± 0.048 (n=14) vs. EB 0.241 ± 0.068 (n=12); $t(24)=9.292$, $p=2.0217 \times 10^{-9}$, two-tailed unpaired t test; Fig. 8C). Similarly, the overall BRP signal intensity within the VM7 glomerulus is reduced by EB exposure during the critical period compared to vehicle controls (Oil 1.0 ± 0.0596 (n=14) vs. EB 0.179 ± 0.103 (n=12); ($U=13$, $p=7.704 \times 10^{-5}$, two-tailed Mann Whitney test; Fig. 8D). These results indicate that critical period olfactory experience induces OSN synapse elimination, with fewer synapses persisting after the odorant exposure. The greater BRP reduction compared to OSN glomerulus volume suggests that synapse loss precedes retraction of Or42a axons. Taken together, these results show that EB odorant exposure during the critical period drives rapid synapse elimination from the Or42a OSNs innervating the VM7 glomerulus.

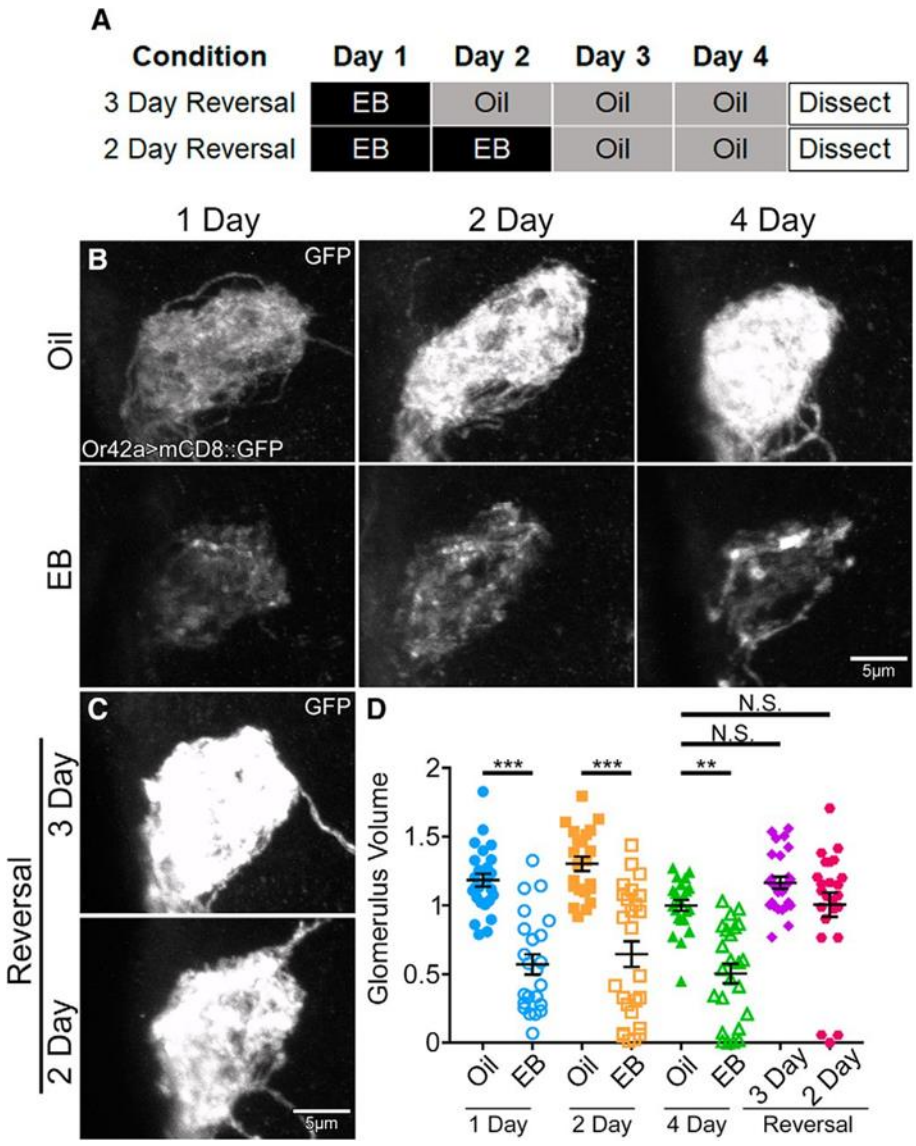

Figure 7: Critical period OSN innervation remodeling is reversible by odorant removal
A, Schematic illustrating the timing of exposure to either mineral oil vehicle (oil) or ethyl butyrate in oil (EB; 25%) for reversal experiments. Animals were exposed to EB for either 1 day (top) or 2 days (bottom) before shifting to the oil vehicle condition. All animals were dissected at the end of 4 days, testing 3 day reversal (top) or 4 day reversal (bottom). **B,** Representative gray scale confocal images of Or42a-Gal4 driven UAS-mCD8::GFP membrane marker in olfactory sensory neurons (OSNs) innervating the antennal lobe (AL) glomerulus VM7. Animals exposed to either oil vehicle(top) or EB (bottom) for 1 day (left), 2 days (middle) and 4 days (right) post-eclosion. **C,** Representative gray scale images as in B, but with 1 day of 25% EB exposure followed by 3 days of oil (3-day reversal, top) or 2 days of EB exposure followed by 2 days of oil (2-day reversal, bottom). **D,** Quantification of Or42a OSN innervation volume of the VM7 glomerulus for all 8 conditions. Scatter plots show all data points and the mean ± SEM. The significance is indicated from Kruskal-Wallis one-way ANOVA with follow up Dunn's multiple comparisons tests as not significant (N.S.; $p>0.05$), or significant at $p<0.01$ (**) and $p<0.001$ (***).

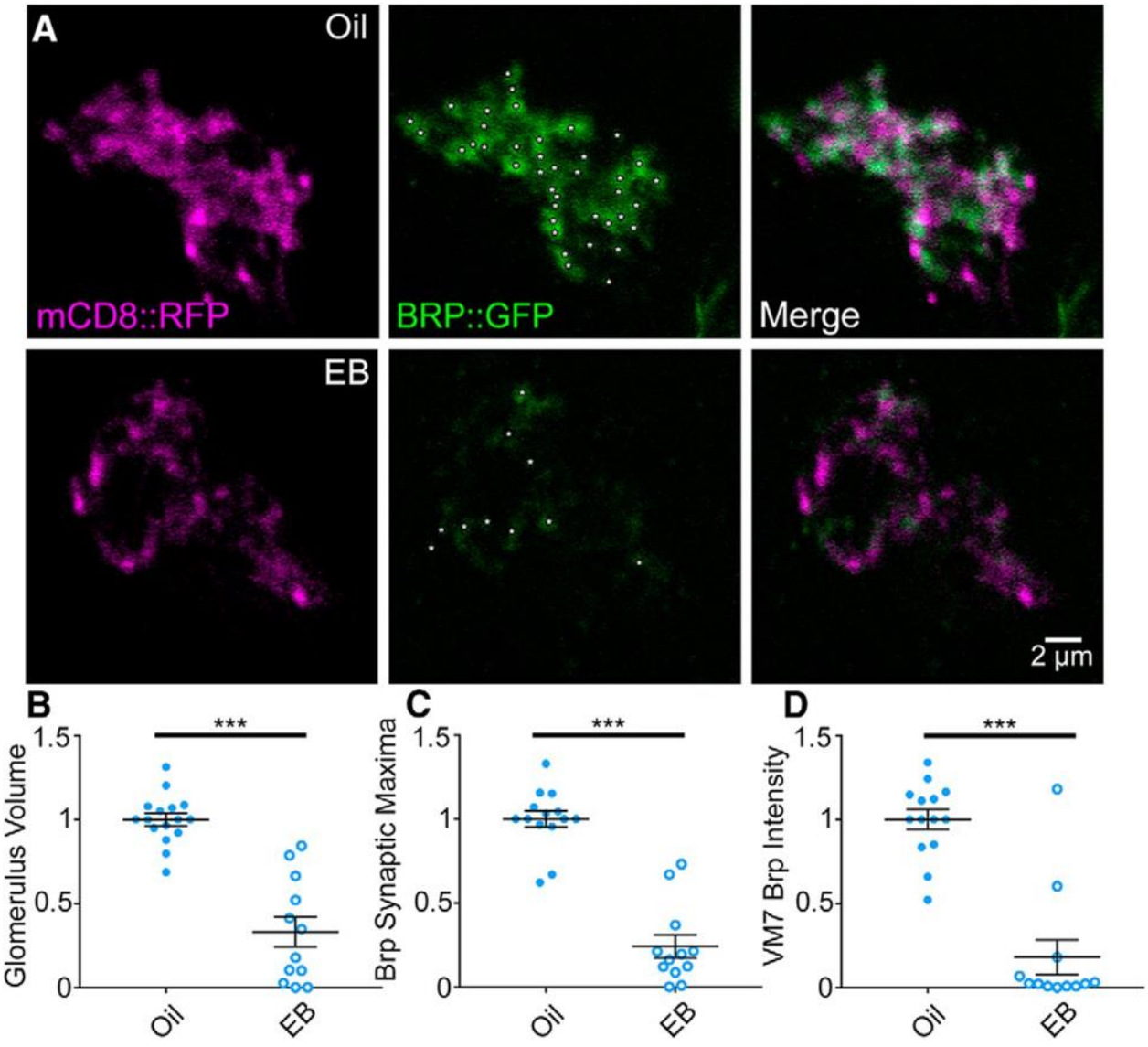

Figure 8: Critical period olfactory experience drives glomeruli synapse elimination
A, Representative confocal images of Or42a-Gal4 driven UAS-mCD8::RFP membrane marker (mCD8::RFP, magenta, left) and UAS-Bruchpilot::GFP (BRP::GFP, green, middle) with the merged overlap (right) in olfactory sensory neurons (OSNs) innervating the antennal lobe (AL) glomerulus VM7. BRP local maxima punctae at OSN synapses (white asterisks) in single confocal sections (1 µm). Exposure to the mineral oil vehicle (top) or ethyl butyrate (EB) odorant at 25% (%V/V; bottom) during the early-use critical period (0-2 days post-eclosion; dpe). Quantification of the Or42a OSN innervation volume of the VM7 glomerulus (**B**), BRP synaptic maxima (**C**) and BRP intensity (**D**). Scatter plots show all the data points and the mean ± SEM. Significance from two-tailed unpaired *t* tests is indicated as $p<0.001$ (***).

Ultrastructural analyses of odorant exposure effects on Or42a OSN innervation

We next sought to test and extend the above light microscopy study at higher resolution using transmission electron microscopy (TEM) ultrastructural analyses (Vita and Broadie, 2017). The antennal lobe VM7 glomerulus contains multiple neuron types in addition to Or42a OSNs (Grabe et al., 2016; Golovin and Broadie 2016, 2017), making it impossible to identify specific synaptic terminals using standard TEM sample preparations. Therefore, to specifically assay Or42a OSN synaptic terminals within the VM7 glomerulus, we made use of a photoconversion labeling technique to render the Or42a OSNs electron-dense compared to all other surrounding VM7 neurons. The genetically-encoded mini Singlet Oxygen Generator (miniSOG) construct produces oxygen free radicals when exposed to blue light (480 nm), which can then interact with diaminobenzidine (DAB) to generate a dark, electron-dense precipitate at the location of the reaction (Shu et al., 2011; Ng et al., 2016). This signal can be readily imaged with TEM. Driving targeted expression of the membrane-tethered mCherry-tagged miniSOG transgene (UAS-myr-miniSOG-mCherry) with Or42a-Gal4, we can label and identify specifically the Or42a OSN synaptic terminals innervating the VM7 glomerulus. Prior to the blue light exposure, Or42a OSNs expressing miniSOG are clearly visible and identifiable via the fluorescent mCherry tag (Fig. 9A, red, left panel). After the blue light exposure (~1 hour), the DAB precipitate labels the Or42a OSNs innervating only the VM7 glomerulus (Fig. 9A, black, right panel), marking these neurons selectively for subsequent TEM analyses.

Due to the shape and location of the VM7 glomerulus, proper brain orientation in the TEM block is imperative to maintain imaging consistency (Fig. 9B). To section the embedded brain, we position the anterior side toward the block face, such that sectional planes proceed in an anterior to posterior direction (Fig. 9B). Moreover, to ensure accurate and consistent depth measurements across compared conditions, we use brain confocal imaging stacks as a guide to determine the depth from the antennal lobe surface to the widest point of the VM7 glomerulus (~40 μm). Starting at this sectioning depth, we image individual ultra-thin brain sections (65 nm) spanning 6.5 μm of

tissue, affording us reproducible image acquisition and analysis (Fig. 9B). During the DAB photoconversion, the visible fluorescence signal will bleach swiftly (typically 5-10 minutes of light exposure), but singlet oxygens are still being generated and blue light exposure must be maintained until the precipitate is clearly seen (~1h for our experiments). Labeled Or42a OSNs are distinctly darker than all surrounding cells, and can be easily identified even at low magnification (6500X) as islets of increased density within VM7 glomeruli (Fig. 9C). In control brains, labeled regions are present throughout the VM7 glomerulus, occupying a large proportion of the neuropil (Fig. 9C, left panel). Under identical acquisition and imaging parameters, EB-exposed animals display a dramatic reduction in labeled Or42a OSNs, with islets sparsely occupying the neuropil (Fig. 9C, right panel). Thus, odorant experience during the critical period results in a dramatic loss of Or42a OSN innervation of the VM7 glomerulus.

Quantification shows a striking decrease in OSN synaptic area following 25% EB critical period treatment (0-2 dpe) compared to vehicle controls (Fig. 9D). Vehicle controls exhibit 6X more terminal area per section compared to EB-treated animals (Oil 33.280$\pm$2.839 μm^2 (n=10 sections) vs. EB 5.103$\pm$0.800 μm^2 (n=10)), with a highly significant reduction after the odorant exposure ($t(18)=9.554$, $p<0.0001$, two-tailed unpaired t test; Fig. 6D). Higher magnification reveals DAB precipitate throughout the cytoplasm (30,000X; Fig. 9E), consistent with all published miniSOG labeling results (Shu et al., 2011; Ng et al., 2016), likely due to membrane trafficking within the neuron (Winkle and Gupton, 2016). Synaptic regions characterized by presynaptic active zone T-bars (Fig. 9E, asterisks; enlarged in insets), with mitochondria (M), endosomes (E) and synaptic vesicles, are clearly apparent in the Or42a OSN terminals innervating VM7. To test for synapse changes, we quantified T-bars in two ways; 1) T-bars per EM image, and 2) T-bar density. In both cases, there is a large decrease in synaptic T-bars (asterisks) after critical period EB exposure (Fig. 9E,F). In both counts, oil vehicle controls contain significantly more T-bars than EB-treated animals (Oil 12.480$\pm$0.763 t-bars/image (n = 46 images) vs. EB 4.583$\pm$0.704 T-bars/image (n=24 images); Oil 1.57$\pm$0.082 T-bars/μm^2 (n=400 regions) vs. EB 0.591$\pm$0.100 T-

bar/μm² (n=136 regions); Fig. 9F). Taken together, these results indicate that axonal retraction and synapse elimination in the Or42a OSNs innervating the VM7 glomerulus follows EB odorant sensory experience during the critical period.

Or42a olfactory reception is required for critical period remodeling of Or42a OSN innervation

In addition to the strong activation of Or42a OSNs innervating only the VM7 glomerulus, EB can activate several other AL glomeruli, particularly with higher odorant concentrations (Couto et al., 2005; Semmelhack and Wang, 2009; Münch and Galizia, 2016). This is a very important consideration since AL lateral connections from other activated olfactory sensory neurons could possibly affect VM7 critical period development. Indeed, recent work has demonstrated that altered lateral inhibition in the antennal lobe can modulate olfactory sensory processing and change olfactory behavioral outputs (Acebes et al., 2011, 2012; Franco et al., 2017; Golovin and Broadie, 2017). We therefore tested whether the specific activation of Or42a receptors is required for critical period synaptic remodeling of Or42a OSNs within the VM7 glomerulus. To test the role of Or42a receptor activity, we compared control animals expressing mCD8::GFP under the Or42a promoter (Or42a-mCD8::GFP; Stephan et al., 2012) with the characterized *Or42a* mutants that completely eliminate the receptor response to the EB odorant (*Or42a*^{F04305}, Or42a-mCD8::GFP; Olsen et al., 2007). As above, Or42a OSN innervation of the VM7 glomerulus was compared between the odorant vehicle controls (mineral oil) and EB odorant dissolved in the oil at 25% concentration. The odorant exposure was for 48 hours at 0-2 dpe, within the initial, early-use critical period. Sample images and quantified VM7 glomerular volume data for the four conditions are shown in Figure 10.

Compared to vehicle controls, EB-treated animals show strong loss of OSN innervation, marked by Or42a-mCD8::GFP punctae characteristic of axonal retraction (Fig. 10A, arrows). Quantification shows a significant effect of EB exposure on Or42a OSN innervation ($F(1, 79) = 13.74$, $p=0.0004$, two-way ANOVA; Fig. 10B, left). Follow up multiple comparisons tests reveal a

significant difference between the vehicle control (Oil; 1.0 ± 0.059, n=26) and EB-treated animals (0.543 ± 0.091, n=21; t(79)=5.226, p=4.13x10^{-6}, Sidak's multiple comparisons test). In sharp contrast, *Or42a* mutants exposed to EB exhibit Or42a OSN innervation indistinguishable from oil-exposed mutants (Fig. 10A, right). Note that membrane punctae characteristic of axonal retraction (Ertürk et al., 2007) are widely present in EB-treated VM7 control glomeruli (Fig. 10A, arrows), but do not occur in EB-treated *Or42a* mutants (Fig. 10A, right), which resembles the vehicle controls in both genotypes. Quantification shows no significant difference between the vehicle control in the *Or42a* mutant (0.817 ± 0.043, n=19) and the EB-treated *Or42a* mutant (0.783 ± 0.047, n=17; t(79)=0.3427, p=0.980, Sidak's multiple comparisons test; Fig. 10B, right). The effect of EB exposure on genetic controls vs. *Or42a* mutants is also significant (exposure x genotype interaction, F(1, 79)=10.19, p=0.002, two-way ANOVA; Fig. 10B, top dashed bar). These results demonstrate that specific Or42a receptor odorant activation is required for the critical period remodeling of the Or42a OSN innervation of the VM7 glomerulus, suggesting a cell intrinsic, activity-dependent mechanism.

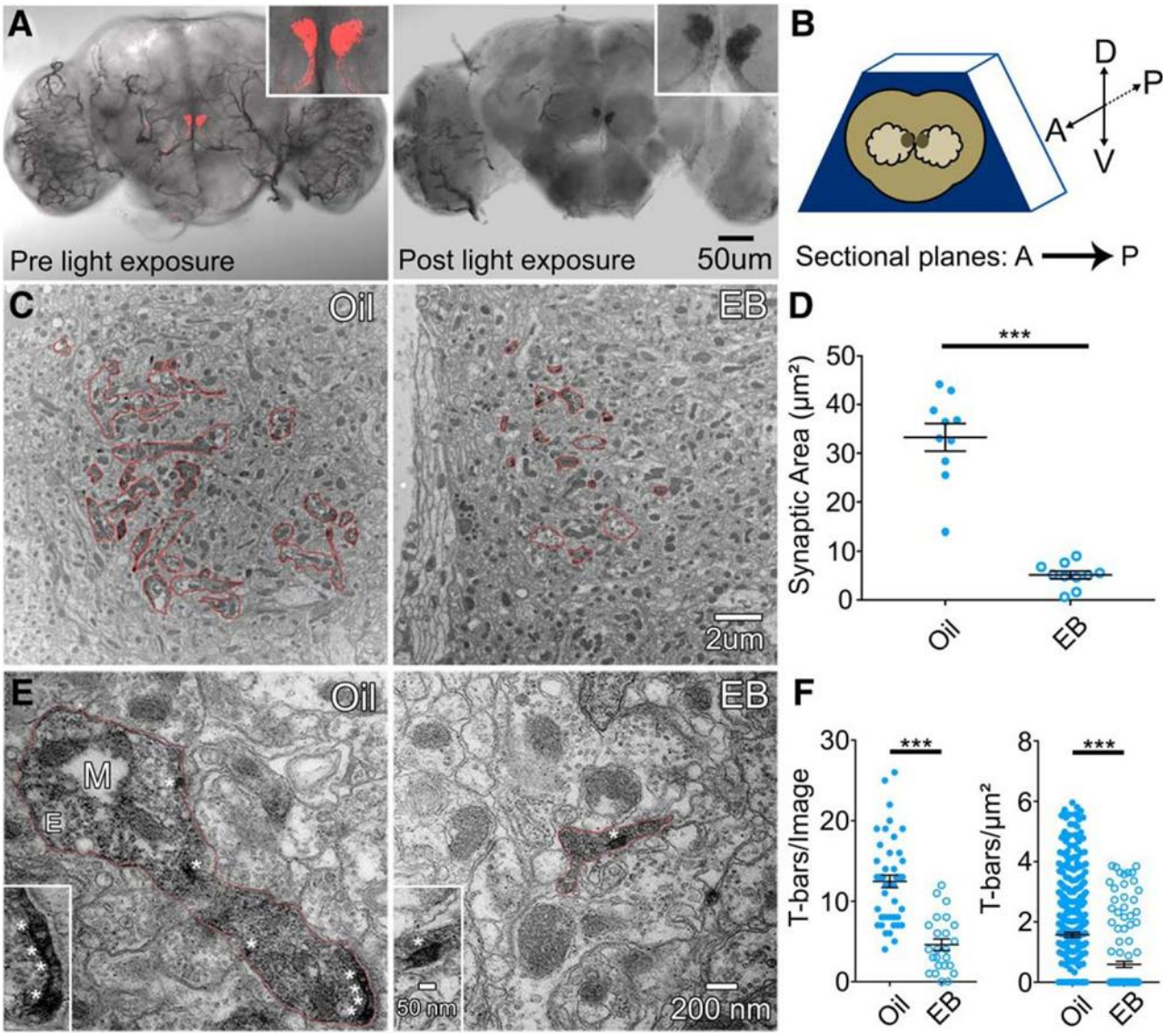

Figure 9: Ultrastructure analysis of critical period odorant exposure on Or42a innervation
A, Light microscope brain images of membrane-tethered mCherry-tagged miniSOG transgene (UAS-myr-miniSOG-mCherry) driven by Or42-Gal4 before blue light (480 nm) exposure (left) and after light exposure forming DAB precipitate (right). Insets show enlarged VM7 glomerulus with fluorescent signal (red, left) and DAB precipitate (black, right). **B**, Schematic depicting brain orientation in resin block for sectioning, with coordinates; anterior (A), posterior (P), dorsal (D) and ventral (V). Direction of sectional plane is A to P. **C**, Representative low magnification electron micrographs (6500X) of vehicle control (Oil, left) and 48 hour ethyl butyrate exposure (EB, right). Red outlines depict DAB labeled regions in the VM7 glomerulus. **D**, Quantification of area measurements depicted in C. **E**, Representative high magnification electron micrographs (30,000X) of vehicle control (Oil, left) and 48 hour EB exposure (right). Red outlines depict DAB labeled boutons in VM7 glomerulus. Abbreviations: M, mitochondrion; E, endosome; *, t-bars. Insets show enlarged synaptic t-bars from each bouton. **F**, Quantification of synaptic active zone t-bar count per image (left graph) and density within labeled area (right graph). All experiments use Or42a-Gal4 driving myr-miniSOG-mCherry. Scatter plots show all data points and mean ± SEM. Significance is shown between conditions by two-tailed unpaired *t* tests or a Mann-Whitney test (t-bars/area). Analysis of t-bars per area was performed following ROUT outlier test with Q set to 1%. Significance is indicated as $p<0.001$ (***).

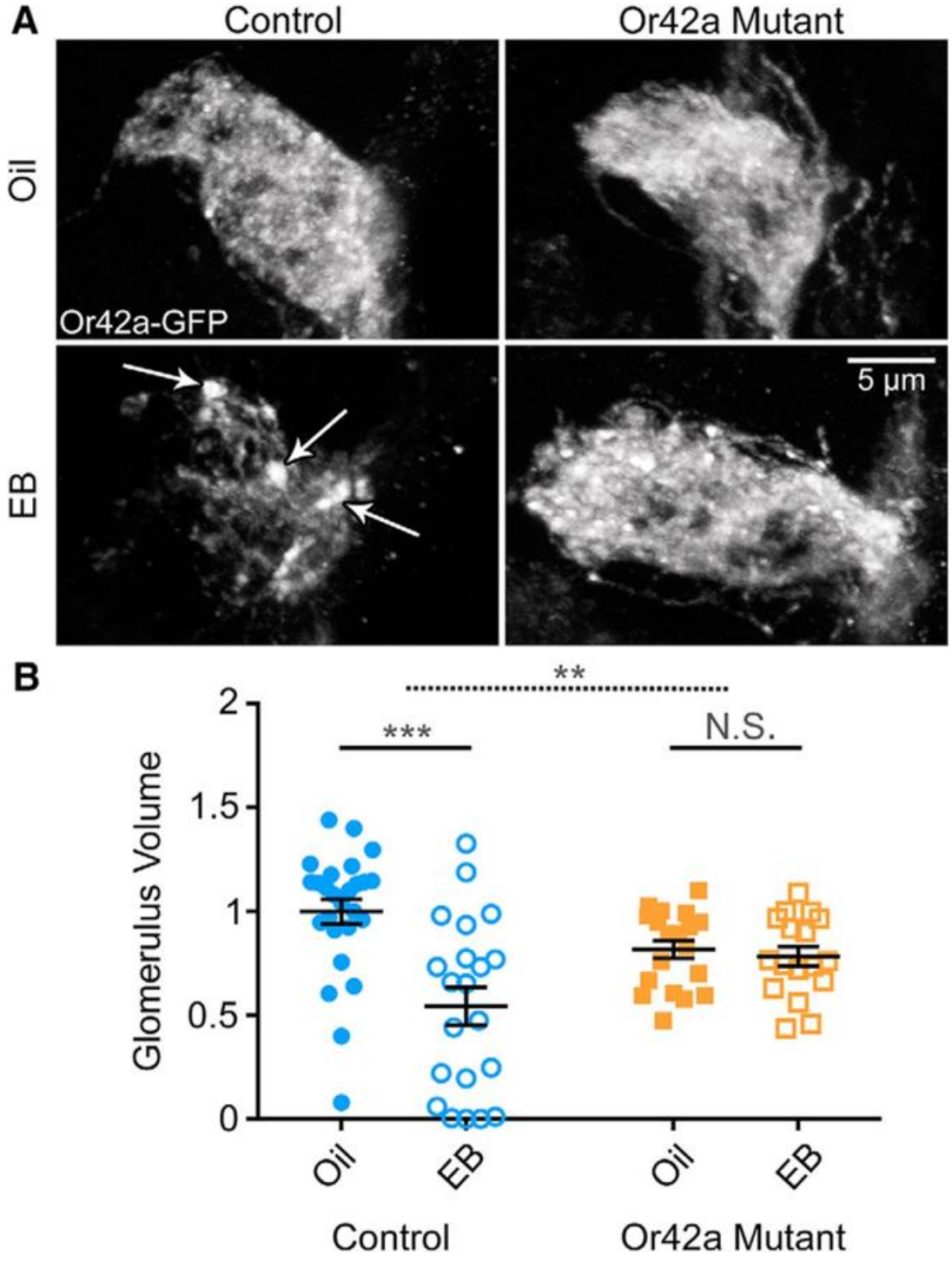

Figure 10: Or42a olfactory receptors required for Or42a OSN critical period remodeling
A, Representative confocal images of Or42a -mCD8::GFP in olfactory sensory neurons (OSNs) innervating the antennal lobe VM7 glomerulus. Early critical period exposure (0-2 dpe) to the vehicle only (oil, top) or 25% ethyl butyrate (EB, bottom) in the Or42a-mCD8::GFP genetic background (control, left) and the Or42a-mCD8::GFP; *Or42a*^{F04305} null (*Or42a* mutant, right). White arrows in EB control indicate axonal membrane retraction punctae. **B,** Quantification of Or42a OSN innervation volume of the VM7 glomerulus for all 4 conditions. Scatter plots show all the data points and the mean ± SEM. Significance from two-way ANOVA with Sidak's multiple comparisons tests between vehicle and EB conditions within each genotype. Top dashed significance bar indicates the interaction between genotype and odor exposure. Significance is indicated as not significant (N.S.; p>0.05), or significant at p<0.01 (**) and p<0.001 (***).

Activity-dependent modulation of OSN critical period remodeling of glomeruli innervation

Activity has long been established to mediate critical period neural circuit remodeling, both within specific neuron classes (Devaud et al., 2003b; Sachse et al., 2007) and between different neurons at a circuit level (Acebes et al., 2011; Das et al., 2011; Lieber et al., 2011; Sudhakaran et al., 2014). We therefore tested whether activity within the Or42a OSNs specifically, or the activation of downstream neurons via synaptic neurotransmission within the neural circuit, plays a role in critical period remodeling in the VM7 glomerulus. In order to test both activity levels, we used two widely-employed transgenic tools: 1) UAS-targeted expression of the tetanus toxin light chain (TeTxLC) protease, which cleaves the vSNARE synaptobrevin to block synaptic vesicle fusion and eliminate neurotransmission (Sweeney, Broadie et al., 1995), and 2) UAS-targeted expression of the exogenous inward rectifying potassium channel 2.1 (Kir2.1), which increases K^+ permeability, hyperpolarizes the neuron, and thus inhibits action potential firing within the targeted neuron (Baines et al., 2001). Both UAS constructs were driven with Or42a-Gal4 only within the targeted Or42A OSNs innervating the VM7 glomerulus. To examine VM7 innervation, Or42a OSNs co-express the UAS-mCD8::GFP membrane label. Comparisons were done for each genotype between a vehicle oil control and EB dissolved in the oil at 25% for 0-2 dpe. Sample images for all conditions and quantified VM7 glomerular innervation for all six conditions are shown in Figure 11.

Transgenic controls respond to EB exposure with a strong decrease in innervation and characteristic axonal punctae (Fig. 11A, left). Quantification again shows the significant effect of odorant exposure ($F(1, 144)=298.4$, $p=1.29x10^{-36}$, two-way ANOVA; Fig. 11B, left). Follow-up multiple comparisons reveal a significant decrease of OSN innervation in transgenic controls (Oil 1.0 ± 0.037 (n=27) vs. EB 0.500 ± 0.062 (n=25); $t(144)=9.064$, $p=6.22x10^{-15}$, Sidak's multiple comparisons test). TeTxLC neurotransmission blockade specifically in Or42a OSNs does not prevent critical period remodeling, but rather results in a further loss of innervation (Fig. 11A, middle). This increased remodeling is accompanied by lack of axon retraction punctae (compare

to Fig. 11A, left, arrows), suggesting a more rapid, complete axonal retraction process. In general, axonal punctae are observed less frequently with the greatest innervation loss, suggesting a nearly complete absence of Or42a OSNs within VM7 (Fig. 11A, middle). We hypothesize TeTxLC has a clear developmental effect on VM7 innervation as the oil TeTxLC condition has a larger Or42a OSN volume compared to controls ($t(144)=3.135$, $p=0.014$ Sidak's multiple comparison test). Quantification with follow up multiple comparisons test between the oil control TeTxLC condition (1.179 ± 0.049, n=22) and EB-treated TeTxLC condition (0.043 ± 0.011, n=21) reveals significant volume reduction ($t(144) = 18.74$, $p=1.32x10^{-39}$, Sidak's multiple comparisons test; Fig. 11B). A linear regression analysis shows that TeTxLC block significantly increases the effect of EB exposure compared to controls (-0.636 ± 0.007, $t(144)=-7.195$, $p=2.21 \times 10^{-10}$, two-tailed unpaired t test with Sidak's correction; Fig. 11B, middle dashed bar).

We next tested critical period remodeling with the Kir2.1 suppression of action potential firing in the Or42A OSNs. Like the *Or42a* mutant, EB exposure did not significantly alter OSN innervation in Kir2.1 compared to the vehicle controls (Fig. 11A, right). However, a complication to this interpretation is that Kir2.1 activity suppression in Or42a OSNs strongly reduces VM7 innervation in the vehicle controls (Fig. 11A; compare control and Kir2.1 oil-exposed conditions). The striking effect shows activity-dependent control of OSN refinement, but may indicate a need for activity for the initial innervation of the VM7 glomerulus (Chiang et al., 2009). Note also that despite the overall effect of Kir2.1 activity suppression on OSN innervation, EB-treatment still produces axonal retraction punctae similar to controls (Fig. 11A, Kir2.1 EB). Quantification of innervation volume shows a strong reduction already in the vehicle control Kir2.1 condition (Oil; 0.210 ± 0.030, n=28) with no significant loss with EB exposure (0.154 ± 0.028, n=27; $t(144)=1.043$, $p=0.917$, Sidak's multiple comparisons test; Fig. 11B, right). Linear regression analyses show Kir2.1 activity suppression attenuates the EB treatment effect compared to controls by 0.441 ± 0.007, and is significantly reduced compared to the controls ($t(144)= 5.327$, $p=2.63 \times 10^{-6}$, two-tailed unpaired t test with Sidak's correction; Fig. 11B, top dashed bar). Thus,

suppression of Or42A OSN activity reduced baseline innervation and blocks critical period remodeling. Overall, these results indicate cell intrinsic OSN activity is important for innervation, and that OSN synaptic signaling limits OSN remodeling during the critical period.

Critical period remodeling requires NMDA glutamatergic transmission, but not GABA signaling

Given neurotransmission is important for control of critical period remodeling, we next dissected intercellular signaling mechanisms. Previous work suggests both GABAergic and glutamatergic signaling play important roles in regulating AL-dependent behavior (Das et al., 2011). Labeling studies indicate GABAb R2/3 and NMDA R1/R2 receptors are present in the AL (Xia et al. 2005; Raccuglia et al. 2016). To independently test GABAergic and glutamatergic signaling, we used transgenic RNAi to knockdown GABA receptors (*GABAb R3*;) and NMDA receptors (*NMDAR1*) specifically in the Or42a OSNs (Ni et al., 2009). We then assessed Or42a innervation of the VM7 glomerulus as above, comparing oil vehicle controls with 25% EB during the critical period (0-2 dpe; Fig. 12). A two-way ANOVA analysis shows a significant effect of odorant exposure ($F(1, 143)=66.27$, $p=3.5x10^{-13}$; Fig. 12A,B, left). Compared to controls, *GABAb R3* RNAi flies show similar reduction of VM7 innervation after EB exposure (Fig. 12A, middle). Quantification shows the transgenic control reduction in Or42a OSN volume in VM7 with EB exposure (Oil 1.0 ± 0.067 (n=26) vs. EB control 0.373 ± 0.079 (n=24); $t(143)=6.376$, $p=1.18x10^{-8}$, Sidak's multiple comparisons test) is similar to the effects in the *GABAb R3* RNAi condition (Oil 1.096 ± 0.053 (n=22) vs. EB 0.547 ± 0.095 (n=24); $t(143)=5.348$, $p=1.72x10^{-6}$, Sidak's multiple comparisons test; Fig. 12B, middle). There is no significant difference due to *GABAb R3* RNAi on EB reduction compared to controls (average difference 0.0787 ± 0.0126, $t(143)=0.5242$, $p=0.99$, two-tailed unpaired t test with Sidak's correction; dashed middle bar).

Given that *GABAb R3*-mediated GABAergic signaling has no detectable effect on critical period OSN innervation remodeling, we next assayed roles of *NMDAR1*-mediated glutamatergic signaling. In the transgenic controls, EB exposure during the critical period (0-2 dpe) results in a

highly significant reduction in OSN innervation compared to the odorant vehicle (Fig 8A,B left). In sharp contrast, *NMDAR1* RNAi OSN knockdown strikingly suppresses this EB-dependent remodeling (Fig. 12A, right). Despite the decreased change in Or42a OSN innervation, the VM7 glomerulus with *NMDAR1* RNAi still shows axonal retraction punctae, consistent with an incomplete axonal retraction process in the absence of effective NMDA signaling. Quantification shows that the vehicle exposed *NMDAR1* RNAi condition (Oil; 1.019 ± 0.047, n=26) is not significantly different from the EB-treated *NMDAR1* RNAi condition (EB; 0.800 ± 0.068, n=27; t(143)=2.284, p=0.114, Sidak's multiple comparisons test; Fig. 12B, right). *NMDAR1* knockdown significantly attenuates the effect of critical period EB exposure on Or42a OSN innervation compared to controls (0.423 ± 0.0111, t(143)=3.1851, p=0.0088, two-tailed unpaired t test with Sidak's correction; Fig. 12B, top dashed bar). Glutamatergic interneurons are the only known source of glutamate in the antennal lobe (Das et al., 2010; Liu and Wilson, 2013), suggesting these cells are the signal source. These results indicate that NMDA glutamatergic signaling onto OSNs, but not GABAb GABAergic signaling, is important for critical period OSN remodeling.

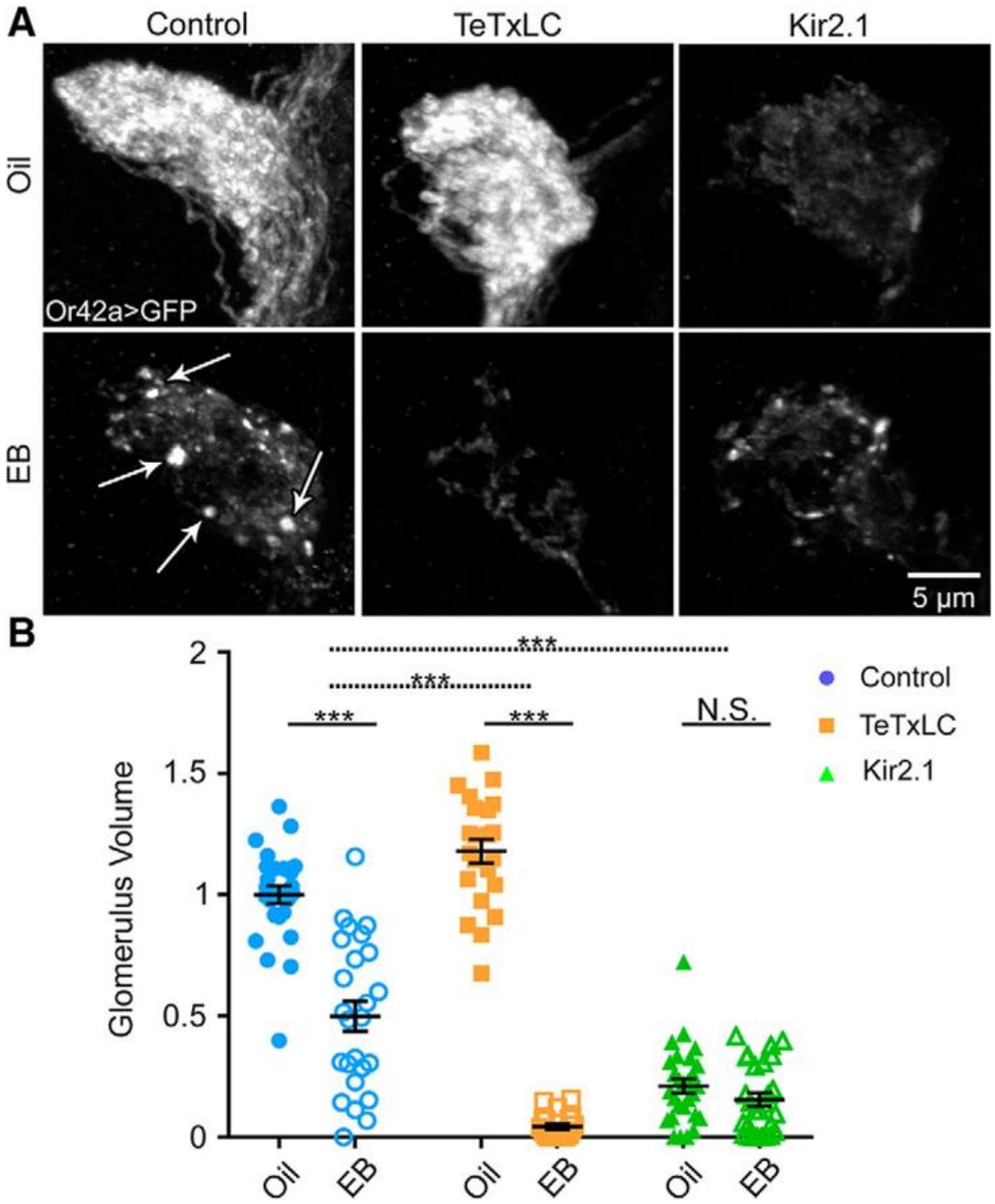

Figure 11: Activity-dependent critical period remodeling of olfactory glomeruli innervation
A, Representative confocal images of Or42a OSNs innervating the VM7 olfactory glomerulus (Or42a-GAL4 driven UAS-mCD8::GFP) following critical period exposure (0-2 dpe) to vehicle only (oil, top) or 25% ethyl butyrate (EB, bottom). Three genotypes are compared: 1) the background control w^{1118}; UAS-mCD8::GFP/+; Or42a-GAL4/+ (control, left), 2) same genotype with UAS-tetanus toxin light chain (TeTxLC, middle) to block synaptic transmission, and 3) the same genotype with UAS-inward rectifying potassium channel 2 (Kir2.1, right) to block action potentials. White arrows in EB control (left) indicate OSN axonal membrane retraction punctae. **B,** Quantification of Or42a OSN innervation volume of the VM7 glomerulus for all 6 conditions. Scatter plots show all the data points and the mean ± SEM. Significance is shown within genotypes from two-way ANOVA with Sidak's multiple comparisons tests (bottom bars), or from multiple regression with two-tailed unpaired *t* tests to test interactions between genotype and treatment for TeTxLC (dashed middle bar) and Kir2.1 (dashed top bar) conditions. Significance is indicated as not significant (N.S.; p>0.05) or significant at $p<0.001$ (***).

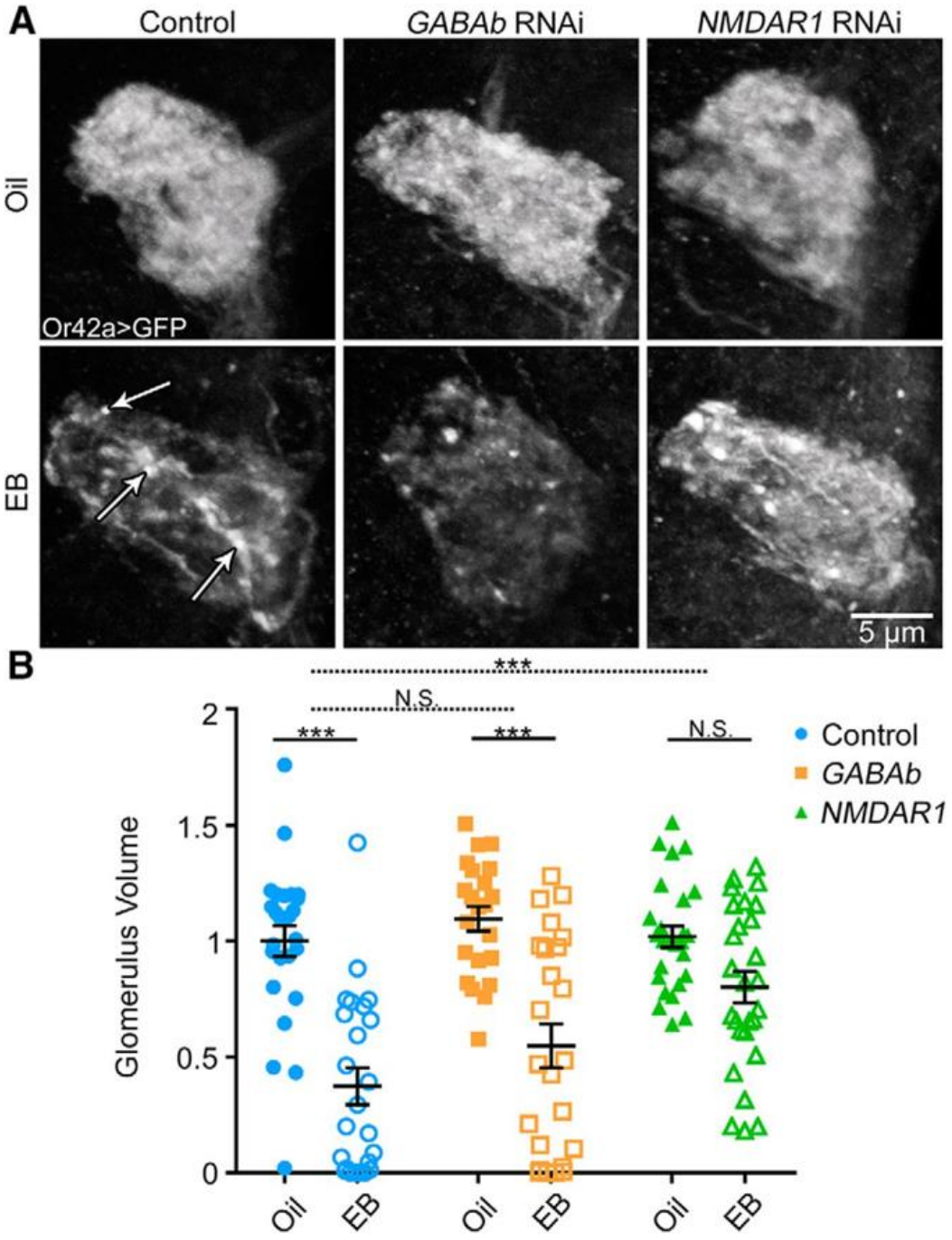

Figure 12: NMDAR glutamatergic transmission required for critical period OSN remodeling
A, Representative confocal images of Or42a OSNs innervating the VM7 olfactory glomerulus (Or42a-GAL4 driven UAS-mCD8::GFP) following critical period exposure (0-2 dpe) to vehicle only (oil, top) or 25% ethyl butyrate (EB, bottom). Three genotypes are compared: 1) the background control w^{1118}; UAS-mCD8::GFP/+; Or42a-GAL4/+ (control, left), 2) same genotype with UAS-*GABAb R3* RNAi (middle) or 3) UAS-*NMDAR1* RNAi (right). White arrows in EB control indicate OSN membrane retraction punctae. **B,** Quantification of Or42a OSN innervation volume of the VM7 glomerulus for all 6 conditions. Scatter plots show all the data points and the mean ± SEM. Significance is shown within genotypes from two-way ANOVA with Sidak's multiple comparisons tests (bottom bars), or multiple regression with two-tailed unpaired *t* tests to test the interactions between genotype and odorant treatment for *GABAb* RNAi (dashed middle bar) and *NMDAR1* RNAi (dashed top bar). The significance is indicated as not significant (N.S.; p>0.05) or significant at $p<0.001$ (***).

Wingless/Wnt-1 signaling is not involved in critical period Or42a remodeling

Other forms of *trans*-synaptic signaling reportedly play key roles in sensory experience remodeling (Huang et al., 1999; Chiang et al., 2009; Lieber et al., 2011). Wingless (W*g*; Wnt-1) is a prominent example, with Wg ligand activating the *Drosophila* Frizzled 2 (*dFz2*) receptor to inhibit *Drosophila* GSK3β Shaggy (*Sgg*) and regulate connectivity (Packard et al., 2002; Chiang et al., 2009; Korkut et al., 2009; Tsai et al., 2012; Friedman et al., 2013; Kopke et al., 2017). We used genetic approaches to interrogate this Wg signaling pathway in OSN critical period remodeling. We first removed one copy of *wg* (*wg*$^{l\text{-}17}$/+*;* Baker, 1987; Kopke et al., 2017) to reduce the Wg ligand level. In controls, 25% EB exposure in the critical period (0-2 dpe) causes the expected loss of OSN innervation and appearance of axonal retraction punctae (Fig. 13A, top, arrows), and quantification shows the typical loss of VM7 glomerulus innervation (Oil 1.0 ± 0.035 (n=25), EB 0.485 ± 0.058 (n=25); t(138)=7.093, p=4.37x10^{-10}, Sidak's multiple comparisons test; odorant exposure, effects F(1, 138)=210.8, p=2.84x10^{-29}, two-way ANOVA; Fig. 13B, left). Heterozygous *wg*$^{l\text{-}17}$/+ does not impact the effect of EB exposure on OSNs, with innervation indistinguishable from matched controls (Fig. 13A). Quantification shows a significant difference between vehicle and EB exposure (Oil *wg*$^{l\text{-}17}$/+ 0.901 ± 0.059 (n=12) vs. EB-treated *wg*$^{l\text{-}17}$/+ 0.266 ± 0.063 (n=17); t(138)=6.564, p6.86x10^{-9}, Sidak's multiple comparisons test; Fig. 13B). There is no significant effect on EB exposure between *wg*$^{l\text{-}17}$/+ and controls (0.120 ± 0.009, t(138)=-1.0997,p=0.893, two-tailed unpaired t test on interaction terms from linear regression with Sidak's correction; Fig. 13B, third dashed bar).

Despite the lack of Wg effect, we used stronger transgenic manipulations to further test the signaling pathway. We targeted a *dFz2* dominant-negative (*dFz2*-DN; Zhang and Carthew, 1998) to Or42a OSNs. This reduces VM7 innervation in vehicle controls (Fig. 13A), but does not significantly impact the effect of EB exposure (Oil 0.554 ± 0.097 (n=15) vs. EB 0.029 ± 0.021 (n=19); t(138) = 5.926, p=1.65x10^{-7}, Sidak's multiple comparisons test; Fig. 13B). In *dFz2*-DN flies, the EB treatment effect compared to controls is weakly augmented by -0.0104 ± 0.01023,

which is not significantly different (t(138)=-0.086, p=0.999, two-tailed unpaired t test with Sidak's Correction; Fig. 13B, second dashed bar). We also expressed a *Sgg* dominant-negative (*Sgg*-DN; Bourouis, 2002) in Or42a OSNs to inhibit Wg signaling. Compared to controls, *Sgg*-DN increases the effect of critical period EB exposure on innervation (Fig. 13A, bottom). Quantification shows vehicle controls (1.135 ± 0.073, n=18) are significantly different from EB-treated *Sgg*-DN (0.273 ± 0.070, n=15; t(138)=9.607, $p=3.48x10^{-16}$, Sidak's multiple comparisons test; Fig. 13B, right). In *Sgg*-DN flies, the OSN volume reduction from EB exposure compared to control is augmented by -0.347 ± 0.0104, which is significant (t(138)=-2.849, p=0.035, two-tailed unpaired t test with Sidak's correction; Fig. 13B, first dashed bar). However, a Sgg role in remodeling is likely independent of Wg signaling, as the other Wg manipulations do not impact remodeling, other pathways regulate Sgg activity, and Sgg independently affects glomerulus synapse number and behavior (Acebes et al., 2011). Overall, Wg signaling does not appear to be involved in regulating EB-dependent critical period remodeling.

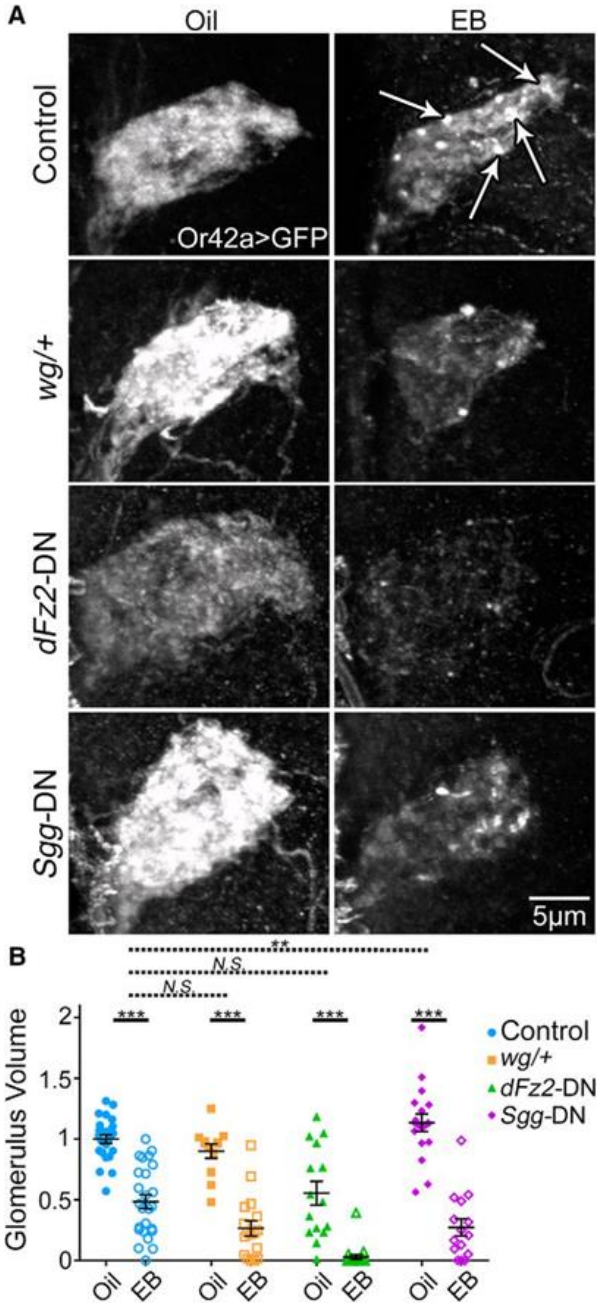

Figure 13: Wnt Wg signaling not involved in critical period sensitive OSN remodeling
A, Representative confocal images of Or42a OSNs innervating the VM7 olfactory glomerulus (Or42a-GAL4 driven UAS-mCD8::GFP) following critical period exposure (0-2 dpe) to vehicle only (oil, left) or 25% ethyl butyrate (EB, right). Four genotypes are compared: 1) background control w^{1118}; UAS-mCD8::GFP/+; Or42a-GAL4/+ (control, top), 2) same genotype with a heterozygous *wingless* null ($wg^{l\text{-}17}$/+, second row), 3) same genotype with UAS-*Drosophila frizzled-2 dominant negative* (*dFz2*-DN, third row) or 4) the UAS-*shaggy dominant negative* (*Sgg*-DN, bottom). White arrows in EB control indicate OSN axonal membrane retraction punctae. Female brains were used for these experiments. **B,** Quantification of OSN innervation volume of the VM7 glomerulus for all 8 conditions. Scatter plots show all the data points and the mean ± SEM. Significance within genotypes from two-way ANOVA with Sidak's multiple comparisons tests (bottom bars), or from multiple regression with two-tailed unpaired *t* tests to test interactions between genotype and treatment for *Sgg*-DN (dashed top bar), *dFz2*-DN (dashed second bar) and *wg/+* (dashed third bar). Significance is indicated as not significant (N.S.; $p>0.05$), or significant at $p<0.01$ (**) and $p<0.001$ (***).

Discussion

In *Drosophila*, the first few days of sensory experience are a use-dependent critical period for central olfactory circuit refinement with a greatly heightened capacity for synaptic remodeling (Devaud et al., 2003a; Sachse et al., 2007; Tessier and Broadie, 2009; Doll and Broadie, 2015, 2016; Doll et al., 2017). Here, we test this early post-eclosion time window (0-2 days) in contrast to maturity (7-9 days). We find odorant exposure only during the early period causes a striking reduction of Or42a OSN innervation onto their target VM7 synaptic glomerulus. This remodeling is odorant concentration-dependent and developmentally regulated. Despite early work clearly showing critical period odorant experience reduces glomerulus innervation volume (Devaud et al., 2001, 2003a, 2003b), no other work, to our knowledge, has shown an odorant-dependent decrease in OSN glomerular innervation, and only previous work from our lab has demonstrated reduction at the level of the postsynaptic PNs (Doll and Broadie, 2015). The current study thus refutes the conclusion that glomeruli activated by an odorant during the critical period always respond with an innervation increase, and presents a more complicated landscape. The current study also reveals larger magnitude innervation remodeling changes in comparison with earlier studies reporting reductions approaching ~30% (Devaud et al., 2001, 2003a). These differences likely reflect dosage-dependent effects (10% vs. 15% or 25% concentration), and the more careful monitoring of critical period timing.

Similar to a previous report on CO_2-sensitive olfactory sensory neurons, we demonstrate Or42a innervation remodeling is reversible with removal from the odorant (Sachse et al. 2007). Removing animals from EB for 2 or 3 days during the critical period leads to complete reversal of lost glomerulus innervation. Importantly, however, a few animals with 2 days reversal do not manifest re-innervation. This result suggests that remodeling capacity is reduced with odorant exposure time and the critical period endpoint threshold prevents reversal remodeling to make the OSN glomerulus innervation largely permanent. This conclusion agrees with classical critical period studies (Hubel and Wiesel, 1970; Blakemore et al., 1978; Ma et al., 2014; Tsai and Barnea,

2014; Huang et al., 2015), and is supported by the all-or-nothing nature of the reversal. We test synaptic remodeling using OSN-targeted STaR synapse labeling (Chen et al., 2014). Using the STaR technique, we show odorant-induced synapse elimination is more extensive than process loss, suggesting loss of synaptic connections precedes axon retraction. MiniSOG electron microscopy confirms synapse elimination (Devaud et al., 2001). This loss of synaptic connectivity likely modifies odorant-induced behaviors following EB exposure during the critical period (Das et al., 2011; Sudhakaran et al., 2014), which results in long-term habituation with flies avoiding the EB odorant more weakly than naïve flies.

We used three manipulations to test the activity-dependence of critical period remodeling. First, using *Or42a*^{F04305} receptor mutants that render OSNs EB-insensitive (Olsen et al., 2007), we find that critical period refinement is eliminated. This result indicates Or42a receptor activity is necessary in a cell-intrinsic mechanism controlling activity specifically within the Or42a OSNs. Second, expressing the tetanus protease to block synaptic vesicle fusion and neurotransmission (Sweeney, Broadie et al., 1995), we find that OSN synaptic output is not only dispensable for the odorant-induced remodeling, but acts to limit the extent of glomerular retraction. This intriguing finding suggests a mechanism acting *trans*-synaptically to limit critical period refinement of Or42a OSN innervation of VM7 glomerulus. A strong candidate is Notch signaling, which was recently shown to mediate Or82a OSN remodeling (Kidd and Lieber, 2016). Third, targeted Kir2.1 expression to suppress cell-intrinsic OSN electrical activity (Baines et al., 2001) blocks critical period innervation remodeling, similarly to the loss of Or42a receptor function. However, Kir2.1 silencing reduces glomerular innervation in both the vehicle- and EB-exposed animals, suggesting that activity is required for OSN axonal maintenance (Chiang et al., 2009). Together, these results demonstrate that activity-dependent critical period remodeling requires OSN cell-autonomous olfactory receptor activity modulated by downstream neuronal communication within the neural circuit.

The loss of critical period remodeling in OSNs lacking the Or42a EB odorant receptor indicates the mechanism requires olfactory reception in the specific OSN, and lateral communication between different OSN classes within the antennal lobe is not sufficient to cause remodeling (Acebes et al., 2011, 2012; Franco et al., 2017; Golovin and Broadie, 2017). The maintenance of OSN critical period remodeling with tetanus toxin blockade does not exclude electrical synapse involvement, which are not affected by the neurotoxin (Sweeney and Broadie et al., 1995). However, OSN electrical synapses have not been described, and electrical synapse loss does not alter OSN function (Yaksi and Wilson, 2010). Nevertheless, innexin mutants could be used to test possible electrical synapse roles (Phelan et al., 1996). Our studies indicate tetanus toxin has a consequence on OSN development, since animals have increased glomerulus innervation in the vehicle controls. This confirms previous results that tetanus toxin produces increased axon branching in olfactory PNs (Doll et al., 2017). Interpretation of our Kir2.1 result is likewise complicated by decreased Or42a OSN-VM7 innervation in vehicle controls. Although remodeling is eliminated with Kir2.1 silencing, the assay may not be sensitive enough to detect changes with the reduced innervation. Future studies using optogenetics to conditionally silence OSNs in the critical period may avoid the developmental effects of constitutive Kir2.1 silencing.

Our results indicate that NMDAR1-mediated glutamatergic neurotransmission is required for critical period OSN remodeling, consistent with previous work showing NMDAR1 is required for glomerulus volume increases and long-term habituation after EB exposure (Das et al., 2011). The only known source of AL glutamate release is a population of ventral LNs (Das et al., 2010), suggesting that these interneurons regulate critical period remodeling. GABAergic signaling also regulates Or42a OSN activity (Olsen and Wilson, 2008; Raccuglia et al., 2016), but our results indicate that AL-expressed GABAb R3 receptors (Okada et al., 2009) are not necessary for remodeling. This finding is consistent with previous reports that GABAergic signaling impacts long-term habituation, but not AL circuit changes (Das et al., 2011). We conclude that NMDA receptor, but not GABAb receptor, signaling combines with odorant dependent activity in Or42a

OSNs to drive synaptic remodeling during the critical period. The role of activity and NMDA receptor signaling is in agreement with previous studies on OSN response to odorant exposure (Das et al., 2011). However, the direction and magnitude of remodeling changes reported here differ from earlier reports. The loss of Or42a OSN VM7 innervation is somewhat reminiscent of the progressive loss of axonal processes in *Or83b* (*orco*) mutants that lack olfactory sensory reception (Chiang et al., 2009). These *orco* mutants also display axonal punctae similar to the mCD8::GFP membrane retractions reported here.

The punctae in retracting OSN axon processes closely resembles mammalian retraction bulbs (Li and Raisman, 1995). However, for this characterization we would need to establish the punctae are long-lived and display a disorganized microtubule architecture (Ertürk et al., 2007). Despite the striking similarities between EB-exposed OSNs and *orco* mutants, the time course is enormously different, with odorant-dependent critical period remodeling occurring immediately after eclosion (0-2 dpe) and *orco* retraction phenotypes starting much later (Chiang et al., 2009). Also, unlike the *orco* mutant retraction, critical period refinement does not involve Wg signaling (Packard et al., 2002; Chiang et al., 2009; Korkut et al., 2009; Tsai et al., 2012), as both *Wg* heterozygotes and targeted *dFz2*-DN in Or42a OSNs fails to impact axon retraction. Curiously, targeted *Sgg*-DN in Or42a OSNs enhances odorant-induced critical period remodeling, with a greater degree of VM7 innervation loss following EB exposure. However, *Sgg*-DN effects likely do not act via the Wg signaling pathway, as this mechanism would be expected to limit OSN innervation reduction. Importantly, Sgg acts independently to regulate glomerulus synapse number (Acebes et al., 2011). The Wg pathway studies reported here support a role in the maintenance of OSN glomerular innervation, but do not indicate a role in the regulation of critical period remodeling.

This study demonstrates a novel mode of odorant-dependent critical period remodeling of brain olfactory circuitry. EB odorant exposure during an early-use critical period causes an extensive retraction of Or42a OSN innervation of the AL VM7 glomerulus. This striking loss of

innervation is independent of changes in number of Or42a OSNs, consistent with previous reports that show glomerular innervation changes occur independently of the peripheral OSN cell bodies (Sachse et al. 2007, Chiang et al. 2009). The reduction of axonal innervation is presaged by striking elimination of OSN synaptic connections. Ultrastructural studies confirm synapse elimination due to heightened critical period odorant experience. Synapse remodeling requires Or42a receptor activity and NMDA receptor signaling. These results extend our knowledge of AL critical period remodeling by demonstrating how activity diminishes innervation of an olfactory glomerulus. At a molecular level, this remodeling likely relies on an unidentified *trans*-synaptic signal. The previously identified Wingless signaling pathway is not detectably involved (Chiang et al., 2009), and Notch *trans*-synaptic signaling is the future candidate (Kidd and Lieber, 2016). This work has important implications for our understanding of critical period remodeling of sensory circuits, and provides a step towards our understanding of the developing nervous system in both health and disease.

Acknowledgments

We are particularly grateful to Ilona Grunwald-Kadow (Munich Center for Neurosciences, Germany) for Or42a-mCD8:GFP lines, S. Laurence Zipursky (UCLA, USA) for STaR lines, Gregory Jefferis and Julian Ng (Cambridge University, UK) for UAS-miniSOG lines, the Bloomington *Drosophila* Stock Center (Indiana University, USA) for numerous fly lines, and the Developmental Studies Hybridoma Bank (University of Iowa, USA) for many antibodies. We thank Edward van Opstal and Jessamyn Perlmutter in the Bordenstein Lab for assistance with the quantitative PCR experiments. Transmission electron microscopy was performed within the Vanderbilt University Cell Imaging Shared Resource (supported by CA68485, DK20593). We thank Tyler Kennedy, Danielle Kopke, Jim Sears and Broadie Lab members for input on this manuscript. This study was supported by National Institutes of Health Grant MH084989 to K.B.

Chapter III

Neuron-Specific FMRP Roles in Experience-Dependent Remodeling of Olfactory Brain Innervation During an Early-life Critical Period[2]

Introduction

Abstract

Critical periods are developmental windows during which neural circuits effectively adapt to the new sensory environment. Animal models of Fragile X syndrome (FXS), a common monogenic autism spectrum disorder (ASD), exhibit profound impairments of sensory experience-driven critical periods. However, it is not known whether the causative Fragile X Mental Retardation Protein (FMRP) acts uniformly across neurons, or instead manifests neuron-specific functions. Here, we use the genetically-tractable *Drosophila* brain antennal lobe (AL) olfactory circuit of both sexes to investigate neuron-specific FMRP roles in the odorant experience-dependent remodeling of the olfactory sensory neuron (OSN) innervation during an early-life critical period. We find targeted OSN class-specific FMRP RNAi impairs innervation remodeling within AL synaptic glomeruli, whereas global *dfmr1* null mutants display relatively normal odorant-driven refinement. We find both OSN cell autonomous and cell non-autonomous FMRP functions mediate odorant experience-dependent remodeling, with AL circuit FMRP imbalance causing defects in overall glomerulus innervation refinement.

[2] This work has been adapted from a published paper under the same name. See additional information below.

This chapter is adapted from *Neuron-Specific FMRP Roles in Experience-Dependent Remodeling of Olfactory Brain Innervation During an Early-life Critical Period* published in The Journal of Neuroscience and has been reproduced with the permission of the publisher and my co-authors, Jacob Vest and Kendal Broadie. Golovin, R. M., Vest, J. & Broadie, K. Neuron-Specific FMRP Roles in Experience-Dependent Remodeling of Olfactory Brain Innervation During an Early-life Critical Period. J Neurosci JN-RM-2167-20 (2021) doi:10.1523/jneurosci.2167-20.2020. The authors declare no competing financial interests. Abbreviated Title: FMRP Roles in Critical Period Circuit Remodeling

This chapter is adapted from *Neuron-Specific FMRP Roles in Experience-Dependent Remodeling of Olfactory Brain Innervation During an Early-life Critical Period* published in The Journal of Neuroscience and has been reproduced with the permission of the publisher and my co-authors, Jacob Vest and Kendal Broadie. Golovin, R. M., Vest, J. & Broadie, K. Neuron-Specific FMRP Roles in Experience-Dependent Remodeling of Olfactory Brain Innervation During an Early-life Critical Period. J Neurosci JN-RM-2167-20 (2021) doi:10.1523/jneurosci.2167-20.2020. The authors declare no competing financial interests. Abbreviated Title: FMRP Roles in Critical Period Circuit Remodeling

We find OSN class-specific FMRP levels bidirectionally regulate critical period remodeling, with odorant experience selectively controlling OSN synaptic terminals in AL glomeruli. We find OSN class-specific FMRP loss impairs critical period remodeling by disrupting responses to lateral modulation from other odorant-responsive OSNs mediating overall AL gain control. We find that silencing glutamatergic AL interneurons reduces OSN remodeling, while conversely, interfering with the OSN class-specific $GABA_A$ signaling enhances remodeling. These findings reveal control of OSN synaptic remodeling by FMRP with neuron-specific circuit functions, and indicate how neural circuitry can compensate for global FMRP loss to reinstate normal critical period brain circuit remodeling.

Significance statement

Fragile X syndrome (FXS), the leading monogenic cause of intellectual disability (ID) and autism spectrum disorder (ASD), manifests severe neurodevelopmental delays. Likewise, FXS disease models display disrupted neurodevelopmental critical periods. In the well-mapped *Drosophila* olfactory circuit model, perturbing the causative Fragile X Mental Retardation Protein (FMRP) within a single olfactory sensory neuron (OSN) class impairs odorant-dependent remodeling during an early-life critical period. Importantly, this impairment requires activation of other OSNs, and the olfactory circuit can compensate when FMRP is removed from all OSNs. Understanding the neuron-specific FMRP requirements within a developing neural circuit, as well as the FMRP loss compensation mechanisms, should help us engineer FXS treatments. This work suggests FXS treatments could use homeostatic mechanisms to alleviate circuit-level deficits.

Background

Critical periods are time windows when brain circuitry is particularly susceptible to initial sensory input driving activity-dependent remodeling (Hubel and Wiesel, 1970; Hensch, 2005). This refinement is impaired in a range of heritable neurological disorders (Dölen et al., 2007;

Greenhill et al., 2015; Krishnan et al., 2015; Meredith, 2015). Fragile X syndrome (FXS) patients exhibit profound developmental delays (Bailey et al., 1998; Roberts et al., 2016), and FXS disease models display disrupted critical periods (Dölen et al., 2007; Contractor et al., 2015). This leading monogenic cause of both intellectual disability and autism spectrum disorder is characterized by hypersensitivity to sensory stimuli and childhood activity-dependent seizures (Crawford et al., 2001; Hersh et al., 2011; Contractor et al., 2015). The causal Fragile X Mental Retardation Protein (FMRP) regulates activity-dependent protein synthesis enabling experience-dependent synaptic plasticity (Brown et al., 2001; Darnell et al., 2001; Zalfa et al., 2003; Dölen et al., 2007), especially during critical periods (Bureau et al., 2008; He et al., 2014; Doll et al., 2017). Building evidence suggests specific FMRP roles in different brain circuits and cell types (Dahlhaus, 2018). Neuron class-specific FMRP genetic manipulations reveal striking differences controlling activity-dependent connectivity remodeling (Doll and Broadie, 2015), channel-binding (Brandalise et al., 2020), and translational control (Sawicka et al., 2019). Thus, it is crucial to test FMRP functions within specific neurons of defined brain circuits, and particularly FMRP roles during activity-dependent neural circuit remodeling in early sensory critical periods.

The *Drosophila* brain antennal lobe (AL) olfactory circuit provides an excellent model to study odorant sensory experience-dependent critical period remodeling (Devaud et al., 2003a). Numerous studies have shown that exposing young animals to selected odorants changes AL circuit structure and function (Devaud et al., 2003a; Sachse et al., 2007; Doll et al., 2015; Golovin et al., 2019; Chodankar et al., 2020). Early work established that critical period odor exposure alters olfactory sensory neuron (OSN) connectivity in activated AL regions (Devaud et al., 2003a; Sachse et al., 2007). Subsequent work showed that odorant exposure or optogenetic activity stimulation during just the first day following eclosion drives FMRP-dependent PN structural and functional remodeling (Doll and Broadie, 2015, 2016). Recently, we discovered a new form of experience-dependent OSN remodeling (Golovin et al., 2019), which reduces Or42a-expressing OSN innervation of a specific AL synaptic glomerulus following ethyl butyrate (EB) odorant

exposure during the first two days of life, but not a week later. Furthermore, this remodeling requires functional odorant receptors, but not OSN output, and is reversed following prolonged removal from the odorant (Golovin et al., 2019). Together these studies demonstrate that temporally restricted critical period odor experience refines AL glomeruli innervation and activity-dependent function. However, it remains unclear how reversible critical period OSN remodeling employs FMRP, and whether neuron-specific FMRP actions operate in AL circuit mechanisms.

Based on the key roles of FMRP in regulating critical period remodeling within the AL, we hypothesized an FMRP requirement in OSNs. To test this hypothesis, we assayed Or42a OSN innervation of the VM7 glomerulus following EB exposure during the well-mapped critical period (Golovin et al., 2019). Surprisingly, we find FMRP null mutants manifest normal OSN innervation refinement following EB exposure, whereas *Or42a*-targeted FMRP RNAi strongly attenuates experience-dependent remodeling. Consistently, global FMRP RNAi mimics null mutants by not affecting synaptic remodeling, whereas *Or42a*-targeted FMRP overexpression strongly enhances remodeling following EB exposure. These results indicate that balanced FMRP levels across EB-activated OSNs are required to tune LN input. We find that *Or42a*-targeted FMRP RNAi does not affect OSN remodeling after *Or42a*-specific optogenetic activation, but still attenuates circuit remodeling when Or42a OSN synaptic output is blocked. Importantly, we find that blocking glutamatergic AL interneuron neurotransmission as well as $GABA_AR$ signaling disrupts Or42a OSN remodeling, suggesting that imbalanced FMRP levels perturb LN to Or42a OSN activity. Together these results reveal neuron-specific FMRP functions in AL circuit critical period remodeling, and demonstrate that this circuit can restore normal function in the absence of FMRP.

Materials and Methods

Drosophila genetics

All animals were reared at 25°C prior to odor/light exposure. Animals were reared on a 12:12 hr light/dark cycle except for light exposure experiments, for which animals were kept in darkness. All animals were fed on the standard *Drosophila* cornmeal molasses food. Initial experiments used animals of both sexes, but males show reduced critical period OSN innervation remodeling compared to females. Therefore, later experiments were conducted using only females in order to control the remodeling variability, and ensure a robust response to the odorant-dependent critical period OSN remodeling across the many experimental genotypes. All genotypes were confirmed with visible markers and/or PCR. Transgenic controls include w^-; UAS-mCD8::GFP/+; *Or42a*-Gal4/+, w^-; *Or42a*-mCD8::4xGFP/*Or42a*-mCD8::4xGFP, w^-; *Or42a*-mCD8::4xGFP/+; *Or42a*-mCD8::4xGFP/+ and w^-; *Or42a*-mCD8::4xGFP/*Or42a*-mCD8::4xGFP. The genetic lines used for each figure are listed in Table 1.

Table 1 – List of Experimental Genotypes

Figure	Genotype	References
Fig. 1A	*w⁻; +/+; Or42a*-Gal4,UAS-*GtACR1::eYFP*/ *Or42a*-Gal4,UAS-*GtACR1::eYFP*	BDSC#9969 Fishilevich and Vosshall, 2005 Mohammad et al., 2017
Fig. 1B	*w⁻*; +/+;*Or42a*-Gal4,UAS-*Cschrimson::mVenus*/ *Or42a*-Gal4,UAS-*Cschrimson::mVenus*	BDSC#9969 Fishilevich and Vosshall, 2005 BDSC#55136 Klapoetke et al., 2014
Fig. 1C	*Peb*-Gal4/*w⁻*; UAS-mCD8::RFP/+; *Or42a*-mCD8::4xGFP/ *Or42a*-mCD8::4xGFP	BDSC#80570 Sweeney et al., 2007 BDSC#32219 Barret Pfeiffer, Janelia, HHMI Stephan et al., 2012
Fig. 1D	NP3481-Gal4(VM7 PNs)/ *w⁻*;UAS-mCD8::RFP/+; *Or42a*-mCD8::4xGFP/*Or42a*-mCD8::4xGFP	Hayashi et al., 2002 BDSC#32219 Barret Pfeiffer, Janelia, HHMI Stephan et al., 2012
Fig. 1E	*Peb*-Gal4/*w⁻*; UAS-mCD8::RFP/+; *Or42a*-mCD8::4xGFP/ *Or42a*-mCD8::4xGFP	BDSC#80570 Sweeney et al., 2007 BDSC#32219 Barret Pfeiffer, Janelia, HHMI Stephan et al., 2012
Fig. 1F	*w⁻*;GH146-Gal4/UAS-mCD8::GFP;+/+	BDSC#30026 Stocker et al., 1997 BDSC#5137 Lee and Luo, 1999
Fig. 1G	*w⁻*;NP1227-Gal4/UAS-mCD8::GFP;+/+	Hayashi et al., 2002 BDSC#5137 Lee and Luo, 1999
Fig. 1H	*w⁻*;UAS-mCD8::GFP/+;+/+;OK107-Gal4/+	Connolly et al., 1996 BDSC#5137 Lee and Luo, 1999
Fig. 2A	*w⁻*;UAS-mCD8::GFP/+;*Or42a*-Gal4/+	BDSC#5137 Lee and Luo, 1999 BDSC#9969 Fishilevich and Vosshall, 2005
Fig. 2A	*w⁻*;UAS-mCD8::GFP/+; *Or42a*-Gal4,*dfmr1$^{\Delta 50M}$*/ *dfmr1$^{\Delta 50M}$*	DSC#5137 Lee and Luo, 1999 BDSC#9969 Fishilevich and Vosshall, 2005 BDSC#6930 Zhang et al., 2001b
Fig. 2A	*w⁻*;UAS-mCD8::GFP/+; *Or42a*-Gal4/UAS-*dfmr1* RNAi (1-1-7)	BDSC#5137 Lee and Luo, 1999 BDSC#9969 Fishilevich and Vosshall, 2005 Bolduc et al., 2008
Fig. 2B	*w⁻*; UAS-mCD8::GFP/+; *Or42a*-Gal4/+	BDSC#5137 Lee and Luo, 1999 BDSC#9969 Fishilevich and Vosshall, 2005
Fig. 2B	*w⁻*; UAS-mCD8::GFP/+; *Or42a*-Gal4,*dfmr1$^{\Delta 50M}$*/ *dfmr1$^{\Delta 50M}$*	DSC#5137 Lee and Luo, 1999 BDSC#9969 Fishilevich and Vosshall, 2005 BDSC#6930 Zhang et al., 2001b
Fig. 2B	*w⁻*; UAS-mCD8::GFP/+; *Or42a*-Gal4/UAS-*dfmr1* RNAi TRiP.GL00075	BDSC#5137 Lee and Luo, 1999 BDSC#9969 Fishilevich and Vosshall, 2005 BDSC#35200 Flockhart et al., 2006
Fig. 3A,B	*w⁻*;UAS-mCD8::GFP/+;*Or42a*-Gal4/+	BDSC#5137 Lee and Luo, 1999 BDSC#9969 Fishilevich and Vosshall, 2005
Fig.3 A,B	*w⁻*;UAS-mCD8::GFP/+; *Or42a*-Gal4/UAS-*dfmr1* RNAi (2-1)	BDSC#5137 Lee and Luo, 1999 BDSC#9969 Fishilevich and Vosshall, 2005 Bolduc et al., 2008
Fig. 4A,B	*w⁻*; *Or42a*-mCD8::4xGFP/ *Or42a*-mCD8::4xGFP;UH1-Gal4/+	Stephan et al., 2012 Wodarz et al., 1995
Fig. 4A,B	*w⁻*; *Or42a*-mCD8::4xGFP/*Or42a*-mCD8::4xGFP;UH1-Gal4/ UAS- *dfmr1* RNAi TRiP.GL00075	Stephan et al., 2012; Wodarz et al., 1995 BDSC#35200 Flockhart et al., 2006
Fig. 4A,B	*w⁻*; *Or42a*-mCD8::4xGFP/ *Or42a*-mCD8::4xGFP;*dfmr1^{B55}*/*dfmr1^{B55}*	Stephan et al., 2012 Inoue et al., 2002
Fig. 5A	*w⁻*; UAS-mCD8::GFP/+;*Or42a*-Gal4/+	BDSC#5137 Lee and Luo, 1999 BDSC#9969 Fishilevich and Vosshall, 2005
Fig. 5A	*w⁻*; UAS-mCD8::GFP/+; *Or42a*-Gal4/UAS-FMRP 9557-3	BDSC#5137 Lee and Luo, 1999 BDSC#9969 Fishilevich and Vosshall, 2005 BDSC#6931 Zhang et al., 2001b
Fig. 6A	*Peb*-Gal4/*w⁻*; *Or42a-Or42a*-mCD8::4xGFP/+; *Or42a-Or42a*-mCD8::4xGFP/+	BDSC#80570 Sweeney et al., 2007 Stephan et al., 2012
Fig. 6A	*Peb*-Gal4/*w⁻*; *Or42a-Or42a*-mCD8::4xGFP/+; *Or42a-Or42a*-mCD8::4xGFP/UAS-*dfmr1* RNAi TRiP.GL00075	BDSC#80570 Sweeney et al., 2007 Stephan et al., 2012 BDSC#35200 Flockhart et al., 2006
Fig. 6C	*w⁻*; *Or42a-Or42a*-mCD8::4xGFP/*Or42a-Or42a*-mCD8::4xGFP; Orco-Gal4/+	Stephan et al., 2012 BDSC#23292 John Carlson
Fig. 6C	*w⁻*; *Or42a-Or42a*-mCD8::4xGFP/*Or42a-Or42a*-mCD8::4xGFP; Orco-Gal4/ UAS-FMRP 9557-3	Stephan et al., 2012 BDSC#23292 John Carlson BDSC#6931 Zhang et al., 2001b
Fig. 7A	*w⁻*; +/+; *Or42a-Or42a*-Gal4,UAS-*Cschrimson::mVenus*/ *Or42a-Or42a*-Gal4,UAS-*Cschrimson::mVenus*	BDSC#9969 Fishilevich and Vosshall, 2005 BDSC#55136 Klapoetke et al., 2014
Fig. 7C	*w⁻*; UAS-mCD8::GFP/+; *Or42a-Or42a*-Gal4/+	BDSC#5137 Lee and Luo, 1999 BDSC#9969 Fishilevich and Vosshall, 2005
Fig. 7C	*w⁻*; UAS-mCD8::GFP/+; *Or42a-Or42a*-Gal4,*orco^{2}*/*orco^{1}*	BDSC#5137Lee and Luo, 1999 BDSC#9969Fishilevich and Vosshall, 2005 BDSC#23129 and #23130 Larsson et al. 2004
Fig. 7C	*w⁻*; UAS-mCD8::GFP/UAS-Orco; *Or42a-Or42a*-Gal4,*orco^{2}*/*orco^{1}*	BDSC#5137 Lee and Luo, 1999 BDSC#9969 Fishilevich and Vosshall, 2005 BDSC#23129, #23130 and BDSC#23145 Larsson et al. 2004
Fig. 8A,D	*w⁻*/*y^{1}*,*v^{1}*; +/+; *Or42a-Or42a*-Gal4,UAS-*Cschrimson::mVenus*/TRiP control	BDSC#9969 Fishilevich and Vosshall, 2005 BDSC#55136 Klapoetke et al., 2014 BDSC#36303 Flockhart et al., 2006
Fig. 8B,E	*w⁻*/ *y^{1}*,*v^{1}*,*sc^{1}*,*sev^{21}*; +/+; *Or42a-Or42a*-Gal4,UAS-*Cschrimson::mVenus*/ UAS-*dfmr1* RNAi TRiP.GL00075	BDSC#9969 Fishilevich and Vosshall, 2005 BDSC#55136 Klapoetke et al., 2014

		BDSC#35200 Flockhart et al., 2006
Fig. 9A	*w*⁻; UAS-mCD8::GFP/+; *Or42a*-*Or42a*-Gal4/+	BDSC#5137 Lee and Luo, 1999 BDSC#9969 Fishilevich and Vosshall, 2005
Fig. 9A	*w*⁻; UAS-mCD8::GFP/+; *Or42a*-*Or42a*-Gal4/ UAS-*dfmr1* RNAi TRiP.GL00075	BDSC#5137 Lee and Luo, 1999 BDSC#9969 Fishilevich and Vosshall, 2005 BDSC#35200 Flockhart et al., 2006
Fig. 9A	*w*⁻; UAS-mCD8::GFP/ UAS-TeTxLc; *Or42a*-*Or42a*-Gal4/+	BDSC#5137 Lee and Luo, 1999 BDSC#9969 Fishilevich and Vosshall, 2005 BDSC#28838 Sweeney et al. 1995
Fig. 9A	*w*⁻; UAS-mCD8::GFP/ UAS-TeTxLc; *Or42a*-*Or42a*-Gal4/ UAS-*dfmr1* RNAi TRiP.GL00075	BDSC#5137 Lee and Luo, 1999 BDSC#9969 Fishilevich and Vosshall, 2005 BDSC#28838 Sweeney et al. 1995 BDSC#35200 Flockhart et al., 2006
Fig. 10A	*w*⁻; UAS-mCD8::GFP/+; *Or42a*-*Or42a*-Gal4/+	BDSC#5137 Lee and Luo, 1999 BDSC#9969 Fishilevich and Vosshall, 2005
Fig. 10A	*w*⁻; UAS-mCD8::GFP/ UAS-TeTxLc; *Or42a*-*Or42a*-Gal4/+	BDSC#5137 Lee and Luo, 1999 BDSC#9969 Fishilevich and Vosshall, 2005 BDSC#28838 Sweeney et al. 1995
Fig. 11A,B	NP3481-Gal4(VM7 PNs)/ *w*⁻; UAS-mCD8::RFP/+; *Or42a*-*Or42a*-mCD8::4xGFP/*Or42a*-*Or42a*-mCD8::4xGFP	Hayashi et al., 2002 BDSC#32219 Barret Pfeiffer, Janelia, HHMI Stephan et al., 2012
Fig. 12A	*w*⁻; *Or42a*-*Or42a*-mCD8::4xGFP/+; *Or42a*-*Or42a*-mCD8::4xGFP/+;OK107-Gal4/+	Stephan et al., 2012 Connolly et al., 1996
Fig. 12A	*w*⁻; *Or42a*-*Or42a*-mCD8::4xGFP/+; *Or42a*-*Or42a*-mCD8::4xGFP/UAS-TeTxLc;OK107-Gal4/+	Stephan et al., 2012 Connolly et al., 1996 Wang et al., 2012
Fig. 12C	*w*⁻; *Or42a*-*Or42a*-mCD8::4xGFP/ *Or42a*-*Or42a*-mCD8::4xGFP;MB247-Gal4/+	Stephan et al., 2012 BDSC#50742 Zars et al. 2000
Fig. 12C	*w*⁻; *Or42a*-*Or42a*-mCD8::4xGFP/ *Or42a*-*Or42a*-mCD8::4xGFP;MB247-Gal4/UAS-TeTxLc	Stephan et al., 2012 BDSC#50742 Zars et al. 2000 Wang et al., 2012
Fig. 13A	*w*⁻; *Or42a*-*Or42a*-mCD8::4xGFP/*Or42a*-*Or42a*-mCD8::4xGFP;+/+	Stephan et al., 2012
Fig. 13A	*w⁻; Or42a-Or42a-mCD8::4xGFP/Or42a-Or42a-mCD8::4xGFP; Nmdar1*^{MI11796}*/ Nmdar1*^{MI11796}	Stephan et al., 2012
Fig. 13A	*w⁻; Or42a-Or42a-mCD8::4xGFP/Or42a-Or42a-mCD8::4xGFP; Nmdar1*^{EP331}*/ Nmdar1*^{MI11796}	Stephan et al., 2012 BDSC#56692 Nagarkar-Jaiswal et al., 2015 BDSC#17112 Xia et al., 2005
Fig. 14A	*w*⁻; UAS-mCD8::GFP/+; *Or42a*-*Or42a*-Gal4/+	BDSC#5137 Lee and Luo, 1999 BDSC#9969 Fishilevich and Vosshall, 2005
Fig. 14A	*w*⁻; UAS-mCD8::GFP/+; *Or42a*-*Or42a*-Gal4/UAS-*Rdl* RNAi 8-10J	BDSC#5137 Lee and Luo, 1999 BDSC#9969 Fishilevich and Vosshall, 2005 Liu et al., 2007

Odorant exposure

Critical period odorant exposure was done as we previously reported (Golovin et al., 2019). Briefly; Animals were staged as dark pupa (4 days after puparium formation at 25°C), separated based on both the sex and genotype. Fine wire mesh caps were secured onto the animal vials to allow good airflow, and the vials were then placed within larger airtight containers (3700 mL, Glasslock). In 1.5 mL microcentrifuge tubes, 1 mL of mineral oil (Sigma-Aldrich) was placed alone (vehicle control), or with 10%, 15%, 20% or 25% ethyl butyrate (EB; % v/v in mineral oil; Sigma-Aldrich). Containers were placed in humidified 23°C incubators with a 12:12 hr light/dark cycle. After 24 hrs, the adult animals were rapidly transferred to new vials in clean chambers with a fresh odorant supply. Animals were then kept in the odorant chambers for another 24 hrs. The entire odorant exposure period was two days; 0-2 days post-eclosion (dpe).

Light exposure

The optogenetic light exposure matched the above critical period odorant exposure paradigm. Dark-reared animals were staged as dark pupa, separated based on sex and genotype, and then transferred to a petri dish (35x10 mm Falcon, Corning, NY) with 3mL of food. The petri dish was then placed in the same containers used above (3700 mL, Glasslock) in dark, humidified 23°C incubators. Light was supplied through a custom-built cyan LED array (515nm) controlled by an Arduino Uno (Arduino) using a custom script. The light exposure was 5Hz 50ms pulses (337μW/mm^2). After 24 hrs, animals were rapidly transferred to a new dish in a clean chamber. The entire adult animal light exposure period was 2 days; 0-2 days post-eclosion (dpe).

Confocal imaging

Staged animals were anesthetized on ice for at least 1-2 mins, and then brains were dissected using fine forceps (Dumont #5) in physiological saline ([in mM]: 128 NaCl, 2 KCl, 4 $MgCl_2$, 1.8 $CaCl_2$, 64.6 sucrose, 5 HEPES, pH 7.2; Sigma-Aldrich). Dissected brains were fixed for 30 mins at room temperature (RT) in 4% PFA (EMS)/4% sucrose in PBS, pH 7.4 (Invitrogen). Brains were washed 3× with PBS and then blocked for 1 hr in 1% BSA (Sigma-Aldrich) in PBS-T (0.2% Triton X-100 in PBS; Fisher Chemical). Brains were then incubated with primary antibodies diluted in 0.2% BSA in PBS-T at 4°C overnight (O/N). Primary antibodies used were as follows: rabbit anti-GFP (Abcam 290; 1:3000), rat anti-RFP (Chromotek 5F8; 1:500), mouse anti-dFMRP (Abcam a10299 [6A15]; 1:125) and mouse anti-BRP (Developmental Studies Hybridoma Bank (DSHB), nc82; 1:50). Brains were washed 3× for 20 mins with PBS-T and then incubated O/N with secondary antibodies. Secondary antibodies used were as follows: AlexaFluor-488 goat anti-rabbit, AlexaFluor-555 donkey anti-mouse and AlexaFluor-546 goat anti-rat (all at 1:250). Brains were then washed in PBS-T 3× for 20 mins, followed by PBS 1× for 20 mins. Brains were then rinsed with dH_2O and mounted in Fluoromount (EMS 17984-25) on a glass slide (ProbeOn Microscope Slides, Fisherbrand) with a glass coverslip (No. 1.5H, Carl Zeiss). Double-sided adhesive tape (Scotch) was used to raise the coverslips above the brains, and clear nail polish (Sally Hansen) was used to seal the coverslip to the slide. For maxillary palp studies, whole proboscises were dissected and processed as above, except with longer fixation (45 mins), longer primary/secondary antibody incubations (38-42 hrs) and no double-sided tap used for mounting. The whole head image (see Figure 14) was taken using an iPhone 6 (Apple) through the oculars of a Leica dissecting scope with both white light and filtered mercury lamp light for illumination. Confocal images were collected on a 510 META laser-scanning confocal microscope (Carl Zeiss) with 40× and 63× oil-immersion objectives. Images taken with the 40× lens were collected at 1024 × 1024 resolution with a *Z*-slice of 1 µm thickness. Images taken with the 63× lens were collected

at 2048 × 2048 resolution with a *Z*-slice thickness of 0.8 µm. The microscope and imaging settings were kept constant within every experiment.

Quantification

Antennal lobe glomeruli measurements were done as previously reported (Golovin et al., 2019). Briefly, blinded brain images were visualized in ImageJ (NIH) with the quantification channel isolated. A maximum intensity projection that captured the whole VM7 glomerulus was used to generate a region of interest (RoI). This RoI was used with the FIJI plugin 3D Object Counter (Schindelin et al., 2012) to quantify the RoI volume. For every experiment, the threshold was set at a constant value that minimized the noise. In controls, the 3D Object Counter output typically contained two RoIs, which were summed. In experimental conditions, when the glomerular RoI was more discontinuous, all the regions were summed. To control for variations of signal across the different labeling constructs, antibody aliquots and experimental days, glomerulus volumes were normalized to the control mean for each experimental replicate. For the maxillary palp, blinded Z-stack images were analyzed using ImageJ. A maximum intensity projection was used to capture all the Or42a OSNs. For the fluorescence intensity measurements, one RoI for each *Or42a*-positive soma was generated using the GFP signal. ImageJ was then used to quantify the mean intensity for each soma in both the GFP and FMRP channels.

Statistics

All tests were done using *Prism 8* (GraphPad). For comparisons with ≥2 genotypes, a two-way ANOVA was used with odorant/light and genotype as independent variables. Follow-up pairwise comparisons were done using t-tests, with Sidak's multiple comparisons correction. Interactions between genotype and odorant/light exposure were tested with the two-way ANOVA interaction term. A ROUT outlier test was done for data with Q set to 1%. Some genotypes showed altered basal glomerulus innervation volumes in the vehicle-exposed control animals. While the ANOVA

post-hoc test can distinguish whether the EB-treated means are different, it does not account for differences in glomerulus volume of vehicle-treated controls. With only 2 independent variables, an ANOVA (2x2) interaction term can be attributed to the specific genotype/odorant exposure. However, if >2 independent variables occur, the interaction term cannot be used for pairwise comparisons between genotypes. Therefore, in all the cases with >2 independent variables, a linear regression with *t*-tests comparing pairwise interaction terms was used to assess EB treatment effects while controlling for any changes in the basal glomerulus innervation volume. Regression coefficients for each genotype interaction term represent the differences in the treatment effect on the experimental genotype compared to the control genotype. If the interaction term of an experimental genotype were zero, this would indicate the effect of treatment had not changed in the genotype compared to the matched control (glomerular innervation changed by the same amount). If the interaction term were significantly greater than zero, this would indicate that the treatment had not reduced innervation as much in the experimental condition as in control. If the interaction term were significantly less than zero, this would indicate that the treatment had reduced the innervation by more in the experimental condition compared to the control. To display regression analyses, bar values of each genotype show the difference between vehicle and treatment conditions. Error bars are the sum of the error of the EB effect regression plus the error of the genotype effect regression. The sample size (n) is the number of brains, except only Figure 23B,C, where it is the number of maxillary palps. Figure 23B,C employ *t*-tests. Pairwise comparisons in Figure 24C are two Sidak's corrected *t*-tests, while the lines in Figure 24D are linear regressions. ANOVAs are displayed as scatter plots with mean ± SEM. The EB effects from the linear regression analyses are displayed as bar graphs with mean ± standard error of the regression (SER). Significance is shown as not significant (N.S.; $p>0.05$) or significant at $p<0.05$ (*), $p<0.01$ (**) and $p<0.001$ (***).

Results

OSN-specific FMRP loss disrupts odor experience critical period remodeling of AL innervation

The well-mapped and genetically tractable neuron classes of the *Drosophila* antennal lobe (AL) olfactory circuit make it a very powerful system to study the mechanisms of sensory experience-dependent remodeling. The AL is the first brain synaptic node of the olfactory circuit (Fig. 14A,B; Wilson, 2013). Odorants transduced by olfactory sensory neurons (OSNs) in both the antenna and maxillary palps (Fig. 14C) project axons along antennal and labial nerves (Fig. 14B, bottom arrow), respectively, to innervate OSN-specific AL synaptic glomeruli (Fig. 14D; Fig. 14E, top left; Wilson, 2013). Each OSN generally expresses a single olfactory receptor (e.g. Or42a, Fig. 14A-D), in addition to the pan-OSN Orco co-receptor (Larsson et al., 2004; Couto et al., 2005). Each AL glomerulus receives convergent OSNs that express only that single olfactory receptor (Fig. 14B, boxed region; Fig. 14D). Within each AL glomerulus, OSNs synapse onto projection neurons (PNs; Fig. 14D; Fig. 14E, top right). PNs subsequently send olfactory information to the central brain mushroom body and lateral horn (Fig. 14B; Jefferis et al., 2002; Marin et al., 2002). Within the AL, multiple local interneurons (LNs) synapse broadly to provide modulation of OSN-PN excitatory (cholinergic) connections. The LNs release a variety of neuromodulators that can both inhibit and excite this olfactory neurotransmission, including GABA (Fig. 14E, bottom left) and glutamate (Fig. 14E, bottom right; Chou et al., 2010; Wilson, 2013). In addition, LNs can also signal through gap junction mediated electrical synapses (Huang et al., 2010). OSN-AL synaptic connectivity is strongly altered by critical period olfactory experience, providing an ideal system to test circuit level FMRP roles in different neuron classes during synaptic remodeling.

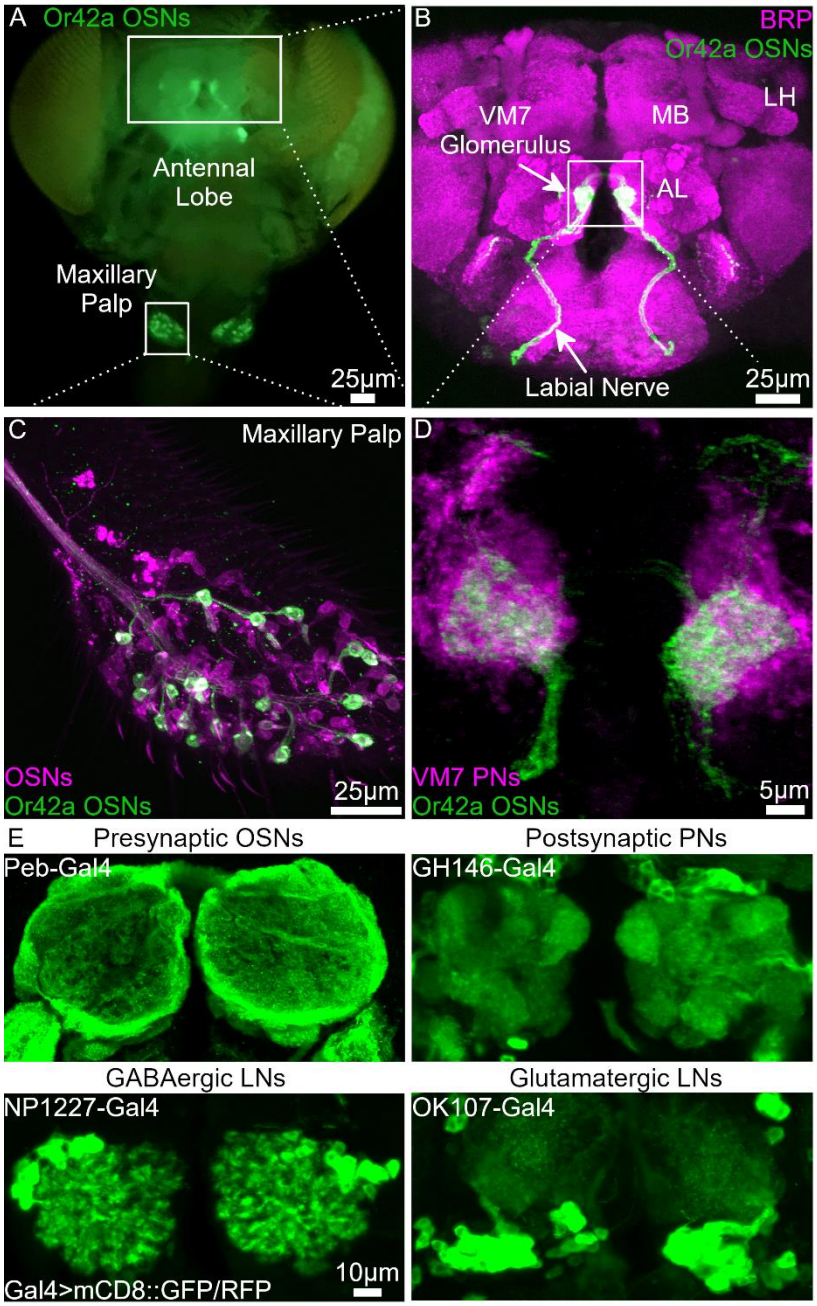

Figure 14: Maxillary palp to antennal lobe olfactory circuitry and neuron class-specific drivers **A)** Whole *Drosophila* head showing Or42a olfactory sensory neuron (OSN) innervation pattern (*Or42a*-Gal4>UAS-GtACR1-eYFP; green). OSN cell bodies in the maxillary palp (MP) project to the antennal lobe (AL). **B)** Or42a OSN innervation (*Or42a*-Gal4>UAS-*CsChrimson::mVenus*; green) of central brain (larger box in A) co-labeled for presynaptic Bruchpilot (BRP; magenta). Or42a OSNs extend axons via the labial nerve (bottom arrow) to terminate in the VM7 glomeruli (top arrow) of each AL. AL glomeruli postsynaptic projection neurons (PNs) send axons to the mushroom body (MB) and lateral horn (LH) in each brain hemisphere. **C)** Or42a OSN cell bodies (*Or42a*-mCD8-4xGFP; green) in MP (smaller box in A) co-labeled for all OSN somata (*Pebbled (Peb)*-Gal4>UAS-mCD8::RFP; magenta). **D)** Or42a OSN axonal termini (*Or42a*-mCD8-4xGFP; green) and postsynaptic PNs (NP3481-Gal4>UAS-mCD8::RFP; magenta) in the AL VM7 (white box in B). **E-H)** Neuron class-specific Gal4 drivers expressing UAS-mCD8::GFP in **E)** presynaptic OSNs (*Peb*-Gal4), **F)** postsynaptic PNs (GH146-Gal4), **G)** GABAergic local interneurons (LNs, NP1227-Gal4) and **H)** Glutamatergic LNs (OK107-Gal4) of the brain AL.

We have reported that odorant exposure to ethyl butyrate (EB) during the critical period (0-2 days post eclosion; dpe) causes a large-scale reduction of Or42a OSN innervation of the AL VM7 glomerulus (Fig. 14A-D; Golovin et al., 2019). Based on previous work from our lab and others on the role of FMRP in mediating AL circuit remodeling (Sudhakaran et al., 2014; Doll and Broadie, 2015), and FMRP roles in regulating the critical period plasticity in other neural circuits (Dölen et al., 2007; Bureau et al., 2008; Gonçalves et al., 2013), we hypothesized that FMRP has a role in OSN remodeling. To test this idea, we assayed Or42a OSN innervation of the AL VM7 glomerulus following 0-2 dpe critical period EB exposure in *dfmr1* null mutants (*dfmr1*^{50M}), Or42a OSN-targeted *dfmr1* RNAi, and matched genetic background controls. To visualize Or42a OSN innervation of the VM7 glomerulus, the membrane marker UAS-mCD8::GFP was driven with *Or42a*-Gal4 (Fig. 15). Innervation volume was assayed between animals exposed to the mineral oil vehicle compared to EB dissolved in the oil at lower concentrations (15% EB, Fig. 15A) or higher concentrations (25% EB, Fig. 15B) during the 0-2 dpe critical period. The three genotypes compared were the transgenic control (*Or42a*-Gal4>mCD8::GFP; Fig. 15A,B, top panels), *dfmr1* null mutant (*dfmr1*^{50M}; Fig. 15A,B, middle panels), and Or42a OSN-targeted *dfmr1* knockdown (*Or42a*-Gal4>*dfmr1* RNAi; Fig. 15A,B, bottom panels). Sample images of Or42a OSN AL innervation, quantified VM7 glomerular innervation volumes, and quantified genotype effect comparisons are all shown in Figure 15.

Control animals exposed to EB during the 0-2 dpe critical period show striking reduction of Or42a OSN innervation of the VM7 glomerulus (Fig. 15A,B, top). In contrast to our working hypothesis, animals completely lacking FMRP (*dfmr1*^{50M} null) exhibit a similar large reduction in VM7 innervation following critical period EB odorant exposure, despite an increase in the basal glomerulus innervation (Fig. 15A,B middle). In stark contrast, Or42a OSN-targeted FMRP RNAi strongly suppresses the EB odorant-dependent loss of Or42a OSN innervation, supporting the hypothesis (Fig. 15A,B, bottom). An ANOVA (3x2) was used to compare the effects on the three genotypes exposed to vehicle control versus 15% EB (Fig. 15C). Quantification of the Or42a OSN

innervation volume shows significant effects of both genotype (F(2,123)=17.20, p=2.59e-7) and EB exposure (F(1,123)=14, p=0.0003), with a significant interaction between genotype and odorant exposure (F(2,123)=12.21, p=1.45e-5). The remodeling is EB concentration-dependent, as increasing the odorant concentration (25% EB) causes a larger innervation reduction (Fig. 15A vs. 2B). An ANOVA (3x2) comparing transgenic control, *dfmr1* null, and Or42a OSN-targeted FMRP RNAi shows significant effects of both genotype (F(2,170)=29.09, p=1.363e-11) and EB exposure (F(1,170)=329.7, p=3.113e-59), with a significant interaction between the genotype and the odorant (F(2, 170)=33.20, p=6.732e-13; Fig. 15E). Quantitative analyses with pairwise comparisons as well as linear regression models further indicate that Or42a OSN-specific FMRP loss suppresses critical period remodeling.

Unpaired t-tests with Sidak's corrections were done to compare the ANOVA conditions. In controls, VM7 innervation is significantly reduced following 15% EB critical period exposure (normalized vehicle control (oil) 1.0 ± 0.046 (n=24 brains) vs. 15% EB 0.592 ± 0.065 (n=23); t(123)=3.331, p=0.017; Fig. 15C, bottom left bar). A stronger reduction (91.2% vs. 40.8%) occurs with 25% EB (oil control 1.0 ± 0.033 (n=37 brains) vs. 25% EB 0.088 ± 0.019 (n=32); t(170) = 12.47, p=1.38e-24; Fig. 15E, bottom left). Compared to vehicle control animals, *dfmr1* nulls have significantly greater VM7 basal innervation in both 15% EB (oil *dfmr1* null 1.698 ± 0.2 (n=12); t(123)=4.705, p=0.0001; Fig. 15C, middle bar) and 25% EB experiments (oil *dfmr1* null 1.41 ± 0.098 (n=28); t(170) = 5.41, p=3.18e-6; Fig. 15E, middle bar). Nevertheless, there is still a strong reduction in innervation following critical period EB odorant exposure (Fig. 15A,B, middle). Following 15% EB, null mutants show a significant loss of innervation volume (oil *dfmr1* null vs. 15% EB *dfmr1* null 1.03 ± 0.12 (n=17); t(123)=4.224, p=0.0007; Fig. 15C, bottom center bar). Likewise, null *dfmr1* VM7 glomerular innervation is significantly reduced following 25% EB exposure compared to the oil-exposed controls (25% EB *dfmr1* null 0.12 ± 0.041 (n=19); t(170)=14.33, p=7.12e-30; Fig. 15E, bottom center). Similar to control animals, the effect of the higher 25% EB exposure is greater than the lower 15% EB exposure in the *dfmr1* null mutants

(91.5% vs. 39.3%). These results indicate FMRP loss has an experience-independent function regulating basal glomerulus innervation, but little impact on experience-dependent remodeling.

In direct contrast to *dfmr1* nulls, FMRP RNAi targeted only to Or42a OSNs using two different constructs (1-1-7, Bolduc et al., 2008; TRiP GL00075, Flockhart et al., 2006; Greenblatt and Spradling, 2018) strongly impairs critical period remodeling (Fig. 15A,B, bottom). Innervation volume in vehicle knockdown animals is not significantly different from controls (15% EB: oil Or42a OSN-targeted FMRP RNAi 1.01 ± 0.069 (n=27); t(123)=0.1197, p>0.9999; 25% EB: oil Or42a OSN-targeted FMRP RNAi 1.12 ± 0.053 (n=32); t(170)=1.663, p=0.79). Moreover, 15% EB critical period exposure does not significantly alter VM7 innervation (15% EB 1.23 ± 0.09 (n=26); t(123)=1.841, p=0.6527; Fig. 15C, bottom right bar). At 25% EB, innervation remodeling is also suppressed with Or42a OSN-targeted FMRP knockdown compared to vehicle controls (25% EB 0.78 ± 0.064 (n=28); t(170)=4.335, p=0.0004; Fig. 15E, bottom right). Since targeted FMRP removal in Or42a OSNs significantly reduces odorant experience-dependent remodeling of VM7 innervation, EB exposure in the knockdown condition was directly compared to the EB control to show a significantly reduced effect on VM7 innervation, at both 15% and 25% EB concentrations (15% EB control vs. 15% EB Or42a OSN-targeted FMRP RNAi; t(123)=5.279, p=8.52e-6; Fig. 15C top bar; 25% EB control vs. 25% EB Or42a OSN-targeted FMRP RNAi; t(170)=8.847, p=1.69e-14; Fig. 15E, top). The inability of FMRP RNAi to completely block OSN remodeling after 25% EB exposure could indicate that rather than impairing the mechanism directly it alters the OSN response to the odorant, thereby increasing the stimulus threshold needed for innervation loss. These results suggest that Or42a OSN-specific FMRP removal within the AL circuit has a significant impact on odorant experience critical period remodeling, but required further analyses to account for variations in basal innervation volume.

Differences in basal OSN innervation between genotypes complicates comparing the EB-exposed conditions. Therefore, a linear regression model was used to analyze EB exposure compared to vehicle, while controlling for genotype differences (see Methods). Unpaired t-tests

of the null hypothesis that genotype does not affect the treatment relationship were done compare regression coefficients for each interaction term. Regression analyses show *dfmr1* null interaction with 15% EB exposure is not significant (*dfmr1x*15% EB β=-0.26 ± 0.2; t(123)=1.302, p=0.1953; Fig. 15D, top), indicating no significant impact from global FMRP loss on EB exposure effects. With 25% EB, the *dfmr1* null regression coefficient becomes significant (β=-0.38 ± 0.12; t(170)=3.267, p=0.0013; Fig. 15F, top), indicating FMRP removal augments innervation loss from odorant exposure. Consistent with the pairwise comparisons between the control genotype and Or42a OSN-targeted FMRP RNAi, regression analyses show significant interactions at both 15% and 25% EB (Or42a OSN-targeted FMRP RNAix15% EB β=0.62 ± 0.17; *t*(123)=3.687, *p*=0.0003; Or42a OSN-targeted FMRP RNAix25% EB β=0.57 ± 0.11; *t*(170)=5.334, *p*=4.54e-6; Fig. 15D,F, bottom). Together, these results indicate that FMRP has two roles; 1) a cell non-autonomous role regulating basal Or42a OSN-VM7 innervation, with *dfmr1* nulls displaying experience-independent increased glomeruli innervation, and 2) an OSN cell autonomous role regulating critical period olfactory experience-dependent remodeling, with *Or42a*-specific FMRP removal, but not global FMRP loss, limiting innervation refinement.

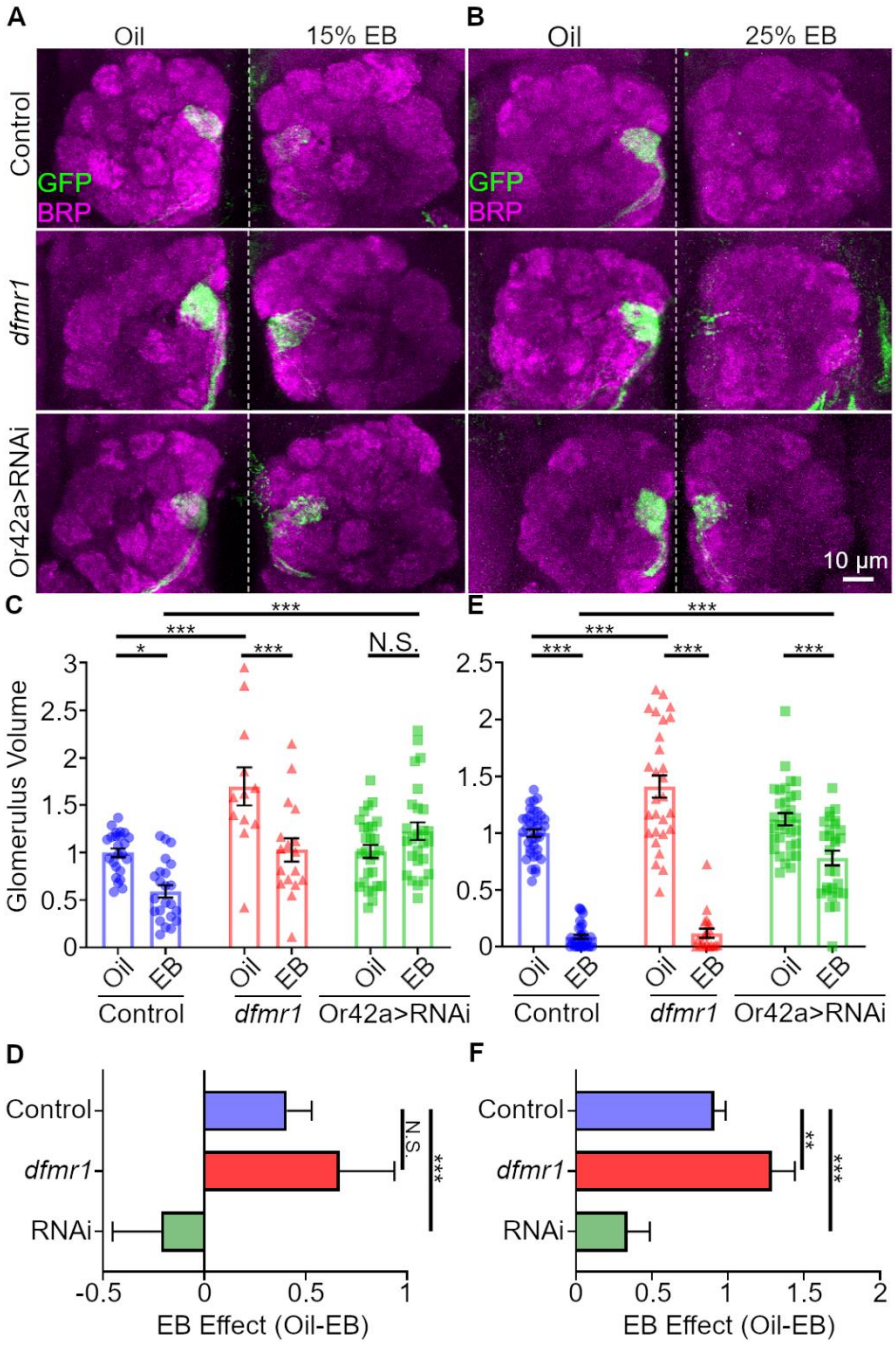

Figure 15: Or42a OSN-specific FMRP loss impairs VM7 innervation critical period remodeling **A-B)** Representative confocal maximum intensity projections of antennal lobe (AL) innervation by Or42a olfactory sensory neurons (OSNs; *Or42a*-Gal4>UAS-mCD8::GFP; green) co-labeled for presynaptic Bruchpilot (BRP; magenta). Exposure to mineral oil vehicle (Oil; left) or odorant (ethyl butyrate; EB) during the critical period (0-2 days post eclosion; dpe) at either **A)** 15% EB or **B)** 25% EB (%V/V). Three genotypes are shown: *Or42a*-Gal4>mCD8::GFP transgenic control (top), *dfmr1* null (*dfmr1*^{50M}; middle), and *Or42a*-Gal4 targeted *dfmr1* RNAi (A: 1-1-7, B: TriP GL00075). **C)** Quantification of *Or42a*-OSN AL VM7 glomerulus innervation volumes comparing oil vehicle and 15% EB, normalized to vehicle control. **D)** The difference between oil and EB exposure for each genotype. **E)** Quantification of the *Or42a*-OSNs VM7 innervation at 25% EB for all three genotypes. **F)** The difference between oil and EB exposure for each genotype. The scatter plots show all data points and the mean ± SEM for each assay. The bar graphs show mean ± SER for each assay. The significance is indicated as not significant (N.S.; p>0.05), or significant at $p<0.05$ (*), $p<0.01$ (**) and $p<0.001$ (***).

Sex-specific differences in early odorant experience critical period remodeling of AL innervation

In experiments testing the role of FMRP in critical period OSN remodeling, we observed that much of the variation between animal responses to EB exposure could be attributed to sex. To quantify this sex difference, we compared male and female animals following exposure to vehicle control and 20% EB from 0-2 dpe. To further validate our finding that Or42a-targeted RNAi against FMRP disrupts EB-dependent AL innervation remodeling, we used a third RNAi targeting FMRP (2-1; Bolduc et al., 2008). After odorant exposure, the volume of the Or42a OSN innervation of the VM7 glomerulus was assessed by quantifying *Or42a*-Gal4>UAS-mCD8::GFP. Animals exposed to EB during the critical period show pronounced changes in VM7 glomeruli, with sparser innervation and the appearance of OSN puncta (Fig. 16A,B). In EB-exposed males, OSN puncta occur in both controls and *dfmr1* RNAi animals, but the exposure has relatively little impact on the glomerulus innervation volume (Fig. 16A). Or42a-targeted *dfmr1* RNAi males lack any VM7 innervation loss but produce more OSN puncta (Fig. 16A, bottom right). In EB-exposed females, there is a much more pronounced response to odorant experience during the critical period, with a strong shift towards greater innervation loss but with fewer OSN puncta (Fig. 16B). As with the males, females expressing Or42a-targeted *dfmr1* RNAi exhibit very altered critical period remodeling, with the appearance of greater numbers of OSN puncta and much less loss of the overall VM7 glomerulus innervation compared to control females (Fig. 16B, bottom right). Representative images for both the sexes and both the genotypes, together with the quantitative innervation measurements, are shown in Figure 16.

A three-way ANOVA (2x2x2) comparing innervation volume reveals significant effects of EB exposure ($F(1,206)=17.47$, $p=4.313e-5$), genotype ($F(1,206)=21.80$, $p=5.45e-6$) and sex ($F(1,206)=57.26$, $p=1.251e-12$; Fig. 16C). There are significant interactions between odorant and genotype ($F(1,206)=26.87$, $p=5.179e-7$) as well as sex ($F(1,206)=63.83$, $p=9.485e-14$), but not genotype and sex ($F(1,206)=0.005$, $p=0.9427$). EB-exposed control males show only a small loss

in innervation volume (oil 1±0.036 (n=26) vs. EB 0.91±0.097 (n=25); multiple comparisons with Sidak's correction, t(206)=0.9129, *p*>0.9999; Fig. 16C bottom left bar) compared to *dfmr1* RNAi males with significantly greater innervation relative to vehicle exposure (oil 0.955±0.1 (n=26) vs. EB 1.412±0.099 (n=25); t(206)=4.636, *p*=0.0002; Fig. 16C, second bottom bar). EB-exposed control females show a much greater loss of innervation (oil 1.0±0.037 (n=28) vs. EB 0.187±0.029 (n=28); t(206)=8.634, *p*=4.55e-14; Fig. 16C, third bottom bar), with *Or42a*-Gal4>*dfmr1* RNAi causing severely attenuated remodeling (RNAi oil 0.996±0.063 (n=28) vs. EB 0.635±0.053 (n=28); t(206)=3.831, *p*=0.0047; Fig. 16C, right bottom bar). Quantification reveals that Or42a-targeted *dfmr1* RNAi causes significantly altered innervation in both sexes (control EB male vs. RNAi EB Male; t(206)=5.042, *p*=2.81e-5; control EB female vs. RNAi EB female; t(206)=4.756, *p*=0.0001; Fig. 16C, second bars). EB-exposed females have significantly less innervation than males in both controls and with *dfmr1* RNAi (control EB male vs. control EB female; t(206)=7.457, *p*=6.78e-11; RNAi EB male vs. RNAi EB female; t(206)=8.02, *p*=2.2e-12; Fig. 16C, top two bars). Together, these results indicate critical period EB exposure causes a more robust loss of glomerulus innervation in control females, with Or42a-targeted *dfmr1* RNAi strongly attenuating this OSN remodeling. For consistency and clarity in dissecting the causal mechanisms, females were employed in subsequent experiments.

Null dfmr1 mutants and global FMRP RNAi animals both maintain critical period remodeling

Due to the above surprising difference between *dfmr1* null mutants and Or42a OSN-targeted *dfmr1* RNAi, we wanted to test the conclusion that neuron class-specific differences (Or42a OSN-targeted vs. global) rather than technical differences (null mutant vs. all 3 RNAi knockdowns) accounts for the result. We differentiated between these two possibilities by testing olfactory experience-dependent remodeling of Or42a OSN VM7 innervation with a global FMRP knockdown (UH1-Gal4>*dfmr1* RNAi; Wodarz et al., 1995) and transgenic control lacking *dfmr1* RNAi, compared to a second *dfmr1* null mutant (*dfmr1*^{B55}; Inoue et al., 2002), Animals of these

three genotypes expressing a membrane-bound GFP under direct control of the *Or42a* promoter (*Or42a*-mCD8::4xGFP; Stephan et al., 2012) were exposed to either oil vehicle or 20% EB during the 0-2 dpe critical period. If all three genotypes show the strong reduction in Or42a OSN VM7 innervation following EB exposure relative to the vehicle control, then the result supports neuron class-specific FMRP roles within the AL olfactory circuit. On the other hand, if the UH1-Gal4>*dfmr1* RNAi animals show an impaired response to odorant experience during the critical period, then this would suggest an important difference between the FMRP null mutant and RNAi knockdown in mediating the olfactory experience-dependent remodeling phenotype. Representative images of brain FMRP levels and VM7 glomerulus innervation, as well as quantifications for all conditions, are shown in Figure 17.

In first testing our genetic tools, both global *dfmr1* RNAi and the homozygous $dfmr1^{B55}$ mutation led to an indistinguishable complete loss of brain FMRP expression compared to the robust FMRP levels in the matched transgenic controls (Fig. 17A; top vs. middle and bottom). This agrees with previous reports on these lines (Inoue et al., 2002; Greenblatt and Spradling, 2018), showing a loss of detectable FMRP. As in the above experiments, exposing control animals to EB during the 0-2 dpe critical period causes a stark reduction of Or42a OSN VM7 glomerulus innervation (Fig. 17B, top). Importantly, the global UH1-Gal4>*dfmr1* RNAi animals look remarkably like the null mutants (Fig. 17B, middle). Global FMRP removal leads to an increase in the basal oil-exposed Or42a OSN innervation volume, while maintaining robust olfactory experience-dependent remodeling. As in the $dfmr1^{50M}$ null mutant above, the alternate $dfmr1^{B55}$ null mutant shows an indistinguishable response to both oil vehicle and EB exposure, with vehicle-treated animals showing a larger innervation volume compared to controls, but still maintaining the robust innervation loss following critical period EB odorant exposure (Fig. 17B, bottom). Note also the characteristic Or42a OSN puncta in the VM7 glomeruli of both the global dfmr1 knockdown and null mutant following critical period EB exposure (Fig. 17B, middle and bottom arrows) suggesting a dynamic stage in the OSN remodeling process, as we reported

previously (Golovin et al., 2019). Together, these results support an OSN-specific FMRP role in olfactory experience-dependent critical period remodeling.

ANOVA (3x2) analyses support the qualitative conclusion with significant effects of odor ($F(1,161)=487.5$, $p=1.411e-50$) and genotype ($F(2,161)=18.08$, $p=8.252e-8$), but no significant interaction ($F(2,161)=2.57$, $p=0.0797$; Fig. 17C). Pairwise *t*-tests with Sidak's correction indicate EB exposure significantly reduces innervation in all 3 genotypes (control oil 1.0 ± 0.05 (n=34) vs. EB 0.008 ± 0.006 (n=35); $t(161)=13.54$, $p=3.4e-27$; UH1-Gal4>*dfmr1* RNAi oil 1.377 ± 0.08 (n=31) vs. EB 0.156 ± 0.04 (n=29); $t(161)=15.52$, $p=1.27e-32$; $dfmr1^{B55}$ oil 1.328 ± 0.06 (n=19) vs. EB 0.318 ± 0.10 (n=19); $t(161)=10.23$, $p=4.62e-18$; Fig. 17C, bottom bars). Vehicle null and RNAi animals both have larger basal innervation volumes (oil control vs. oil UH1-Gal4>*dfmr1* RNAi; $t(161)=4.989$, $p=2.3e-5$; oil control vs. $dfmr1^{B55}$ oil; $t(161)=3.76$, $p=0.0036$; Fig. 17C, middle and top bars). Multiple linear regression to compare vehicle- and EB-exposure while controlling for this innervation difference shows UH1-Gal4>*dfmr1* animals have a slightly larger change (UH1-Gal4>*dfmr1* RNAi x 20% EB β=-0.23 ± 0.11; $t(161)=2.127$, $p=0.035$; Fig. 17D, bottom bar) and *dfmr1* nulls have no significant difference ($dfm1^{B55}$ x 20% EB β=-0.02 ± 0.12; $t(161)=0.147$, $p=0.8833$; Fig. 17D, top bar). Despite this small difference, both the ubiquitous FMRP knockdown and $dfmr1^{B55}$ mutant largely resemble the $dfmr1^{50M}$ mutant. These findings indicate that Or42a OSN-targeted FMRP removal selectively disrupts olfactory experience-dependent critical period remodeling. Together these results further demonstrate that global FMRP loss in the AL circuit can be compensated for, despite the *Or42a* OSN-specific FMRP function.

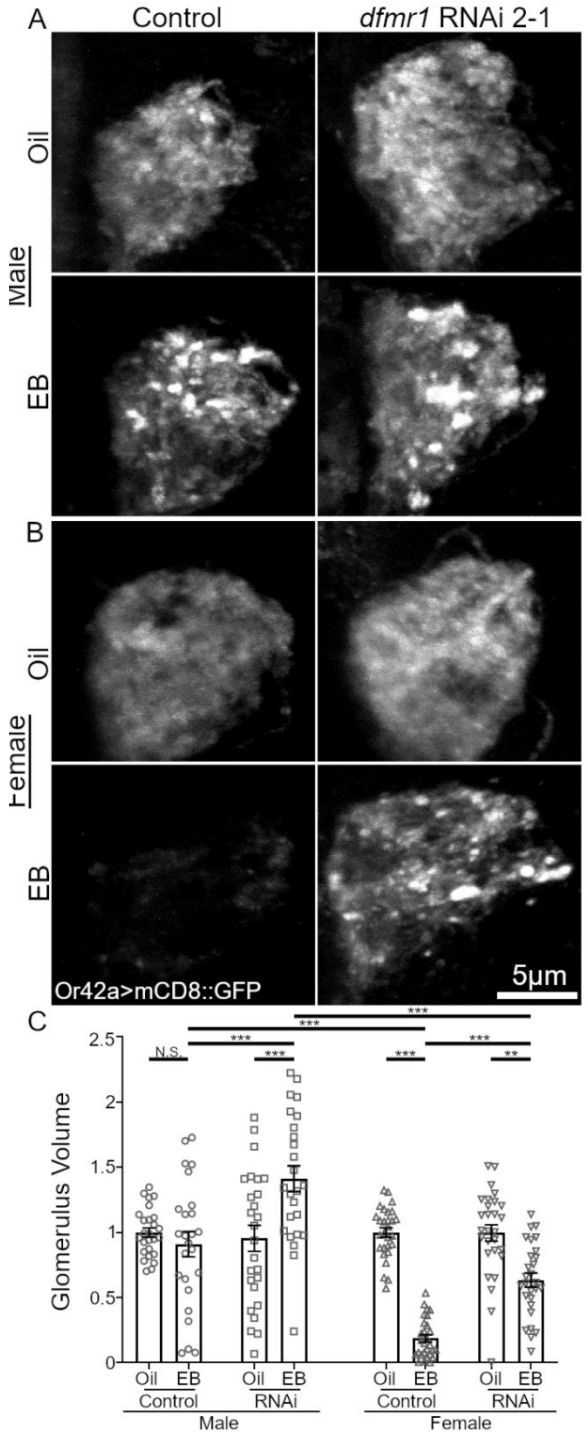

Figure 16: Sex-specific differences in EB-dependent critical period remodeling of AL innervation **A)** Representative confocal maximum intensity projections of Or42a OSNs innervating the male AL VM7 glomerulus (*Or42a*-Gal4>UAS-mCD8::GFP; white). **B)** Representative images from females under identical conditions. All animals were exposed to mineral oil vehicle (top), or 20% EB odorant (bottom) during the 0-2 dpe critical period. The paired genotypes shown are: the transgenic control (*Or42a*-Gal4>mCD8::GFP; left column), and the same transgenic line with *dfmr1* RNAi expression (*Or42a*-Gal4>*dfmr1* RNAi 2-1; right column). **C)** Quantification of the Or42a OSN VM7 innervation volumes for both genotypes, treatment conditions and sexes. Scatter plots show all data points and the mean ± SEM. The significance is indicated as not significant (N.S.; $p>0.05$), or significant at $p<0.01$ (**) and $p<0.001$ (***).

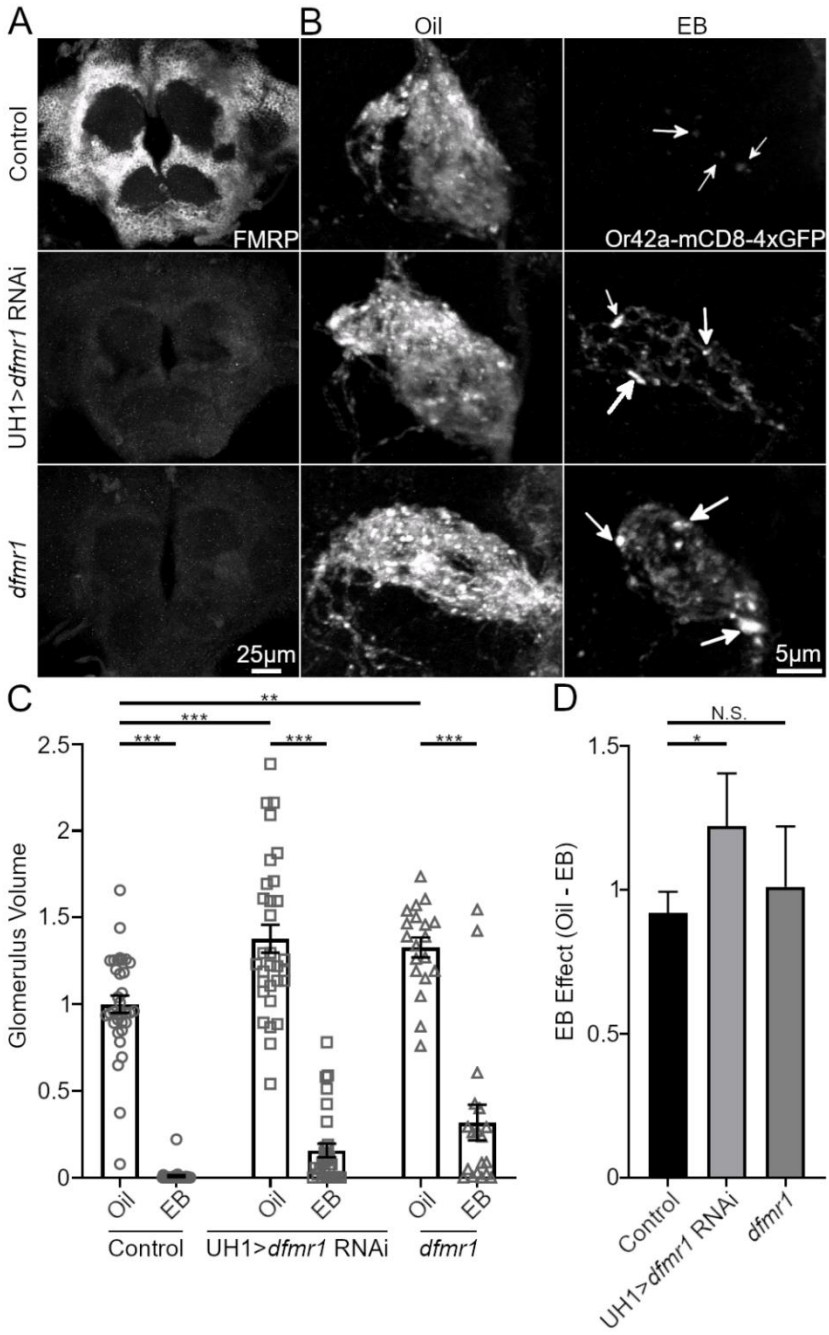

Figure 17: Neither *dfmr1* mutants nor global *dfmr1* RNAi impair OSN critical period remodeling **A)** Representative confocal maximum intensity projections of the entire central brain labeled with anti-FMRP (white) in the *w⁻;Or42a*-mCD8::4xGFP/*Or42a*-mCD8::4xGFP;UH1-Gal4/+ transgenic control (top), with ubiquitous *dfmr1* RNAi (*w⁻;Or42a*-mCD8::4xGFP/*Or42a*-mCD8::4xGFP;UH1-Gal4/ UAS-*dfmr1* RNAi TriP GL00075; middle) and in a *dfmr1* null mutant (*dfmr1*^{B55}; bottom*)*. **B)** Representative confocal maximum intensity projections of Or42a OSNs innervating the female AL VM7 glomerulus (*Or42a*-mCD8-4xGFP; white). The same genotypes above exposed to mineral oil vehicle (left) or 20% EB odorant (right) from 0-2 dpe. The bright puncta following EB exposure are labeled by white arrows. **C)** Quantification of *Or42a*-OSN AL VM7 glomerulus innervation volumes comparing oil vehicle and 20% EB of all three genotypes. **D)** The difference between oil and EB exposure for each genotype. The scatter plots show all data points and the mean ± SEM for each assay. The bar graphs show mean ± SER for each assay. The significance is indicated as not significant (N.S.; p>0.05), or significant at *p*<0.05 (*), *p*<0.01 (**) and *p*<0.001 (***).

Or42a OSN-specific FMRP overexpression enhances critical period odorant remodeling

The above results suggest that a FMRP balance between Or42a OSNs and other circuit neurons is required for proper critical period remodeling. If so, then elevating FMRP levels in OR42a OSNs should also alter experience-dependent remodeling. We have found bidirectional FMRP regulation within other neural circuits (Zhang et al., 2001b; Sears et al., 2019). To test if targeted FMRP overexpression (OE) impacts critical period remodeling, transgenic controls (Or42a>mCD8::GFP) were compared with UAS-FMRP 9557-3 (Or42a>FMRP OE; Zhang et al., 2001b) after exposure to either the oil vehicle or 20% EB during 0-2 dpe. As above, the controls show a striking reduction in Or42a OSN innervation (Fig. 18A; left panels, top vs. bottom). In agreement with the FMRP balance hypothesis, Or42a OSN-targeted FMRP OE greatly enhances this olfactory experience-dependent remodeling (Fig. 18A; right panels, top vs. bottom). Note that the directional disruption of the Or42a OSN innervation volume change is the opposite to Or42a OSN-targeted FMRP knockdown (Fig. 15), indicating a clear bidirectional consequence of FMRP imbalance within the circuit. Both the control and FMRP OE conditions show the OSN puncta characteristic of remodeling (Fig. 18A, arrows), but remnant Or42a OSN innervation is much sparser in the FMRP OE condition, similar to the consequence of increasing EB odorant concentration (Fig. 15). The quantitative assessment of Or42a OSN VM7 innervation volume further supports the role in FMRP balance in regulating olfactory experience-dependent synaptic remodeling during the early-use critical period.

ANOVA (2x2) analyses to compare these conditions show significant effects of both the genotype ($F(1,71)=11.03$, $p=0.0014$) and odorant exposure ($F(1,71)=186.7$, $p=1.471e-21$), with a significant interaction between them ($F(1,71)=13.96$, $p=0.0004$; Fig. 18B). Unpaired t-tests with Sidak's correction pairwise comparisons show EB exposure in controls significantly reduces Or42a OSN innervation (control oil 1.0 ± 0.037 (n=17) vs. 20% EB 0.48 ± 0.054 (n=17); $t(71)=6.714$, $p=2.35e-8$; Fig. 18B, bottom left), with a stronger effect following targeted FMRP OE (oil 1.022 ± 0.07 (n=21) vs. EB 0.11 ± 0.032 (n=20); $t(71)=12.92$, $p=1.53e-19$; Fig. 18B, bottom

right). FMRP OE does not impact the basal innervation ($t(71)=0.2955$, $p=0.9998$), so we directly compared EB-exposed control and FMRP OE conditions. FMRP OE in the Or42a OSNs significantly enhances critical period remodeling from the EB exposure ($t(71)=4.963$, $p=2.75e-5$; Fig. 18B, top bar). This confirms the ANOVA analyses indicating a significant interaction between FMRP OE and odorant exposure. These results support the conclusion that FMRP balance within the AL circuit determines olfactory experience-dependent synaptic remodeling during the critical period. More specifically, the opposite effects of targeted FMRP decrease and increase only in Or42a OSNs indicates a bidirectional regulation of remodeling. When FMRP levels are lower in Or42a OSNs compared to other neurons, remodeling is diminished, and conversely increasing FMRP levels in Or42a OSNs enhances critical period remodeling.

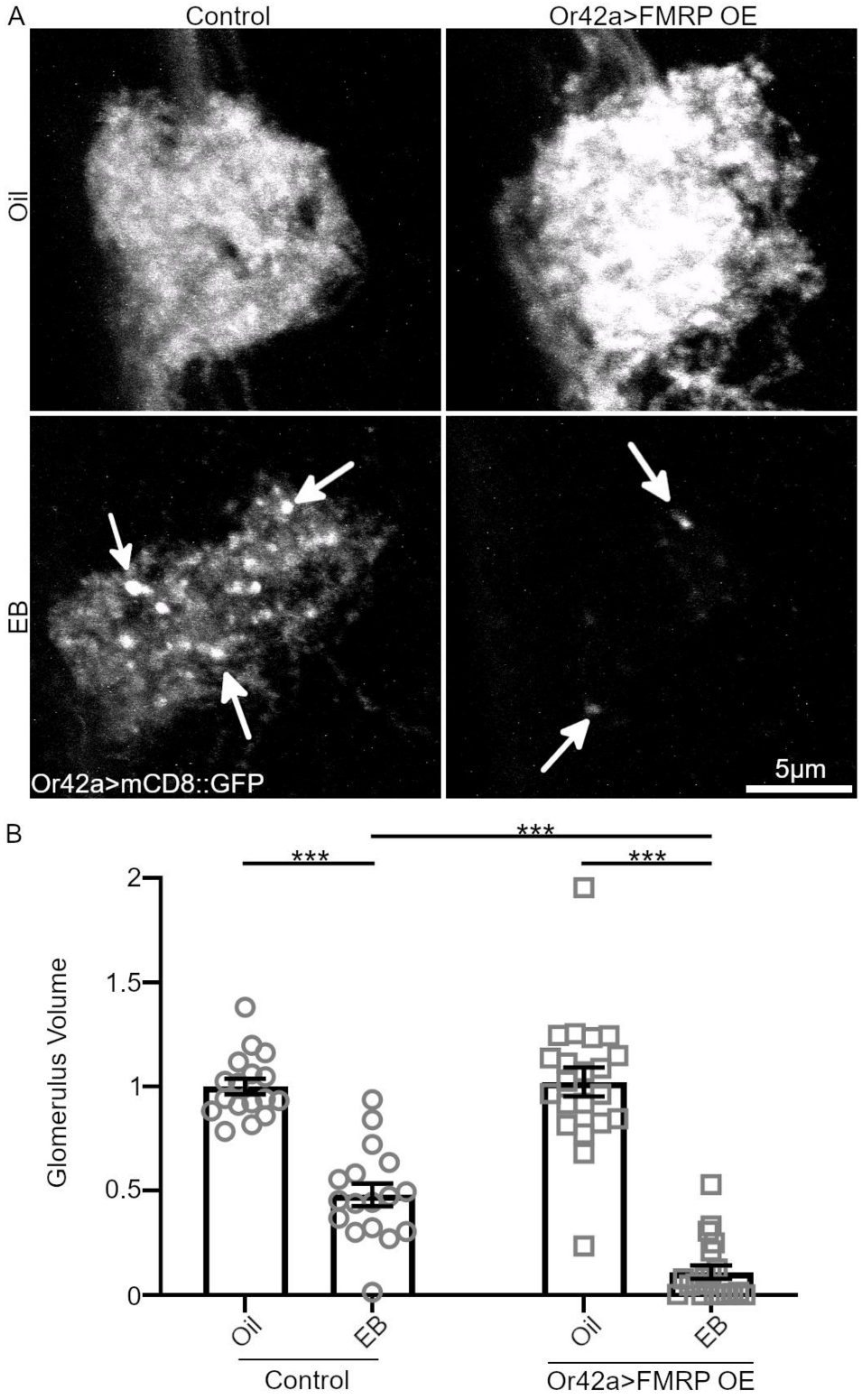

Figure 18: Or42a OSN-specific FMRP overexpression increases VM7 innervation remodeling
A) Representative confocal maximum intensity projections of Or42a OSNs innervating the AL VM7 glomerulus (*Or42a*-Gal4>UAS-mCD8::GFP; white). Females were exposed to mineral oil vehicle (top), or 20% EB odorant (bottom) from 0-2 dpe. Two genotypes are shown: transgenic control (*Or42a*-Gal4>mCD8::GFP; left), and the same transgenic line overexpressing FMRP (*Or42a*-Gal4>FMRP 9557-3; right). The bright puncta following EB exposure are labeled by white arrows. **B)** Quantification of the *Or42a*-OSN VM7 innervation volume for both genotypes and treatment conditions. Scatter plots show all data points and the mean ± SEM. The significance is indicated as $p<0.001$ (***).

Pan-OSN FMRP knockdown does not impact olfactory experience critical period remodeling

The above results indicate FMRP works cell autonomously and cell non-autonomously in opposition to regulate critical period olfactory experience OSN synaptic remodeling. Given the Or42a OSN-specific FMRP functions, the next goal was to identify the neurons providing the cell non-autonomous counterbalance. To begin this new pursuit, Or42a OSN remodeling was tested after altering FMRP levels in all OSNs. The *Orco*-Gal4 line drives expression in all OSNs (Larsson et al., 2004), but comes on relatively late in pupation. *Pebbled*-Gal4 (*Peb*-Gal4) is also expressed in all OSNs (Fig. 14E; Sweeney et al., 2007), and comes on earlier. Since both drivers include the Or42a OSNs, the prediction is that if only the Or42a OSNs are involved in the critical period remodeling, then altering FMRP levels should phenocopy the Or42a OSN-specific driver. Alternatively, if other OSNs contribute to Or42a OSN remodeling, then this should phenocopy the global UH1-Gal4, without affecting Or42a OSN remodeling. To test these two possibilities, *Peb*-Gal4 and *Orco*-Gal4 were used to eliminate and overexpress FMRP throughout the OSN population while assaying specifically for Or42a OSN olfactory experience-dependent critical period remodeling. *Peb*-Gal4 was first used to drive *dfmr1* RNAi, while labeling Or42a OSNs using *Or42a*-mCD8::4xGFP. Transgenic controls (lacking the RNAi) and experimental animals were again exposed to oil vehicle or 20% EB from 0-2 dpe. Sample images of FMRP expression in maxillary palp OSNs and Or42a OSN innervation in VM7 glomeruli, as well as quantified glomerular innervation values, are all shown in Figure 19.

All OSN cell bodies in the maxillary palp express FMRP, and can be co-labeled for the Or42a OSN population (Fig. 19A, top). *Peb*-Gal4 driven FMRP RNAi (*Peb*-Gal4>*dfmr1* RNAi) strongly suppresses FMRP in all OSNs, including Or42a OSNs (Fig. 19A, right). Following EB exposure, transgenic controls exhibit a near complete loss of Or42a OSN innervation (Fig. 19A, bottom). Due to strong loss of Or42a innervation (GFP signal) in the VM7 glomeruli, presynaptic active zone Bruchpilot (BRP) labeling is also shown to outline the AL glomeruli (Fig. 19A, bottom,

magenta). Three distinct glomeruli are thus demarcated, including the central VM7 glomerulus innervated by Or42a OSNs (Fig. 19A, dotted white lines). In the oil-exposed animals, typical innervation is observed. After 20% EB critical period exposure, both transgenic controls and the *Peb*-Gal4>*dfmr1* RNAi animals show near complete loss of VM7 innervation (Fig. 19A, third row vs. bottom). Importantly, Or42a OSN innervation loss corresponds with the loss of synaptic BRP within VM7 glomeruli, and therefore an inability to clearly define the VM7 border with BRP labeling (Fig. 19A bottom, white dotted regions). This loss of BRP synapse after critical period EB exposure is consistent with our previous report that strong olfactory experience during the critical period diminishes BRP volume and intensity within Or42a OSN presynaptic active zones (Golovin et al., 2019). These results indicate that global OSN-targeted FMRP removal does not impact Or42a OSN innervation remodeling due to EB exposure during the critical period, a conclusion next confirmed by quantitative assessment.

ANOVA (2x2) analyses to compare genotypes vs. odorant treatments show a significant effect of odorant ($F(1,57)=378.3$, $p=7.734e-27$), but not genotype ($F(1,57)=1.148$, $p=0.288$), with no significant interaction between genotype and odorant ($F(1,57)=0.7329$, $p=0.396$; Fig. 19B). Unpaired t-tests with Sidak's correction evaluating pairwise comparisons indicate EB-exposed control animals have significantly reduced Or42a OSN innervation (control oil 1.0 ± 0.032 (n=17) vs. 20% EB 0.002 ± 0.001 (n=17); $t(57)=14.02$, $p=4.64e-26$; Fig. 19B, bottom left). FMRP OSN knockdown (*Peb*-Gal4>*dfmr1* RNAi) also causes significantly reduced OSN innervation volumes following EB exposure (*Peb*-Gal4> *dfmr1* RNAi oil 1.103 ± 0.102 (n=15) vs. EB 0.013 ± 0.009 (n=12); $t(57)=13.56$, $p=1.042e-18$; Fig. 19B, bottom right). FMRP removal does not impact the basal extent of VM7 innervation ($t(57)=1.408$, $p=0.6603$), and we therefore can directly compare the two EB-exposed genotypes. *Peb*-Gal4>*dfmr1* RNAi in all the OSNs does not significantly impact the Or42a OSN innervation following critical period EB exposure compared to transgenic controls ($t(57)=0.1478$, $p>0.9999$; Fig. 19B, top bar). This confirms the above ANOVA analyses indicating no significant interaction between EB exposure and the *Peb*-Gal4 FMRP knockdown.

These results bolster the hypothesis that balanced FMRP within the AL circuit acts to regulate Or42a OSN critical period remodeling, and predict that overexpression of FMRP in all OSNs should also have no effect, thus mirroring the results of pan-OSN knockdown.

We next examined FMRP in transgenic control and *Orco*-Gal4>FMRP maxillary palps to find strong FMRP overexpression in all OSNs, including the marked Or42a OSNs (Fig. 19C, top). Similar to global OSN FMRP knockdown, FMRP overexpression throughout OSNs does not impact Or42a OSN critical period remodeling following EB exposure (Fig. 19C, third and bottom rows, compare left vs. right). ANOVA (2x2) quantification confirms the similar EB effect between transgenic controls and *Orco*-Gal4>FMRP OE animals, with a significant main effect of odorant exposure ($F(1,71)=907.8$, $p=3.473e-42$), but not genotype ($F(1,71)=0.518$, $p=0.474$), and no significant interaction between EB exposure and genotype ($F(1,71)=1.506$, $p=0.224$; Fig. 19D). Pairwise comparisons using unpaired t-tests with Sidak's correction reveal that EB exposure significantly reduces VM7 glomerular innervation in both controls and with *Orco*-Gal4>FMRP OE compared to the oil-exposed animals (control oil 1.0 ± 0.05 (n=16) vs. 20% EB 0.049 ± 0.03 (n=19); $t(71)=19.77$, $p=8.28e-30$; *Orco*-Gal4>FMRP oil 1.06 ± 0.04 (n=19) vs. 20% EB 0.033 ± 0.01 (n=21); $t(71)=22.98$, $p=7.91e-34$; Fig. 19D, bottom bars). In addition, these tests show that *Orco*-Gal4>FMRP OE does not alter VM7 innervation after oil or EB exposure (control oil vs. *Orco*-Gal4>FMRP oil; $t(71)=1.331$, $p=0.712$; control 20% EB vs. *Orco*-Gal4>FMRP 20% EB; $t(71)=0.372$, $p=0.999$; Fig. 19D, top bar). These results, along with the results from global OSN FMRP RNAi, all point to a FMRP role in Or42a OSNs and other OSN classes controlling VM7 innervation remodeling driven by critical period olfactory experience.

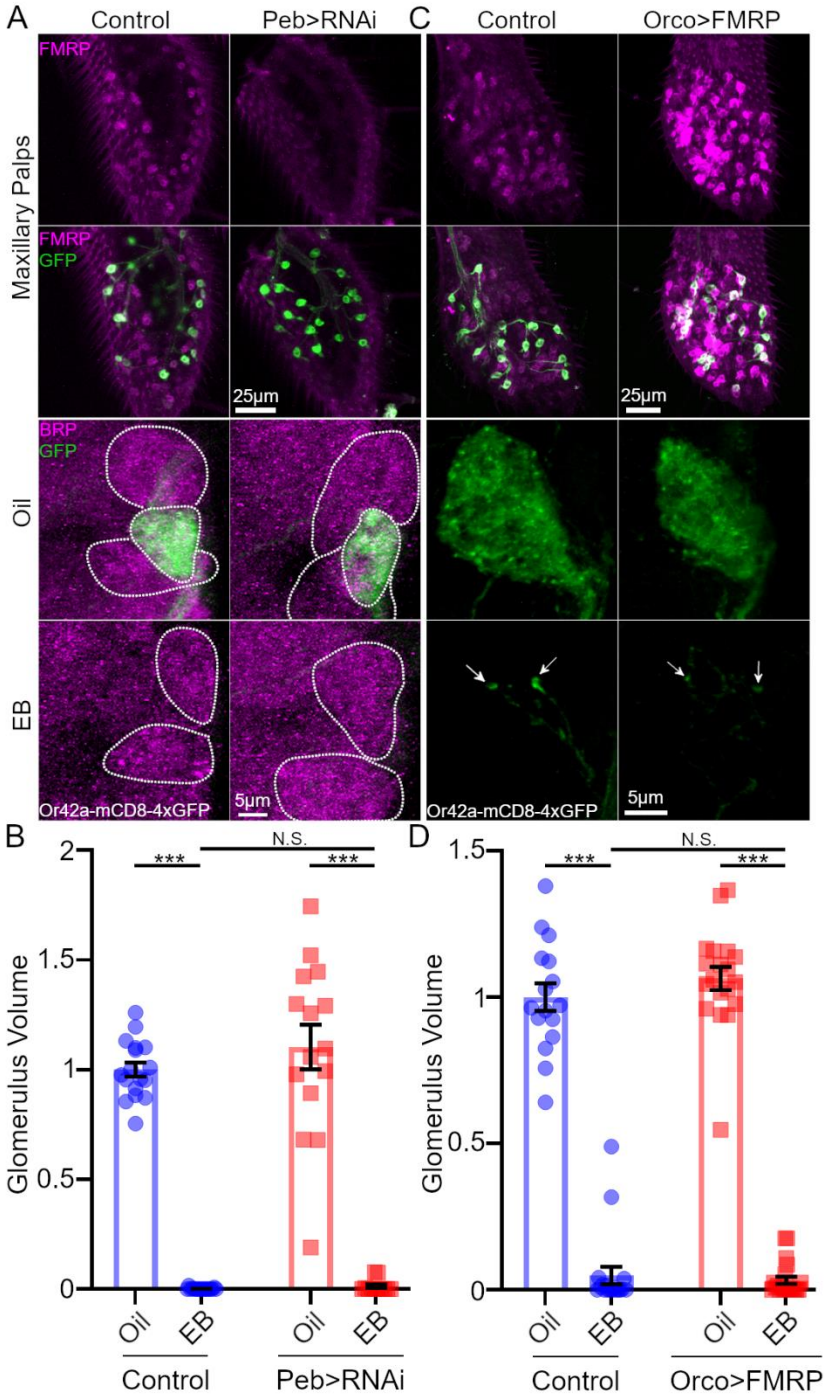

Figure 19: Pan-OSN FMRP knockdown/overexpression does not impact the VM7 remodeling **A)** Maxillary palp anti-FMRP (magenta; top row), co-labeled with Or42a OSNs (*Or42a*-mCD8-4xGFP, green; second row) in transgenic control (*w*⁻;Peb-Gal4/+;*Or42a*-mCD8::4xGFP/+;*Or42a*-mCD8::4xGFP/+; left) and *Peb*-Gal4>*dfmr1* RNAi (*w*⁻;Peb-Gal4/+; *Or42a*-mCD8::4xGFP/+; *Or42a*-mCD8::4xGFP/UAS-*dfmr1* RNAi; right). Bottom two rows: Or42a OSN innervation of VM7 glomerulus after exposure to oil vehicle or 20% EB from 0-2 dpe. BRP labeling (magenta) shows VM7 and surrounding glomeruli (dotted white outlines). **B)** Quantification of Or42a OSN VM7 innervation volume with *Peb*-Gal4 *dfmr1* RNAi. **C)** The same MP labeling of transgenic control (*w*⁻*; Or42a*-mCD8::4xGFP/*Or42a*-mCD8::4xGFP; Orco-Gal4/+; left) and Orco-Gal4 FMRP overexpression (*w*⁻*; Or42a*-mCD8::4xGFP/ *Or42a*-mCD8::4xGFP; Orco-Gal4/UAS-FMRP 9557-3; right). Bottom two rows: the same Or42a OSN-VM7 innervation exposed to either oil vehicle or 20% EB from 0-2 dpe. **D)** Quantification of the *Or42a*-OSN VM7 innervation volume for Orco-Gal4 FMRP overexpression. Scatter plot shows all data points and the mean ± SEM. The significance is indicated as not significant (N.S.; $p>0.05$), or significant at $p<0.001$ (***).

Or42a OSN-specific optogenetic activation is sufficient to drive critical period remodeling

The FMRP role across the OSN population suggests a function mediating Or42a OSN innervation remodeling in response to EB odorant exposure in the critical period. We previously showed that the functional Or42a receptor is required for Or42a OSN critical period remodeling (Golovin et al., 2019). However, EB activates other OSN classes (DoOR v2.0; Münch and Galizia, 2016), and higher EB levels may activate more OSNs (Semmelhack and Wang, 2009). Therefore, it remains possible that critical period remodeling requires both Or42a receptors and EB-sensitive receptors in other OSN classes. To test this hypothesis, parallel approaches were employed. First, *CsChrimson::mVenus* channelrhodopsin (Klapoetke et al., 2014) was targeted to Or42a OSNs (*Or42a*-Gal4>*CsChrimson::mVenus*) for the specific activation of Or42a OSNs with timed cyan (515nm) light stimulation (Fig. 20A,B). Second, removal of the essential olfactory Orco co-receptor required to mediate OSN responses (Larsson et al., 2004) was used to compare *orco* null mutants and *orco* nulls with Orco re-expressed only within Or42a OSNs, compared to transgenic driver controls (Fig. 20C). These tests allow the assessment of 1) the requirement of OSN activity in general, and 2) the sufficiency of Or42a OSN activity specifically, to mediate critical period remodeling. As above, Or42a OSN innervation was imaged within the VM7 glomerulus following 0-2 dpe critical period exposure to either the oil vehicle or 20% EB. Representative images and innervation quantifications for both channelrhodopsin and *orco* mutant experiments are shown in Figure 20.

To mimic the effects of EB odorant exposure during the critical period, *Or42a*-Gal4> *CsChrimson::mVenus* animals were staged and exposed to 515nm light as closely as possible to the manner of EB odorant exposure. However, there were two differences; 1) the animals were kept in constant darkness before exposure to cyan light stimulus, and 2) the animals were raised in petri dishes to allow for stronger optogenetic light stimulation (see Methods). Critical period light exposure of the targeted Or42a OSN *CsChrimson*-expressing animals drives a striking reduction of the Or42a innervation of the VM7 glomerulus, which qualitatively resembles the

remodeling driven by the critical period EB olfactory experience (Fig. 20A, top vs. bottom). Changes include a reduction in intensity, sparse and reduced glomerulus coverage, and appearance of the characteristic OSN puncta. This qualitative assessment is supported by quantitative measurements, which show that *Or42a*-Gal4>*CsChrimson::mVenus* animals exposed to cyan light during the critical period have significantly reduced innervation compared to dark-reared control animals (dark 1.0 ± 0.058 vs. light 0.08 ± 0.02; $t(26)=15.04$; $p= 2.421e-14$, unpaired t-test; Fig. 20B). The ability of channelrhodopsin-driven activity to reduce Or42a OSN innervation similar to olfactory EB exposure indicates that Or42a activity is sufficient for critical period synaptic remodeling of VM7 glomerulus innervation. However, because light and odorant driven activity levels in the Or42a neurons could be different, it is possible that the magnitude of innervation remodeling is different when only Or42a OSNs are activated.

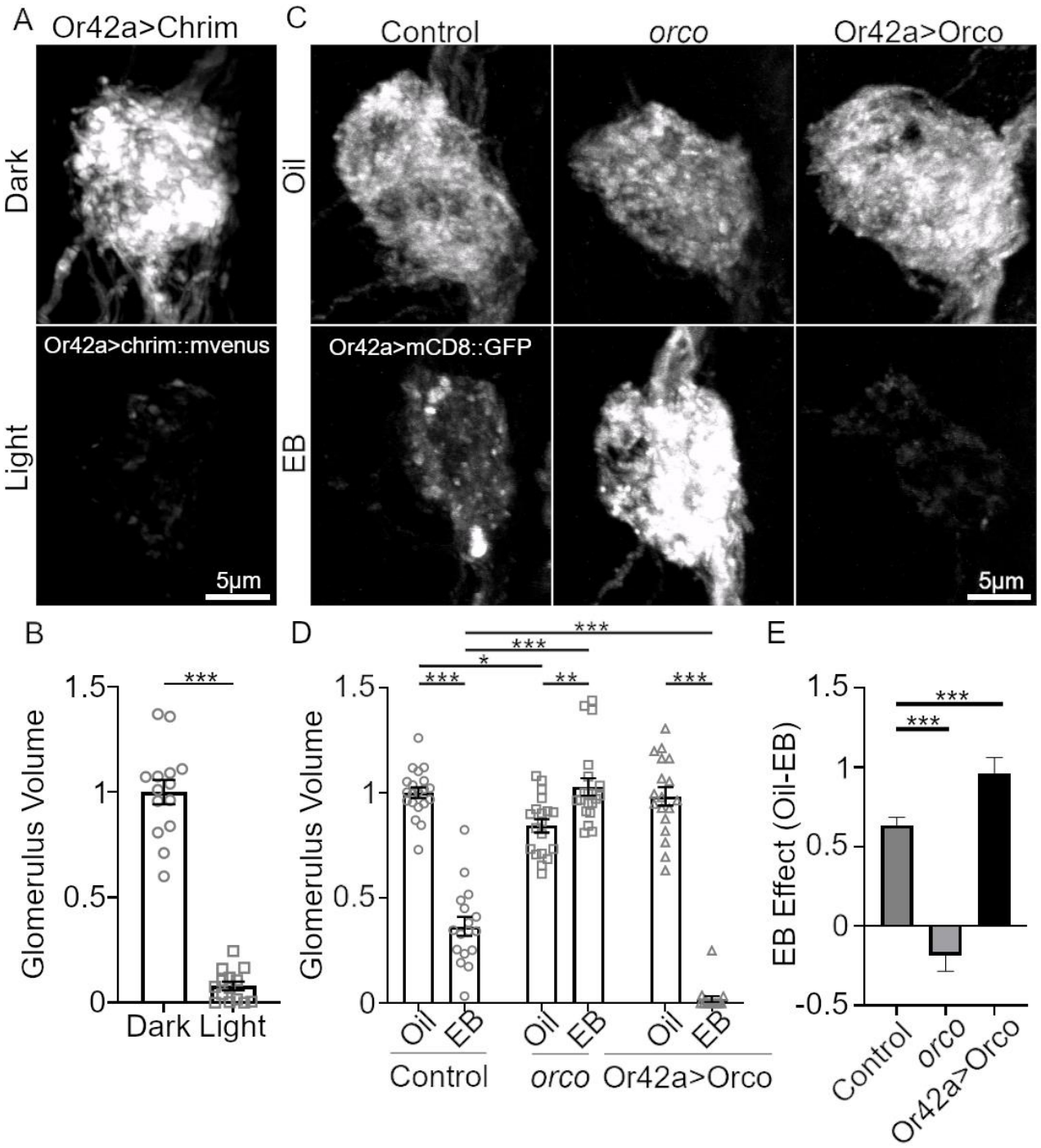

Figure 20: Or42a OSN-targeted neuronal activation drives VM7 critical period remodeling
A) Representative confocal maximum intensity projections of *Or42a*-OSN VM7 innervation, with *Or42a*-Gal4 driven expression of fluorescently tagged channelrhodopsin *Cschrimson*::mVenus. Females were reared in complete darkness (dark, top) or with 515nm cyan light (light, bottom) during the 0-2 dpe critical period. **B)** Quantification of *Or42a*-OSN VM7 innervation volume without activation (dark) and with optogenetic stimulation (light). **C)** Representative images of Or42a OSN VM7 innervation (*Or42a*-Gal4>UAS-mCD8::GFP; white). Females were exposed to the oil vehicle (top) or 20% EB (bottom) during the 0-2 dpe critical period. Three genotypes are shown: transgenic control (*w⁻;* UAS-mCD8::GFP/+; *Or42a*-Gal4/+ ; left), *orco* null mutant ($orco^1/orco^2$; middle), and the *orco* null with Or42a OSN-targeted Orco rescue ($orco^1/orco^2$, *Or42a*-Gal4>UAS-Orco; right). **D)** Quantification of VM7 innervation for all genotypes and conditions. **E)** The difference between the oil vehicle and EB exposures. Scatter plots show all data points and mean ± SEM. Bar graphs show mean ± SER. The significance is indicated as significant at $p<0.05$ (*), $p<0.01$ (**) and $p<0.001$ (***).

Or42a OSN-specific odorant activation is essential for critical period innervation remodeling

To test whether Or42a OSN-specific EB receptor activation produces the same effect as global OSN EB activation, *orco* null mutants were compared to *orco* nulls with targeted Orco rescue only in Or42a OSNs (*Or42a*-Gal4>UAS-Orco; Fig. 20C). As in all the above experiments, the transgenic controls show the normal striking reduction in VM7 innervation caused by 20% EB odorant exposure during the 0-2 dpe critical period, compared to the robust innervation characterizing the oil vehicle alone (Fig. 20C; left, top vs. bottom). Consistent with the role of olfactory reception mediating critical period remodeling (Golovin et al., 2019), *orco* null mutants lack any reduction in VM7 innervation following critical period EB exposure, compared to the matched oil-exposed animals (Fig. 20C; middle, top vs. bottom). In agreement with the above optogenetic studies, when Orco is re-expressed only in Or42a OSNs (*Or42a*-Gal4>Orco) there is again a strong reduction in VM7 innervation following EB olfactory experience during the critical period, compared to the oil-exposed animals (Fig. 20C; right, top vs. bottom). Interestingly, the reduction of VM7 innervation with targeted *Or42a*-Gal4>Orco rescue appears even more extreme than the matched control animals (Fig. 20C; left bottom vs. right bottom). In the targeted *Or42a*-Gal4>Orco rescue animals, critical period EB exposure generates sparser and less intensely labeled VM7 glomeruli innervation. Taken together, these results suggest a highly specific Or42a OSN activity requirement in critical period innervation remodeling, a conclusion supported and expanded by quantitative analyses.

ANOVA (3x2) quantification comparing the controls and *orco* null mutants exposed to either EB or oil vehicle alone during the 0-2 dpe critical period shows significant effects of genotype ($F(2,105)=76.63$ $p=3.016e-21$) and odorant exposure ($F(1,105)=266.3$, $p=1.455e-30$), with a significant interaction between the two ($F(2,105)=142.3$, $p=1.273e-30$; Fig. 20D). Unpaired t-tests with Sidak's correction evaluating pairwise comparisons show EB-exposed transgenic controls (*Or42a*-Gal4>mCD8::GFP) have significantly reduced innervation volumes (control oil

1.0 ± 0.025 (n=20) vs. EB 0.365 ± 0.045 (n=17); t(105)=12.69, p=9.46e-22; Fig. 20D, bottom left bar). Unexpectedly, the oil-exposed *orco* null mutants (*orco*^{1}/*orco*^{2}, Larsson et al., 2004) exhibit significantly lower innervation volumes compared to matched controls (control oil vs. *orco* oil 0.842 ± 0.032 (n=19); t(105)=3.245, p=0.0234; Fig. 20D, second from bottom bar). Although the *orco* null AL has been reported to have grossly normal overall morphology (Larsson et al., 2004), this basal difference could mark the beginnings of the later glomerular degeneration that later occurs in *orco* null mutants (Chiang et al., 2009). Also surprisingly, *orco* null mutants exposed to 20% EB during the critical period have significantly larger glomerulus innervation volumes than the oil-exposed *orco* mutants (*orco* oil vs. *orco* EB 1.028 ± 0.041 (n=20); t(105)=3.814, p=0.0035; Fig. 20D, bottom middle bar). These results show that complete loss of olfaction in all the OR-expressing OSNs has striking impacts on the olfactory circuitry and may shift the AL circuit connectivity in unexpected ways.

Since the oil-exposed control animals and EB-exposed *orco* mutants show no significant difference in VM7 glomerulus innervation (t(105)=0.577, p>0.9999), one possible explanation is that EB exposure prevents the glomerular degeneration starting to appear in *orco* mutants via the lateral excitation onto Or42a OSNs triggered by other OSN classes (Huang et al., 2010). Despite the above unanticipated results, the *orco* null mutants clearly show the expected lack of VM7 innervation remodeling after critical period EB exposure (Fig. 20C,D). There is a significantly increased innervation volume in *orco* nulls exposed to EB, compared to EB-exposed controls (t(105)=13.25, p=5.71e-23; Fig. 20D, third from bottom bar). Targeted restoration of Orco only in Or42a OSNs in otherwise *orco* null mutants prevents the innervation loss occurring in the *orco* nulls alone, leading to innervation volumes that are not significantly different compared to the oil-exposed controls (control oil = vs. *Or42a*-Gal4>Orco oil 0.983 ± 0.043 (n=18); t(105)=0.3539, p>0.9999; Fig. 20D). The *Or42a*-Gal4>Orco rescue condition also restores the VM7 innervation remodeling caused by critical period EB exposure, compared to the oil vehicle condition alone (EB 0.02 ± 0.015 (n=17); t(105)=18.77, p=3.74e-34; Fig. 20D, bottom right bar). Moreover, the

VM7 innervation reduction is significantly greater than within EB-exposed control animals ($t(105)=6.636$, $p=2.17e-8$; Fig. 20D, top bar). These results demonstrate that Orco-dependent Or42a OSN activation is the main driver of critical period AL innervation remodeling, but that other OSNs can fine-tune the response.

To directly compare interactions between critical period EB exposure and each genotype separately, a linear regression model was used to generate interaction terms interrogated to determine whether genotypes significantly alter innervation following EB exposure (Fig. 20E). There is a significant interaction between the critical period EB exposure and the *orco* null mutant genotype, with a significant regression coefficient (20% EB x *orco* $\beta=0.82 \pm 0.07$; $t(105)=11.76$, $p=7.082e-21$; Fig. 20E, left bar). This result indicates that introduction of the *orco* null prevents the olfactory experience-dependent innervation loss after critical period EB exposure, compared to the matched controls. The interaction of the odorant exposure with the *Or42a*-Gal4>Orco rescue in an otherwise *orco* null mutant is in the opposite direction, with another very significant regression coefficient (20% EB x Or42a>Orco $\beta=-0.328 \pm 0.071$; $t(105)=4.574$, $p=1.315e-5$; Fig. 20E, right bar). This result indicates that the critical period EB odorant exposure leads to a greater reduction of VM7 innervation volume in the *orco* null mutants with Orco re-expressed only in the Or42a OSNs, compared to the transgenic control animals. Taken together, these results provide very strong evidence that Or42a OSN-specific activity is sufficient to drive critical period remodeling of the VM7 glomerulus innervation. However, although only Or42a OSN activity is required for the innervation remodeling, other OSNs appear to modulate the level of EB experience remodeling through lateral inhibition, as the innervation reduction seen when Orco is only targeted to Or42a OSNs is greater than in the matched transgenic control animals.

Or42a OSN-targeted activation is not affected by Or42a OSN-targeted FMRP knockdown

The Or42a OSN presynaptic terminals innervating the VM7 glomerulus receive lateral inhibition from antennal lobe GABAergic local interneurons (LNs; Fig. 14E, bottom left; Olsen and

Wilson, 2008). This inhibition scales with OSN olfactory activation and is effectively blocked by removing or shielding from external odorant stimuli (Olsen and Wilson, 2008). Based on the role of balanced OSN FMRP levels (Fig. 19), and the impact of silencing many OSNs (Fig. 20) in mediating the Or42a OSN critical period remodeling, we next hypothesized that FMRP might regulate the local lateral modulation downstream of broad EB-driven OSN activation. To test this hypothesis, we took advantage of Or42a OSN-targeted *CsChrimson::mVenus* channelrhodopsin (Klapoetke et al., 2014) to specifically activate just the target OSNs (as in Figure 20), while also targeting FMRP removal (*Or42a*-Gal4>UAS-*CsChrimson::mVenus*, UAS-*dfmr1* RNAi; Fig. 21). These animals were compared to animals raised in total darkness, and to transgenic control animals (lacking the RNAi) raised in either darkness or in the same light conditions. As further controls, we examined the effect of oil vehicle alone or 20% EB on the same genotypes raised in complete darkness. All light and odorant treatments were done in the 0-2 dpe critical period. Representative images of Or42a OSN terminals in the VM7 glomerulus, and the innervation quantifications for all genotypes and treatments, are shown in Figure 21.

Transgenic controls show the expected strong reduction in Or42a OSN innervation of the VM7 glomerulus following critical period light stimulation, compared to animals raised in total darkness (Fig. 21A). Or42a OSN-specific optogenetic activation in *Or42a*-Gal4>UAS-*dfmr1* RNAi animals causes a similar decrease in VM7 innervation compared with the dark-reared animals (Fig. 21A vs. B), indicating the EB-driven OSN activity is an important driver of the FMRP effect. ANOVA (2x2) analyses of glomeruli innervation for each condition show a significant light stimulation effect ($F(1,73)=114.3$, $p=1.368e-16$), but no FMRP genotype effect ($F(1,73)=0.05$, $p=0.8158$), with no significant interaction between stimulation and genotype ($F(1,73)=1.71$, $p=0.195$). Pairwise comparisons using *t*-tests with Sidak's correction show that critical period EB exposure significantly reduces innervation in both transgenic controls and *Or42a*-Gal4>UAS-*dfmr1* RNAi animals (control dark 1.0 ± 0.04 (n=21) vs. light 0.41 ± 0.06 (n=21); $t(73)=8.9$, $p=1.71e-12$; RNAi dark 0.947 ± 0.02 (n=18) vs. light 0.486 ± 0.07 (n=17); $t(73)=6.35$, $p=9.7e-8$;

Fig. 21C, bottom bars). Further comparisons show that transgenic controls raised in darkness or light-stimulated during the 0-2 dpe critical period have VM7 glomerulus innervation volumes not statistically different from *Or42a*-Gal4>UAS-*dfmr1* RNAi animals under the same conditions (control dark vs. RNAi dark; $t(73)=0.766$, $p=0.9712$; control light vs. RNAi light; $t(73)=1.08$, $p=0.8641$; Fig. 21C, top bar). Together, these results indicate that broad OSN activation is required for the effect of Or42a OSN-targeted FMRP removal.

Consistent with previous results, transgenic controls exposed to 20% EB show reduced Or42a OSN VM7 innervation compared to oil-exposed animals (Fig. 21D, top vs. bottom). The effect of Or42a OSN-targeted FMRP RNAi also agrees with previous experiments, showing impaired innervation remodeling compared to the transgenic controls (Fig. 21E). ANOVA (2x2) quantification of the effects of oil vs. 20% EB exposure on the two genotypes show a significant effect of both odorant ($F(1,75)=284.1$, $p=3.211e-27$) and genotype ($F(1,75)=17.3$, $p=8.4e-5$), with a significant interaction between exposure and genotype ($F(1,75)=5.02$, $p=0.028$). Pairwise comparisons using *t*-tests with Sidak's correction show that EB exposure significantly reduces VM7 glomerulus innervation volume for both transgenic controls and *Or42a*-Gal4>UAS-*dfmr1* RNAi animals (control oil 1.0 ± 0.03 (n=21) vs. 20% EB 0.359 ± 0.04 (n=21); $t(75)=13.95$, $p=9.38e-22$; RNAi oil 1.064 ± 0.04 (n=19) vs. 20% EB 0.574 ± 0.02 (n=18); $t(75)=10.02$, $p=1.05e-14$; Fig. 21F, bottom bars). *Or42a*-Gal4>UAS-*dfmr1* RNAi animals exposed to the oil vehicle have statistically similar glomerulus innervation volumes to the transgenic controls (control oil vs. RNAi oil; $t(75)=1.37$, $p=0.687$). In line with our previous experiments, *Or42a*-Gal4>UAS-*dfmr1* RNAi animals had significantly greater VM7 innervation compared to transgenic controls after critical period EB exposure (control EB vs. RNAi EB; $t(75)=4.49$, $p=0.0002$; Fig. 21F, top bar). Overall, these results suggest lateral connections from broadly branching AL LNs are the likely mediators of critical period remodeling.

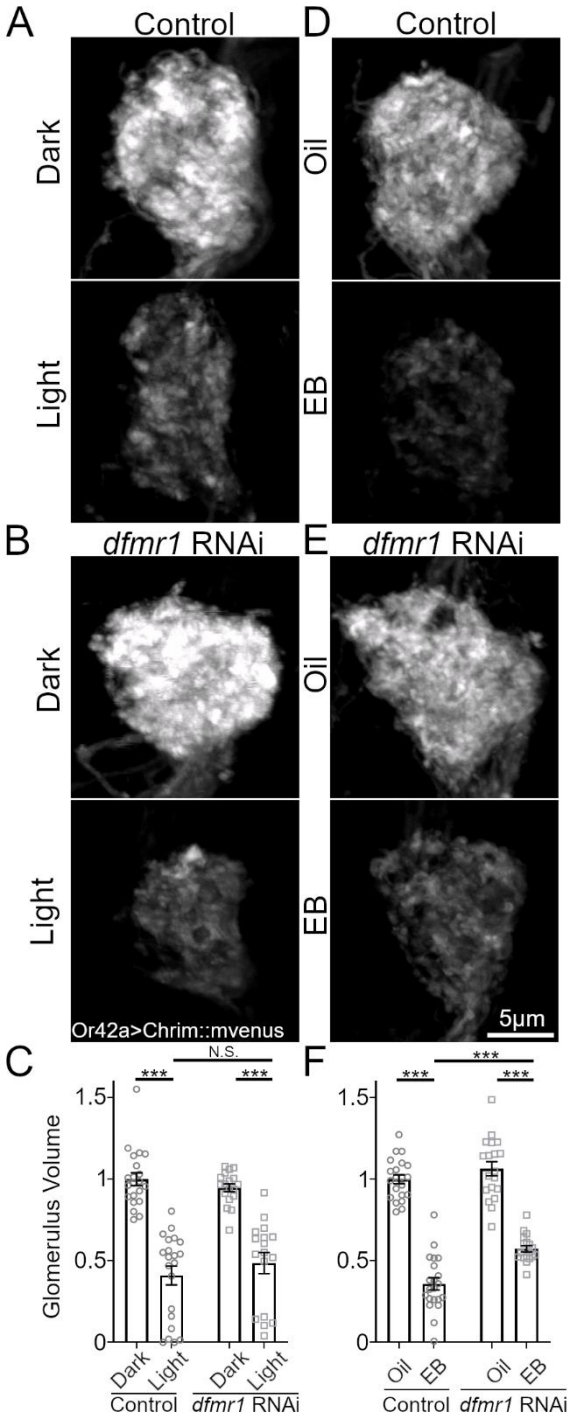

Figure 21: *Or42a*-targeted optogenetic activation is not affected by *Or42a*-targeted FMRP RNAi All images show confocal maximum intensity projections of *Or42a*-OSN VM7 innervation, with *Or42a*-Gal4 driven expression of fluorescently tagged channelrhodopsin *Cschrimson*::*mVenus*. **A,B**) Females were reared in total darkness (dark, top) or with 515nm cyan light (light, bottom). **A)** Or42a>*Cschrimson::mVenus* transgenic controls and **B)** *Or42a*-targeted *dfmr1* RNAi (TriP GL00075). **C)** Quantification of VM7 innervation in control and Or42a>*dfmr1* RNAi animals following dark and light treatment. **D,E**) Females were reared with oil vehicle (top) or 20% EB odorant (bottom) during the 0-2 dpe critical period. **D)** Or42a>*Cschrimson::mVenus* transgenic controls and **E)** *Or42a*-targeted *dfmr1* RNAi (TriP GL00075). **F)** Quantification of VM7 innervation in control and Or42a>*dfmr1* RNAi animals following oil and 20% EB exposure. Scatter plots show all data points and the mean ± SEM. The significance is indicated as not significant (N.S.; $p>0.05$) and significant at $p<0.001$ (***).

Or42a OSN synaptic output is not required for Or42a-targeted FMRP RNAi remodeling effects

Results up to this point indicate that Or42a OSN-specific activity is needed for critical period remodeling and that refinement is impaired if FMRP levels are not balanced between OSNs. We previously reported that Or42a OSN synaptic output does not drive critical period remodeling, but rather serves to limit the effect of EB odorant experience (Golovin et al., 2019). Due to the known FMRP roles controlling *trans*-synaptic signaling that coordinates with neurotransmitter release (Friedman et al., 2013), we hypothesized that FMRP roles in critical period remodeling require synaptic output. To block synaptic output in Or42a OSNs, we used a targeted tetanus toxin light chain (*Or42a*-Gal4>UAS-TeTxLc), while unbalancing FMRP levels using targeted FMRP RNAi (*Or42a*-Gal4>UAS-*dfmr1* RNAi), with *Or42a*-Gal4>UAS-mCD8::GFP labeling. The combined *Or42a*-Gal4>UAS-TeTxLc, UAS-*dfmr1* RNAi animals were compared to the controls (*Or42a*-Gal4>UAS-mCD8::GFP), as well as TeTxLc (*Or42a*-Gal4>UAS-TeTxLc) and FMRP RNAi (*Or42a*-Gal4>UAS-*dfmr1* RNAi) alone. Animals of each genotype were exposed to either the oil vehicle or 10% EB during the 0-2 dpe critical period. The lower EB concentration was used for this experiment because our previous work with *Or42a*-Gal4>UAS-TeTxLc animals showed that Or42a OSN innervation of the VM7 glomerulus was completely eliminated at higher EB concentrations (Golovin et al., 2019). Representative images of Or42a OSN terminals in the VM7 glomerulus, innervation quantifications, and EB effect quantifications for all genotypes and treatments are shown in Figure 22.

Unlike the higher EB exposures, 10% EB from 0-2 dpe has little effect on Or42a OSN innervation in transgenic control animals (Fig. 22A, top), although characteristic OSN punctae still occur after odorant exposure. The 10% EB-exposed controls show some regions of thinner VM7 innervation, with other areas containing the OSN puncta often occurring in EB-exposed animals (Fig. 22A, top, right arrows). Comparing *Or42a*-Gal4>UAS-*dfmr1* RNAi animals exposed to oil vehicle or EB odorant also reveals similar OSN puncta (Fig. 22A second row, right arrows).

However, unlike the control animals, *Or42a*-target FMRP RNAi animals have more widespread OSN puncta with little thinning of the innervation, which leads to a small expansion of the overall glomerulus innervation (Fig. 22A, second row). Consistent with our previous experimental report (Golovin et al., 2019), *Or42a*-Gal4>UAS-TeTxLc causes both more expansive basal innervation and a stronger EB odorant-induced reduction than matched controls (Fig. 22A, third row). These TeTxLc-expressing animals show a response to critical period 10% EB exposure that appears similar to the control response to 20% EB. In addition, examining animals expressing both *Or42a*-targeted *dfmr1* RNAi and TeTxLc blockade shows basal glomerulus innervation even further increased compared to controls (Fig. 22A, bottom row). Moreover, EB-exposed animals with both *dfmr1* RNAi and TeTxLc synapse blockade show impaired remodeling compared to TeTxLc alone (Fig. 22A, bottom right). These results indicate that blocking Or42a OSN synaptic output does not impair the effect of *Or42a*-targeted FMRP RNAi.

ANOVA (2x2x2) quantitative analyses of VM7 glomerulus innervation for each condition strongly support the above conclusions (Fig. 22B,C). Comparisons show a significant effect of the EB odorant exposure ($F(1,316)=335.9$, $p=1.272e-51$), TeTxLc synaptic transmission blockade ($F(1,316)=34.04$, $p=1.336e-8$) and targeted *dfmr1* RNAi ($F(1,316)=102.4$, $p=4.924e-21$), with significant two-way interactions between odorant and TeTxLc ($F(1,316)=428.4$, $p=9.46e-61$), odor and *dfmr1* RNAi ($F(1,316)=15.9$, $p=8.3e-5$), and TeTxlc and *dfmr1* RNAi ($F(1,316)=7.96$, $p=0.0051$), but no significant three-way interaction ($F(1,316)=0.0014$, $p=0.9697$). Pairwise comparisons using *t*-tests with Sidak's correction show that critical period EB exposure does not significantly change VM7 glomerulus innervation for the transgenic controls compared to the oil-exposed animals (control oil 1.0 ± 0.03 (n=42) vs. 10% EB 0.959 ± 0.03 (n=41); $t(316)=0.8375$, $p>0.9999$; Fig. 22B, bottom left bar). Interestingly, *Or42a*-Gal4>UAS-*dfmr1* RNAi animals have significantly larger VM7 glomerulus innervation volumes after EB exposure compared to the oil vehicle (RNAi oil 1.082 ± 0.04 (n=39) vs. 10% EB 1.242 ± 0.04 (n=41); $t(316)=3.179$, $p=0.0445$; Fig. 22B, second bottom bar). Critical period 10% EB exposure in *Or42a* OSN-targeted TeTxLc

animals, with or without *dfmr1* RNAi, leads to a significant reduction in VM7 innervation compared to the oil-exposed animals (TeTxLC oil 1.3 ± 0.03 (n=41) vs. 10% EB 0.226 ± 0.03 (n=38); *t*(316)=21.22, *p*=2.69e-61; RNAi+TeTxLc oil 1.525 ± 0.04 (n=42) vs. 10% EB 0.648 ± 0.05 (n=40); *t*(316)=17.65, *p*=1.5e-47; Fig. 22B, bottom third and right bars).

Further comparisons show that oil-exposed transgenic controls have similar Or42a OSN VM7 innervation compared to *Or42a*-Gal4>UAS-*dfmr1* RNAi, but significantly smaller than with *Or42a*-Gal4>UAS-TeTxLc (control oil vs. RNAi oil; *t*(316)=1.636, *p*=0.9519; control oil vs. TeTxLc oil; *t*(316)=6.079, *p*=9.75e-8; Fig. 22B, second and third from bottom left bars). Combining both *dfmr1* RNAi and TeTxLc significantly increases the glomerulus innervation of oil-exposed animals, possibly indicating an odor experience-independent interaction (TeTxLc oil vs. dfmr1 RNAi + TeTxLc oil; *t*(316)=4.553, *p*=0.0002; Fig. 22B, second from bottom bar right). As expected, following 10% EB exposure, *Or42a* OSN-targeted *dfmr1* RNAi impairs and *Or42a* OSN-targeted TeTxLc enhances VM7 glomerulus innervation, compared to matched controls (control 10% EB vs. RNAi 10% EB; *t*(316)=5.7, *p*=7.69e-7; control 10% EB vs. TeTxLc 10% EB; *t*(316)=14.47, *p*=2.58e-35; Fig. 22B, fourth from bottom and top left bars). Glomerulus innervation was also compared in *Or42a*-Gal4>UAS-TeTxLc animals after 10% EB exposure, with or without *dfmr1* RNAi. Similar to Or42a OSNs with intact synaptic output, transmission-blocked animals with *dfmr1* RNAi show significantly increased VM7 innervation, implying the remodeling impairment from imbalanced FMRP levels does not require synaptic transmission from Or42a OSNs (TeTxLC 10% EB vs. RNAi + TeTxLc 10% EB; *t*(316)=8.289, *p*=9.265e-14; Fig. 22B, right, fourth bar from bottom). The ANOVA quantification indicates that FMRP effects Or42a OSN critical period remodeling independent of OSN synaptic output.

To compare interactions between the critical period EB exposure and each of the genotypes, a linear regression model was generated to test for significant interactions (Fig. 22C). There is significant interaction between critical period EB experience and targeted *dfmr1* RNAi, with a significant regression coefficient (10% EB x *dfmr1* RNAi β=0.22 ± 0.07; *t*(316)=3.108,

p=0.0021; Fig. 22C, bottom left bar), indicating that targeted *dfmr1* RNAi significantly mitigates EB-induced innervation remodeling. The interaction of critical period EB exposure and TeTxLc is in the opposite direction, with another very significant regression coefficient (10% EB x TeTxLc β=-1.009 ± 0.07; *t*(316)=13.96, *p*= 7.849e-35; Fig. 22C, top bar), indicating that EB exposure causes a greater reduction of VM7 innervation in *Or42a*-targeted TeTxLc animals. The interaction between EB exposure and targeted *dfmr1* RNAi is not altered by the TeTxLc blockade (10% EB x *dfmr1* RNAi x TeTxLc β=-0.027 ± 0.1; *t*(316)=0.26, *p*=0.795). To test more specifically for an effect of *Or42a*-targeted *dfmr1* RNAi on EB exposure in the TeTxLc animals, we built a second linear regression model using only the TeTxLc blockade data. The regression coefficient for the interaction between critical period EB exposure and Or42a OSN-targeted *dfmr1* RNAi in the TeTxLc model is still significant (10% EB x *dfmr1* RNAi β=0.1973 ± 0.07; *t*(157)=2.77, *p*=0.0063; Fig. 22C, bottom right bar). Taken together, these findings indicate that the cell autonomous FMRP role on odorant experience-dependent innervation remodeling does not rely on the Or42a OSN synaptic output.

It is possible that OSN-targeted TeTxLc synaptic transmission blockade might be having effects by modifying FMRP levels in these neurons. In the above FMRP overexpression studies, elevating FMRP levels in the Or42a OSNs enhances the effect of EB experience-dependent critical period remodeling (Fig. 17). Therefore, rather than TeTxLc blockade acting independently from FMRP, OSN-targeted TeTxLc could possibly increase FMRP expression and thus mimic the effects of FMRP overexpression. In order to test this possibility, we used FMRP antibody labeling to compare controls to animals expressing TeTxLc in Or42a OSNs. Silencing synaptic output of Or42a OSNs does not detectably alter FMRP levels in these neurons (Fig. 23). Comparisons of Or42a OSN somata in maxillary palps reveal no differences in the intensity or extent of FMRP labeling (Fig. 23A). Quantification shows that Or42a OSN FMRP levels do not significantly differ between the controls and *Or42a-Gal4>*TeTxLc animals (control 2723±161.4 FMRP intensity (A.U.; n=20 palps) vs. Or42a-Gal4>TeTxLc 2445±417.8 A.U. (n=12); unpaired t-test,

t(30)=0.7262, *p*=0.4733; Fig. 23B). Moreover, the ratio between Or42a OSN FMRP and total FMRP (i.e. FMRP in all maxillary palp OSNs) is not different between controls and TeTxLc animals (control 1.151±0.03487 (n=20) vs. Or42a-Gal4>TeTxLc 1.176±0.2347 (n=12); unpaired t-test, t(30)=0.3627, *p*=0.7193; Fig. 23C). Together, these results suggest silencing Or42a OSN synaptic output does not detectably alter FMRP levels, again implicating the importance of lateral connections from other neurons rather than a direct feedback mechanism.

Previous work from our lab and others has shown that critical period odorant experience can drive dendritic arbor changes in postsynaptic projection neurons (PNs) downstream of OSN glomerular innervation (Sachse et al., 2007; Doll and Broadie, 2015; Chodankar et al., 2020). However, a recent study has suggested that Or42a OSN presynaptic remodeling is a completely separable mechanism (Chodankar et al., 2020). This recent study, combined with Or42a OSN remodeling in absence of synaptic output to VM7 PNs, made it unclear whether presynaptic innervation changes would be mirrored in a comparable PN postsynaptic refinement. We therefore next jointly assayed both the presynaptic OSNs and the postsynaptic PNs following the critical period odorant exposure. To simultaneously image pre- and postsynaptic partners within the VM7 glomerulus, we labeled the Or42a OSNs with *Or42a*-mCD8::4xGFP (Fig. 24A; left, green), while using NP3481-Gal4 (Olsen and Wilson, 2008) to drive UAS-mCD8::RFP (NP3481>mCD8::RFP) in the PNs (Fig. 24A; middle, magenta). The co-labeling shows the RFP-marked PNs overlap with the GFP-marked Or42a OSNs within the VM7 glomerulus in merged single slice confocal images (Fig. 24A; right, merged). These animals were exposed to either oil vehicle or 20% EB during the 0-2 dpe critical period. Representative images of the pre- and postsynaptic processes in the VM7 glomerulus, and the innervation quantifications for both Or42a OSNs and VM7 PNs following critical period treatments, are shown in Figure 24.

Following 20% EB critical period exposure, the control animals show the typical strong reduction of Or42a OSN innervation (Fig. 24B, green, left vs. right). Despite loss of presynaptic innervation, postsynaptic PNs are largely unchanged between oil- and EB-exposed conditions

(Fig. 24B, magenta, left vs. right). Pre- and postsynaptic volumes were quantified and compared with *t*-tests with Sidak's correction and a simple linear regression. Compared to oil-exposed animals, EB-exposed animals show significantly reduced Or42a OSN innervation, but no significant difference in the PN volume in the VM7 glomerulus (Or42a OSN oil 1.0 ± 0.07 (n=18) vs. 20% EB 0.15 ± 0.06 (n=18); $t(34)=9.43$, $p=1.04e-10$; VM7 PN oil 1.24 ± 0.04 (n=18) vs. 20% EB 1.1 ± 0.11 (n=18) PN volumes normalized to Or42a OSN oil volume mean; $t(34)=1.12$, $p=0.47$; Fig. 24C). Note that there is some increased variability in the VM7 PN volumes in the EB-exposed animals compared to vehicle controls (SEM oil 0.04 vs. 20% EB 0.11; Fig. 24C). We therefore tested whether Or42a OSN innervation and PN dendritic arborization might correlate, and possibly account for some of the odorant-induced variability. A simple linear regression was used to compare the pre- and postsynaptic volumes, but only a very weak, EB-independent relationship is apparent (oil $R^2=0.1591$ vs. EB $R^2=0.1387$; Fig. 24D). In summary, these results show that critical period odorant exposure drives striking remodeling in the presynaptic Or42a OSNs, but not the postsynaptic PNs, and therefore separates this process from similar processes that have mirrored pre- and postsynaptic alterations.

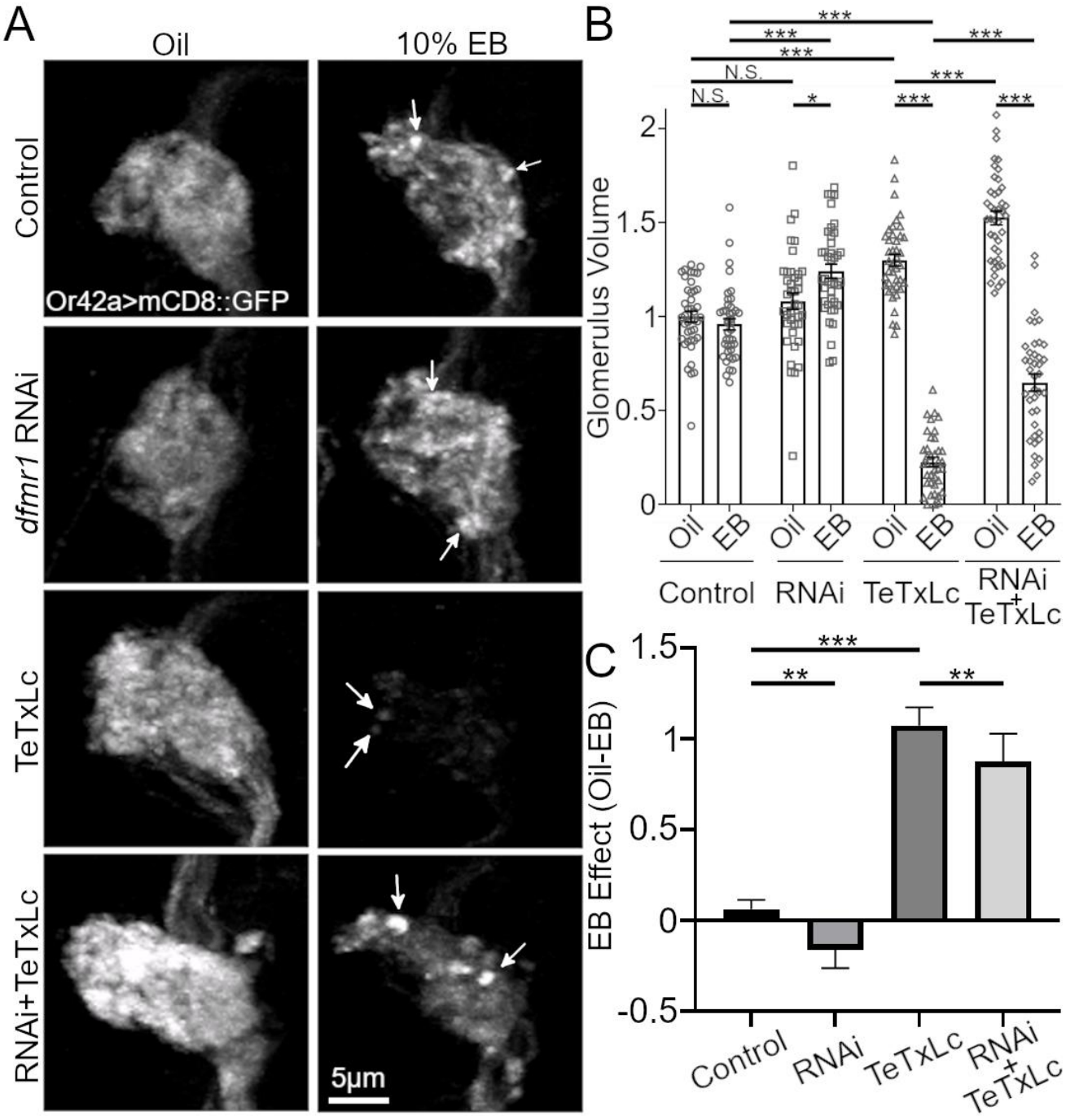

Figure 22: Or42a OSN synaptic output is not required for *Or42a*-targeted FMRP RNAi effect
A) Representative confocal maximum intensity projections of Or42a OSN VM7 innervation (*Or42a*-Gal4>UAS-mCD8::GFP; white) following exposure to oil vehicle (left) or 10% EB (right) during the 0-2 dpe critical period. Four genotypes are shown: the transgenic control (*Or42a*-Gal4>mCD8::GFP; top), with *Or42a*-targeted *dfmr1* RNAi (TriP GL00075; second), with *Or42a*-targeted tetanus toxin light chain (TeTxLc; third), and with both *Or42a*-targeted *dfmr1* RNAi and TeTxLc (bottom). The bright puncta following EB odorant exposure are labeled by white arrows. **B)** Quantification of the Or42a OSN VM7 innervation volume for each genotype and condition. **C)** Difference between oil vehicle and EB odorant shown for each genotype. Scatter plots show all data points and mean ± SEM. Bar graphs show mean ± SER. The significance is indicated as not significant (N.S.; p>0.05), or significant at $p<0.05$ (*), $p<0.01$ (**) and $p<0.001$ (***).

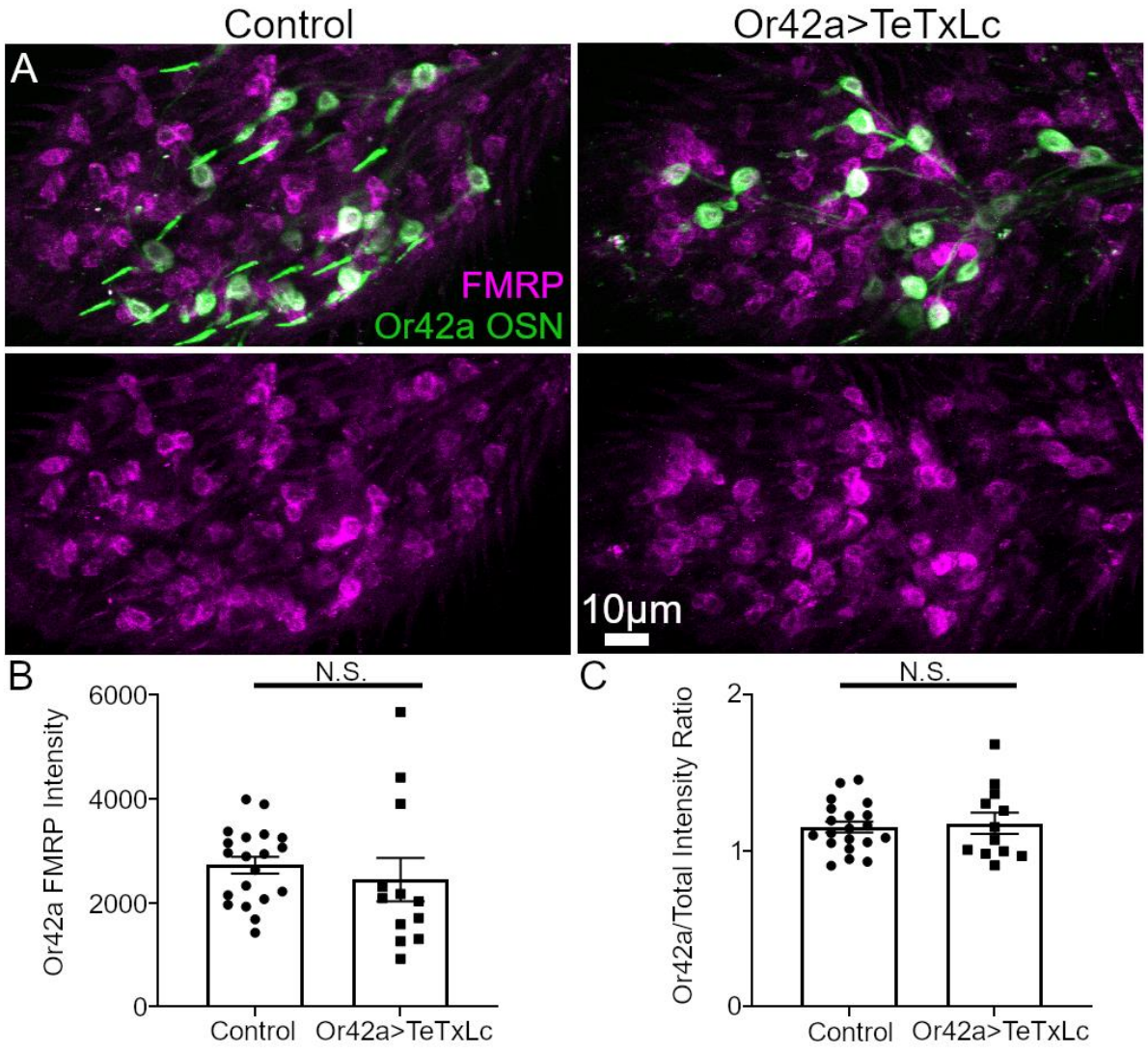

Figure 23: Or42a OSN-targeted TeTxLc neurotransmission block does not alter FMRP levels
A) Representative confocal maximum intensity projections of maxillary palp OSNs labeled with anti-FMRP (magenta) and *Or42a*-Gal4>mCD8::GFP (green); showing both channels (merged, top) or the FMRP channel alone (bottom). The maxillary palps are from the transgenic controls (*Or42a*-Gal4>Or42a-mCD8::GFP, left) and with TeTxLc expression (*Or42a*-Gal4>TeTxLc, right). **B)** Quantification of the mean FMRP fluorescence intensity levels within the GFP-positive Or42a OSNs comparing the controls and TeTxLc-expressing animals. **C)** Quantification of the ratio of mean FMRP fluorescence intensity in Or42a OSNs compared to all OSNs. Scatter plots show all data points and mean ± SEM. The significance is indicated as not significant (N.S.; $p>0.05$).
Critical period olfactory experience selectively remodels presynaptic OSN innervation

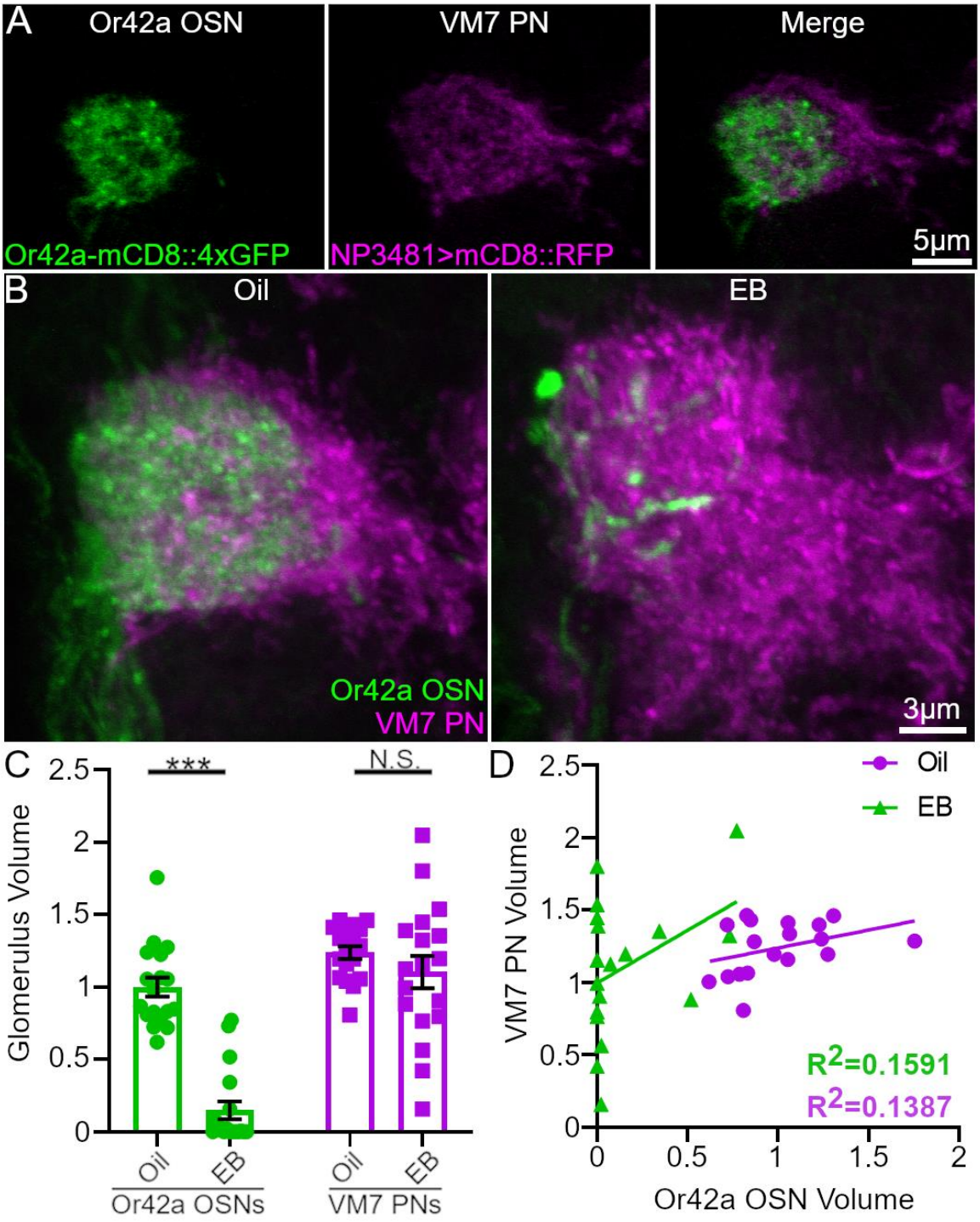

Figure 24: Odorant exposure selectively remodels presynaptic OSNs in the VM7 glomerulus
A) Representative confocal slices showing presynaptic Or42a OSNs (*Or42a*-mCD8::4xGFP, green; left) and postsynaptic PNs (NP3481-Gal4>mCD8::RFP, magenta; middle), with the merged image (right). **B)** Representative VM7 merged images after exposure to the oil vehicle alone (left) or 20% EB odorant (right) during the 0-2 dpe critical period. **C)** Quantification of VM7 glomerulus volume of Or42a OSNs (green) and VM7 PNs (magenta), normalized to the vehicle control. Data shown as a scatter plot of all data points with mean ± SEM. **D)** Quantification of the relationship between the presynaptic Or42a OSN volume and postsynaptic PN volume within the VM7 glomerulus. Data shown as a scatter plot with lines fit to vehicle (magenta) and EB (green) conditions. R^2 values given for each condition. Significance is presented as not significant (N.S; $p>0.05$), and significant at $p<0.001$ (***).

Silencing AL glutamatergic interneurons reduces Or42a OSN critical period remodeling

AL local interneurons (LNs) are prime candidates to regulate critical period remodeling. LNs interconnect OSNs for lateral modulation of OSN activity (Chou et al., 2010; Fig. 21) receive broad synaptic output from many OSNs (Olsen and Wilson, 2008; Fig. 22), and innervate OSN presynaptic terminals (Wilson, 2013; Fig. 24). LNs release neuromodulators including GABA and glutamate (Jackson et al., 1990; Das et al., 2010). We previously found that *Or42a*-targeted knockdown of the glutamate receptor NMDAR1 subunit strongly impairs Or42a OSN critical period remodeling (Golovin et al., 2019). Glutamatergic LNs (GluLNs; Fig. 14E, bottom right) provide the major source of glutamate neurotransmission in the AL circuit (Liu and Wilson, 2013). Therefore, we next tested the contribution of the GluLNs to Or42a OSN critical period remodeling. GluLN synaptic output was silenced as above, using OK107-Gal4 to drive tetanus toxin (OK107-Gal4>TeTxLc), with Or42a OSNs labeled by *Or42a*-mCD8::4xGFP. Since the OK107-Gal4 driver has extensive expression in the mushroom body (MB; Connolly et al., 1996), we also used the MB-restricted driver MB247-Gal4 (Zars et al., 2000) as a control to express TeTxLc (MB-247-Gal4>TeTxLc) and assess the effect of MB silencing on Or42a critical period remodeling. The same transgenic lines lacking TeTxLc were used as controls. Staged animals from all genotypes were exposed to either the oil vehicle or 20% EB during the 0-2 dpe critical period. Representative VM7 images and glomerulus innervation quantifications for all genotypes and conditions are shown in Figure 25.

As above, transgenic control animals show a striking reduction in VM7 glomerulus innervation with 20% EB critical period exposure (Fig. 25A, top). In contrast, animals with GluLN silencing by TeTxLc (OK107-Gal4>TeTxLc) have impaired Or42a OSN remodeling following the EB odorant exposure (Fig. 25A, top vs. bottom). Quantification of glomerulus innervation and ANOVA (2x2) analyses show a significant effect of the odor ($F(1,74)=367.9$, $p= 1.946e-30$) and the GluLN TeTxLc silencing ($F(1,74)=10.24$, $p=0.002$), with a significant interaction between experience and genotype ($F(1,74)=25.61$, $p=2.95e-6$; Fig. 25B). Pairwise comparisons using the

t-tests with Sidak's corrections show that EB-exposed animals have significantly reduced innervation compared to oil-exposed transgenic controls and OK107-Gal4>TeTxLc animals (control oil 1.0 ± 0.03 (n=26) vs. 20% EB 0.003 ± 0.001 (n=25); $t(74)=20.61$, $p=1.31e-31$; TeTxLc oil 0.923 ± 0.06 (n=13) vs. 20% EB 0.343 ± 0.07 (n=14); $t(74)=8.73$, $p=3.23e-12$; Fig.10B, bottom bars). Silencing GluLNs does not alter the basal glomerulus innervation under control oil-exposed conditions (control oil vs. TeTxLc oil; $t(74)=1.304$, $p=0.7303$), but does significantly increase Or42a OSN innervation following the critical period EB odorant exposure (control 20% EB vs. TeTxLc 20% EB; $t(74)=5.893$, $p=6.27e-7$; Fig. 25B, top bar). Together, these results suggest a role for GluLN glutamatergic signaling in Or42a OSN olfactory-experience-dependent critical period remodeling, but it is possible that some or all of this effect is due to OK107-Gal4 expression within the downstream MB learning/memory center.

MB-restricted silencing with MB247-Gal4 slightly enhances the Or42a OSN remodeling (Fig. 25C). Like transgenic controls, MB247-Gal4>TeTxLc animals exposed to 20% EB show reduced VM7 innervation, but the effect is even stronger than in the controls. Quantification of innervation and ANOVA (2x2) analyses show a significant effect of both odor ($F(1,64)=136.9$, $p=1.513e-17$) and genotype ($F(1,64)=4.459$, $p=0.0386$), but no significant interaction between them ($F(1,64)=0.743$, $p=0.3919$; Fig. 25D). Pairwise comparisons using *t*-tests with Sidak's corrections show that EB-exposed animals have significantly reduced innervation compared to both oil-exposed transgenic controls and MB247-Gal4>TeTxLc animals (control oil 1.0 ± 0.03 (n=25) vs. 20% EB 0.357 ± 0.07 (n=20); $t(64)=9.287$, $p=1.07e-12$; TeTxLc oil 0.926 ± 0.07 (n=12) vs. 20% EB 0.181 ± 0.08 (n=11); $t(64)=7.736$, $p=5.65e-10$; Fig.12D, bottom bars). Silencing the MB does not significantly alter basal glomerulus innervation under oil-exposed control conditions (control oil vs. TeTxLc oil; $t(64)=0.9146$, $p=0.3639$), but does significantly decrease Or42a OSN innervation following critical period EB exposure (control 20% EB vs. TeTxLc 20% EB; $t(64)=2.036$, $p=0.0459$; Fig. 25D, top bar). Despite the significant decrease in innervation volume in the MB247>TeTxLc EB condition compared to the transgenic control, the lack of a significant

interaction term between genotype and odorant exposure in the ANOVA complicates interpretation. Taken together, these results indicate GluLNs role in critical period OSN remodeling, but do not clearly demonstrate a potential MB role.

Based on the above findings, we hypothesized that GluLN-released glutamate binds to Or42a OSN NMDARs to modulate critical period remodeling. To further test this hypothesis, we next set forth to assess whether NMDAR1 specifically regulates critical period remodeling. Transgenic controls with Or42a OSNs labeled using *Or42a*-mCD8::GFP were compared in two *Nmdar1* mutant combinations; 1) *Nmdar1* null mutants homozygous for a Mi{MIC} insertion (*Nmdar1*$^{MI11796/MI11796}$; Nagarkar-Jaiswal et al., 2015), and 2) heterozygous mutants with a copy of *Nmdar1*^{MI11796} over a hypomorphic mutation (*Nmdar1*$^{EP331/MI11796}$; Rorth et al., 1996; Xia et al., 2005). Control and mutant animals were exposed to either oil vehicle or 20% EB in the 0-2 dpe critical period. Representative images of the Or42a OSN VM7 glomerular innervation, as well as innervation quantifications and the effect of EB exposure for all genotypes and conditions, are all shown in Figure 26. Transgenic control animals show the characteristic strong reduction in VM7 innervation following 20% EB critical period exposure (Fig. 26A, left). Surprisingly, we found that both mutants also show a very similar response to the EB exposure. Mutants exhibit a strong reduction in Or42a OSN axon terminal innervation and the characteristic OSN bright puncta (Fig. 26A, middle and right). This suggests two possibilities; 1) the effect of GluLNs silencing on Or42a OSN critical period remodeling does not rely on NMDAR1-dependent signaling, or 2) *Or42a*-targeted NMDAR1 knockdown may have a similar effect as with FMRP with only circuit imbalance having an impact on critical period remodeling.

ANOVA (3x2) quantification shows a significant effect of both odorant ($F(1, 128)=567.7$, $p=6.876e-49$) and genotype ($F(2, 128)=6.084$, $p=0.003$), but no significant interaction between them ($F(2, 128)=2.089$, $p=0.128$; Fig. 26B). Pairwise comparisons using Sidak's corrected *t*-tests show that both control and mutants significantly reduce innervation volumes with critical period EB exposure (control oil 1.0 ± 0.03 (n=32) vs. 20% EB 0.085 ± 0.03 (n=33); $t(128)=17.73$,

p=4.25e-35; *Nmdar1*$^{MI11796/MI11796}$ oil 0.873 ± 0.06 (n=13) vs. 20% EB 0.078 ± 0.03 (n=18); *t*(128)=10.5, *p*=8.29e-18; *Nmdar1*$^{EP331/MI11796}$ oil 1.149 ± 0.08 (n=19) vs. 20% EB 0.147 ± 0.05 (n=19); *t*(128)=14.85, *p*=1.9e-28; Fig. 26B, bottom bars), but there is no significant difference in the basal innervation with vehicle exposure (control oil vs. *Nmdar1*$^{MI11796/MI11796}$ oil; *t*(128)=1.858, *p*=0.6376; control oil vs. *Nmdar1*$^{EP331/MI11796}$ oil; *t*(128)=2.467, *p*=0.202) or in odor-dependent remodeling (control EB vs. *Nmdar1*$^{MI11796/MI11796}$ EB; *t*(128)=0.113, *p*>0.9999; control EB vs. *Nmdar1*$^{EP331/MI11796}$ EB; *t*(128)=1.029, *p*=0.9958; Fig. 26B, middle and top bars). Quantification of EB effects using multiple linear regression shows that all genotypes have similar responses without significantly different regression coefficients (20% EB x *Nmdar1*$^{MI11796/MI11796}$ β=0.1203 ± 0.09; *t*(128)=1.312, *p*=0.1918; 20% EB x *Nmdar1*$^{EP331/MI11796}$ β=-0.08699 ± 0.08; *t*(128)=1.024, *p*=0.3079; Fig. 26C). Together, these results suggest that NMDAR1 signaling functions in an Or42a OSN-specific pattern similar to FMRP to mediate the olfactory experience-dependent critical period remodeling of Or42a OSN presynaptic terminals.

Or42a OSN-targeted GABA$_A$R knockdown enhances critical period innervation remodeling

Inhibitory GABAergic LNs oppose excitatory inputs, with the excitatory and inhibitory LN balance controlling AL circuit output (Acebes et al., 2011, 2012). Excitatory/inhibitory imbalance characterizes FXS disease models (Contractor et al., 2015). Therefore, we hypothesized altering inhibitory LN signaling might imbalance the AL circuit and impair Or42a OSN refinement. We showed above that remodeling depends on neural activity specifically within the Or42a OSNs. In addition, we showed that Or42a OSN critical period remodeling is augmented when other OSNs cannot transduce odorants. Since the overall impact of OSN population interactions on Or42a OSNs is lateral inhibition (Olsen and Wilson, 2008), we hypothesized that reducing inhibition should mimic the effects of the *orco* mutant with *Or42a*-Gal4>Orco rescue (Fig. 20). Since a major component of lateral inhibition onto Or42a OSNs comes from ionotropic GABA receptors (Olsen and Wilson, 2008), we used *Or42a*-targeted RNAi to knockdown Resistant to Dieldrin (RDL), a

principle $GABA_AR$ subunit (Aronstein and Ffrench-Constant, 1995; Okada et al., 2009). In order to examine the role of RDL in the critical period remodeling of Or42a OSNs, we used *Or42a*-Gal4>mCD8::GFP to label the neurons and compared the RDL RNAi expressing animals (*Or42a*-Gal4>*Rdl* RNAi) to a transgenic control expressing only the membrane-bound GFP. Staged animals were exposed to either oil vehicle or 20% EB during the 0-2 dpe critical period. Representative images of Or42a OSN innervation of the VM7 glomerulus as well as innervation quantifications for all conditions are shown in Figure 27.

As in all studies above, control animals EB-exposed during the critical period exhibit a strong reduction in Or42a OSN innervation of the VM7 glomerulus (Fig. 27A, top). When $GABA_A$ signaling is reduced with Or42a OSN-targeted *Rdl* RNAi, basal innervation is similar to controls following oil exposure (Fig. 27A; left, top vs. bottom). However, when *Or42a*-Gal4>*Rdl* RNAi animals are exposed to EB during the critical period, they have a larger reduction in Or42a OSN innervation compared to controls (Fig. 27A; right, top vs. bottom). ANOVA (2x2) quantification shows significant effects of odor ($F(1,98)=259.6$, $p=2.671e-29$) and *Rdl* RNAi (($F(1,98)=19.78$, $p=2.3e-5$), with a significant interaction between the two ($F(1,98)=17.11$, $p=7.5e-5$; Fig. 27B). Pairwise comparisons with *t*-tests and Sidak's correction show both control and *Rdl* RNAi animals have significantly reduced Or42a OSN innervation after EB exposure (control oil 1.0 ± 0.03 (n=26) vs. 20% EB 0.538 ± 0.04 (n=28); $t(98)=8.729$, $p=4.14e-13$; *Rdl* RNAi oil 0.988 ± 0.04 (n=23) vs. 20% EB 0.206 ± 0.04 (n=25); $t(98)=14.57$, $p=1.73e-25$; Fig. 27B, bottom bars). Although the two genotypes had comparable innervation with vehicle (control oil vs. *Rdl* RNAi oil; $t(98)=0.2161$, $p>0.9999$), *Or42a*-Gal4>*Rdl* RNAi significantly decreases the VM7 glomerulus innervation following critical period EB exposure (control EB vs. *Rdl* RNAi EB; $t(98)=6.193$, $p=8.32e-8$; Fig. 27B, top bar). These results reveal a role of $GABA_AR$-mediated inhibition in regulating Or42a OSN synaptic remodeling, and provide a mechanism by which FMRP acts to modulate olfactory experience-dependent critical period refinement.

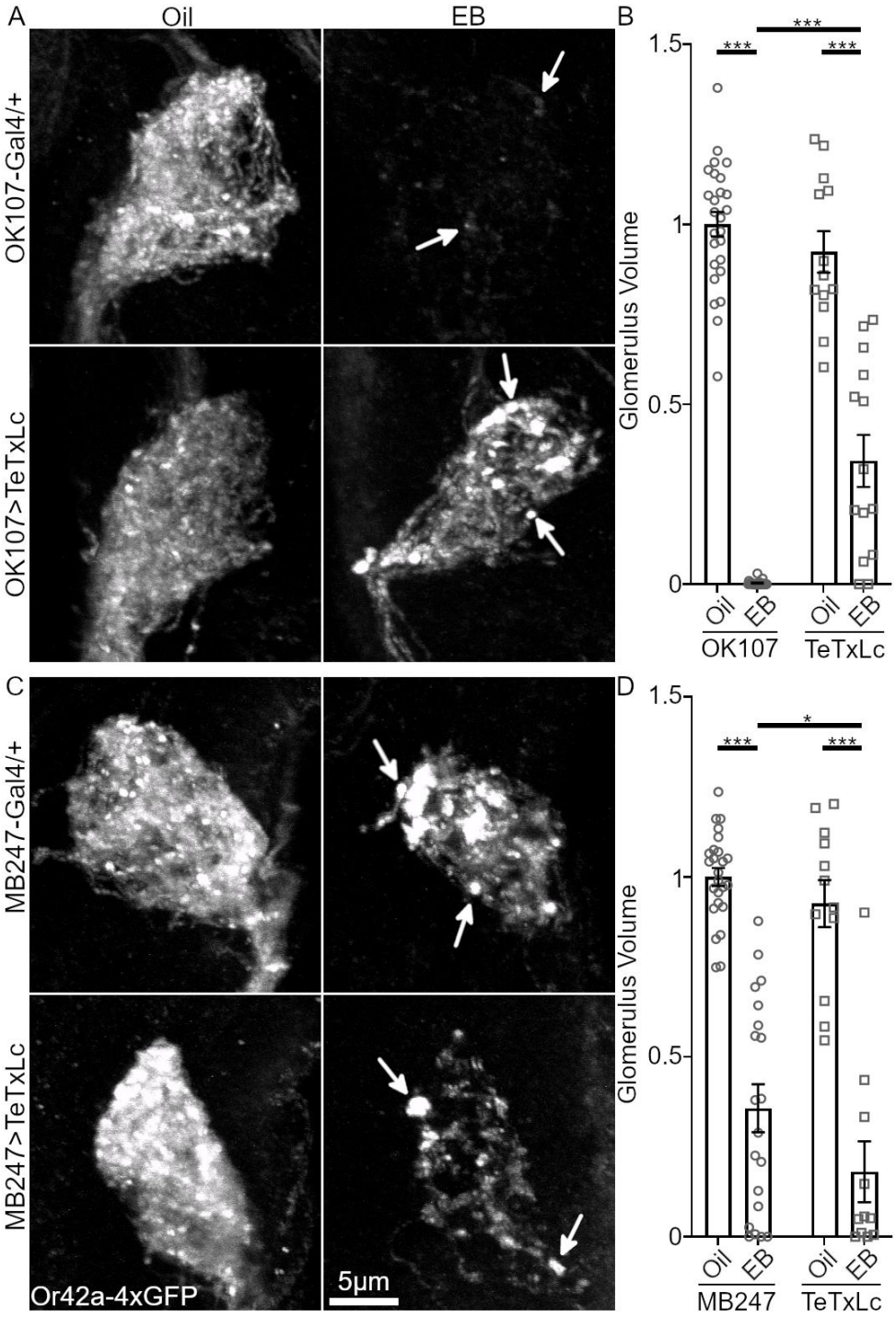

Figure 25: Silencing AL glutamatergic neurons reduces Or42a OSN critical period remodeling **A)** Representative confocal maximum intensity projections of Or42a OSN VM7 innervation (two copies of *Or42a*-mCD8::4xGFP; white). Transgenic control (w^-; *Or42a*-mCD8::4xGFP/+; *Or42a*-mCD8::4xGFP/+; OK107-Gal4/+; top) and with OK107-Gal4 driving UAS-tetanus toxin (OK107>TeTxLc; bottom). Females exposed to oil vehicle alone (left) or 20% EB odorant (right) during the 0-2 dpe critical period. **B)** Quantification of VM7 innervation for the OK107-Gal4 control and TeTxLc blocked animals exposed to either oil or EB. **C)** Imaging as above in A**,** transgenic control (w^-/w^-; *Or42a*-mCD8::4xGFP/*Or42a*-mCD8::4xGFP; MB247-Gal4/+; top) and with MB247-Gal4 driving UAS-TeTxLc (bottom). Females exposed to oil (left) or 20% EB (right) during the critical period. **D)** Quantification of VM7 innervation for MB247-Gal4 control and TeTxLc animals exposed to oil or EB. Scatter plots show all data points and the mean ± SEM. Significance is indicated as $p<0.05$ (*) and $p<0.001$ (***).

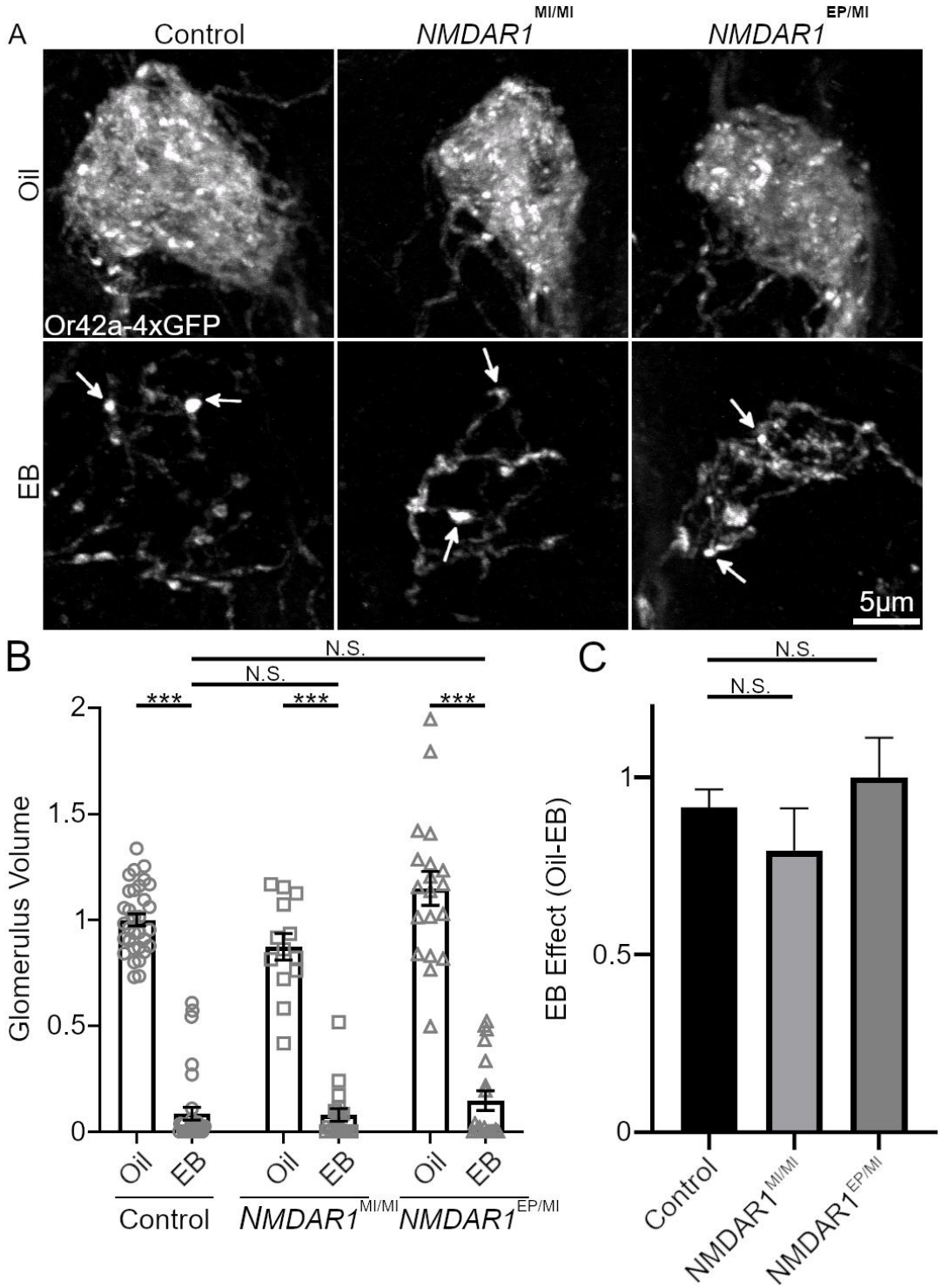

Figure 26: *NMDAR1* signaling is not required for OSN critical period innervation remodeling
A) Representative confocal maximum intensity projections of Or42a OSN VM7 innervation (two copies of *Or42a*-mCD8::4xGFP; white) following exposure to oil vehicle (top) or 20% EB (bottom) during the 0-2 dpe critical period. Three genotypes are shown: transgenic control (*w⁻; Or42a*-mCD8::4xGFP/*Or42a*-mCD8::4xGFP; left), *NMDAR1* mutant (*NMDAR1*^{MI11796}; middle) and a second *NMDAR1* mutant (*NMDAR1*^{EP331}/*NMDAR1*^{MI11796}; right). Remnant puncta following EB exposure are labeled by white arrows. **B)** Quantification of VM7 innervation volume for each genotype and condition. **C)** The difference between oil and EB conditions for each genotype. Scatter plots show all data points and the mean ± SEM. Bar graphs show mean ± SER. Significance is indicated as not significant (N.S.; $p>0.05$) and $p>0.001$ (***).

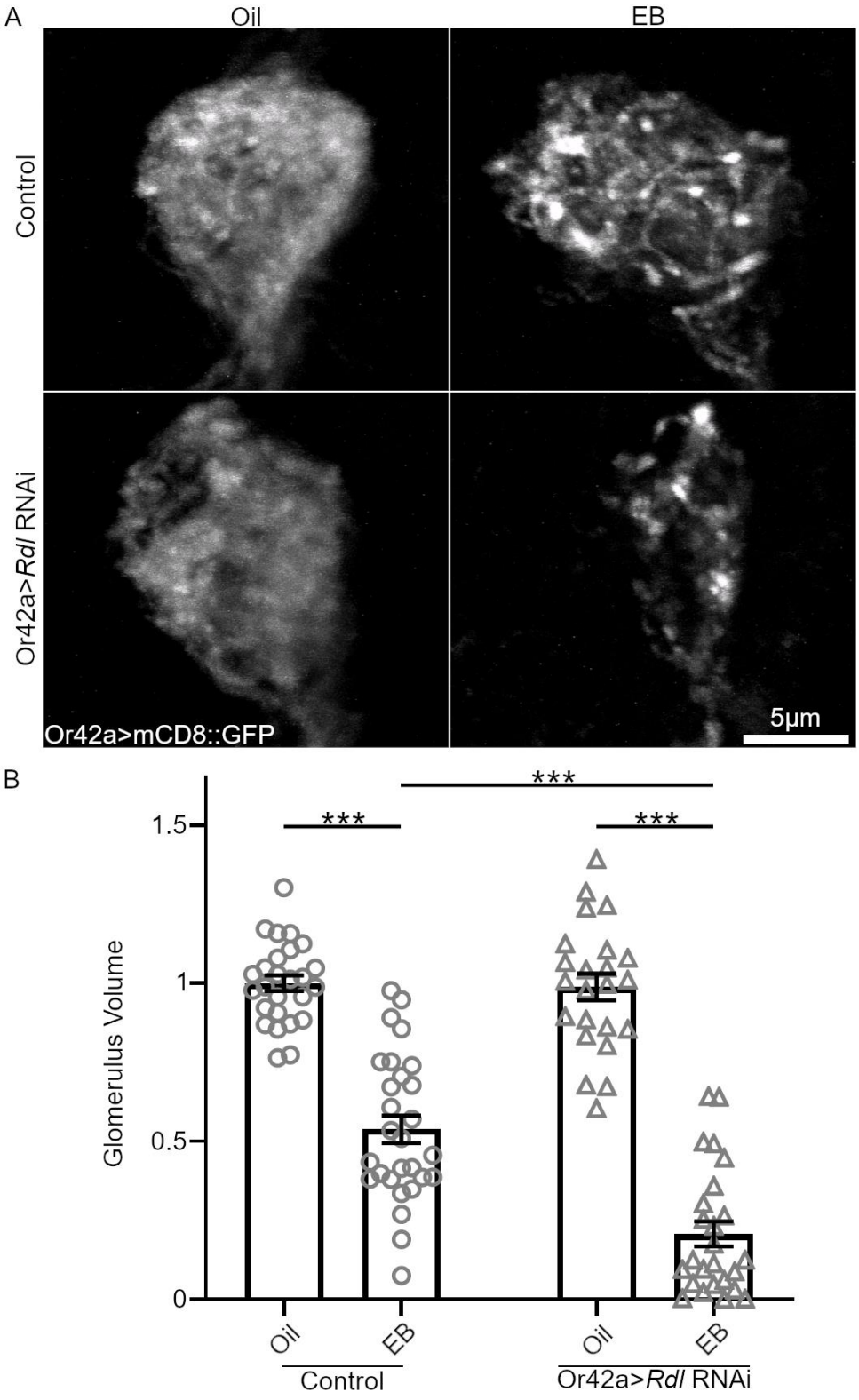

Figure 27: Or42a OSN-targeted $GABA_AR$ knockdown enhances critical period remodeling
A) Representative confocal maximum intensity projections of Or42a OSN VM7 innervation (*Or42a*-Gal4>UAS-mCD8::GFP; white) following exposure to oil vehicle (top) or 20% EB odorant (bottom) during the 0-2 dpe critical period. Two genotypes are shown; transgenic control (*Or42a*-Gal4>mCD8::GFP; top) and *Or42a*-targeted *Rdl* RNAi (*Rdl* RNAi 8-10J; bottom). **B)** Quantification of VM7 innervation for the two genotypes and conditions. Scatter plots show all data points with the mean ± SEM. The significance is indicated as $p<0.001$ (***).

Discussion

The first days of *Drosophila* adulthood mark a critical period for the remodeling of brain olfactory circuitry (Devaud et al., 2003a; Sachse et al., 2007; Tessier and Broadie, 2009; Doll and Broadie, 2015; Golovin et al., 2019; Chodankar et al., 2020). During this developmental window, olfactory sensory neurons (OSNs) manifest heightened adaptability to the new odorant sensory environment. Vertebrates show similarly heightened responsiveness to early odorant exposure. Rodents exposed to odors during development show increased or decreased effects dependent on conditions examined (Dalland and Døving, 1981; Geramita and Urban, 2016; Liu and Urban, 2017). Zebrafish also exhibit olfactory imprinting from developmental odorant exposure (Gerlach et al., 2019). We previously described OSN innervation remodeling that is restricted to an early-life critical period (0-2 days post-eclosion; Golovin et al., 2019). Here, we expand our knowledge of this remodeling by testing the role of FMRP, a protein strongly implicated in activity-dependent critical periods (Dölen et al., 2007; Tessier and Broadie, 2009; Contractor et al., 2015). Based on this study, we propose that FMRP functions to regulate the lateral interactions between OSNs mediated by local interneurons (LNs; Acebes et al., 2011). Previous studies have shown that each OSN receives lateral presynaptic GABAergic inhibition that scales with the total activity of all OSNs, and serves as a gain control mechanism by reducing OSN activity to odorants that activate multiple OSN classes (Olsen and Wilson, 2008). High EB concentrations likely activate multiple OSN classes, in addition to the Or42a OSNs, and should therefore recruit presynaptic inhibition. We would expect this inhibition to limit activity in response to EB exposure and reduce remodeling. Indeed, when we block lateral inhibition either through 1) specifically activating Or42a OSNs or 2) selectively removing Or42a OSN $GABA_A$ receptors, EB odorant exposure has a greater effect on critical period remodeling.

In addition, our previous work showed that *Or42a*-targeted NMDAR1 knockdown impairs Or42a OSN innervation remodeling, likely via reduced lateral excitation (Golovin et al., 2019). However, NMDAR signaling on OSNs has not been directly shown. *Or42a*-targeted FMRP RNAi

impairs the critical period remodeling of Or42a OSNs. Or42a-specific FMRP loss likely alters the OSN response to circuit lateral inputs both by enhancing inhibition and also reducing excitation. This role represents a novel FMRP function for regulating acute OSN remodeling specifically on the presynaptic side (Sudhakaran et al., 2014; Doll and Broadie, 2015, 2016; Franco et al., 2017). Previous studies have found that FMRP is required for mediating long-term habituation (LTH), a form of structural and functional adaption that leads to a reduction in innate avoidance behavior (Das et al., 2011). More specifically, FMRP interacts with a second RNA-binding protein (Ataxin2), contributing to LTH by acting in both the PNs and LNs (Sudhakaran et al., 2014). FMRP-dependent PN remodeling likewise occurs following a single day of activation within a cell-autonomous mechanism (Doll and Broadie, 2015, 2016). The results presented here extend beyond this earlier work in three ways; 1) Or42a OSN remodeling involves lateral inhibition mechanisms, 2) Or42a OSN remodeling is a purely presynaptic process, and 3) Or42a OSN remodeling manifests acute reversibility (Chodankar et al., 2020). The neuron-specific FMRP functions in the AL olfactory circuit highlight an increasingly appreciated FMRP role specificity within different neuron classes.

FMRP is widely expressed in the nervous system (Khandjian et al., 1995; Zhang et al., 2001b), where it binds multiple different target mRNAs, including neuron class-specific transcripts (Darnell et al., 2011). For example, a recent study in mice showed that FMRP binds to circadian protein-encoding mRNAs preferentially in hippocampal CA1 pyramidal neurons compared to cerebellar granule neurons (Sawicka et al., 2019). Therefore, it is important to identify how FMRP loss perturbs the function of specific neuron classes to affect particular neural circuits. The current study describes how unbalancing FMRP levels between neurons of the *Drosophila* olfactory circuit can alter odorant experience-dependent remodeling, revealing how dissecting FMRP functions at a fine cellular resolution can uncover FXS circuit-level impairments (Contractor et al., 2015; Franco et al., 2017; Goel et al., 2018; Lovelace et al., 2019). Neuron class-specific FMRP functions are also revealed by activity-dependent dissection, with optogenetic stimulation causing

opposite phenotypes in the olfactory PN and MB output neurons, but both effects failing when FMRP is absent (Doll and Broadie, 2015). Functionally, recent work on the FMRP role in binding to HCN cation channels demonstrates opposing excitability consequences in hippocampal CA1 compared to layer 5 prefrontal cortex (Brandalise et al., 2020). Together with the results presented here, this work underscores the importance of neuron-specific FMRP mechanisms, and the need to understand how these altered roles combine to generate circuit-level FXS phenotypes.

One intriguing result from our experiments is that despite the important FMRP role in Or42a remodeling, FMRP null mutants maintain normal remodeling capacity. We suggest that this compensation is due to AL LN circuitry that allows for OSN activity to be modified based on the total input to the system (Olsen and Wilson, 2008). LNs excitation scales with the total OSN activity, so when FMRP is altered (LOF/GOF) only in Or42a OSNs there is little change to LN output. However, when FMRP is manipulated in all OSNs equally, the output of LNs is adjusted based on the responsiveness of all the OSNs, thereby balancing the circuit (Olsen et al., 2010; Mohamed et al., 2019). Although this result was unexpected by us, it is not unprecedented for homeostatic mechanisms to be able to overcome FMRP loss (Antoine et al., 2019; Domanski et al., 2019). For instance, in a recent analysis of four monogenic mouse autism models, including FXS, there was an increase in the excitatory-to-inhibitory ratio of pyramidal neurons within the primary somatosensory cortex, which in general served as a homeostatic mechanism to maintain the overall network activity, but there was not increased excitatory spiking (Antoine et al., 2019). Another example from mouse barrel cortex demonstrates that although the development of NMDA-dependent LTP is disrupted in the FXS disease model, there is no apparent defect in lesion-induced plasticity owing to homeostatic compensation (Harlow et al., 2010). In order to more fully understand the FXS condition, we must grasp not only neuron-specific FMRP functions, but also how these functions balance across circuits.

Our results indicate the balanced roles of inhibitory $GABA_AR$ and excitatory NMDAR signaling in OSN remodeling. In our previous report on critical period remodeling, we found that

Or42a-targeted NMDAR1 RNAi impairs the innervation loss from early-life EB odorant exposure (Golovin et al., 2019). Here, we find that targeted tetanus toxin synaptic silencing of GluLNs, the major source of AL glutamatergic transmission (Das et al., 2010), causes a similar impairment to Or42a OSN-targeted NMDAR1 knockdown. However, global *Nmdar1* mutants lack a detectable phenotype. One explanation is that NMDAR signaling acts in a similar fashion to FMRP function, with targeted removal putting Or42a OSNs out of balance with the rest of the circuit, but global loss not generating this imbalance. Since the AL has both metabotropic glutamate receptors (Devaud et al., 2008) and glutamate-gated chloride channels (Liu and Wilson, 2013), GluLNs could mediate their effect on Or42a remodeling by also altering signaling through these receptors. Another unlikely possibility is that since the OK107-Gal4 driver expresses in a few neurons outside the olfactory circuitry (Aso et al., 2009) these distant populations might be mediating the effects. Future experiments testing broader NMDAR1 functions, as well as studies of possible mGLuR-mediated glutamate signaling in AL, will be important to fully elucidate circuit mechanisms that regulate OSN remodeling.

In conclusion, we discover here that unbalanced neuron class-specific FMRP functions can alter lateral OSN interactions and impact critical period OSN remodeling. The findings show that FMRP acts in Or42a OSNs as well as other EB-responsive OSNs to control the response to lateral input. When FMRP is removed only in Or42a OSNs, they have a lower responsiveness to EB exposure and therefore manifest impaired critical period remodeling. However, when FMRP is removed from all OSNs, balance is restored to reinstate the normal remodeling. The FMRP requirement is bidirectional as targeted FMRP elevation in Or42a OSNs also causes circuit imbalance to enhance the effect of odorant experience on critical period remodeling. Furthermore, unlike other forms of activity-dependent remodeling in the AL circuit, this reversible remodeling occurs only in the presynaptic OSN terminals and requires OSN activity, but not OSN synaptic output. Or42a OSN-targeted optogenetic activation drives critical period remodeling, but this activity-dependent mechanism does not require FMRP function in the Or42a OSNs. Despite the

clear involvement of LN glutamatergic and GABAergic signaling in regulating OSN critical period remodeling, their exact circuit connectivity remains to be fully elucidated. The innervation loss and retraction characteristics following critical period odorant experience resemble developmental pruning during *Drosophila* metamorphosis, which suggests similar underlying mechanisms of cytoskeleton disassembly and glial phagocytosis (Yu and Schuldiner, 2014). In addition, the mechanism(s) by which FMRP regulates OSN responses to lateral inputs will be an important avenue for future research. Overall, this work provides a new example of neuron class-specific FMRP function, neural circuit compensation for FMRP loss, and an avenue to inform therapies addressing FXS circuit-level symptoms.

Acknowledgments

We are very grateful to Francois Bolduc for UAS-*dfmr1* RNAi lines (1-1-7, 2-1; University of Alberta, Canada), Ron Davis for UAS-*Rdl* RNAi (8-10J; The Scripps Research Institute Florida, USA), Ilona Grunwald-Kadow for *Or42a*-mCD8:GFP (Technical University of Munich, Germany), Craig Montell for GtACR1-eYFP (University of California Santa Barbara, USA), Mani Ramaswami for NP1227(LN1)-Gal4 (Trinity College Dublin, Ireland), and Bloomington *Drosophila* Stock Center (Indiana University, USA) for many lines. We thank Dominic Vita, Danielle Kopke and Jim Sears for their input. This work was supported by National Institutes of Health Grant MH084989 to K.B.

Chapter IV

Conclusions and Future Directions

Through the course of my thesis work, I discovered *Drosophila* exposed to EB odorant from the end of development (final day of pupation) through the early-use critical period (2 days post eclosion, dpe) show reduced innervation volume of presynaptic axon terminals of O42a olfactory sensory neurons (OSNs) in the target ventral metdial 7 (VM7) synaptic glomerulus within the brain antennal lobe (AL; Fig. 5). This innervation loss within the olfactory glomerulus likely represents a glial-dependent phagocytosis and removal of the Or42a processes for three reasons (Fig. 28). 1) The signal from membrane-bound fluorescent markers is dimmer following EB exposure. 2) The persistent processes are more sparsely distributed within the glomerulus. 3) Bright puncta appear that resemble retraction bulbs following synaptic pruning (Low and Cheng, 2006) or blebbing during Wallerian degeneration (Conforti et al., 2014). The EB odorant sensory experience drives these changes by activating EB odorant receptors on the O42a OSNs (Fig. 10). The activation of the odorant receptor likely leads to cation influx driving the synaptic remodeling as the same phenotype is driven by a light-activated cation channel using optogenetics (Fig. 20). I demonstrated that the Or42a innervation remodeling can be altered by Or42a OSN-targeted reduction of FMRP, which acts to alter responses from LNs and unbalance homeostatic compensation mechanisms in the brain AL circuit. Overall, my work reveals a novel form of critical period synaptic remodeling and demonstrates a new role for FMRP in regulating sensory experience-dependent critical period refinement in neuron class-specific in brain olfactory AL circuit mechanisms.

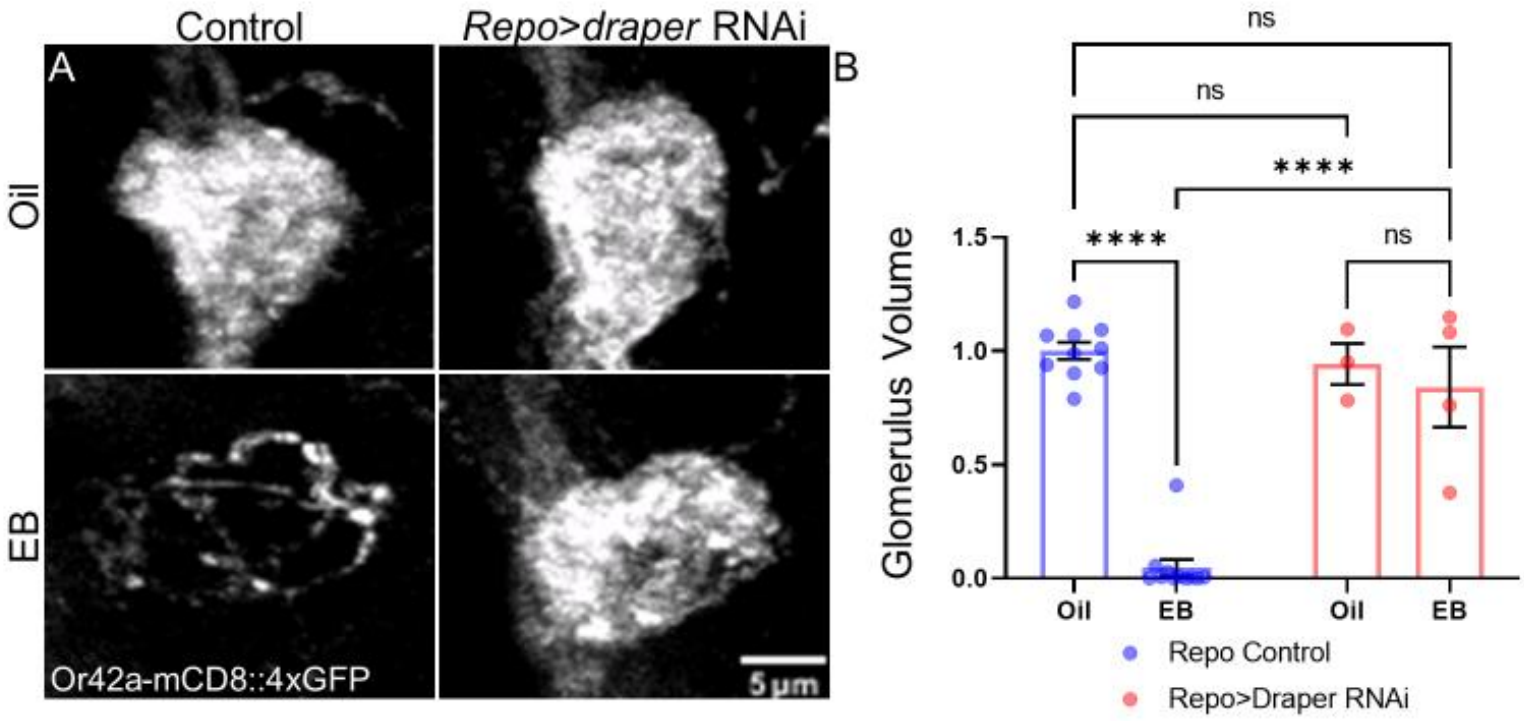

Figure 28. Glial-targeted Knockdown of *draper* Blocks Or42a Remodeling
A) Representative confocal maximum intensity projections of Or42a olfactory sensory neurons (OSNs) innervating the antennal lobe (AL) ventral medial 7 (VM7) glomerulus (*Or42a*-mCD8::4xGFP; white). Females were exposed to mineral oil vehicle (top), or 20% ethyl butyrate (EB) odorant (bottom) from 0-2 days post eclosion. Two genotypes are shown: transgenic control (*w';Or42a*-mCD8::4xGFP/+;*Or42a*-mCD8::4xGFP/+; left), and the same transgenic with glial-targeted *draper* RNAi (*Repo*-Gal4>*draper* RNAi; right). **B)** Quantification of the *Or42a*-OSN VM7 innervation volume for both genotypes and treatment conditions. Scatter plots show all data points and the mean ± SEM. The significance is indicated as non-significant (ns) or significant at $p<0.0001$ (****).

How Does Or42a OSN Remodeling Fit as a Critical Period?

Early-use critical periods have four major phases: pre-experience, onset of experience, refinement and stabilization (Fig. 1, 29). The remodeling of Or42a OSNs explored here fits within these phases. Prior to the onset of olfactory sensory experience, the AL has a genetically “hard-wired” structure representing a glomerular map (Fig. 29; Vosshall et al., 2000). OSNs are the final neurons to innervate the AL and are targeted to the correct glomerulus by a combination of secreted signaling molecules and cell-surface adhesion molecules (Hong and Luo, 2014). The maxillary palp OSNs reach the AL prior to eclosion at around 32 hours after puparium formation (APF) and begin to infiltrate the AL by 36 hours APF (Sweeney et al., 2007). OSNs have been shown to respond to odors if the fly is removed from the pupal case prior to birth (Dubin and Harris, 1997), but my results indicate that exposure to the EB odorant prior to eclosion did not lead to altered Al glomerulus innervation. This indicates that the eclosion transition initiates the activity-dependent response of OSNs to EB, although the events that are triggered by eclosion to affect use-dependent neuronal structure and function are not known (Fig. 29). Just the emergence from the pupal case would certainly allow for greater odorant responses following eclosion, however other hormonal shifts might be important triggers (Nässel and Zandawala, 2020). The innervation remodeling studied here falls into the refinement phase of the odor-exposure critical period (Fig. 29). Several papers have explored the role of early odorant experience on OSN structure/function and behavioral output during this same critical period (Devaud et al., 2001, 2003; Sachse et al., 2007; Kidd et al., 2015; Chodankar et al., 2020).

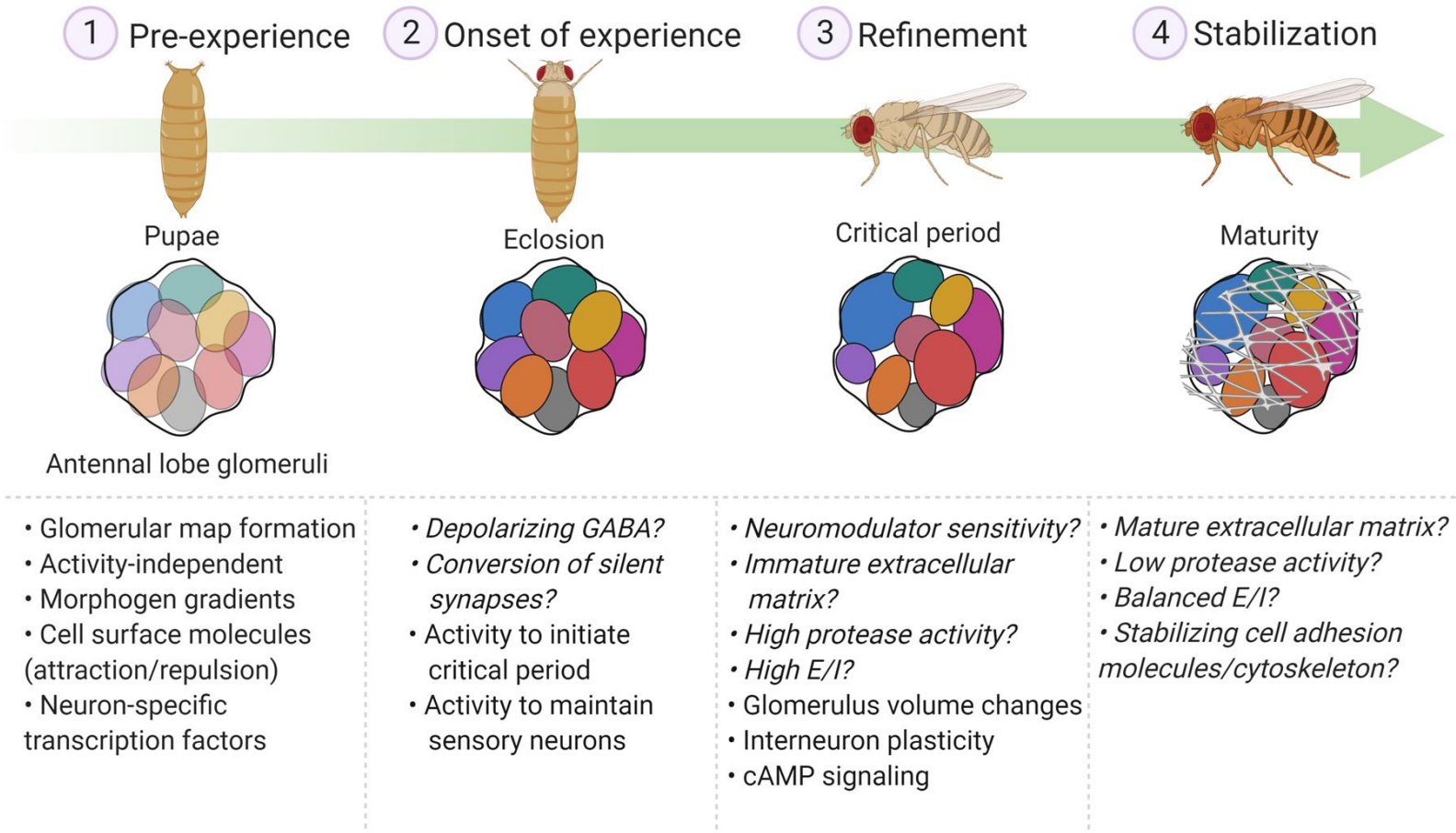

Figure 29. Proposed Phases of Critical Period in *Drosophila* Antennal Lobe
1) Pre-experience. Prior to experience, the antennal lobe (AL) generates a glomerular map in an activity-independent fashion. This map is formed by a combination of the morphogen gradients, cell-surface attractants and repellants and glomerulus-specific transcription factors. **2) Onset of Experience.** The onset of sensory stimulation of the AL occurs at elcosion as the fly emerges from the pupal case. This burst of activity at ecolsion marks the onset of the olfactory critical period and serves to maintain OSN stability until maturation about a week later. It is currently unknown whether the AL has depolarizing GABA signaling at the onset of the critical period or whether the primary cholinergic AL synapses undergo the equivalent of silent synapse conversion. **3) Refinement**. During the critical period the volume and function of AL neurons shifts in response to the odor environment. This refinement relies on the activity of local interneurons and downstream cyclic AMP signaling. Whether the AL olfactory critical period requires neuromodulators, depends on immature extracellular matrix and high protease activity or a relativity high excitation to inhibition ratio remain to be established. **4) Stabilization.** Nothing is currently known about the molecular mechanisms that lead to the closure of the critical period in the AL. Based on work on mammalian critical periods, maturation of extracellular matrix structures, lower protease activity, balancing of excitation and inhibition and stabilizing cell adhesion and cytoskeleton are all strong candidates. Created with BioRender.com.

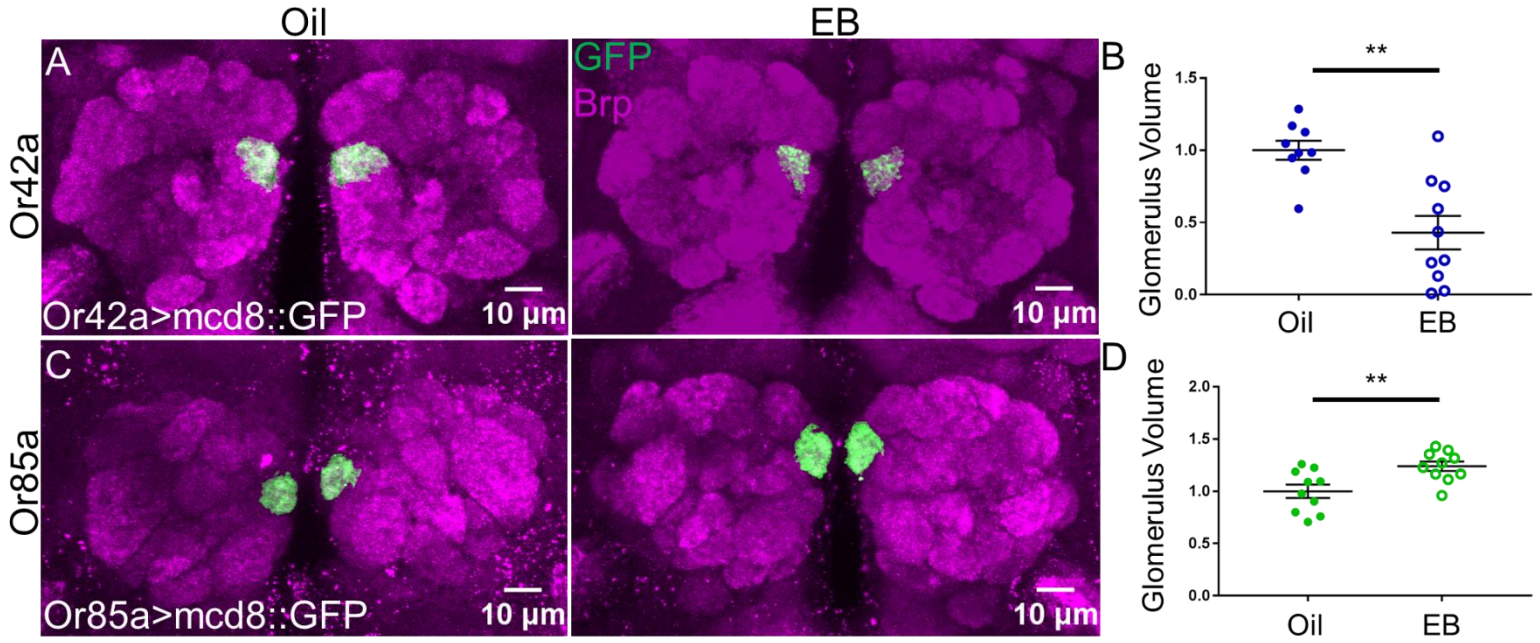

Figure 30. Opposite Responses of Or42a and Or85a OSNs to Critical Period EB Exposure
A,C) Representative confocal maximum intensity projections of olfactory sensory neurons (OSNs) innervating the antennal lobe (AL) co-labeled with presynaptic active zone marker Bruchpilot (BRP) to visualize glomerulus structure (magenta) and OSN-targeted mCD8::GFP (green). Animals were exposed to mineral oil vehicle (left), or 15% ethyl butyrate (EB) odorant (right) from 0-2 days post eclosion. Two genotypes are shown: *Or42a*-Gal4>UAS-mCD8::GFP; top), and Or85a (*Or85a*-Gal4>UAS-mCD8::GFP bottom). **B,D)** Quantification of the *Or42a*-OSN VM7 (top) or *Or85a*-OSN DM5 (bottom) innervation volume for both treatment conditions. Scatter plots show all data points and the mean ± SEM. The significance is indicated as significant at $p<0.01$ (**).

The work presented here has important differences from these previous studies. First, studies from some labs have started from the first day following eclosion while other groups have waited until the second day to begin exposure (Fig. 5; Devaud et al., 2003a; Sachse et al., 2007; Das et al., 2011; Sudhakaran et al., 2014; Doll and Broadie, 2015, 2016; Chodankar et al., 2020). Work from our group has demonstrated that this first day is a key part of the critical period with changes to both Or42a OSNs and Vl1 projection neurons (PNs) (Fig. 5; Doll and Broadie, 2015, 2016). This is in line studies from other systems that show changes at the onset of sensory experience (Fox, 1992; Rheede et al., 2015). Previous work is based on a behavioral study that began a day later (2 dpe), perhaps due to difficulties in precisely timing the developmental exposure around eclosion. The other important difference is when changes are assayed. Some studies looked for the effects of odorant exposure immediately after the animals were removed from the odor (Fig. 5; Devaud et al., 2003a; Sachse et al., 2007; Das et al., 2011; Sudhakaran et al., 2014; Doll and Broadie, 2015, 2016; Chodankar et al., 2020), while others have waited a day following odorant exposure in order to avoid possible effects of habituation on measures of function and behavior (Devaud et al., 2003a; Sachse et al., 2007; Das et al., 2011; Sudhakaran et al., 2014). Overall, eclosion marks the onset of olfactory experience and the start of the phase of refinement.

AL refinement preserves the gross glomerular map, but alters the strength of individual OSN class channels (Fig. 29). The work on glomerulus innervation remodeling during the early-use critical period has found that different classes of OSNs tend to respond differently to activating odors (Fig. 5, 30; Devaud et al., 2001, 2003; Sachse et al., 2007; Chodankar et al., 2020). Early studies showed both increases and decreases in glomerular innervation volume depending on both the odor and the glomerulus assayed. Later studies using targeted genetic tools proposed a model that the activated glomerulus increases innervation volume following exposure to a specific odorant during the critical period (Devaud et al., 2001, 2003; Sachse et al., 2007; Das et al., 2011). However, the work I present here demonstrates that odorant exposure to EB leads to a

decrease in Or42a OSN innervation volume. Similarly, work from our lab on pyrrolidine odorant exposure during the first day of the critical period showed that VL1 PNs have reduced volume (Doll and Broadie, 2015). However, neuronal volume changes do not reliably predict changes in function. For example, EB exposure increases the volume of DM5 neurons, but decreases their function (Das et al. 2011). A similar trend holds true for CO_2 exposure and the innervation of the V glomerulus (Sachse et al. 2007), but geranyl acetate exposure leads to an increase in the volume of the VA6 glomerulus and a concomitant increase in function (Kidd et al. 2015). However, the decrease in the VL1 PN volume in response to optogenetic activation is matched by an increase in function (Doll and Broadie, 2015, 2016).

Although I did not directly measure the functional changes associated with EB exposure on Or42a OSNs, the dramatic reduction of presynaptic sites suggests decreased function (Fig. 8, 9). One importance difference, however, is that the Or42a volume reduction is suggested to be relatively short lived, at least without maintained sensory experience (Fig. 7; Chodankar et al. 2020), which makes discriminating between habituation versus remodeling potentially challenging. The direction of the response to odorant likely depends on the connections to local interneurons (Das et al., 2011; Acebes et al., 2012). Although all critical period changes in the AL may rely on interneuron connectivity, the longer lasting changes seem to be directly regulating interneuron synapses (Sachse et al., 2007; Das et al., 2011). In contrast, Or42a remodeling reduces OSN presynaptic terminals without altering postsynaptic PN volume, indicating a differential mechanism (Fig. 24). My Or42a OSN-targeted optogenetic experiments indicate that innervation volume reduction is dependent on specific neuron expression rather than differences in the response to odorants from Or42a receptors. This could be directly tested by exogenously expressing other classes of receptors to drive the effect with different odorants, or alternatively by expressing Or42a receptors in all sensory neurons and testing the response to EB. Together, these experiments suggest that both the identity of the neuron and the timing of the exposure and

analysis determine the direction of structural and functional changes that occur during early sensory experience critical period AL refinement.

The stabilization phase of the *Drosophila* early-life odorant exposure critical period is not well studied (Fig. 29). Work has focused mainly on reversibility studies (Fig. 7; Devaud et al., 2003a; Sachse et al., 2007), with one recent study exploring routes to extend the critical period (Chodankar et al., 2020). In general, critical periods are considered to be times of heightened sensitivity when the sensory environment can lead to long-lasting changes in brain circuitry and behavioral outputs (Reh et al., 2020). However, if the environmental stimulus is removed during the critical period neural circuits and behaviors can shift back towards the basal state (Hubel and Wiesel, 1970; Sachse et al., 2007). The reversibility of structural changes driven by critical period odorant exposure has been tested in several paradigms (Fig. 7; Devaud et al., 2003a; Sachse et al., 2007; Chodankar et al., 2020), but only one study has tested the timing of the reversibility (Sachse et al., 2007). My studies did not directly address when the reversibility of the Or42a OSN remodeling could occur. I showed that Or42a OSN volume reduction occurs following just 24 hours of EB odorant exposure, and that removing animals from the odor leads to re-innervation of the target glomerulus within the first 4 days of life. Another group demonstrated a large amount of re-innervation happening within 12 hours after 4 days of EB exposure (Chodankar et al., 2020).

It remains to be seen if Or42a remodeling can be reversed if the odor is removed later in life. If sensory experience can only drive volume reduction during the critical period, but can be reversed any time after the critical period, then it would not fit into the strict definition of a critical period as leading to long-lasting changes (Knudsen, 2004). One result that might hint at there being a time restriction for the reversal of remodeling comes from my experiments which show that a small number of animals did not reverse, possibly indicating that 4 days might be around the end of the period when the innervation changes are reversible. Alternatively, this could indicate that once denervation of the Or42a OSNs reaches a certain point, the neurons are no longer able to reinnervate the target glomerulus. A recent paper demonstrated that, for some

odor-glomerulus pairs, temporally silencing of the OSN input to the target glomerulus for 2 days following eclosion could extend the critical period (Chodankar et al. 2020). This study is interesting as it agrees with ocular dominance plasticity in the primary visual cortex of mammals, which can be extended by dark-rearing animals from birth (Cynader, 1983). Future work is needed to test whether temporary silencing of Or42a OSNs can extend the critical period to olfactory sensory experience.

Molecular Mechanisms of the Antennal Lobe Glomerular Remodeling

It is clear from my work and previous studies that the first few days of *Drosophila* life mark a critical period for AL glomerular innervation and function. This window is closed by the end of the first week and possibly as early as the third day (Fig. 5; Devaud et al., 2003a; Sachse et al., 2007; Chodankar et al., 2020). Despite knowledge of the timing of the critical period, molecular and circuit mechanisms that control the closure of heightened sensitivity are unknown. The extensive work done in the mammalian visual system points to structural, functional and epigenetic changes controlling this critical period end point (Fig. 1; Hensch, 2004; Reh et al., 2020). It is likely that all three of these levels of change also act together to close the critical period for AL glomerular innervation remodeling. The stabilization of synaptic structure involves trans-synaptic adhesion and signaling molecules, cytoskeletal elements and extracellular matrix proteoglycans (Hensch and Quinlan. 2018; Ribic and Biederer, 2019). Instruction of AL glomerular map formation during pupal development relies on a code of adhesion molecules and cell-surface receptors (Hong and Luo, 2014). It is appealing to speculate that at least some components of this program are involved in critical period remodeling.

Notch signaling is required in response to odorant exposure for growth of the V and VA6 glomeruli while silencing of Or22a OSNs leads to a slow degeneration that can be ameliorated by overexpression of the wingless (Wg) ligand (Chiang et al., 2009; Kidd et al., 2015). Within the AL

Notch signals by binding to its cell-surface ligand Delta or through a poorly understood non-canonical mechanism. Upon activation, the Notch intercellular domain is cleaved and translocated to the nucleus to drive transcription of target genes (Kidd and Lieber, 2016). However, EB-driven remodeling of Or42a OSN innervation was not mediated by either of these pathways based on my work using RNAi mediated knockdowns and mutants. Despite the lack of effect on the EB-dependent remodeling, both signaling pathways had a significant impact on the basal innervation of Or42a OSNs to the VM7 glomerulus. Or42a-targeted RNAi against the Notch ligand Delta reduced basal innervation volume, while reducing Notch levels had no effect on volume (Fig. 31). A more comprehensive assessment of Wg signaling indicates an involvement of a non-canonical pathway in controlling basal Or42a OSN volume. Although Wg heterozygote mutants had normal basal innervation volume, Or42a expression of a dominant-negative form of the Wg receptor, Frizzled-2 (Zhang and Carthew, 1998), reduces basal volume. Conversely, expressing a dominant-negative form of Shaggy, a protein typically downregulated by Wg signaling (Bourouis, 2002), increases basal volume. In addition, Notch and Wg signaling may intersect as Notch activation can alter the function of disheveled in the Wg signaling pathway (Axelrod et al., 1996; Collu et al., 2012). My studies have not indicated a role for the previously implicated signaling molecules, but a more compressive assessment of both signaling and adhesion molecules is needed to determine the role these proteins play in structural remodeling during the critical period.

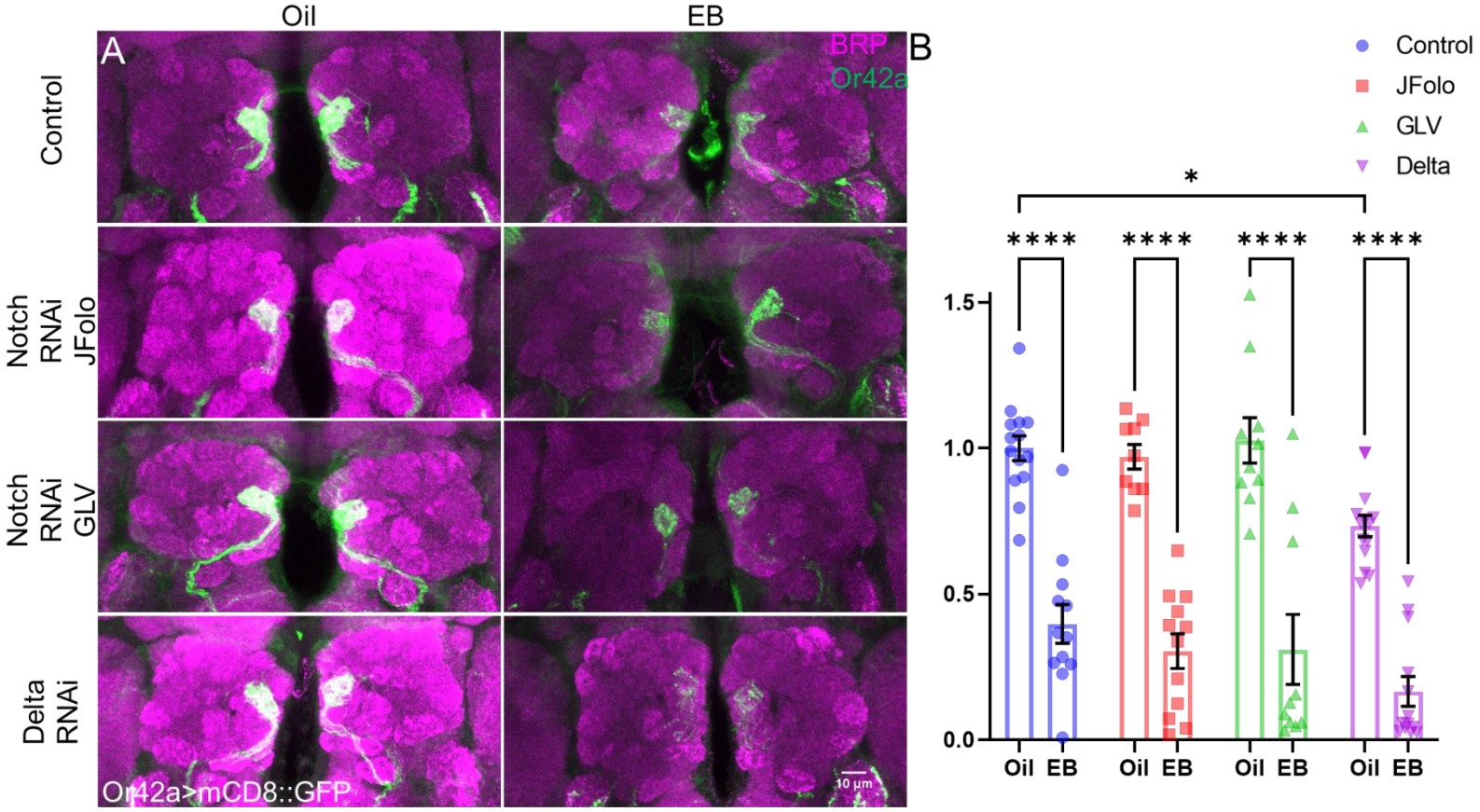

Figure 31. Effect of Notch Pathway Manipulations on Or42a Remodeling
A) Representative confocal maximum intensity projections of Or42a olfactory sensory neurons (OSNs) innervating the antennal lobe (AL) ventral medial 7 (VM7) glomerulus (*Or42a*-Gal4>UAS-mCD8::4xGFP). Females co-labeled with presynaptic active zone marker Bruchpilot (BRP) to visualize glomerulus structure (magenta) and mCD8::GFP (green) were exposed to mineral oil vehicle (left), or 20% ethyl butyrate (EB) odorant (right) from 0-2 days post eclosion. Four genotypes are shown: transgenic control (*w*⁻;UAS-mCD8::GFP/+;*Or42a*-Gal4/+; top), the same transgenic with *Or42a*-targeted weak *Notch* RNAi (*Or42a*-Gal4>*Notch* RNAi JFolo; second), *Or42a*-targeted strong *Notch* RNAi (*Or42a*-Gal4>*Notch* RNAi GLV; third) and *Or42a*-targeted weak *Delta* RNAi (*Or42a*-Gal4>*Delta* RNAi; bottom). **B)** Quantification of the *Or42a*-OSN VM7 innervation volume for both genotypes and treatment conditions. Scatter plots show all data points and the mean ± SEM. The significance is indicated as significant at $p<0.0001$ (****) and $p<0.05$(*).

Critical periods employ the cytoskeleton to control the stability of synaptic processes. In mammals, live imaging shows dendritic spines are more motile and plastic during the critical period and become stabilized following its closure (Majewska and Sur, 2003). Currently, the role of the cytoskeleton in Or42a critical period remodeling is unknown. My preliminary experiments testing Or42a-targeted knockdown of the microtubule-associated protein 1B (MAP1B) homolog Futsch did not impact remodeling. Futsch is strongly present in OSN axons, but does not extend into the synaptic regions of the AL. The microtubule-binding protein Jupiter is a more interesting target, with expression in the AL synaptic region (Nagarkar-Jaiswal et al., 2015). The involvement of the actin cytoskeleton in regulating AL critical period remodeling is even less explored. It is likely that actin dynamics play a key role in remodeling, as cyclic AMP (cAMP) signaling downstream of calcium/calmodulin-dependent kinase II (CAMKII) activation has been shown to play an important role in regulating the volume increase in the dorsal medial 5 (DM5) and ventral (V) glomeruli following odorant exposure (Das et al., 2011; Sudhakaran et al., 2014). Due to the connection of calcium binding proteins like CAMKII with cytoskeleton dynamics differential calcium influx in response to odors (Wang et al., 2003; Halty-deLeon et al., 2018) and/or the differential expression of calcium-binding proteins (Mukunda et al., 2014) are prime candidates for controlling the regulation of glomerular volume changes and for dictating whether a given glomerulus will increase or decrease in volume following prolonged exposure. The role of the cytoskeleton in regulating critical period dynamics is largely untapped in the AL and represents a fruitful are for further research.

The dynamic regulation of the cytoskeleton by calcium influx, trans-synaptic signaling and cell adhesion molecules allows for the tremendous connectivity changes during the critical period. However, what leads to the stabilization of synapses at the close of the critical period is the maturation of the extracellular matrix surrounding the synapses (Pizzorusso et al., 2006). This maturation is punctuated by the formation of dense proteoglycan networks, which serve to limit neuronal motility and regulate synaptic signaling molecules (Pizzorusso et al., 2006; Sugiyama et

al., 2008). In mammals, the proteoglycan network is called the perineuronal net (PNN) and disruptions of these networks using enzymes can reinstate critical period-like plasticity (Pizzorusso et al., 2006). An equivalent structure has not been characterized in the *Drosophila* AL, but work at the larval neuromuscular junction has uncovered a rich cohort of proteoglycans that regulate synapse formation (Rushton et al., 2020). It is likely similar mechanisms occurs at the central AL synapses, as many of the same signaling molecules that rely on proteoglycan function are present. Glia may also can play an instrumental role. For instance, astrocytes help to close a critical period for the *Drosophila* larval motor circuit through interaction with adhesion molecules neurexin and neuroligin, which act to reduce dendrite dynamics (Ackerman et al., 2020). In the mouse visual cortex, maturing glia reduce their secretion of the protease MMP9 during the critical period, which allows proliferation of the extracellular PNNs (Ribot et al., 2020). It will be interesting to test the role of extracellular matrix proteoglycans in neuronal stabilization at the close of the AL critical period by using glycan-targeting enzymes like chondroitnase (Pizzorusso et al., 2006) or heparinase (Pérez et al., 2016; Dear et al., 2017) and look for critical period like refinement in mature animals. Overall, the creation and expansion of extracellular proteoglycan networks serves to limit trans-synaptic signaling and cytoskeletal dynamics leading to the close of the critical period.

Functional and Behavioral Changes Associated with Critical Period Odorant Exposure

In concert with the structural maturation during the critical period, the function of the AL circuit is profoundly modified during the critical period. I found that animals exposed to EB during the critical period had a large reduction in presynaptic active zone Bruchpilot (BRP; Fig. 8; Wagh et al., 2006) as well as reduced numbers of ultrastructurally-defined synapses (Fig. 9). Together these results suggest a decrease in presynaptic function following odorant exposure. Due to the complete loss of presynaptic markers in some animals, and the lack of importance of Or42a OSN

synaptic output for critical period remodeling, it seems unlikely that the loss of presynapses would be specific to any type of connection (i.e. OSN-LN or OSN-PN). Therefore, the consequence of EB exposure on Or42a OSN function to presumably is a large decrease in output. Future work is needed to directly measure the changes in output of Or42a OSNs, however a few technical challenges will need to be overcome. First, since the change in innervation is focused on presynaptic terminals, using a genetically coded calcium (e.g. GCaMP) or voltage sensor (e.g. ArcLight) would be useful to provide spatial specificity (Jin et al., 2012; Chen et al., 2013; Lin and Schnitzer, 2016). However, the decrease in the innervation of the VM7 glomerulus and the decreased signal associated with EB exposure might make it difficult to image the diminished signal. An alternative would be to measure the output of the neurons to the postsynaptic PNs with GCaMP or ArcLight. In this experiment, the Or42a OSNs would be activated optogenetically to avoid lateral excitation of the VM7 PNs. A second issue when analyzing the functional consequences of critical period EB exposure is separating the critical period remodeling from short-term habituation (Das et al., 2011). One possibility would be to extend the exposure and hope that the remodeling persists longer than 12 hours after the close to the critical period. If this does not work, an alternative approach would use a *synapsin* mutant to block short-term habituation (Sadanandappa et al., 2013) while assessing functional changes. This method requires testing to make sure these mutants do not have an altered remodeling phenotype. The Or42a OSN remodeling following EB odorant exposure suggests that it does not share a similar circuit mechanism to previous studies.

Previous work on other odorant exposure paradigms has shown that functional changes rely on a change in OSN-LN and PN-LN connections (Sachse et al., 2007; Das et al., 2011; Sudhakaran et al., 2014). Although not directly shown for VL1 PNs, this type of mechanism would fit with these neurons reducing their connections with inhibitory GABAergic LNs and thereby leading to the observed increase in activity with decreasing volume (Doll and Broadie 2016). The remodeling of Or42a OSNs following critical period EB exposure is both quantitatively and

qualitatively different from other forms of remodeling. Quantitatively, the percentage change in volume is much greater (20-30% vs. 50-100%) and the duration of the shift is shorter (12-24h vs. at least 48h). Qualitatively, Or42a OSNs display large (up to 1 micron) puncta that appear similar to retraction bulbs (Fig. 16; Low and Cheng, 2006) and similar structures also occur in degenerative processes (Chiang et al., 2009). I therefore speculate that the mechanisms underlying Or42a OSN remodeling are closer to those of large-scale pruning during *Drosophila* metamorphosis (Watts et al., 2003), or loss of closed-eye inputs during monocular deprivation (Antonini and Stryker, 1993), than the fine-scale refinement of individual boutons or spines. One way to test this hypothesis could be to examine the extent of caspase activity since fine-scale refinement uses local caspase activation while large scale refinement would have broader activity (Mukherjee and Williams, 2017).

There are some studies that produce phenotypes reminiscent of the Or42a remodeling. First, work on glial phagocytosis following OSN axon severing leads to a slow degeneration of the axon processes over several days and a generally sparser innervation over that time (Macdonald et al. 2006). Or42a OSN remodeling appears to use a similar pathway, as my preliminary data suggests glial draper is required for the volume reduction, implicating glial phagocytosis in this critical period process (Fig. 28). A second study demonstrated that OSNs without functional olfactory co-receptor protein (Orco), necessary to form the ion conducting pore the olfactory receptors (Butterwick et al., 2018), or that are genetically silenced undergo a progressive degeneration of OSN axons that likely depends on glial draper signaling (Chiang et al. 2009). Finally, a third study implicated the presentation of cell surface phosphatidylserine (PS) as an “eat me” signal to induce the glial-dependent phagocytosis of OSNs (Sapar et al. 2018). Interestingly, overexpression of a calcium-dependent scramblase (TMEM16F) led to increased PS expression and rapid neuron degeneration in response to strong odorant exposure of OSNs. EB exposure of Or42a neurons during the critical period could lead to a prolonged increase in calcium levels at the axon terminals facilitating the activation of calcium-dependent proteins to promote

degeneration. The TMEM16F scramblase could be a promising starting point to investigate calcium-dependent mechanisms. Together these results suggest that prolonged activation of Or42a OSNs during the critical period promotes activity (possibly calcium) dependent recruitment of phagocytic glia, which break down presynaptic terminals, but spare postsynaptic neurons.

In all other cases of critical period remodeling following odorant exposure, there is aligned pre- and postsynaptic changes (Sachse et al., 2007; Chodankar et al., 2020). In contrast, my EB exposure studies show a specific presynaptic change, and I suggest three possible hypotheses for this difference. First, EB exposure greatly increases the variability in postsynaptic VM7 PN volume, which might resolve into a more persistent change observable at a later time point (Fig. 24). A second hypothesis suggests the difference between Or42a OSNs and other glomeruli is that these OSNs are the most activated by EB exposure (Münch and Galizia, 2016), but inhibitory neurons limit the activation of the downstream PNs (Olsen and Wilson, 2008). In other words, Or42a OSN activity could increase linearly over a greater odor concentration range than VM7 PNs, leading to a plateauing of PN activity. This hypothesis would suggest that VM7 PNs may have the capacity to remodel, but are suppressed by circuit inhibition. Direct activation of VM7 PNs using optogenetics could test this idea by activating these neurons in the absence of OSN input. A third hypothesis incorporates an interaction between pre- and postsynaptic neurons. Since inhibition can differentially affect OSNs and PNs (Olsen et al., 2010), at the high EB concentrations used in my experiments VM7 PNs could be near completely inhibited while Or42a OSNs are still strongly activated. This mismatch between pre- and postsynaptic activity could trigger a breakdown of the synaptic connections via a mechanism similar to mammalian spike-timing dependent long-term depression (Feldman, 2000; Froemke and Dan, 2002). Altogether these functional alterations could correspond to my strong reduction in VM7 glomerular innervation and loss of presynaptic markers seen after critical period EB exposure.

Despite the profound changes on the Or42a OSN-dependent olfactory circuitry by critical period olfactory experience, the impact on animal behavior may be much more subtle. Animals

exposed to four days of EB during the critical period show reduced long-term habituation (LTH), an avoidance to aversive concentrations of EB in a Y-maze test (Das et al., 2011). However, the Or42a remodeling appears to be shorter lived and regulated by different mechanisms than LTH. Therefore, similar to the functional analysis, an assessment of behavioral changes following EB exposure would need to use either timing or genetic technics to separate critical period changes with short-term habituation. Based off of the loss of innervation and reduction of Or42a OSN synapses following critical period EB exposure, the simplest interpretation would be a reduction in Or42a-dependent behavior. In order to test changes to Or42a-dependent behavior, three different methods could be employed to test for attraction or avoidance behavior: 1) Use of an odor that elicits spiking in only VM7 PNs (Olsen and Wilson 2008). 2) Optogenetic activation of Or42a OSNs using the specific Or42a-Gal4 line. 3) Using animals with functional Orco rescued only in Or42a OSNs in order to eliminate the influence of most other olfactory glomeruli.

Based on optogenetic activation experiments, the response of animals to Or42a odorant is attraction or approach behavior (Gomez-Marin et al., 2011; Bell and Wilson, 2016). From this it would follow that EB exposure by reducing Or42a innervation and synapse number would decrease Or42a-based attraction. The behavioral response to EB, which more broadly activates many OSN classes (DoOR 2.0; Münch and Galizia, 2016), would likely be more complex. The overall response to high concentrations of EB is avoidance, while lower concentrations are attractive (Semmelhack and Wang, 2009). Targeted expression of Orco protein in an *orco* null background has demonstrated that expression in Or42a, Or42ab or Or92a OSNs is sufficient to restore attraction and Or85a expression is sufficient to restore avoidance (Semmelhack and Wang, 2009; Asahina et al., 2009). I observed decreased volume of Or42a OSNs and increased volume of Or85a OSNs following critical period EB exposure (Fig. 5, 30). However, I did not assess the synaptic strength of the Or85a OSNs at the structural or functional levels, and therefore it is difficult to conclude the direction of the change. Based on the results from the LTH experiments from other groups, the increase in volume would reduce activity by forming more

connections with inhibitory GABAergic LNs (Das et al., 2011). All of these changes together would suggest a decreased response to both high and low concentrations of EB with less avoidance and attraction, respectively. Future experiments are needed to understand the extent of behavioral changes seen after critical period Or42a OSN remodeling, and how it compares to other critical period changes in the AL.

The Role of Or42a Synaptic Output in Controlling Critical Period Remodeling

One of the most intriguing findings from my experiments on Or42a OSN critical period remodeling is the unexpected effects of Or42a-targeted tetanus toxin light-chain (TeTxLc; Sweeney and Broadie, 1995; Fig. 11, 22) expression and other neuronal silencing techniques. A comparison of different approaches to "silence" Or42a OSNs unveils a variety of different outcomes. The inward rectifying potassium channel Kir2.1 (Baines et al., 2001) hyperpolarizes the membrane of neurons and leads to a reduction in action potential generation. Or42a OSNs expressing Kir2.1 show a large reduction of basal Or42a OSNs signal, but little change in volume in response to EB exposure during the critical period. These experiments are difficult to interpret as it is unclear whether the basal reduction in OSN innervation volume reflects fewer processes within the VM7 glomerulus, or simply less GFP expression of the neurons. Interestingly, despite little change to innervation volume in Or42a>Kir2.1 animals there is still the appearance of bright puncta indicating some level of process remodeling. This perhaps indicates that a lower level of spiking is still happening in these animals as a similar lack of volume change and appearance of puncta is seen in control animals exposed to lower concentrations of EB. In contrast to Kir2.1, expressing of the outward rectifying potassium channel, Open rectifier K+ channel (ORK; Nitabach et al., 2002), has no effect on the response of Or42a OSNs to EB experience during the critical period. This is perhaps due to extracellular potassium levels around Or42a OSNs or ineffective expression of this channel in these OSNs. It will be interesting to test whether

expressing DN potassium channels can lead to the opposite effects of Kir2.1 (Venken et al. 2011) and whether some of the challenges of Kir2.1 expression can be overcome by using a temporally restricted Gal80 (Chiang et al., 2009).

Silencing of Or42a OSNs by disrupting of olfactory receptors also prevents remodeling. A reduction in basal innervation volume is seen in *orco* mutants, which is similar but less severe than Kir2.1 expression. This may reflect the progressive degeneration seen with *orco* mutation or Kir2.1 expression in much later Or22a neurons (Larsson et al. 2004; Chiang et al., 2009). However, my experiments with Or42a OSNs show that at the third day after eclosion Kir2.1-expressing animals exposed to only mineral oil have a large reduction in innervation volume without any apparent puncta while *orco* mutants have only a modest reduction in volume more in line with the published Or22a results. This difference might indicate an alteration in membrane trafficking of the GFP in Kir2.1 expressing animals that does not occur in the *orco* mutant animals. Surprisingly, exposing *orco* null animals to EB during the critical period actually *increases* innervation volume, restoring VM7 innervation to control levels. How this is happening is unclear, but two possibilities are that 1) Or42a receptors can form poorly functioning homomeric channels or heteromeric channels with a truncated Orco protein or 2) exposure to high concentrations of EB activates low affinity IR or GR containing OSNs that activate Or42a OSNs through interactions with excitatory LNs (Huang et al., 2010; Seki et al., 2010). Both these hypotheses suggest that Or42a OSNs receive excitatory input in the absence of Orco. Therefore, an initial experiment looking at the activation of Or42a OSNs to high EB concentrations in an *orco* mutant background is necessary. If this experiment supports these hypotheses, then single sensilla recordings (Pellegrino et al., 2010) and calcium imaging of Or42a OSNs in response to IR and GR activation could test the first and second hypotheses, respectively. Mutating the *Or42a* gene had a more predictable effect on Or42a OSNs with no difference in basal volume compared to controls and a complete lack of EB exposure-dependent volume reduction. The mutation of *Or42a* may differ from *orco* mutants in the basal volume change due to Orco having a much greater role in

mediating spontaneous activity. These results point to dissociable roles of neuron spiking, membrane potential and synaptic output.

The use of TeTxLc allowed me to separately test the role of OSN synaptic output. The mechanism of action for TeTxLc is to cleave the v-SNARE synaptobrevin and thus prevent synaptic vesicle (SV) fusion (Sweeney and Broadie et al. 1995). Due to this blockade level, TeTxLc does not disrupt normal OSN sensory transduction or action potential generation. TeTxLc both increases the basal innervation volume of Or42a OSNs and dramatically enhanced the ability of critical period EB exposure to reduce Or42a innervation volume. This presents a stark contrast to *orco* mutants and Kir2.1 expression, indicating that while Or42a OSN membrane depolarization leads to the loss of VM7 glomerulus innervation, the TeTxLc-sensitive output of these neurons actually serves to limit OSN remodeling during the critical period. The importance of SV exocytosis to both basal Or42a OSN volume and odorant-dependent remodeling indicates that neurotransmission might either directly or indirectly regulate important autocrine and paracrine signaling pathways. One interesting model that could explain the TeTxLc results posits that Or42a OSNs expressing TeTxLc fail to form mature synaptic connections. In this model synaptic output is a critical step for the establishment of initial connectivity. In terms of the critical period phases, this model suggests that in animals expressing TeTxLc the OSNs are “stuck” in the first phase unable to make the transition to the second phase with the onset of sensory experience. Due to this immature state the TeTxLc Or42a OSNs would respond to EB exposure more strongly because few if any of the structural stability mechanisms would be triggered in the absence of synaptic output.

Similar to Kir2.1 and *orco* mutant OSNs, sensory neurons expressing TeTxLc show a slow degeneration of processes in the absence of odorant exposure (Chiang et al., 2009). In the case of *orco* mutants, a brief 1-2 days of activity is sufficient for the initial stabilization phase of OSNs even if *orco* is lost later on (Chiang et al., 2009). I would expect a similar result could be seen using conditional TeTxLc expression. Preliminary results indicate that Or42a OSNs expressing

TeTxLc have minor degeneration of the proximal axon segment in basal conditions and profound degeneration of the proximal axon following critical period EB exposure. Control animals have minor if any degeneration of the proximal axon even following EB exposure. Future experiments will be needed to test whether EB exposure TeTxLc animals are a more extreme example of the same critical period phenotype, or a separate phenotype resulting from an already degenerating axon. One experiment that would be useful to help tease apart what is happening with Or42a TeTxLc expression is to expose older animals to EB. If indeed these animals are stalled at an earlier and immature phase of development, than perhaps the critical period would remain open later in life. This would be in line with recent experiments using conditional *orco* mutants to extend the critical period for LTH (Chodankar et al., 2020).

Or42a OSN Critical Period Remodeling in *Dfmr1* Mutants

FMRP has been widely studied as a regulator of activity-dependent plasticity in a variety of different model systems (reviewed in Contractor et al., 2015). More specifically, FMRP is required for both LTH and for the effects of optogenetic stimulation of VL1 volume reduction during the first day after eclosion (Sudhakaran et al., 2014; Doll et al., 2015, 2016). My initial hypothesis was that Or42a OSN critical period remodeling represented a variant of other forms of critical period structural changes in the AL. However, my experimental results alongside findings in the literature suggest that Or42a remodeling is a mechanistically different phenomenon than the slow, long-lasting and postsynaptically driven changes seen previously. Although many different functions have been attributed to FMRP, its role in the AL has been best characterized in LTH where it regulates CaMKII signaling (Sudhakaran et al., 2014). Furthermore, LTH requires cAMP dependent signaling and likely PKA signaling similar to classical learning and memory experiments in *Drosophila*. Although it has not been directly shown, disrupted cAMP and PKA signaling in FMRP mutant animals probably contributes to impaired LTH behavior since it has

recently been shown that FMRP regulates PKA signaling widely in the *Drosophila* brain (Sears et al. 2019). One of the key differences between LTH and critical period remodeling is the timescale, with Or42a remodeling having a more rapid onset and offset (Fig. 7; Das et al., 2011; Chodankar et al., 2020). This faster timescale could indicate that Or42a remodeling can occur without *de novo* protein synthesis, however, direct assessments are needed to test this hypothesis. I predict that Or42a critical period remodeling is driven by the local activity-dependent recruitment of enzymes that mark neurites of glial degradation. Despite Or42a remodeling occurring in the absence of FMRP, multiple AL neurons still utilize FMRP to regulate how Or42a OSNs integrate into the AL circuit.

Different Responses to EB Exposure of *Dfmr1* Null Mutants and Or42a-targeted RNAi

Typically, *dfmr1* null mutants display the strongest phenotypes, whereas cell type-specific RNAi knockdowns produce similar or weaker effects. Therefore, the much stronger impact on Or42a OSN critical period remodeling by the Or42a-targeted RNAi knockdown of FMRP compared to a *dfmr1* null mutant came as a total surprise and upended my initial hypothesis that FMRP controls Or42a remodeling in a cell-autonomous manner similar to other forms of odorant-dependent structural changes in the developing AL circuit. From this unexpected result, I came up with four testable hypotheses that might explain the difference between the mutant and RNAi conditions: 1) RNAi knockdown produces a reduced level of FMRP, which leads to different phenotype than a complete elimination as in the mutant. 2) RNAi affects the levels of an off-target protein, which leads to the phenotype. 3) The *dfmr1* mutant takes away FMRP throughout life while the targeted RNAi reduces the protein only when the receptor expression begins in mid-pupal development. 4) The null mutant removes FMRP from all cells while the targeted RNAi is limited to only the Or42a-expressing cells. From my experiments, the fourth hypothesis has the most support. The first hypothesis is unlikely since expressing an RNAi using *Or42a*-Gal4 and

Orco-Gal4 lines produces a similar reduction in FMRP levels, but different effects on Or42a remodeling. A more conclusive experiment to rule out the first hypothesis would be to do an Or42a-restricted knockout of the *dfmr1* gene using CRISPR/Cas9 (Housden et al., 2017). However, I was not able to technically establish this experiment. I found expression of the CRISPR/Cas9 components in all neurons from embryonic development using *elav*-Gal4 led to a complete loss of detectable FMRP protein in the adult brain (Fig. 32). Despite this promising result, using *Or42a*-Gal4 to express the CRISPR components failed to eliminate FMRP immunoreactivity by the end of the second day of adult life. Since FMRP has a half-life of about 30 hours (Ceman et al., 2003) and *Or42a*-Gal4 turns on expression prior to eclosion (Sweeney et al., 2007), inefficient cutting of the DNA is the most likely issue with this experimental design. Two changes to the experiment might help to overcome these issues and allow for Or42a-targeted mutation of the *dfmr1* gene. First, the levels of the CRISPR components could be increased by boosting the copy numbers of the UAS and Gal4 transgenes. Second, a more efficient Cas9 enzyme could be used to make DNA cuts more frequent. The tradeoff with this increase in mutation rate is that there would be a greater probability of *dmfr1* mutation in off target cells where leaky expression of the CRISPR components is present. Altering the cell-targeted CRISPR technique in this way would open the door to experiments on tight developmental time windows.

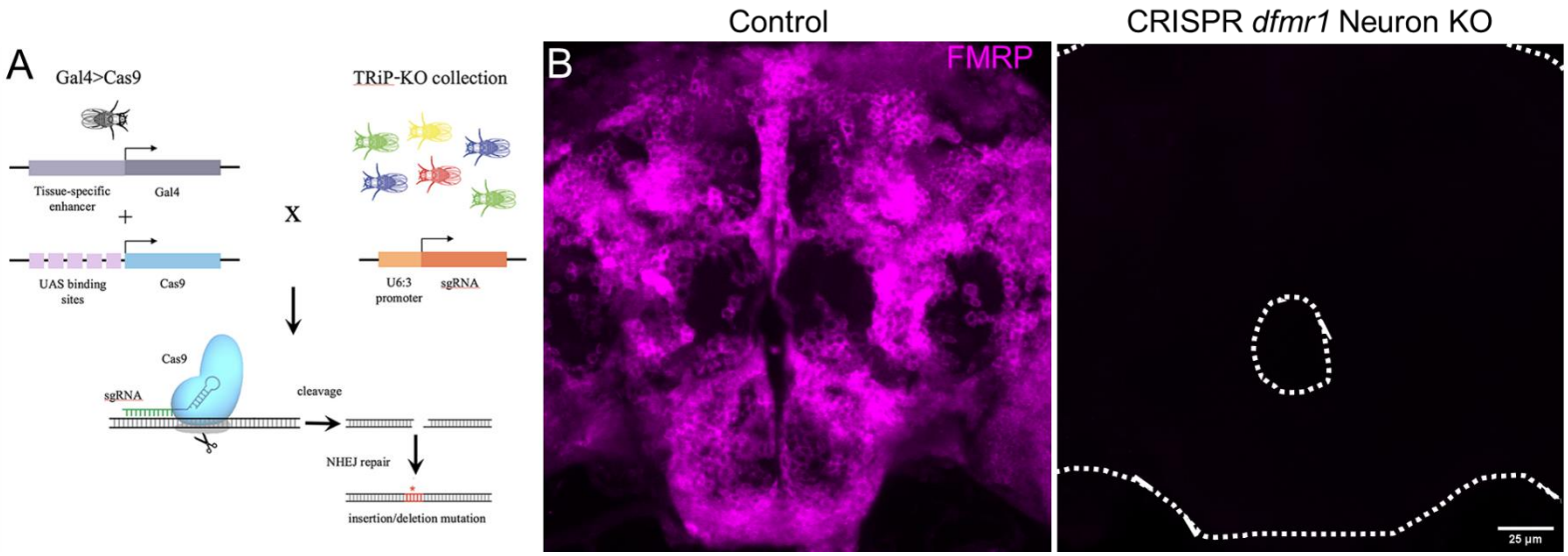

Figure 32. Neuron-targeted *in vivo* CRISPR of *dfmr1*
Schematic of *in vivo* CRISPR/Cas9 mediated mutagenesis. Flies containing tissue-specific Gal4 and UAS-Cas9 crossed to animals ubiquitously expressing an sgRNA under U6:3 promoter control produce progeny with the necessary components for tissue specific DNA mutagenesis. Cas9 causes double-stranded DNA breaks targeted to a location based on the sgRNA. Imprecise nonhomologous end-joining repair of the DNA can produce mutates that disrupt gene function. **B)** Representative confocal maximum intensity projections of the *Drosophila* central brain stained with an antibody against FMRP (magenta). Two genotypes are shown: transgenic control (*elav*-Gal4; UAS-Cas9.P2/+; left) or the same transgenic line with *dfmr1* sgRNA (CRISPR *dfmr1* Neuron KO; right). Adapted from https://fgr.hms.harvard.edu/vivo-crispr-0.

Two main pieces of evidence argue against the second hypothesis. First, I was able to replicate the effect of Or42a-targeted FMRP RNAi on critical period remodeling using four different RNAi constructs. Since these RNAi sequences would have different off-target activity is it very unlikely that all of them would produce the same result. Second, Or42a-targeted overexpression, but not pan-OSN overexpression enhanced the effect of EB exposure on Or42a glomerulus innervation. Since the overexpression of FMRP would not produce off-target effects like RNAi this also indicates that off-target effects are unlikely to be the cause of the Or42a-targeted RNAi phenotype. A similar rational argues against the third hypothesis. In addition to *Or42a*-Gal4 and *Orco*-Gal4 having similar levels of FMRP knockdown, these two promoters also begin expression around the same point in mid-pupal development. An alternative approach to test this hypothesis would be to use a heat-shock protein promoter to control the expression of the Gal4 protein and FMRP RNAi knockdown. By using a microscope laser to heat up targeted cells, the temporal and spatial expression of expression of the RNAi can be finely controlled (Halfon et al., 1997). The fourth hypothesis is supported by a number of published experiments (Figs. 15-26). Another experiment which would have further solidified this hypothesis, I was also not able to technically establish. The experiment combined a broadly expressing Gal4 line with an Or42a-Gal80 to block the expression an FMRP RNAi only in Or42a neurons. The issue with this experiment is that the broad Gal4 lines have expression levels much greater than Or42a. This led to an ineffective block of the RNAi knockdown by the Gal80. This technical limitation could be overcome by taking advantage of a heat-shock promoter. By controlling the strength and duration of a heat-shock the expression of the Gal4 could be titrated to a level amenable to an Or42a-Gal80 block (Eliason et al., 2018). Alternatively, controlling Gal80 expression by a heat-shock promoter and restricting expression using a microscope laser could also achieve a similar effect (Halfon et al., 1997). Together with my published data these experiments would combine to bolster my FMRP balance model in controlling Or42a critical period remodeling.

Balanced AL Circuit FMRP Levels Maintain Proper Or42a Critical Period Remodeling

A major conclusion from my work on Or42a OSN critical period remodeling is the role of FMRP in regulating responses to local interneurons. Interestingly, I found that altered responsiveness only seemed to impact remodeling when the 'balance' of FMRP within the OSN population is shifted. Three important unanswered questions remain in regards to the FMRP role in regulating Or42a OSN critical period remodeling: 1) In what neurons do FMRP levels impact remodeling? 2) What does reducing FMRP levels in Or42a neurons do to affect their response to EB exposure? 3) How does the AL circuit compensate for FMRP loss to restore a strong EB exposure responsiveness? Although my work points strongly to FMRP levels in OSNs being a major player in controlling Or42a remodeling, I have experimental results that suggest other AL neurons as well as mushroom body (MB) neurons are also involved (Figs. 33, 34). Thus far, I have tested how targeted knockdown of FMRP impacts Or42a structural remodeling using 4 additional Gal4 lines: GH146, OK107, MB247 and OK371. GH146-Gal4 is expressed in ~90 olfactory PNs of the AL including ones postsynaptic to Or42a OSNs (Marin et al. 2005). The reduction of FMRP within the GH146 population did not impact Or42a remodeling (Fig. 33), consistent with my other findings that remodeling does not impact VM7 PNs and does not rely on the output of Or42a OSNs. A reduction of FMRP levels using the OK107-Gal4 significantly blunted the effect of critical period EB exposure on Or42a glomerular innervation. Since OK107-Gal4 expresses mainly in the MB and the glutamatergic ventral lateral LNs of the AL (Connolly et al., 1996, I conducted FMRP knockdown experiments with MB247-Gal4 (MB expression; Zars et al., 2000) and OK371-Gal4 (glutamatergic neuron expression including the AL and MB; Meyer and Aberle, 2006) to attempt and tease apart where the action of FMRP is

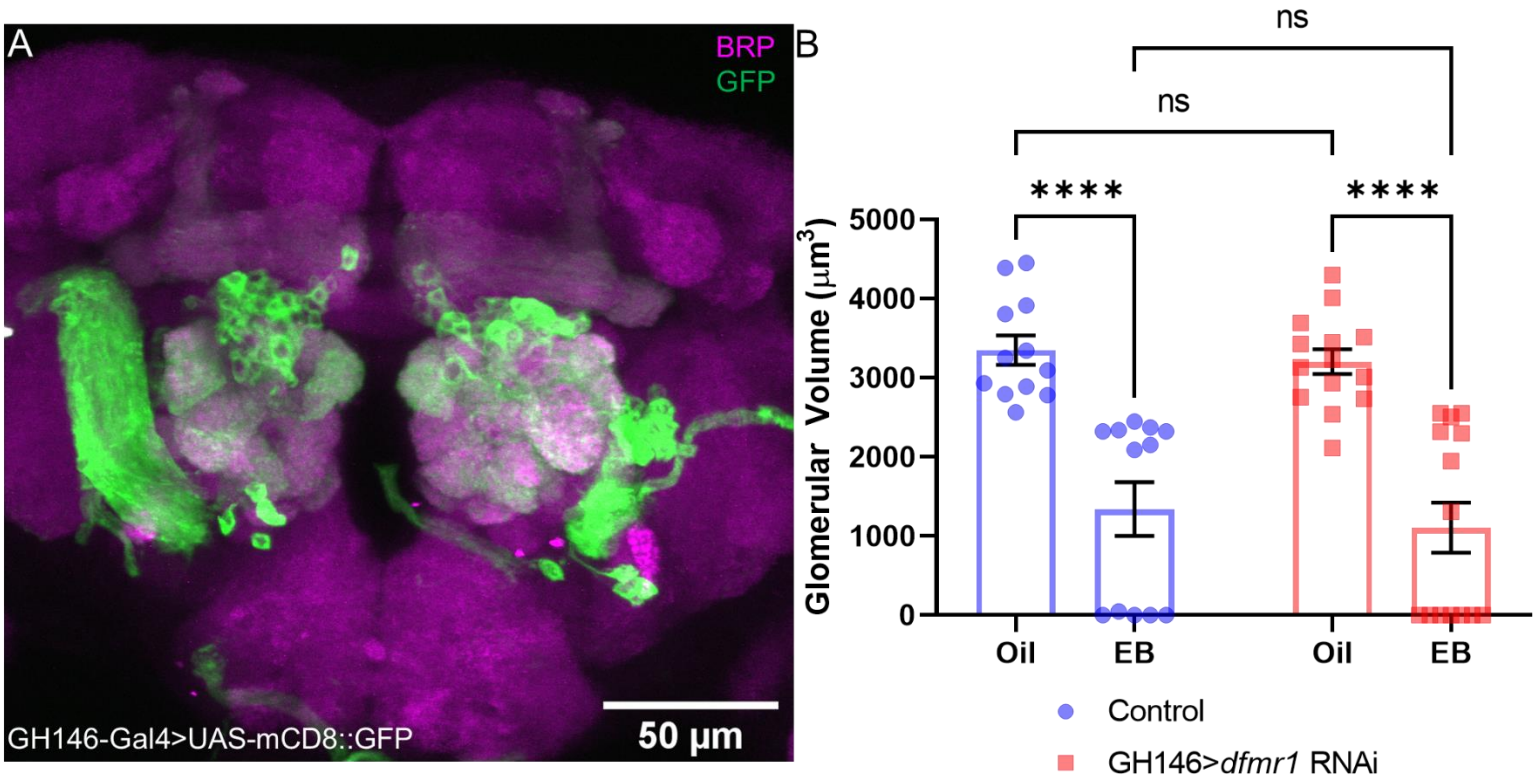

Figure 33. Projection Neuron FMRP is not Required for Or42a Critical Period Remodeling
A) Representative confocal maximum intensity projection of olfactory projection neurons (PNs) co-labeled with presynaptic neuropil marker Bruchpilot (BRP; magenta) and PN-targeted membrane GFP (GH146-Gal4>UAS-mCD8::GFP; green). **B)** Quantification of the *Or42a*-OSN VM7 innervation volume for both genotypes and treatment conditions. Scatter plots show all data points and the mean ± SEM. The significance is indicated as non-significant (ns) or significant at $p<0.0001$ (****).

I found that both MB247-Gal4 and OK371-Gal4 also blunted the response to EB exposure similar to OK107 (Fig. 34). The results of these knockdown experiments were not completely clear, but most likely indicate a role for MB neurons as all three lines express in at least a subset of the MB. In addition, these knockdown results do not rule out an FMRP role within glutamatergic LNs of the AL. Since feedback connections from the MB to the AL have only been shown by one study (Hu et al. 2010), it will be important to further characterize these connections. One method to look at feed-forward connections is to use the *trans* Tango system (Talay et al. 2017) to identify putative connections and verify their functionality with GCaMP or electrophysiology. In order to establish the role of FMRP within glutamatergic LNs, an intersectional genetic approach could be used by combining OK107-Gal4 or OK371-Gal4 with MB247-Gal80 in order to reduce the MB expression and better isolate the role of this population. In addition to the olfactory circuit neurons, it will be important to test other, non-glutamatergic, classes of interneurons since these cells are the most likely candidates to control lateral interactions between the different olfactory pathways (Olsen and Wilson, 2008; Root et al., 2008; Huang et al., 2010). Of particular interest are the GABAergic LNs, since I showed that limiting the levels of the $GABA_A$ receptor subunit Rdl in Or42a OSNs elevates remodeling following critical period EB exposure (Fig. 27). Overall, I suggest that AL LNs are the critical modifiers of OSN activity through which FMRP can have its influence and the broad connections that LNs form with both AL intrinsic and extrinsic neurons are likely key hubs for FMRP to exert its influence on Or42a remodeling.

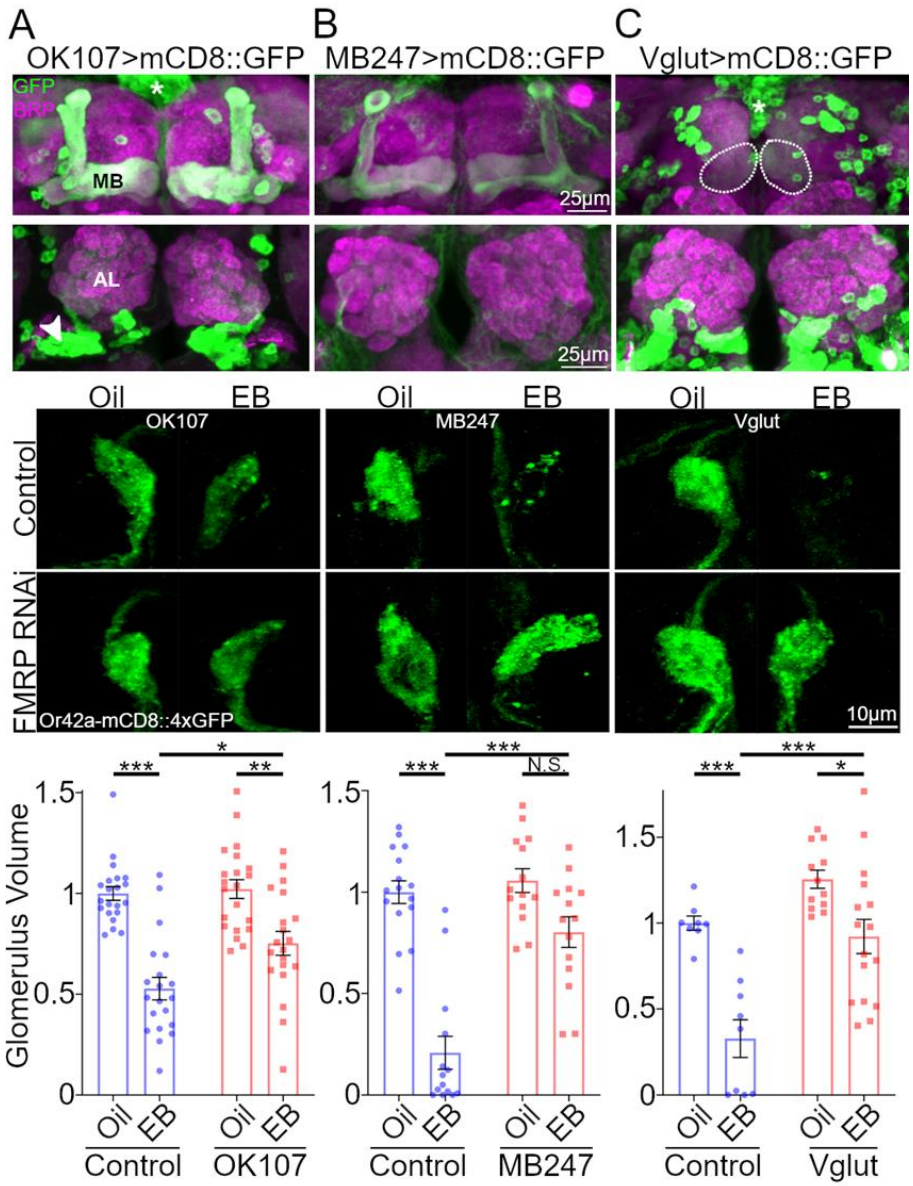

Figure 34. MB-targeted FMRP Knockdown Disrupts Or42a Remodeling
A) Maximum intensity projection of OK107-Gal4 expression patter in the mushroom bodies (MB; top, upper panel) and antennal lobes (AL; top, lower panel). Images are co-labeled with presynaptic bruchpilot (BRP) as a neuropil marker (magenta) and OK107-Gal4>UAS-mCD8::GFP (green). White asterisks indicate insulin-secreting neuron population and white arrowheads are the ventral lateral interneurons of the AL (VLLNs). Middle panels are representative confocal maximum intensity projections of Or42a olfactory sensory neurons (OSNs) innervating the AL ventral medial 7 (VM7) glomerulus (*Or42a*-mCD8::4xGFP; green). Females were exposed to mineral oil vehicle (top), or 15% ethyl butyrate (EB) odorant (bottom) from 0-2 days post eclosion. Two genotypes are shown: transgenic control (*w';Or42a*-mCD8::4xGFP/+;*Or42a*-mCD8::4xGFP/+; middle, upper panel), and the same transgenic with OK107-targeted *dfmr1* RNAi (*OK107*-Gal4>*dfmr1* RNAi; middle, lower panel). Bottom graph is a quantification of the *Or42a*-OSN VM7 innervation volume for both genotypes and treatment conditions. Scatter plots show all data points and the mean ± SEM. **B)** Same as in A except MB247-Gal4 was used to specifically target the MB and animals were exposed to 20% EB. **C)** Same as in A except Vglut-Gal4 was used and animals were exposed to 20% EB. White dotted outlines show vglut-Gal4 expression in part of the MB. The significance is indicated as non-significant (N.S.) or significant at $p<0.05$ (*), $p<0.01$ (**) or $p<0.001$ (***).

The central importance of the AL LNs to the regulation of Or42a neurons by FMRP provides a starting point to studying the mechanism by which FMRP acts within these cells. I showed that Or42a-targeted knockdown of FMRP does not impact remodeling when Or42a neurons are activated optogenetically (Fig. 22). I interpreted this result as meaning that the activation of LNs by the activation of other EB-responsive OSNs was required for the effect of FMRP knockdown on Or42a remodeling. This conclusion could be further supported by testing for an effect of Or42a-targeted FMRP knockdown in animals that only express Orco within the Or42a OSNs thereby eliminating other EB-responsive OSNs from the circuit. If this result holds true, it would indicate that reducing FMRP in Or42a OSNs impacts how these neurons respond to input from LNs. Groups of LNs are characterized by the type of neurotransmitter they release (Chou et al., 2010). Therefore, experiments using RNAi knockdown, cell-type specific CRISPR or mutants of different neurotransmitter receptors could narrow in on the pathway(s) through which FMRP is exerting its influence. Once potential pathways are identified Or42a-targeted *dfmr1* RNAi combined with trans-heterozygous mutants to the individual pathway components could indicate which part of the pathway is likely influenced by FMRP knockdown. Finally, the putative target(s) would be verified by testing for regulation at the RNA or protein level. Since my data suggests that FMRP may be acting similarly in all EB-responsive OSNs, the target should also be altered in these neurons and show changes similar changes in regulation. This proposed experimental pipeline provides a route to pinpoint how FMRP knockdown alters the response of OSNs to LN input and affects Or42a OSN remodeling.

One implication of the difference between the Or42a-targeted FMRP knockdown and the *dmfr1* null mutant is that animals with global loss of FMRP must be able to compensate for the effects of FMRP loss in Or42a neurons. My current model to explain the compensation in *dfmr1* null mutants builds off work on exploring lateral inhibition that targets the presynaptic OSNs and depends on both $GABA_A$ and $GABA_B$ receptors (Olsen and Wilson 2008). This lateral inhibition scales with the total amount of activity of the OSNs and can act as a gain control mechanism by

providing greater inhibition when many OSNs are activated. Based on my current results, a compensation model focused on lateral inhibition would predict that reducing FMRP increases OSN responsiveness to inhibitory signaling through $GABA_A$ and $GABA_B$ channels which is restored to near control levels by reducing the activity of the corresponding LNs. Although possible, a GABAergic LN focused hypothesis does not fit with a study showing loss of FMRP increases the activity of GABAergic LNs (Franco et al. 2017). I predict that a related mechanism exists to boost the signal of early-activated OSNs through glutamatergic signaling. Odorants do not activate all OSNs simultaneously. OSNs with higher affinity receptors will more rapidly generate spikes in response to stimulation (Wilson et al., 2017). In the case of a strong odorant stimulation like the EB exposure used in my experiments, the early activated high-affinity receptor OSNs drive the activity of both GABAergic and glutamatergic LNs. The activation of these LNs would trigger widespread release of GABA and Glutamate and bind to inhibitory $GABA_A$, $GABA_B$, GluCl receptors, excitatory NMDA receptors and modulatory mGlu receptors. Since NMDA receptors require both membrane depolarization to remove the magnesium block and glutamate binding to open its pore, only the early-activated OSNs would have NMDAR-dependent depolarization. Although, the overall effect of glutamate on short-duration activation is inhibition (Liu and Wilson, 2013), it is possible that NMDARs exert more of an influence on longer structural and functional plasticity. For instance, NMDARs have been shown to regulate a non-specific excitotoxic response of OSNs to high concentrations of ethanol (French and Heberlein, 2009).

The most straightforward experiments to test for functional changes and compensation in *dfmr1* mutants employ a combination of functional imaging and pharmacology. Three hypotheses could be tested. First, the response of Or42a OSNs in control and *dfmr1* mutant animals is similar to prolonged high concentration EB exposure. Since control and *dfmr1* mutant animals have similar levels of Or42a remodeling, I expect that their electrical activity to be similar with critical period EB exposure. This experiment could be carried out by expressing GCaMP in Or42a neurons and examining fluorescence responses in animals either chronically exposure to EB

during the critical period with an imaging window (Huang et al. 2018) or by measuring the response to a few hours of EB exposure which could be done in a more acute experiment. Second, the response of *dfmr1* mutant Or42a OSNs to different pharmacological agents which activate glutamate, GABA or other LN neurotransmitter receptors should be altered. This experiment would be easiest to perform if the relevant LN class was identified through the experiments suggested in the previous section. The responses of Or42a OSNs could be monitored again with GCaMP and the effect of the different agents can be assessed either by modifying the relatively high spontaneous activity of OSNs or by using Or42a-targeted optogenetics. Third, the activity of the LNs should be changed in order to compensate for the shift in Or42a responses. To test for changes in the release of LN neurotransmitters onto Or42a OSNs, fluorescent sensors sensitive to different neurotransmitters (Helassa et al., 2018; Patriarchi et al., 2018; Marvin et al., 2019; Wan et al., 2020) could be expressed in Or42a OSNs and the response to strong EB stimulation assessed. Since the levels of the sensors will likely be similar between control and *dfmr1* mutants, this experiment would show changes in the amount of a given neurotransmitter released by a given LN population. Altogether, these experiments will help extend the findings from my thesis work and uncover the method that the AL uses to overcome the loss of FMRP.

What Controls Basal Glomerulus Innervation Volume?

Null *dfmr1* mutants have expanded Or42a OSN innervation volume of the VM7 glomerulus. In theory, the increase in volume could be explained by an expansion of the processes from a similar number of O42a OSNs or an increase in the number of OSNs. One study suggested that the number OSNs is a major determinant of glomerular volume (Grabe et al. 2016), but overall accounted for only ~30% of the volume variation. This indicates that other factors can play an important role in determining innervation volume. Since *dfmr1* nulls do not have a

noticeable difference in Or42a OSN number, it is likely that the processes are expanded as has been seen in other AL neurons of *dfmr1* mutants (Doll and Broadie 2015, Vita and Broadie, 2017). Based on my assays of basal Or42a OSN glomerular innervation, Wg signaling, PKA signal transduction and spontaneous electrical activity through olfactory receptors (Larsson et al., 2004) seem promising areas for future study. Wg signaling has a well-characterized role in controlling synaptic architecture at the *Drosophila* neuromuscular junction (NMJ, Packard et al. 2002). In addition, *dfmr1* mutants have expanded NMJ structure due, in part, to elevated levels of Wg ligand (Friedman et al., 2013). Few studies have examined the role of Wg in the adult brain, but one report indicates that Wg ligand is expressed in the AL and its levels are increased following high potassium stimulation (Chiang et al., 2009). Furthermore, this work demonstrated that Wg acts through a non-canonical signaling pathway, similar to the NMJ, to control OSN survival following genetic silencing.

In this signaling pathway, Wg activates presynaptic frizzled-2 receptors (Fz2) to inhibit GSK-3β homolog shaggy (Sgg) and prevent breakdown of the local cytoskeleton. Targeted expression of Sgg in AL LNs can decrease their synapse number and apparent size indicating that this pathway might be broadly relevant for controlling AL structure (Acebes et al., 2011). My experiments manipulating Wg signaling in Or42a OSNs indicated a likely role in controlling basal volume. While Wg heterozygous mutants did not have significantly altered volumes, expressing of a Fz2 dominant negative (DN) dramatically decreased volume, while expression of a Sgg-DN increased basal OSN volume. These results suggest a model where *dfmr1* mutants release more Wg ligand around Or42a OSNs leading to activation of Fz2 and inhibition of Sgg thereby increasing glomerulus volume similar to the Sgg-DN. One simple experiment to test for an interaction between FMRP and Wg in controlling Or42a basal volume is to combine a *dfmr1* null mutant with a *wg* heterozygous null mutant. Previous experiments using this design have been able to observe phenotypic reduction indicating an interaction of FMRP with the Wg signaling pathway (Kopke et al., 2017). If a connection between Wg and FMRP can be established follow-

up work will be needed to determine where FMRP functions to regulate Wg levels. Although knockdown of FMRP in Or42a does not produce significant changes in basal volume, Wg is released from neurons and glia at the NMJ (Kerr et al., 2014) and therefore FMRP loss in multiple cell types may be required to see a phenotype similar to a global manipulation. Wg signaling represents a fruitful path for future research exploring the regulation of basal Or42a OSN volume by FMRP.

While the Wg signaling pathway shows much promise for interacting with FMRP to control basal Or42a OSN innervation volume, recent work from my lab colleagues as well as my own experiments point to PKA signaling as area ripe for investigation. Loss of FMRP leads to a concurrent decrease in PKA signaling, which is likely related to altered cAMP production (Sears et al., 2019). Within the *Drosophila* MB learning and memory center, long-term memories are generated by the activation of the adenylyl cyclase Rutabaga, production of cAMP and recruitment of PKA (Heisenberg, 2003). PKA phosphorylates the kinase Meng Po and prevents the breakdown of cAMP-responsive element binding protein B (CREB-B; Lee et al., 2018). In my thesis work, I discovered that reducing Meng Po levels in Or42a OSNs did not block EB-dependent remodeling, but did increase the basal volume of Or42a innervation (Fig. 35). This result is similar to that seen for *dfmr1* null mutants and may indicate a shared underlying mechanism. Since *dfmr1* mutants have decreased levels of PKA, and PKA is known to phosphorylate and activate Meng Po (Lee et al., 2018), the activation of Meng Po may be diminished in *dfmr1* mutants and lead to a similar phenotype as my RNAi knockdown experiment. Although the exact role of PKA signaling in OSN development remains to be determined, mutants of the cAMP, *dunce* and *rutabaga* show impairments in olfaction (Martín et al., 2001) and the development of OSNs into glomeruli is altered in mutants of the PKA-binding protein AKAP200 (Zhang et al., 2006). Future experiments are needed to assess whether Meng Po and PKA signaling are linked in Or42a OSNs and to what extent FMRP may regulate PKA signaling within these neurons.

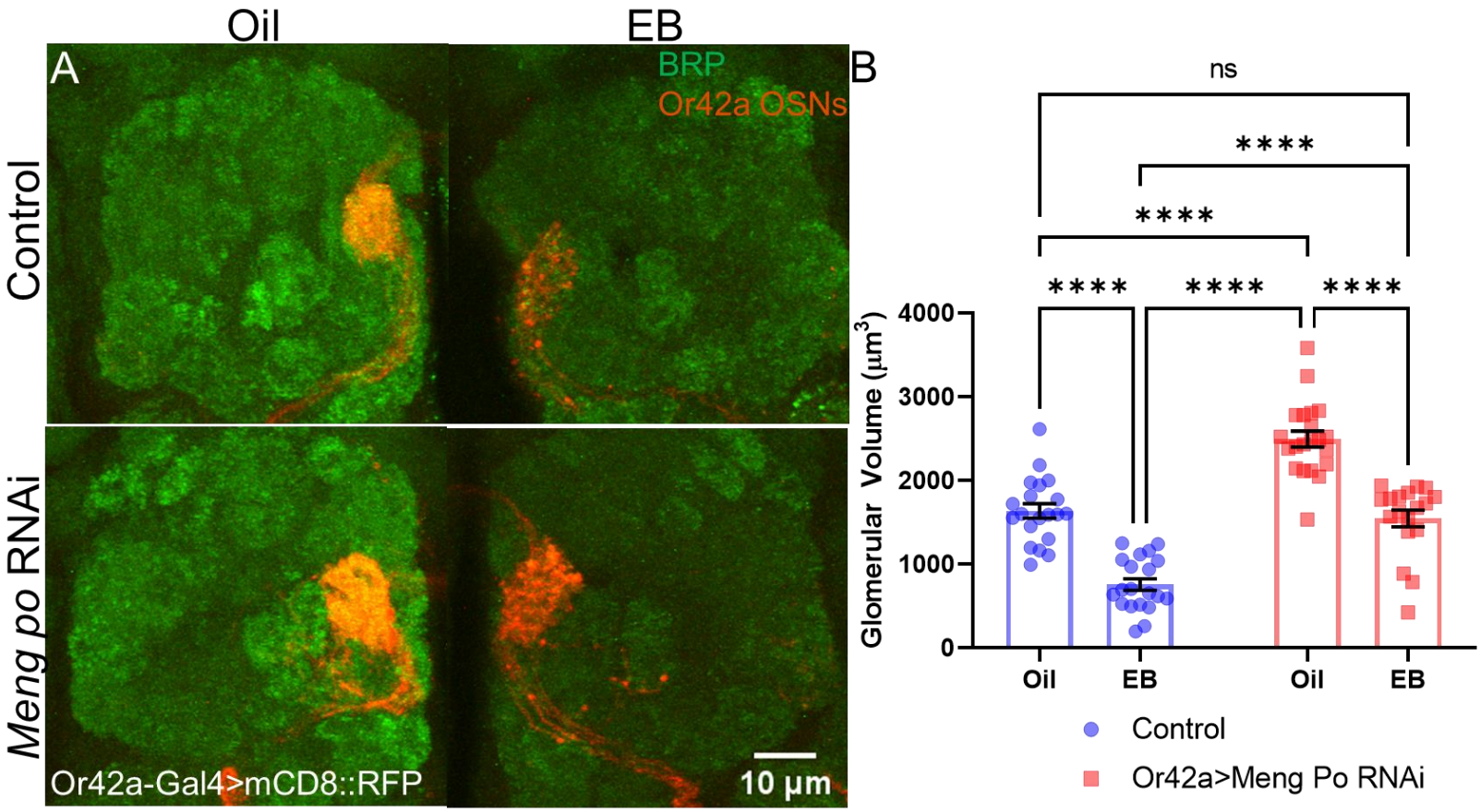

Figure 35. Meng Po Limits the Basal Volume of Or42a OSNs, but not Remodeling
A) Representative confocal maximum intensity projections of olfactory sensory neurons (OSNs) innervating the antennal lobe (AL) co-labeled with presynaptic active zone marker Bruchpilot (BRP) to visualize glomerulus structure (green) and OSN-targeted mCD8::RFP (red). Females were exposed to mineral oil vehicle (left), or 20% ethyl butyrate (EB) odorant (right) from 0-2 days post eclosion. Two genotypes are shown: transgenic control (*w*⁻*;*UAS-mCD8::RFP/+;*Or42a*-Gal4/+; top), and the same transgenic with *Or42a*-targeted *meng po* RNAi (*Or42a*-Gal4>*meng po* RNAi; bottom). **B)** Quantification of the *Or42a*-OSN VM7 innervation volume for both genotypes and treatment conditions. Scatter plots show all data points and the mean ± SEM. The significance is indicated as non-significant (ns) or significant at $p<0.0001$ (****).

Neuronal activity may provide a link between FMRP, Wg signaling and PKA signal transduction. FMRP has well-characterized roles controlling neuronal excitability and activity-dependent plasticity (Contractor et al. 2015). While Or42a OSNs lacking FMRP do not show altered remodeling in response to EB exposure during development, changes in earlier spontaneous activity in these neurons might alter their development and affect basal innervation volume of the VM7 glomerulus. Both Wg and PKA signaling can be initiated by activity and within AL OSNs depolarization has been shown to induce Wg release and cAMP production (Chiang et al., 2009; Miazzi et al. 2016). While a direct link between activity, Wg signaling and PKA signal transduction within Or42a neurons is still needed, my studies genetically manipulating activity within Or42a OSNs has demonstrated changes to basal volume innervation of the VM7 glomerulus. The detailed description of my silencing experiments has already been discussed above, but in general manipulations that reduce Or42a OSN spiking below baseline levels lead to a reduction in basal volume. I predict Or42a neurons with genetically increased activity would have the opposite phenotype with increased basal volume. The role of increased activity in Or42a OSNs could be tested by expressing DN potassium channels in Or42a OSNs and examining changes to basal innervation volume (Venken et al. 2011). Since *dfmr1* mutants have larger Or42a OSN basal volume, I would expect that these neurons have either increased spontaneous neuronal activity or altered signaling that mimics such increased activity. Overall, my current hypothesis is that loss of FMRP acts to increase spontaneous activity of Or42a OSNs, leading to enhanced trans-synaptic signaling through the Wg pathway and reduced PKA signaling, perhaps by a diminished capacity for cAMP production.

Conclusions

My thesis work expanded the *Drosophila* critical period field by identifying a new form of innervation remodeling that occurs in Or42a OSNs strongly activated by olfactory sensory experience. While the type of remodeling occurring in Or42a OSNs seems to be different from other published forms in the AL, the timing of the critical period has been largely consistent over many studies, occurring in the first few days of life (Sachse et al., 2007; Doll and Broadie, 2015; Chodaharkan et al., 2020). This suggests a shared underlying mechanism for controlling critical period timing and separate mechanism controlling structural and functional remodeling of specific AL circuit elements. More work is needed to explore timing controls of the critical period in the *Drosophila* AL, but maturation of the OSN-PN synapses, incorporation of inhibitory LNs and stabilization of extracellular matrix structure are prime candidate mechanisms. Although some studies have explored the molecular mechanisms controlling LTH, it is still unknown whether remodeling of the VL1 glomerulus is controlled by similar processes. Despite a limited understanding of the molecular mechanisms which control Or42a OSN remodeling, I made substantial headway in uncovering the AL circuitry important for the process. I found that depolarization of Or42a OSNs is the major driver of remodeling, and that LNs can mediate excitatory and inhibitory modulation of OSN depolarization in order to influence the extent of innervation changes. Interestingly, I discovered that FMRP can influence the response of Or42a OSNs to LNs, and that when FMRP is relatively lower in Or42a OSNs compared to the AL circuit Or42a OSNs have a diminished remodeling response to EB olfactory experience. Overall, my discoveries expand our understanding of odorant-dependent critical periods in the AL and provide a model to study how FMRP in different cell types can influence experience-dependent remodeling and interact with AL circuitry.

Fragile X Syndrome (FXS) is a well-studied neurodevelopmental disorder with numerous investigations in a variety of model systems from *Drosophila* to human tissue. Despite this extensive body of work, there are no effective FXS treatments available. Towards this end, many

scientists have moved away from the traditional study of FMRP in regulating individual target proteins, to studies testing how FMRP loss influences neuronal circuits at a holistic level. My work provides a framework for exploring how FMRP in different neuron classes impacts brain circuit development. I show here that the AL circuitry is at least partially resistant to the loss of FMRP, with *dfmr1* mutants showing near-normal critical period Or42a OSN remodeling in response to olfactory experience. On the other hand, neuron-specific FMRP loss from OSNs, LNs and PNs blocks odorant-dependent plasticity during this critical period (Sudhakaran et al., 2014; Doll and Broadie, 2015, 2016). This points to two interesting avenues to explore for the treatment of FXS. First, since FMRP acts in a neuron-type specific manner, treatment should be designed to target different neuronal populations with higher precision. Second, the FXS brain is not irreversibly impaired and devoid of critical period plasticity. Therefore, targeted behavioral therapies administered during critical periods of early-life should prove highly effective in improving patient outcomes. In conclusion, this body of work represents a small, but important step in the understanding of critical periods, *Drosophila* olfaction and the treatment of the FXS disease state.

References

Acebes A, Devaud J-M, Arnés M, Ferrús A (2012) Central Adaptation to Odorants Depends on PI3K Levels in Local Interneurons of the Antennal Lobe. J Neurosci 32:417–422.

Acebes A, Martín-Peña A, Chevalier V, Ferrús A (2011) Synapse Loss in Olfactory Local Interneurons Modifies Perception. J Neurosci 31:2734–2745.

Ackerman SD, Perez-Catalan NA, Freeman MR, Doe CQ (2020) Astrocytes close a critical period of motor circuit plasticity. Biorxiv:2020.05.15.098608.

Akerman CJ, Cline HT (2006) Depolarizing GABAergic Conductances Regulate the Balance of Excitation to Inhibition in the Developing Retinotectal Circuit In Vivo. J Neurosci 26:5117–5130.

Antoine MW, Langberg T, Schnepel P, Feldman DE (2019) Increased Excitation-Inhibition Ratio Stabilizes Synapse and Circuit Excitability in Four Autism Mouse Models. Neuron 101:648-661.e4.

Antón-Bolaños N, Sempere-Ferràndez A, Guillamón-Vivancos T, Martini FJ, Pérez-Saiz L, Gezelius H, Filipchuk A, Valdeolmillos M, López-Bendito G (2019) Prenatal activity from thalamic neurons governs the emergence of functional cortical maps in mice. Science 364:eaav7617.

Antonini A, Stryker M (1993) Rapid remodeling of axonal arbors in the visual cortex. Science 260:1819–1821.

Araque A, Carmignoto G, Haydon PG, Oliet SHR, Robitaille R, Volterra A (2014) Gliotransmitters Travel in Time and Space. Neuron 81:728–739.

Aronstein, K., Ffrench-Constant, R. (1995). Immunocytochemistry of a novel GABA receptor subunit Rdl in *Drosophila melanogaster.* Invertebrate Neuroscience 1(1), 25-31.

Asahina K, Louis M, Piccinotti S, Vosshall LB (2009) A circuit supporting concentration-invariant odor perception in Drosophila. J Biology 8:9.

Ashley C, Wilkinson K, Reines D, Warren S (1993) FMR1 protein: conserved RNP family domains and selective RNA binding. Science 262:563–566.

Aso, Y., Grübel, K., Busch, S., Friedrich, A., Siwanowicz, I., Tanimoto, H. (2009). The mushroom body of adult *Drosophila* characterized by GAL4 drivers. Journal of Neurogenetics 23(1-2), 156-72.

Axelrod JD, Matsuno K, Artavanis-Tsakonas S, Perrimon N (1996) Interaction Between Wingless and Notch Signaling Pathways Mediated by Dishevelled. Science 271:1826–1832.

Banner SJ, Fray AE, Ince PG, Steward M, Cookson MR, Shaw PJ (2002) The expression of the glutamate re-uptake transporter excitatory amino acid transporter 1 (EAAT1) in the normal human CNS and in motor neuron disease: an immunohistochemical study. Neuroscience 109:27–44.

Bailey, D., Hatton, D., Skinner, M. (1998). Early Developmental Trajectories of Males With Fragile X Syndrome. American Journal on Mental Retardation 103(1), 29.

Baines RA, Uhler JP, Thompson A, Sweeney ST, Bate M (2001) Altered Electrical Properties in *Drosophila* Neurons Developing without Synaptic Transmission. J Neurosci 21:1523–1531.

Baker N (1987) Molecular Cloning of Sequences from Wingless, a Segment Polarity Gene in *Drosophila*: the Spatial Distribution of a Transcript in Embryos. EMBO J 6:1765–1773.

Baroncelli L, Scali M, Sansevero G, Olimpico F, Manno I, Costa M, Sale A (2016) Experience Affects Critical Period Plasticity in the Visual Cortex through an Epigenetic Regulation of Histone Post-Translational Modifications. J Neurosci 36:3430–3440.

Bear MF, Singer W (1986) Modulation of visual cortical plasticity by acetylcholine and noradrenaline. Nature 320:172–176.

Béïque J-C, Lin D-T, Kang M-G, Aizawa H, Takamiya K, Huganir RL (2006) Synapse-specific regulation of AMPA receptor function by PSD-95. Proc National Acad Sci 103:19535–19540.

Bell JS, Wilson RI (2016) Behavior Reveals Selective Summation and Max Pooling among Olfactory Processing Channels. Neuron 91:425–438.

Belle SJ, Heisenberg M (1994) Associative odor learning in Drosophila abolished by chemical ablation of mushroom bodies. Science 263:692–695.

Ben-Ari Y, Cherubini E, Corradetti R, Gaiarsa JL (1989) Giant synaptic potentials in immature rat CA3 hippocampal neurones. J Physiology 416:303–325.

Benton R, Vannice KS, Gomez-Diaz C, Vosshall LB (2009) Variant Ionotropic Glutamate Receptors as Chemosensory Receptors in Drosophila. Cell 136:149–162.

Berry-Kravis E, Hicar M, Ciurlionis R (1995) Reduced Cyclic AMP Production in Fragile X Syndrome: Cytogenetic and Molecular Correlations. Pediatr Res 38:638–643.

Bian W-J, Miao W-Y, He S-J, Qiu Z, Yu X (2015) Coordinated Spine Pruning and Maturation Mediated by Inter-Spine Competition for Cadherin/Catenin Complexes. Cell 162:808–822.

Bicks LK, Yamamuro K, Flanigan ME, Kim JM, Kato D, Lucas EK, Koike H, Peng MS, Brady DM, Chandrasekaran S, Norman KJ, Smith MR, Clem RL, Russo SJ, Akbarian S, Morishita H (2020) Prefrontal parvalbumin interneurons require juvenile social experience to establish adult social behavior. Nat Commun 11:1003.

Blanco-Suarez E, Liu T-F, Kopelevich A, Allen NJ (2018) Astrocyte-Secreted Chordin-like 1 Drives Synapse Maturation and Limits Plasticity by Increasing Synaptic GluA2 AMPA Receptors. Neuron 100:1116-1132.e13.

Blakemore C, Garey L, Vital-Durand F (1978) The physiological effects of monocular deprivation and their reversal in the monkey's visual cortex. J Physiology 283:223–262.

Bolduc, F., Bell, K., Cox, H., Broadie, K., Tully, T. (2008). Excess protein synthesis in *Drosophila* Fragile X mutants impairs long-term memory. Nature Neuroscience 11(10), nn.2175.

Bourouis M (2002) Targeted Increase in Shaggy Activity Levels Blocks Wingless Signaling. Genesis 34:99–102.

Brand AH, Perrimon N (1993) Targeted gene expression as a means of altering cell fates and generating dominant phenotypes. Development (Cambridge, England) 118:401–415.

Brandalise, F., Kalmbach, B., Mehta, P., Thornton, O., Johnston, D., Zemelman, B., Brager, D. (2020). Fragile X Mental Retardation Protein bidirectionally controls dendritic Ih in a cell-type specific manner between mouse hippocampus and prefrontal cortex. The Journal of Neuroscience 40(27), 5327-5340.

Brochtrup A, Hummel T (2011) Olfactory map formation in the Drosophila brain: genetic specificity and neuronal variability. Curr Opin Neurobiol 21:85–92.

Broeder MJ den, Linde H van der, Brouwer JR, Oostra BA, Willemsen R, Ketting RF (2009) Generation and Characterization of Fmr1 Knockout Zebrafish. Plos One 4:e7910.

Brown MR, Kronengold J, Gazula V-R, Chen Y, Strumbos JG, Sigworth FJ, Navaratnam D, Kaczmarek LK (2010) Fragile X mental retardation protein controls gating of the sodium-activated potassium channel Slack. Nat Neurosci 13:819–821.

Brown V, Jin P, Ceman S, Darnell JC, O'Donnell WT, Tenenbaum SA, Jin X, Feng Y, Wilkinson KD, Keene JD, Darnell RB, Warren ST (2001) Microarray Identification of FMRP-Associated Brain mRNAs and Altered mRNA Translational Profiles in Fragile X Syndrome. Cell 107:477–487.

Bureau I, Shepherd GM, Svoboda K (2008) Circuit and Plasticity Defects in the Developing Somatosensory Cortex of Fmr1 Knock-Out Mice. The Journal of Neuroscience 28:5178–5188.

Butterwick JA, Mármol J del, Kim KH, Kahlson MA, Rogow JA, Walz T, Ruta V (2018) Cryo-EM structure of the insect olfactory receptor Orco. Nature 560:447–452.

Byers D, Davis RL, Kiger JA (1981) Defect in cyclic AMP phosphodiesterase due to the dunce mutation of learning in Drosophila melanogaster. Nature 289:79–81.

Cadwell CR, Bhaduri A, Mostajo-Radji MA, Keefe MG, Nowakowski TJ (2019) Development and Arealization of the Cerebral Cortex. Neuron 103:980–1004.

Ceman S, O'Donnell WT, Reed M, Patton S, Pohl J, Warren ST (2003) Phosphorylation influences the translation state of FMRP-associated polyribosomes. Hum Mol Genet 12:3295–3305.

Chang S, Bray SM, Li Z, Zarnescu DC, He C, Jin P, Warren ST (2008) Identification of small molecules rescuing fragile X syndrome phenotypes in Drosophila. Nat Chem Biol 4:256–263.

Chen Y, Akin O, Nern A, Tsui CY, Pecot MY, Zipursky LS (2014) Cell-type-Specific Labeling of Synapses In Vivo through Synaptic Tagging with Recombination. Neuron 81:280–293.

Chen T-W, Wardill TJ, Sun Y, Pulver SR, Renninger SL, Baohan A, Schreiter ER, Kerr RA, Orger MB, Jayaraman V, Looger LL, Svoboda K, Kim DS (2013) Ultrasensitive fluorescent proteins for imaging neuronal activity. Nature 499:295.

Chiang A, Priya R, Ramaswami M, VijayRaghavan K, Rodrigues V (2009) Neuronal activity and Wnt signaling act through Gsk3-β to regulate axonal integrity in mature *Drosophila* olfactory sensory neurons. Development 136:1273–1282.

Chodankar, A., Sadanandappa, M., VijayRaghavan, K., Ramaswami, M. (2020). Glomerulus-Selective Regulation of a Critical Period for Interneuron Plasticity in the *Drosophila* Antennal Lobe. The Journal of Neuroscience 40(29), 5549-5560.

Chou, Y., Spletter, M., Yaksi, E., Leong, J., Wilson, R., Luo, L. (2010). Diversity and wiring variability of olfactory local interneurons in the *Drosophila* antennal lobe. Nature Neuroscience 13(4), 439-49.

Chung W-S, Clarke LE, Wang GX, Stafford BK, Sher A, Chakraborty C, Joung J, Foo LC, Thompson A, Chen C, Smith SJ, Barres BA (2013) Astrocytes mediate synapse elimination through MEGF10 and MERTK pathways. Nature 504:394–400.

Cingolani LA, Goda Y (2008) Actin in action: the interplay between the actin cytoskeleton and synaptic efficacy. Nat Rev Neurosci 9:344–356.

Collu GM, Hidalgo-Sastre A, Acar A, Bayston L, Gildea C, Leverentz MK, Mills CG, Owens TW, Meurette O, Dorey K, Brennan K (2012) Dishevelled limits Notch signalling through inhibition of CSL. Development 139:4405–4415.

Conforti L, Gilley J, Coleman MP (2014) Wallerian degeneration: an emerging axon death pathway linking injury and disease. Nat Rev Neurosci 15:394–409.

Connolly JB, Roberts IJH, Armstrong JD, Kaiser K, Forte M, Tully T, O'Kane CJ (1996) Associative Learning Disrupted by Impaired Gs Signaling in Drosophila Mushroom Bodies. Science 274:2104–2107.

Contractor A, Klyachko VA, Portera-Cailliau C (2015) Altered Neuronal and Circuit Excitability in Fragile X Syndrome. Neuron 87:699–715.

Consortium TD-BFX et al. (1994) Fmr1 knockout mice: A model to study fragile X mental retardation. Cell 78:23–33.

Couto A, Alenius M, Dickson BJ (2005) Molecular, Anatomical and Functional Organization of the *Drosophila* Olfactory System. Curr Biol 15:1535–1547.

Crawford, D., Acuña, J., Sherman, S. (2001). FMR1 and the Fragile X syndrome: Human genome epidemiology review. Genetics in Medicine 3(5), 359-371.

Curia G, Papouin T, Séguéla P, Avoli M (2009) Downregulation of Tonic GABAergic Inhibition in a Mouse Model of Fragile X Syndrome. Cereb Cortex 19:1515–1520.

Dahlhaus, R. (2018). Of Men and Mice: Modeling the Fragile X Syndrome. Frontiers in Molecular Neuroscience 11, 41.

Cynader M (1983) Prolonged sensitivity to monocular deprivation in dark-reared cats: Effects of age and visual exposure. Dev Brain Res 8:155–164.

Dalland, T., Døving, K. (1981). Reaction to olfactory stimuli in odor-exposed rats. Behavioral and Neural Biology 32(1), 79-88.

Darabid H, Arbour D, Robitaille R (2013) Glial Cells Decipher Synaptic Competition at the Mammalian Neuromuscular Junction. J Neurosci 33:1297–1313.

Darnell, J., Jensen, K., Jin, P., Brown, V., Warren, S., Darnell, R. (2001). Fragile X Mental Retardation Protein Targets G Quartet mRNAs Important for Neuronal Function. Cell 107(4), 489-499.

Darnell, J., Van Driesche, S., Zhang, C., Hung, K., Mele, A., Fraser, C., Stone, E., Chen, C., Fak, J., Chi, S., Licatalosi, D., Richter, J., Darnell, R. (2011). FMRP Stalls Ribosomal Translocation on mRNAs Linked to Synaptic Function and Autism. Cell 146(2), 247-261.

Das A, Chiang A, Davla S, Priya R, Reichert H, VijayRaghavan K, Rodrigues V (2010) Identification and Analysis of a Glutamatergic Local Interneuron Lineage in the Adult *Drosophila* Olfactory System. Neural Syst Circuits 1:1–13.

Das S, Sadanandappa MK, Dervan A, Larkin A, Lee J, Sudhakaran IP, Priya R, Heidari R, Holohan EE, Pimentel A, Gandhi A, Ito K, Sanyal S, Wang JW, Rodrigues V, Ramaswami M (2011) Plasticity of Local GABAergic Interneurons Drives Olfactory Habituation. Proc National Acad Sci 108:646–654.

Dear ML, Shilts J, Broadie K (2017) Neuronal activity drives FMRP- and HSPG-dependent matrix metalloproteinase function required for rapid synaptogenesis. Sci Signal 10:eaan3181.

Dehorter N, Pino ID (2020) Shifting Developmental Trajectories During Critical Periods of Brain Formation. Front Cell Neurosci 14:283.

Deidda G, Allegra M, Cerri C, Naskar S, Bony G, Zunino G, Bozzi Y, Caleo M, Cancedda L (2015) Early depolarizing GABA controls critical-period plasticity in the rat visual cortex. Nature neuroscience 18:87–96.

Deng P-Y, Rotman Z, Blundon JA, Cho Y, Cui J, Cavalli V, Zakharenko SS, Klyachko VA (2013) FMRP Regulates Neurotransmitter Release and Synaptic Information Transmission by Modulating Action Potential Duration via BK Channels. Neuron 77:696–711.

Devaud J, Acebes A, Ramaswami M, Ferrús A (2003a) Structural and Functional Changes in the Olfactory Pathway of Adult *Drosophila* Take Place at a Critical Age. J Neurobiol 56:13–23.

Devaud J, Keane J, Ferrús A (2003b) Blocking Sensory Inputs to Identified Antennal Glomeruli Selectively Modifies Odorant Perception in *Drosophila*. J Neurobiol 56:1–12.

Devaud J-M, Acebes A, Ferrús A (2001) Odor Exposure Causes Central Adaptation and Morphological Changes in Selected Olfactory Glomeruli in *Drosophila*. J Neurosci 21:6274–6282.

Devaud, J., Clouet-Redt, C., Bockaert, J., Grau, Y., Parmentier, M. (2008). Widespread brain distribution of the *Drosophila* metabotropic glutamate receptor. NeuroReport 19(3), 367-371.

Dolan M-J et al. (2019) Neurogenetic dissection of the Drosophila lateral horn reveals major outputs, diverse behavioural functions, and interactions with the mushroom body. Elife 8:e43079.

Dölen G, Osterweil E, Rao BS, Smith GB, Auerbach BD, Chattarji S, Bear MF (2007) Correction of Fragile X Syndrome in Mice. Neuron 56:955–962.

Doll CA, Broadie K (2015) Activity-dependent FMRP Requirements in Development of the Neural Circuitry of Learning and Memory. Development 142:1346–1356.

Doll CA, Broadie K (2016) Neuron Class-Specific Requirements for Fragile X Mental Retardation Protein in Critical Period Development of Calcium Signaling in Learning and Memory Circuitry. Neurobiol Dis 89:76–87.

Doll CA, Vita DJ, Broadie K (2017) Fragile X Mental Retardation Protein Requirements in Activity-Dependent Critical Period Neural Circuit Refinement. Curr Biol 27:2318-2330.e3.

Doll CA, Yergert KM, Appel BH (2020) The RNA binding protein fragile X mental retardation protein promotes myelin sheath growth. Glia 68:495–508.

Domanski, A., Booker, S., Wyllie, D., Isaac, J., Kind, P. (2019). Cellular and synaptic phenotypes lead to disrupted information processing in Fmr1-KO mouse layer 4 barrel cortex. Nature Communications 10(1), 4813.

Dong T, He J, Wang S, Wang L, Cheng Y, Zhong Y (2016) Inability to activate Rac1-dependent forgetting contributes to behavioral inflexibility in mutants of multiple autism-risk genes. Proc National Acad Sci 113:7644–7649.

Dubin AE, Harris GL (1997) Voltage-activated and odor-modulated conductances in olfactory neurons of Drosophila melanogaster. J Neurobiol 32:123–137.

Dudai Y, Jan Y, Byers D, Quinn W, Benzer S (1976) dunce, a mutant of Drosophila deficient in learning. Proceedings of the National Academy of Sciences of the United States of America 73:1684–1688.

Dweck HK, Ebrahim SA, Khallaf MA, Koenig C, Farhan A, Stieber R, Weißflog J, Svatoš A, Grosse-Wilde E, Knaden M, Hansson BS (2016) Olfactory channels associated with the Drosophila maxillary palp mediate short- and long-range attraction. Elife 5:e14925.

Eliason J, Afify A, Potter C, Matsumura I (2018) A GAL80 Collection To Inhibit GAL4 Transgenes in Drosophila Olfactory Sensory Neurons. G3 Genes Genomes Genetics 8:g3.200569.2018.

Ertürk A, Hellal F, Enes J, Bradke F (2007) Disorganized Microtubules Underlie the Formation of Retraction Bulbs and the Failure of Axonal Regeneration. J Neurosci 27:9169–9180.

Espinosa J, Stryker MP (2012) Development and plasticity of the primary visual cortex. Neuron 75:230–249.

Fagiolini M, Hensch TK (2000) Inhibitory threshold for critical-period activation in primary visual cortex. Nature 404:183–186.

Feldman DE (2000) Timing-Based LTP and LTD at Vertical Inputs to Layer II/III Pyramidal Cells in Rat Barrel Cortex. Neuron 27:45–56.

Ferron L, Nieto-Rostro M, Cassidy JS, Dolphin AC (2014) Fragile X mental retardation protein controls synaptic vesicle exocytosis by modulating N-type calcium channel density. Nat Commun 5:3628.

Fiacco TA, McCarthy KD (2018) Multiple Lines of Evidence Indicate That Gliotransmission Does Not Occur under Physiological Conditions. J Neurosci 38:3–13.

Fielde AM (1904) Power of Recognition Among Ants. Biological Bulletin 7: 227-250.

Fishilevich E, Vosshall LB (2005) Genetic and Functional Subdivision of the *Drosophila* Antennal Lobe. Curr Biol 15:1548–1553.

Fişek M, Wilson RI (2014) Stereotyped connectivity and computations in higher-order olfactory neurons. Nature neuroscience 17:280–288.

Flockhart I, Booker M, Kiger A, Boutros M, Armknecht S, Ramadan N, Richardson K, Xu A, Perrimon N, Mathey-Prevot B (2006) FlyRNAi: the *Drosophila* RNAi Screening Center Database. Nucleic Acids Res 34:D489–D494.

Fox K (1992) A Critical Period for Experience-dependent Synaptic Plasticity in Rat Barrel Cortex. J Neurosci 12:1826–1838.

(2021) Fragile X Syndrome: Prevalence. Available at: https://fragilex.org/understanding-fragile-x/fragile-x-101/prevalence/.

(2021) Fragile X Syndrome – Symptoms and Signs. Available at: https://www.fraxa.org/fragile-x-syndrome/symptoms/.

Franco LM, Okray Z, Linneweber GA, Hassan BA, Yaksi E (2017) Reduced Lateral Inhibition Impairs Olfactory Computations and Behaviors in a *Drosophila* Model of Fragile X Syndrome. Curr Biol 27:1111–1123.

French RL, Heberlein U (2009) Glycogen synthase kinase-3/Shaggy mediates ethanol-induced excitotoxic cell death of Drosophila olfactory neurons. Proc National Acad Sci 106:20924–20929.

Froemke RC, Dan Y (2002) Spike-timing-dependent synaptic modification induced by natural spike trains. Nature 416:433–438.

Friedman, S., Dani, N., Rushton, E., Broadie, K. (2013). Fragile X Mental Retardation Protein regulates trans-synaptic signaling in *Drosophila*. Disease Models & Mechanisms 6(6), 1400-1413.

Fuentes-Medel Y, Logan MA, Ashley J, Ataman B, Budnik V, Freeman MR (2009) Glia and Muscle Sculpt Neuromuscular Arbors by Engulfing Destabilized Synaptic Boutons and Shed Presynaptic Debris. Plos Biol 7:e1000184.

Gatto CL, Pereira D, Broadie K (2014) GABAergic circuit dysfunction in the Drosophila Fragile X syndrome model. Neurobiology of disease 65:142–159.

Geramita, M., Urban, N. (2016). Postnatal Odor Exposure Increases the Strength of Interglomerular Lateral Inhibition onto Olfactory Bulb Tufted Cells. The Journal of Neuroscience 36(49), 12321-12327.

Gerlach, G., Tietje, K., Biechl, D., Namekawa, I., Schalm, G., Sulmann, A. (2019). Behavioural and neuronal basis of olfactory imprinting and kin recognition in larval fish. Journal of Experimental Biology 222(1), jeb189746.

Gholizadeh S, Halder SK, Hampson DR (2015) Expression of fragile X mental retardation protein in neurons and glia of the developing and adult mouse brain. Brain research 1596:22–30.

Goel A, Cantu DA, Guilfoyle J, Chaudhari GR, Newadkar A, Todisco B, Alba D de, Kourdougli N, Schmitt LM, Pedapati E, Erickson CA, Portera-Cailliau C (2018) Impaired perceptual learning in a mouse model of Fragile X syndrome is mediated by parvalbumin neuron dysfunction and is reversible. Nat Neurosci 21:1404–1411.

Golovin RM, Broadie K (2016) Developmental Experience-Dependent Plasticity in the First Synapse of the *Drosophila* Olfactory Circuit. J Neurophysiol 116:2730–2738.

Golovin RM, Broadie K (2017) Neural Circuits: Reduced Inhibition in Fragile X Syndrome. Curr Biol 27:298–300.

Golovin, R., Vest, J., Vita, D., Broadie, K. (2019). Activity-Dependent Remodeling of *Drosophila* Olfactory Sensory Neuron Brain Innervation During an Early-Life Critical Period. The Journal of Neuroscience 39(16), 2223-2218.

Gomez-Marin A, Stephens GJ, Louis M (2011) Active sampling and decision making in Drosophila chemotaxis. Nat Commun 2:441.

Gonçalves, J., Anstey, J., Golshani, P., Portera-Cailliau, C. (2013). Circuit level defects in the developing neocortex of Fragile X mice. Nature Neuroscience 16(7), 903-909.

Grabe V, Baschwitz A, Dweck H, Lavista-Llanos S, Hansson BS, Sachse S (2016) Elucidating the Neuronal Architecture of Olfactory Glomeruli in the *Drosophila* Antennal Lobe. Cell Reports 16:3401–3413.

Grabe V, Sachse S (2018) Fundamental principles of the olfactory code. Biosystems 164:94–101.

Greenblatt, E., Spradling, A. (2018). Fragile X mental retardation 1 gene enhances the translation of large autism-related proteins. Science 361(6403), 709-712.

Greenhill, S., Juczewski, K., Haan, A., Seaton, G., Fox, K., Hardingham, N. (2015). Adult cortical plasticity depends on an early postnatal critical period. Science 349(6246), 424-427.

Groschner LN, Miesenböck G (2019) Mechanisms of Sensory Discrimination: Insights from Drosophila Olfaction. Annu Rev Biophys 48:1–21.

Gross C, Yao X, Pong DL, Jeromin A, Bassell GJ (2011) Fragile X Mental Retardation Protein Regulates Protein Expression and mRNA Translation of the Potassium Channel Kv4.2. J Neurosci 31:5693–5698.

Gu Q, Singer W (1995) Involvement of Serotonin in Developmental Plasticity of Kitten Visual Cortex. Eur J Neurosci 7:1146–1153.

Halfon MS, Kose H, Chiba A, Keshishian H (1997) Targeted gene expression without a tissue-specific promoter: Creating mosaic embryos using laser-induced single-cell heat shock. Proc National Acad Sci 94:6255–6260.

Halty-deLeon L, Hansson BS, Wicher D (2018) The Drosophila melanogaster Na+/Ca2+ Exchanger CALX Controls the Ca2+ Level in Olfactory Sensory Neurons at Rest and After Odorant Receptor Activation. Front Cell Neurosci 12:186.

Hara C, Morishita K, Takayanagi-Kiya S, Mikami A, Uchino K, Sakurai T, Kanzaki R, Sezutsu H, Iwami M, Kiya T (2017) Refinement of ectopic protein expression through the GAL4/UAS system in Bombyx mori: application to behavioral and developmental studies. Sci Rep-uk 7:11795.

Hallem EA, Carlson JR (2006) Coding of Odors by a Receptor Repertoire. Cell 125:143–160.

Harlow, E., Till, S., Russell, T., Wijetunge, L., Kind, P., Contractor, A. (2010). Critical period plasticity is disrupted in the barrel cortex of FMR1 knockout mice. Neuron 65(3), 385-98.

Hayashi, S., Ito, K., Sado, Y., Taniguchi, M., Akimoto, A., Takeuchi, H., Aigaki, T., Matsuzaki, F., Nakagoshi, H., Tanimura, T., Ueda, R., Uemura, T., Yoshihara, M., Goto, S. (2002). GETDB, a database compiling expression patterns and molecular locations of a collection of gal4 enhancer traps. Genesis 34(1-2), 58-61.

He, Q., Nomura, T., Xu, J., Contractor, A. (2014). The developmental switch in GABA polarity is delayed in Fragile X mice. The Journal of Neuroscience 34(2), 446-450.

Heisenberg M (2003) Mushroom body memoir: from maps to models. Nature reviews Neuroscience 4:266–275.

Helassa N, Dürst CD, Coates C, Kerruth S, Arif U, Schulze C, Wiegert JS, Geeves M, Oertner TG, Török K (2018) Ultrafast glutamate sensors resolve high-frequency release at Schaffer collateral synapses. Proc National Acad Sci 115:5594–5599.

Hensch TK, Fagiolini M, Mataga N, Stryker MP, Baekkeskov S, Kash SF (1998) Local GABA Circuit Control of Experience-Dependent Plasticity in Developing Visual Cortex. Science 282:1504–1508.

Hensch TK (2004) Critical Period Regulation. Annu Rev Neurosci 27:549–579.

Hensch, T. (2005). Critical period plasticity in local cortical circuits. Nature Reviews Neuroscience 6(11), 877-888.

Hensch TK, Bilimoria PM (2012) Re-opening Windows: Manipulating Critical Periods for Brain Development. Cerebrum Dana Forum Brain Sci 2012:11.

Hensch TK, Quinlan EM (2018) Critical periods in amblyopia. Visual Neurosci 35:E014.

Hersh, J., Saul, R., Genetics, C. (2011). Health Supervision for Children With Fragile X Syndrome. Pediatrics 127(5), 994-1006.

Hess EH (1958) “Imprinting” in Animals. Sci Am 198:81–90.

Higashimori H, Schin CS, Chiang MS, Morel L, Shoneye TA, Nelson DL, Yang Y (2016) Selective Deletion of Astroglial FMRP Dysregulates Glutamate Transporter GLT1 and Contributes to Fragile

X Syndrome Phenotypes In Vivo. The Journal of neuroscience : the official journal of the Society for Neuroscience 36:7079–7094.

Hige T, Aso Y, Rubin GM, Turner GC (2015) Plasticity-driven individualization of olfactory coding in mushroom body output neurons. Nature 526:258–262.

Hilu-Dadia R, Kurant E (2020) Glial phagocytosis in developing and mature Drosophila CNS: tight regulation for a healthy brain. Curr Opin Immunol 62:62–68.

Hong W, Luo L (2014) Genetic control of wiring specificity in the fly olfactory system. Genetics 196:17–29.

Hong W, Mosca TJ, Luo L (2012) Teneurins instruct synaptic partner matching in an olfactory map. Nature 484:201–207.

Hooks BM, Chen C (2007) Critical Periods in the Visual System: Changing Views for a Model of Experience-Dependent Plasticity. Neuron 56:312–326.

Housden BE, Muhar M, Gemberling M, Gersbach CA, Stainier DYR, Seydoux G, Mohr SE, Zuber J, Perrimon N (2017) Loss-of-function genetic tools for animal models: cross-species and cross-platform differences. Nat Rev Genet 18:24–40.

Hu A, Zhang W, Wang Z (2010) Functional feedback from mushroom bodies to antennal lobes in the Drosophila olfactory pathway. Proc National Acad Sci 107:10262–10267.

Huang ZJ, Kirkwood A, Pizzorusso T, Porciatti V, Morales B, Bear MF, Maffei L, Tonegawa S (1999) BDNF Regulates the Maturation of Inhibition and the Critical Period of Plasticity in Mouse Visual Cortex. Cell 98:739-755.

Huang, J., Zhang, W., Qiao, W., Hu, A., Wang, Z. (2010). Functional connectivity and selective odor responses of excitatory local interneurons in *Drosophila* antennal lobe. Neuron 67(6), 1021-1033.

Huang X, Stodieck SK, Goetze B, Cui L, Wong MH, Wenzel C, Hosang L, Dong Y, Löwel S, hlüter O (2015) Progressive maturation of silent synapses governs the duration of a critical period. Proceedings of the National Academy of Sciences of the United States of America 112:E3131-40.

Huang C, Maxey JR, Sinha S, Savall J, Gong Y, Schnitzer MJ (2018) Long-term optical brain imaging in live adult fruit flies. Nat Commun 9:872.

Hubel, D., Wiesel, T. (1970). The period of susceptibility to the physiological effects of unilateral eye closure in kittens. The Journal of Physiology 206(2), 419-436.

Hummel T, Vasconcelos ML, Clemens JC, Fishilevich Y, Vosshall LB, Zipursky SL (2003) Axonal Targeting of Olfactory Receptor Neurons in Drosophila Is Controlled by Dscam. Neuron 37:221–231.

Hummel T, Zipursky SL (2004) Afferent Induction of Olfactory Glomeruli Requires N-Cadherin. Neuron 42:77–88.

Inoue, S., Shimoda, M., Nishinokubi, I., Siomi, M., Okamura, M., Nakamura, A., Kobayashi, S., Ishida, N., Siomi, H. (2002). A Role for the *Drosophila* Fragile X-Related Gene in Circadian Output. Current Biology 12(15), 1331-1335.

Jackson, F., Newby, L., Kulkarni, S. (1990). *Drosophila* GABAergic Systems: Sequence and Expression of Glutamic Acid Decarboxylase. Journal of Neurochemistry 54(3), 1068-1078.

Jawaid S, Kidd GJ, Wang J, Swetlik C, Dutta R, Trapp BD (2018) Alterations in CA1 hippocampal synapses in a mouse model of fragile X syndrome. Glia 66:789–800.

Jeanne JM, Fişek M, Wilson RI (2018) The Organization of Projections from Olfactory Glomeruli onto Higher-Order Neurons. Neuron 98:1198-1213.e6.

Jefferis GS, Marin EC, Stocker RF, Luo L (2001) Target Neuron Prespecification in the Olfactory Map of *Drosophila*. Nature 414:204.

Jefferis, G., Marin, E., Watts, R., Luo, L. (2002). Development of neuronal connectivity in *Drosophila* antennal lobes and mushroom bodies. Current Opinion in Neurobiology 12, 80-86.

Jefferis GS, Vyas RM, Berdnik D, Ramaekers A, Stocker RF, Tanaka NK, Ito K, Luo L (2004) Developmental Origin of Wiring Specificity in the Olfactory System of *Drosophila*. Development 131:117–130.

Jin L, Han Z, Platisa J, Wooltorton JRA, Cohen LB, Pieribone VA (2012) Single Action Potentials and Subthreshold Electrical Events Imaged in Neurons with a Fluorescent Protein Voltage Probe. Neuron 75:779–785.

Jin X, Pokala N, Bargmann CI (2016) Distinct Circuits for the Formation and Retrieval of an Imprinted Olfactory Memory. Cell 164:632-643.

Joo WJ, Sweeney LB, Liang L, Luo L (2013) Linking Cell Fate, Trajectory Choice, and Target Selection: Genetic Analysis of Sema-2b in Olfactory Axon Targeting. Neuron 78:673–686.

Kanellopoulos AK, Semelidou O, Kotini AG, Anezaki M, Skoulakis EM (2012) Learning and memory deficits consequent to reduction of the fragile X mental retardation protein result from metabotropic glutamate receptor-mediated inhibition of cAMP signaling in Drosophila. The Journal of neuroscience : the official journal of the Society for Neuroscience 32:13111–13124.

Kanold PO, Shatz CJ (2006) Subplate Neurons Regulate Maturation of Cortical Inhibition and Outcome of Ocular Dominance Plasticity. Neuron 51:627–638.

Kazama H (2015) Systems neuroscience in Drosophila: Conceptual and technical advantages. Neuroscience 296:3–14.

Kelley DJ, Davidson RJ, Elliott JL, Lahvis GP, Yin JCP, Bhattacharyya A (2007) The Cyclic AMP Cascade Is Altered in the Fragile X Nervous System. Plos One 2:e931.

Kerchner GA, Nicoll RA (2008) Silent synapses and the emergence of a postsynaptic mechanism for LTP. Nat Rev Neurosci 9:813–825.

Kerr KS, Fuentes-Medel Y, Brewer C, Barria R, Ashley J, Abruzzi KC, Sheehan A, Tasdemir-Yilmaz OE, Freeman MR, Budnik V (2014) Glial Wingless/Wnt Regulates Glutamate Receptor

Clustering and Synaptic Physiology at the Drosophila Neuromuscular Junction. J Neurosci 34:2910–2920.

Khakh BS, Sofroniew MV (2015) Diversity of astrocyte functions and phenotypes in neural circuits. Nat Neurosci 18:942–952.

Khandjian, E., Anny, F., Thibodeau, A., Tremblay, S., Cote, F., Devys, D., Mandel, J., Rousseau, F. (1995). A heterogeneous set of FMR1 proteins is widely distributed in mouse tissues and is modulated in cell culture. Human Molecular Genetics 4(5), 783-789.

Kidd S, Lieber T (2016) Mechanism of Notch Pathway Activation and Its Role in the Regulation of Olfactory Plasticity in *Drosophila melanogaster*. Plos One 11:e0151279.

Kidd S, Struhl G, Lieber T (2015) Notch is required in adult Drosophila sensory neurons for morphological and functional plasticity of the olfactory circuit. PLoS genetics 11:e1005244.

Kim H, Gibboni R, Kirkhart C, Bao S (2013) Impaired critical period plasticity in primary auditory cortex of fragile X model mice. The Journal of neuroscience : the official journal of the Society for Neuroscience 33:15686–15692.

Klapoetke, N., Murata, Y., Kim, S., Pulver, S., Birdsey-Benson, A., Cho, Y., Morimoto, T., Chuong, A., Carpenter, E., Tian, Z., Wang, J., Xie, Y., Yan, Z., Zhang, Y., Chow, B., Surek, B.,

Knudsen EI (2004) Sensitive Periods in the Development of the Brain and Behavior. J Cognitive Neurosci 16:1412–1425.

Kremer MC, Jung C, Batelli S, Rubin GM, Gaul U (2017) The glia of the adult Drosophila nervous system. Glia 65:606–638.

Kobayashi Y, Ye Z, Hensch TK (2015) Clock genes control cortical critical period timing. Neuron 86:264–275.

Kopke DL, Lima SC, Alexandre C, Broadie K (2017) Notum Coordinates Synapse Development via Extracellular Regulation of Wnt Wingless Trans-Synaptic Signaling. Development 144:3499–3510.

Korkut C, Ataman B, Ramachandran P, Ashley J, Barria R, Gherbesi N, Budnik V (2009) Trans-Synaptic Transmission of Vesicular Wnt Signals through Evi/Wntless. Cell 139:393–404.

Krishnan, K., Wang, B., Lu, J., Wang, L., Maffei, A., Cang, J., Huang, Z. (2015). MeCP2 regulates the timing of critical period plasticity that shapes functional connectivity in primary visual cortex. Proceedings of the National Academy of Sciences USA 112(34), 4782-4791.

LaLonde M, Janssens H, Yun S, Crosby J, Redina O, Olive V, Altshuller Y, Choi S-Y, Du G, Gergen P, Frohman M (2006) A role for Phospholipase D in Drosophilaembryonic cellularization. Bmc Dev Biol 6:60.

Larsson, M., Domingos, A., Jones, W., Chiappe, M., Amrein, H., Vosshall, L. (2004). Or83b encodes a broadly expressed odorant receptor essential for *Drosophila* olfaction. Neuron 43(5), 703-714.

Lee P-T, Lin G, Lin W-W, Diao F, White BH, Bellen HJ (2018) A kinase-dependent feedforward loop affects CREBB stability and long-term memory formation. Elife 7:e33007.

Lee, T., Luo, L. (1999). Mosaic Analysis with a Repressible Cell Marker for Studies of Gene Function in Neuronal Morphogenesis. Neuron 22(3), 451-461.

Lenneberg EH (2016) The Biological Foundations of Language. Hosp Pract 2:59–67.

Levin LR, Han P-L, Hwang PM, Feinstein PG, Davis RL, Reed RR (1992) The Drosophila learning and memory gene rutabaga encodes a Ca2+calmodulin-responsive adenylyl cyclase. Cell 68:479–489.

Li Y, Raisman G (1995) Sprouts from Cut Corticospinal Axons Persist in the Presence of Astrocytic Scarring in Long-Term Lesions of the Adult Rat Spinal Cord. Exp Neurol 134:102–111.

Liang L, Li Y, Potter CJ, Yizhar O, Deisseroth K, Tsien RW, Luo L (2013) GABAergic projection neurons route selective olfactory inputs to specific higher-order neurons. Neuron 79:917–931.

Lieber T, Kidd S, Struhl G (2011) DSL-Notch Signaling in the *Drosophila* Brain in Response to Olfactory Stimulation. Neuron 69:468–481.

Lin B, Kramár EA, Bi X, Brucher FA, Gall CM, Lynch G (2005) Theta Stimulation Polymerizes Actin in Dendritic Spines of Hippocampus. J Neurosci 25:2062–2069.

Lin MZ, Schnitzer MJ (2016) Genetically encoded indicators of neuronal activity. Nat Neurosci 19:1142–1153.

Ling D, Salvaterra P (2011) Robust RT-qPCR Data Normalization: Validation and Selection of Internal Reference Genes during Post-Experimental Data Analysis. Plos One 6:e17762.

Liu H, Gao P-F, Xu H-W, Liu M-M, Yu T, Yao J-P, Yin Z-Q (2013) Perineuronal nets increase inhibitory GABAergic currents during the critical period in rats. Int J Ophthalmol-chi 6:120–125.

Liu, X., Krause, W., Davis, R. (2007). GABAA Receptor RDL Inhibits *Drosophila* Olfactory Associative Learning. Neuron 56(6), 1090-1102.

Liu WW, Wilson RI (2013) Glutamate is an Inhibitory Neurotransmitter in the *Drosophila* Olfactory System. Proc National Acad Sci 110:10294–10299.

Liu, A., Urban, N. (2017). Prenatal and Early Postnatal Odorant Exposure Heightens Odor-Evoked Mitral Cell Responses in the Mouse Olfactory Bulb. eNeuro 4(5), ENEURO.0129-17.2017.

Livak K, Schmittgen T (2001) Analysis of Relative Gene Expression Data Using Real-Time Quantitative PCR and the 2−ΔΔCT Method. Methods 25:402–408

Lovelace, J., Rais, M., Palacios, A., Shuai, X., Bishay, S., Popa, O., Pirbhoy, P., Binder, D., Nelson, D., Ethell, I., Razak, K. (2019). Deletion of Fmr1 from Forebrain Excitatory Neurons Triggers Abnormal Cellular, EEG, and Behavioral Phenotypes in the Auditory Cortex of a Mouse Model of Fragile X Syndrome. Cerebral Cortex 30(3), 969-988.

Lorenz K (1935) Der Kumpan in der Umwelt des Vogels. J Für Ornithol 83:137–213.

Low LK, Cheng H-J (2006) Axon pruning: an essential step underlying the developmental plasticity of neuronal connections. Philosophical Transactions Royal Soc B Biological Sci 361:1531–1544.

Ma Z, Stork T, Bergles DE, Freeman MR (2016) Neuromodulators signal through astrocytes to alter neural circuit activity and behaviour. Nature 539:428–432.

Ma L, Wu Y, Qiu Q, Scheerer H, Moran A, Yu C (2014) A developmental switch of axon targeting in the continuously regenerating mouse olfactory system. Science (New York, NY) 344:194–197.

MacDonald JM, Beach MG, Porpiglia E, Sheehan AE, Watts RJ, Freeman MR (2006) The Drosophila Cell Corpse Engulfment Receptor Draper Mediates Glial Clearance of Severed Axons. Neuron 50:869–881.

Majewska A, Sur M (2003) Motility of dendritic spines in visual cortex in vivo: Changes during the critical period and effects of visual deprivation. Proc National Acad Sci 100:16024–16029.

Marin, E., Jefferis, G., Komiyama, T., Zhu, H., Luo, L. (2002). Representation of the glomerular olfactory map in the *Drosophila* brain. Cell 109(2), 243-255.

Marin EC, Watts RJ, Tanaka NK, Ito K, Luo L (2005) Developmentally programmed remodeling of the Drosophila olfactory circuit. Development (Cambridge, England) 132:725–737.

Martín F, Charro M, Alcorta E (2001) Mutations affecting the cAMP transduction pathway modify olfaction in Drosophila. J Comp Physiology 187:359–370.

Martin BS, Corbin JG, Huntsman MM (2014) Deficient tonic GABAergic conductance and synaptic balance in the fragile X syndrome amygdala. J Neurophysiol 112:890–902.

Martins AR, Froemke RC (2015) Coordinated forms of noradrenergic plasticity in the locus coeruleus and primary auditory cortex. Nature neuroscience 18:1483–1492.

Marvin JS, Shimoda Y, Magloire V, Leite M, Kawashima T, Jensen TP, Kolb I, Knott EL, Novak O, Podgorski K, Leidenheimer NJ, Rusakov DA, Ahrens MB, Kullmann DM, Looger LL (2019) A genetically encoded fluorescent sensor for in vivo imaging of GABA. Nat Methods 16:763–770.

Masse NY, Turner GC, Jefferis GSXE (2009) Olfactory Information Processing in Drosophila. Curr Biol 19:R700–R713.

Mataga N, Mizuguchi Y, Hensch TK (2004) Experience-Dependent Pruning of Dendritic Spines in Visual Cortex by Tissue Plasminogen Activator. Neuron 44:1031–1041.

McGee AW, Yang Y, Fischer QS, Daw NW, Strittmatter SM (2005) Experience-Driven Plasticity of Visual Cortex Limited by Myelin and Nogo Receptor. Science 309:2222–2226.

Melkonian, M., Jayaraman, V., Constantine-Paton, M., Wong, G., Boyden, E. (2014). Independent optical excitation of distinct neural populations. Nature Methods 11(3), 338-346.

Meredith, R. (2015). Sensitive and critical periods during neurotypical and aberrant neurodevelopment: A framework for neurodevelopmental disorders. Neuroscience & Biobehavioral Reviews 50(1), 180-188.

Meredith RM, Holmgren CD, Weidum M, Burnashev N, Mansvelder HD (2007) Increased Threshold for Spike-Timing-Dependent Plasticity Is Caused by Unreliable Calcium Signaling in Mice Lacking Fragile X Gene Fmr1. Neuron 54:627–638.

Meyer F, Aberle H (2006) At the next stop sign turn right: the metalloprotease Tolloid-related 1 controls defasciculation of motor axons in Drosophila. Development 133:4035–4044.

Miazzi F, Hansson BS, Wicher D (2016) Odor-induced cAMP production in Drosophila melanogaster olfactory sensory neurons. J Exp Biol 219:1798–1803.

Mohamed, A., Retzke, T., Chakraborty, S., Fabian, B., Hansson, B., Knaden, M., Sachse, S. (2019). Odor mixtures of opposing valence unveil inter-glomerular crosstalk in the *Drosophila* antennal lobe. Nature Communications 10(1), 1201.

Mohammad, F., Stewart, J., Ott, S., Chlebikova, K., Chua, J., Koh, T., Ho, J., Claridge-Chang, A. (2017). Optogenetic inhibition of behavior with anion channelrhodopsins.. Nature Methods 14(3), 271-274.

Morishita H, Miwa JM, Heintz N, Hensch TK (2010) Lynx1, a Cholinergic Brake, Limits Plasticity in Adult Visual Cortex. Science 330:1238–1240.

Mosca TJ, Luo L (2014) Synaptic Organization of the *Drosophila* Antennal Lobe and its Regulation by the Teneurins. Elife 3:e03726.

Mukherjee A, Williams DW (2017) More alive than dead: non-apoptotic roles for caspases in neuronal development, plasticity and disease. Cell Death Differ 24:1411–1421.

Mukunda L, Miazzi F, Kaltofen S, Hansson BS, Wicher D (2014) Calmodulin modulates insect odorant receptor function. Cell Calcium 55:191–199.

Münch, D., Galizia, C. (2016). DoOR 2.0--Comprehensive Mapping of *Drosophila melanogaster* Odorant Responses. Scientific Reports 6, 21841.

Murase S, Lantz CL, Quinlan EM (2017) Light reintroduction after dark exposure reactivates plasticity in adults via perisynaptic activation of MMP-9. Elife 6:e27345.

Muthukumar AK, Stork T, Freeman MR (2014) Activity-dependent regulation of astrocyte GAT levels during synaptogenesis. Nature neuroscience 17:1340–1350.

Myrick LK, Deng P-Y, Hashimoto H, Oh Y, Cho Y, Poidevin MJ, Suhl JA, Visootsak J, Cavalli V, Jin P, Cheng X, Warren ST, Klyachko VA (2015) Independent role for presynaptic FMRP revealed by an FMR1 missense mutation associated with intellectual disability and seizures. Proceedings of the National Academy of Sciences 112:949–956.

Nagarkar-Jaiswal, S., DeLuca, S., Lee, P., Lin, W., Pan, H., Zuo, Z., Lv, J., Spradling, A., Bellen, H. (2015). A genetic toolkit for tagging intronic MiMIC containing genes. eLife 4, e08469.

Nakai J, Ohkura M, Imoto K (2001) A high signal-to-noise Ca2+ probe composed of a single green fluorescent protein. Nat Biotechnol 19:137–141.

Nardou R, Lewis EM, Rothhaas R, Xu R, Yang A, Boyden E, Dölen G (2019) Oxytocin-dependent reopening of a social reward learning critical period with MDMA. Nature 569:116–120.

Nässel DR, Zandawala M (2020) Hormonal axes in Drosophila: regulation of hormone release and multiplicity of actions. Cell Tissue Res 382:233–266.

Naters W van der van, Carlson JR (2007) Receptors and neurons for fly odors in Drosophila. Current biology : CB 17:606–612.

Nayak T, Trotter J, Sakry D (2018) The Intracellular Cleavage Product of the NG2 Proteoglycan Modulates Translation and Cell-Cycle Kinetics via Effects on mTORC1/FMRP Signaling. Front Cell Neurosci 12:231.

Ng J, Browning A, Lechner L, Terada M, Howard G, Jefferis GS (2016) Genetically Targeted 3D Visualisation of *Drosophila* Neurons Under Electron Microscopy and X-Ray Microscopy Using miniSOG. Sci Reports 6:srep38863.

Ni J-Q, Liu L-P, Binari R, Hardy R, Shim H-S, Cavallaro A, Booker M, Pfeiffer BD, Markstein M, Wang H, Villalta C, Laverty TR, Perkins LA, Perrimon N (2009) A *Drosophila* Resource of Transgenic RNAi Lines for Neurogenetics. Genetics 182:1089–1100.

Nitabach MN, Blau J, Holmes TC (2002) Electrical Silencing of Drosophila Pacemaker Neurons Stops the Free-Running Circadian Clock. Cell 109:485–495.

O'Connor R, Stone E, Wayne C (2017) A Drosophila model of Fragile X syndrome exhibits defects in phagocytosis by innate immune cells.

Oh WC, Lutzu S, Castillo PE, Kwon H-BB (2016) De novo synaptogenesis induced by GABA in the developing mouse cortex. Science (New York, NY).

Okada R, Awasaki T, Ito K (2009) Gamma Aminobutyric Acid (GABA) Mediated Neural Connections in the *Drosophila* Antennal Lobe. J Comp Neurol 514:74–91.

O'Leary DDM (1989) Do cortical areas emerge from a protocortex? Trends Neurosci 12:400–406.

Olmos-Serrano JL, Paluszkiewicz SM, Martin BS, Kaufmann WE, Corbin JG, Huntsman MM (2010) Defective GABAergic Neurotransmission and Pharmacological Rescue of Neuronal Hyperexcitability in the Amygdala in a Mouse Model of Fragile X Syndrome. J Neurosci 30:9929–9938.

Olsen SR, Bhandawat V, Wilson RI (2007) Excitatory Interactions between Olfactory Processing Channels in the *Drosophila* Antennal Lobe. Neuron 54:89–103.

Olsen, S., Bhandawat, V., Wilson, R. (2010). Divisive Normalization in Olfactory Population Codes. Neuron 66(2), 287-299.

Olsen SR, Wilson RI (2008) Lateral presynaptic inhibition mediates gain control in an olfactory circuit. Nature 452:956–960.

Packard M, Koo E, Gorczyca M, Sharpe J, Cumberledge S, Budnik V (2002) The *Drosophila* Wnt, Wingless, Provides an Essential Signal for Pre- and Postsynaptic Differentiation. Cell 111:319–330.

Paluszkiewicz SM, Martin BS, Huntsman MM (2011) Fragile X Syndrome: The GABAergic System and Circuit Dysfunction. Developmental Neuroscience.

Patriarchi T, Cho JR, Merten K, Howe MW, Marley A, Xiong W-H, Folk RW, Broussard GJ, Liang R, Jang MJ, Zhong H, Dombeck D, Zastrow M von, Nimmerjahn A, Gradinaru V, Williams JT, Tian L (2018) Ultrafast neuronal imaging of dopamine dynamics with designed genetically encoded sensors. Science 360:eaat4422.

Pellegrino M, Nakagawa T, Vosshall LB (2010) Single Sensillum Recordings in the Insects Drosophila melanogaster and Anopheles gambiae. J Vis Exp Jove:1725.

Pérez C, Sawmiller D, Tan J (2016) The role of heparan sulfate deficiency in autistic phenotype: potential involvement of Slit/Robo/srGAPs-mediated dendritic spine formation. Neural Dev 11:11.

Phelan P, Nakagawa M, Wilkin, Moffat K, O'Kane C, Davies J, Bacon J (1996) Mutations in shaking-B prevent electrical synapse formation in the Drosophila giant fiber system. J Neurosci 16:1101–1113.

Pizzorusso T, Medini P, Berardi N, Chierzi S, Fawcett JW, Maffei L (2002) Reactivation of Ocular Dominance Plasticity in the Adult Visual Cortex. Science 298:1248–1251.

Pizzorusso T, Medini P, Landi S, Baldini S, Berardi N, Maffei L (2006) Structural and functional recovery from early monocular deprivation in adult rats. Proc National Acad Sci 103:8517–8522.

Potter CJ, Tasic B, Russler EV, Liang L, Luo L (2010) The Q System: A Repressible Binary System for Transgene Expression, Lineage Tracing, and Mosaic Analysis. Cell 141:536–548.

Raccuglia D, McCurdy L, Demir M, nivas Gorur-Shandilya, Kunst M, Emonet T, Nitabach MN (2016) Presynaptic GABA receptors mediate temporal contrast enhancement in Drosophila olfactory sensory neurons and modulate odor-driven behavioral kinetics. eNeuro 3:ENEURO. 0080-16.2016.

Rakic P (1988) Specification of cerebral cortical areas. Science 241:170–176.

Reh RK, Dias BG, Nelson CA, Kaufer D, Werker JF, Kolb B, Levine JD, Hensch TK (2020) Critical period regulation across multiple timescales. Proc National Acad Sci 117:23242–23251.

Remy J-J, Hobert O (2005) An Interneuronal Chemoreceptor Required for Olfactory Imprinting in *C. elegans*. Science 309:787–790.

Rheede JJ van, Richards BA, Akerman CJ (2015) Sensory-Evoked Spiking Behavior Emerges via an Experience-Dependent Plasticity Mechanism. Neuron 87:1050–1062.

Ribic A, Biederer T (2019) Emerging Roles of Synapse Organizers in the Regulation of Critical Periods. Neural Plast 2019:1–9.

Ribot J, Breton R, Calvo C-F, Moulard J, Ezan P, Zapata J, Samama K, Bemelmans A-P, Sabatet V, Dingli F, Loew D, Milleret C, Billuart P, Dallérac G, Rouach N (2020) Astrocytes close the critical period for visual plasticity. Biorxiv:2020.09.30.321497.

Roberts, J., McCary, L., Shinkareva, S., Bailey, D. (2016). Infant Development in Fragile X Syndrome: Cross-Syndrome Comparisons. Journal of Autism and Developmental Disorders 46(6), 2088-2099.

Root CM, Masuyama K, Green DS, Enell LE, Nässel DR, Lee C-H, Wang JW (2008) A Presynaptic Gain Control Mechanism Fine-Tunes Olfactory Behavior. Neuron 59:311–321.

Rorth, P. (1996). A modular misexpression screen in *Drosophila* detecting tissue-specific phenotypes. Proceedings of the National Academy of Sciences USA 93(22), 12418-12422.

Rushton E, Kopke DL, Broadie K (2020) Extracellular heparan sulfate proteoglycans and glycan-binding lectins orchestrate trans-synaptic signaling. J Cell Sci 133:jcs244186.

Russo A, DiAntonio A (2019) Wnd/DLK Is a Critical Target of FMRP Responsible for Neurodevelopmental and Behavior Defects in the Drosophila Model of Fragile X Syndrome. Cell Reports 28:2581-2593.e5.

Sachse, S., Rueckert, E., Keller, A., Okada, R., Tanaka, N., Ito, K., Vosshall, L. (2007). Activity-dependent plasticity in an olfactory circuit. Neuron 56(5), 838-850.

Sadanandappa MK, Redondo BB, Michels B, Rodrigues V, Gerber B, VijayRaghavan K, Buchner E, Ramaswami M (2013) Synapsin Function in GABA-ergic Interneurons Is Required for Short-Term Olfactory Habituation. J Neurosci 33:16576–16585.

Sanes D, Constantine-Paton M (1983) Altered activity patterns during development reduce neural tuning. Science 221:1183–1185.

Sapar ML, Ji H, Wang B, Poe AR, Dubey K, Ren X, Ni J-Q, Han C (2018) Phosphatidylserine Externalization Results from and Causes Neurite Degeneration in Drosophila. Cell Reports 24:2273–2286.

Sawicka, K., Hale, C., Park, C., Fak, J., Gresack, J., Driesche, S., Kang, J., Darnell, J., Darnell, R. (2019). FMRP has a cell-type-specific role in CA1 pyramidal neurons to regulate autism-related transcripts and circadian memory. eLife 8, e46919.

Schafer DP, Lehrman EK, Kautzman AG, Koyama R, Mardinly AR, Yamasaki R, Ransohoff RM, Greenberg ME, Barres BA, Stevens B (2012) Microglia Sculpt Postnatal Neural Circuits in an Activity and Complement-Dependent Manner. Neuron 74:691–705.

Schindelin J, Arganda-Carreras I, Frise E, Kaynig V, Longair M, Pietzsch T, Preibisch S, Rueden C, Saalfeld S, Schmid B, Tinevez J-Y, White D, Hartenstein V, Eliceiri K, Tomancak P, Cardona A (2012) Fiji: an Open-Source Platform for Biological-Image Analysis. Nat Methods 9:676.

Schneider CA, Rasband WS, Eliceiri KW (2012) NIH Image to ImageJ: 25 years of image analysis. Nat Methods 9:671.

Sears JC, Broadie K (2018) Fragile X Mental Retardation Protein Regulates Activity-Dependent Membrane Trafficking and Trans-Synaptic Signaling Mediating Synaptic Remodeling. Frontiers Mol Neurosci 10:440.

Sears JC, Broadie K (2020) FMRP-PKA Activity Negative Feedback Regulates RNA Binding-Dependent Fibrillation in Brain Learning and Memory Circuitry. Cell Reports 33:108266.

Sears, J., Choi, W., Broadie, K. (2019). Fragile X Mental Retardation Protein positively regulates PKA anchor Rugose and PKA activity to control actin assembly in learning/memory circuitry. Neurobiology of Disease 127, 53-64.

Seki Y, Rybak J, Wicher D, Sachse S, Hansson BS (2010) Physiological and morphological characterization of local interneurons in the Drosophila antennal lobe. Journal of neurophysiology 104:1007–1019.

Semmelhack, J., Wang, J. (2009). Select *Drosophila* glomeruli mediate innate olfactory attraction and aversion. Nature 459(7244), 218-223.

Shepard KN, Liles LC, Weinshenker D, Liu RC (2015) Norepinephrine Is Necessary for Experience-Dependent Plasticity in the Developing Mouse Auditory Cortex. J Neurosci 35:2432–2437.

Shiraiwa T (2008) Multimodal Chemosensory Integration through the Maxillary Palp in Drosophila. Plos One 3:e2191.

Shu X, Lev-Ram V, Deerinck TJ, Qi Y, Ramko EB, Davidson MW, Jin Y, Ellisman MH, Tsien RY (2011) A Genetically Encoded Tag for Correlated Light and Electron Microscopy of Intact Cells, Tissues, and Organisms. Plos Biol 9:e1001041.

Sidhu H, Dansie LE, Hickmott PW, Ethell DW, Ethell IM (2014) Genetic Removal of Matrix Metalloproteinase 9 Rescues the Symptoms of Fragile X Syndrome in a Mouse Model. J Neurosci 34:9867–9879.

Stacey SM, Muraro NI, Peco E, Labbé A, Thomas GB, Baines RA, Meyel DJ van (2010) Drosophila Glial Glutamate Transporter Eaat1 Is Regulated by Fringe-Mediated Notch Signaling and Is Essential for Larval Locomotion. J Neurosci 30:14446–14457.

Stephan D, Sánchez-Soriano N, Loschek LF, Gerhards R, Gutmann S, Storchova Z, Prokop A, Kadow IC (2012) *Drosophila* Psidin Regulates Olfactory Neuron Number and Axon Targeting through Two Distinct Molecular Mechanisms. J Neurosci 32:16080–16094.

Stevens B, Allen NJ, Vazquez LE, Howell GR, Christopherson KS, Nouri N, Micheva KD, Mehalow AK, Huberman AD, Stafford B, Sher A, Litke AM, Lambris JD, Smith SJ, John SWM, Barres BA (2007) The Classical Complement Cascade Mediates CNS Synapse Elimination. Cell 131:1164–1178.

Strickfaden H, Xu Z, Hendzel MJ (2015) Visualization of miniSOG Tagged DNA Repair Proteins in Combination with Electron Spectroscopic Imaging (ESI). J Vis Exp Jove.

Stocker, R., Heimbeck, G., Gendre, N., Belle, J. (1997). Neuroblast ablation in *Drosophila* P[GAL4] lines reveals origins of olfactory interneurons. Journal of Neurobiology 32(5), 443-456.

Sudhakaran, I., Hillebrand, J., Dervan, A., Das, S., Holohan, E., Hülsmeier, J., Sarov, M., Parker, R., VijayRaghavan, K., Ramaswami, M. (2014). FMRP and Ataxin-2 function together in long-term olfactory habituation and neuronal translational control. Proceedings of the National Academy of Sciences USA 111(1), 99-108.

Sugiyama S, Nardo AAD, Aizawa S, Matsuo I, Volovitch M, Prochiantz A, Hensch TK (2008) Experience-dependent transfer of Otx2 homeoprotein into the visual cortex activates postnatal plasticity. Cell 134:508–520.

Sweeney, S., Broadie, K., Keane, J., Niemann, H., O'Kane, C. (1995). Targeted expression of tetanus toxin light chain in *Drosophila* specifically eliminates synaptic transmission and causes behavioral defects. Neuron 14(2), 341-351.

Sweeney LB, Chou Y-H, Wu Z, Joo W, Komiyama T, Potter CJ, Kolodkin AL, Garcia KC, Luo L (2011) Secreted Semaphorins from Degenerating Larval ORN Axons Direct Adult Projection Neuron Dendrite Targeting. Neuron 72:734–747.

Sweeney, L., Couto, A., Chou, Y., Berdnik, D., Dickson, B., Luo, L., Komiyama, T. (2007). Temporal Target Restriction of Olfactory Receptor Neurons by Semaphorin-1a/PlexinA-Mediated Axon-Axon Interactions. Neuron 53(2), 185-200.

Szüts D, Bienz M (2000) LexA chimeras reveal the function of Drosophila Fos as a context-dependent transcriptional activator. Proc National Acad Sci 97:5351–5356.

Takano T, Wallace JT, Baldwin KT, Purkey AM, Uezu A, Courtland JL, Soderblom EJ, Shimogori T, Maness PF, Eroglu C, Soderling SH (2020) Chemico-genetic discovery of astrocytic control of inhibition in vivo. Nature 588:296–302.

Takesian AE, Bogart LJ, Lichtman JW, Hensch TK (2018) Inhibitory circuit gating of auditory critical-period plasticity. Nat Neurosci 21:218–227.

Talay M, Richman EB, Snell NJ, Hartmann GG, Fisher JD, Sorkaç A, Santoyo JF, Chou-Freed C, Nair N, Johnson M, Szymanski JR, Barnea G (2017) Transsynaptic Mapping of Second-Order Taste Neurons in Flies by trans-Tango. Neuron 96:783-795.e4.

Tessier CR, Broadie K (2008) *Drosophila* Fragile X Mental Retardation Protein Developmentally Regulates Activity-Dependent Axon Pruning. Development 135:1547–1557.

Tessier CR, Broadie K (2009) Activity-Dependent Modulation of Neural Circuit Synaptic Connectivity. Frontiers Mol Neurosci 2:8.

Tessier CR, Broadie K (2011) The Fragile X Mental Retardation Protein Developmentally Regulates the Strength and Fidelity of Calcium Signaling in *Drosophila* Mushroom Body Neurons. Neurobiol Dis 41:147–159.

Thibault ST et al. (2004) A Complementary Transposon Tool Kit for *Drosophila melanogaster* Using P and piggyBac. Nat Genet 36:283–287.

Till SM, Li H-LL, Miniaci MC, Kandel ER, Choi Y-BB (2011) A presynaptic role for FMRP during protein synthesis-dependent long-term plasticity in Aplysia. Learning & memory (Cold Spring Harbor, NY) 18:39–48.

Tsai L, Barnea G (2014) A critical period defined by axon-targeting mechanisms in the murine olfactory bulb. Science (New York, NY) 344:197–200.

Tsai P-I, Wang M, Kao H-H, Cheng Y-J, Lin Y-J, Chen R-H, Chien C-T (2012) Activity-Dependent Retrograde Laminin A Signaling Regulates Synapse Growth at *Drosophila* Neuromuscular Junctions. Proc National Acad Sci 109:17699–17704.

Tyzio R, Nardou R, Ferrari DC, Tsintsadze T, Shahrokhi A, Eftekhari S, Khalilov I, Tsintsadze V, Brouchoud C, Chazal G, Lemonnier E, Lozovaya N, Burnashev N, Ben-Ari Y (2014) Oxytocin-mediated GABA inhibition during delivery attenuates autism pathogenesis in rodent offspring. Science (New York, NY) 343:675–679.

Vainchtein ID, Chin G, Cho FS, Kelley KW, Miller JG, Chien EC, Liddelow SA, Nguyen PT, Nakao-Inoue H, Dorman LC, Akil O, Joshita S, Barres BA, Paz JT, Molofsky AB, Molofsky AV (2018) Astrocyte-derived interleukin-33 promotes microglial synapse engulfment and neural circuit development. Science 359:eaal3589.

Vay S, Wiesel TN, Hubel DH (1980) The Development of Ocular Dominance Columns in Normal and Visually Deprived Monkeys. J Comp Neurol 191:1–51.

Venken KJT, Simpson JH, Bellen HJ (2011) Genetic Manipulation of Genes and Cells in the Nervous System of the Fruit Fly. Neuron 72:202–230.

Verkerk A et al. (1991) Identification of a gene (FMR-1) containing a CGG repeat coincident with a breakpoint cluster region exhibiting length variation in fragile X syndrome. Cell 65:905–914.

Vetencourt J, Sale A, Viegi A, Baroncelli L, Pasquale R, O'Leary OF, Castrén E, Maffei L (2008) The Antidepressant Fluoxetine Restores Plasticity in the Adult Visual Cortex. Science 320:385–388.

Vita DJ, Broadie K (2017) ESCRT-III Membrane Trafficking Misregulation Contributes To Fragile X Syndrome Synaptic Defects. Sci Reports 7:8683.

Vosshall LB, Wong AM, Axel R (2000) An Olfactory Sensory Map in the Fly Brain. Cell 102:147–159.

Wagh DA, Rasse TM, Asan E, Hofbauer A, Schwenkert I, Dürrbeck H, Buchner S, Dabauvalle M-C, Schmidt M, Qin G, Wichmann C, Kittel R, Sigrist SJ, Buchner E (2006) Bruchpilot, a Protein with Homology to ELKS/CAST, Is Required for Structural Integrity and Function of Synaptic Active Zones in *Drosophila*. Neuron 49:833–844.

Wan J, Peng W, Li X, Qian T, Song K, Zeng J, Deng F, Hao S, Feng J, Zhang P, Zhang Y, Zou J, Pan S, Zhu JJ, Jing M, Xu M, Li Y (2020) A genetically encoded GRAB sensor for measuring serotonin dynamics in vivo. Biorxiv:2020.02.24.962282.

Wang, J., Beck, E., McCabe, B. (2012). A Modular Toolset for Recombination Transgenesis and Neurogenetic Analysis of *Drosophila*. PLoS ONE 7(7), e42102.

Wang Y, Guo H-F, Pologruto TA, Hannan F, Hakker I, Svoboda K, Zhong Y (2004) Stereotyped Odor-Evoked Activity in the Mushroom Body of Drosophila Revealed by Green Fluorescent Protein-Based Ca2+ Imaging. J Neurosci 24:6507–6514.

Wang JW, Wong AM, Flores J, Vosshall LB, Axel R (2003) Two-Photon Calcium Imaging Reveals an Odor-Evoked Map of Activity in the Fly Brain. Cell 112:271–282.

Watts RJ, Hoopfer ED, Luo L (2003) Axon Pruning during Drosophila Metamorphosis Evidence for Local Degeneration and Requirement of the Ubiquitin-Proteasome System. Neuron 38:871–885.

Wen TH, Afroz S, Reinhard SM, Palacios AR, Tapia K, Binder DK, Razak KA, Ethell IM (2017) Genetic Reduction of Matrix Metalloproteinase-9 Promotes Formation of Perineuronal Nets Around Parvalbumin-Expressing Interneurons and Normalizes Auditory Cortex Responses in Developing Fmr1 Knock-Out Mice. Cereb Cortex 28:3951–3964.

Wiesel TN, Hubel DH (1963a) Effects of Visual Deprivation on Morphology and Physiology of Cells in the Cat's Lateral Geniculate. J Neurophysiol 26:978–993.

Wiesel TN, Hubel DH (1963b) Single-Cell Responses in Striate Cortex of Kittens Deprived of Vision in One Eye. J Neurophysiol 26:1003–1017.

Wilson, R. (2013). Early olfactory processing in *Drosophila*: mechanisms and principles. Annual Review of Neuroscience 36, 217-241.

Wilson CD, Serrano GO, Koulakov AA, Rinberg D (2017) A primacy code for odor identity. Nat Commun 8:1477.

Wilton DK, Dissing-Olesen L, Stevens B (2019) Neuron-Glia Signaling in Synapse Elimination. Annu Rev Neurosci 42:107–127.

Winkle, C. C. and Gupton, S. L. (2016). Membrane Trafficking in Neuronal Development: Ins and Outs of Neural Connectivity. Int. Rev. Cell Mol. Biol. 322, 247–280.

Wodarz, A., Hinz, U., Engelbert, M., Knust, E. (1995). Expression of crumbs confers apical character on plasma membrane domains of ectodermal epithelia of *Drosophila*. Cell 82(1), 67-76.

Wu B, Li J, Chou Y-H, Luginbuhl D, Luo L (2017) Fibroblast growth factor signaling instructs ensheathing glia wrapping of Drosophila olfactory glomeruli. Proc National Acad Sci 114:7505–7512.

Wu H-H, Bellmunt E, Scheib JL, Venegas V, Burkert C, Reichardt LF, Zhou Z, Fariñas I, Carter BD (2009) Glial precursors clear sensory neuron corpses during development via Jedi-1, an engulfment receptor. Nat Neurosci 12:1534–1541.

Xia, S., Miyashita, T., Fu, T., Lin, W., Wu, C., Pyzocha, L., Lin, I., Saitoe, M., Tully, T., Chiang, A. (2005). NMDA Receptors Mediate Olfactory Learning and Memory in *Drosophila*. Current Biology 15(7), 603-615.

Yaeger CE, Ringach DL, Trachtenberg JT (2019) Neuromodulatory control of localized dendritic spiking in critical period cortex. Nature 567:100–104.

Yamamuro K, Bicks LK, Leventhal MB, Kato D, Im S, Flanigan ME, Garkun Y, Norman KJ, Caro K, Sadahiro M, Kullander K, Akbarian S, Russo SJ, Morishita H (2020) A prefrontal–paraventricular thalamus circuit requires juvenile social experience to regulate adult sociability in mice. Nat Neurosci 23:1240–1252.

Yaksi E, Wilson RI (2010) Electrical coupling between olfactory glomeruli. Neuron 67:1034–1047.

Yu, F. & Schuldiner, O. (2014). Axon and dendrite pruning in *Drosophila*. Curr Opin Neurobiol 27, 192–198.

Yun S-WW, Platholi J, Flaherty MS, Fu W, Kottmann AH, Toth M (2006) Fmrp is required for the establishment of the startle response during the critical period of auditory development. Brain research 1110:159–165.

Zalfa F, Giorgi M, Primerano B, Moro A, Penta A, Reis S, Oostra B, Bagni C (2003) The fragile X syndrome protein FMRP associates with BC1 RNA and regulates the translation of specific mRNAs at synapses. Cell 112:317–327.

Zars T, Fischer † M., Schulz R, Heisenberg M (2000) Localization of a Short-Term Memory in Drosophila. Science 288:672–675.

Zhang LI, Bao S, Merzenich MM (2001a) Persistent and specific influences of early acoustic environments on primary auditory cortex. Nat Neurosci 4:1123–1130.

Zhang Y, Bailey A, Matthies H, Renden R, Smith M, Speese S, Rubin G, Broadie K (2001b) Drosophila fragile X-related gene regulates the MAP1B homolog Futsch to control synaptic structure and function. Cell 107:591–603.

Zhang Y, Bonnan A, Bony G, Ferezou I, Pietropaolo S, Ginger M, Sans N, Rossier J, Oostra B, LeMasson G, Frick A (2014) Dendritic channelopathies contribute to neocortical and sensory hyperexcitability in Fmr1(-/y) mice. Nature neuroscience 17:1701–1709.

Zhang J, Carthew R (1998) Interactions Between Wingless and DFz2 During *Drosophila* Wing Development. Development 125:3075–3085.

Zhang D, Zhou W, Yin C, Chen W, Ozawa R, Ang L, Anandan L, Aigaki T, Hing H (2006) Misexpression screen for genes altering the olfactory map in Drosophila. Genesis 44:189–201.

Zheng J-J, Li S-J, Zhang X-D, Miao W-Y, Zhang D, Yao H, Yu X (2014) Oxytocin mediates early experience–dependent cross-modal plasticity in the sensory cortices. Nat Neurosci 17:391–399.

Zhu G, Liu Y, Wang Y, Bi X, Baudry M (2015) Different Patterns of Electrical Activity Lead to Long-term Potentiation by Activating Different Intracellular Pathways. J Neurosci 35:621–633.

Zhu H, Hummel T, Clemens JC, Berdnik D, Zipursky SL, Luo L (2006) Dendritic patterning by Dscam and synaptic partner matching in the Drosophila antennal lobe. Nat Neurosci 9:349–355.

Zhu H, Luo L (2004) Diverse functions of N-cadherin in dendritic and axonal terminal arborization of olfactory projection neurons. Neuron 42:63–75.